

KINETIC MODELING OF A SOUR GAS INCINERATOR:
AN ALTERNATIVE STUDY TO SOUR GAS FLARING

CENTRE FOR NEWFOUNDLAND STUDIES

**TOTAL OF 10 PAGES ONLY
MAY BE XEROXED**

(Without Author's Permission)

LORI LYNN M. LYNCH



**Kinetic Modeling of a Sour Gas Incinerator:
An Alternative Study to Sour Gas Flaring**

By

© Lori Lynn M. Lynch, BSc.

A Thesis Submitted to the
School of Graduate Studies
in Partial Fulfilment of the
Requirements for the Degree of
Master of Engineering

Faculty of Engineering and Applied Science
Memorial University of Newfoundland

December 2003

St. John's

Newfoundland



Library and
Archives Canada

Bibliothèque et
Archives Canada

Published Heritage
Branch

Direction du
Patrimoine de l'édition

395 Wellington Street
Ottawa ON K1A 0N4
Canada

395, rue Wellington
Ottawa ON K1A 0N4
Canada

Your file *Votre référence*

ISBN: 0-612-99091-5

Our file *Notre référence*

ISBN: 0-612-99091-5

NOTICE:

The author has granted a non-exclusive license allowing Library and Archives Canada to reproduce, publish, archive, preserve, conserve, communicate to the public by telecommunication or on the Internet, loan, distribute and sell theses worldwide, for commercial or non-commercial purposes, in microform, paper, electronic and/or any other formats.

The author retains copyright ownership and moral rights in this thesis. Neither the thesis nor substantial extracts from it may be printed or otherwise reproduced without the author's permission.

AVIS:

L'auteur a accordé une licence non exclusive permettant à la Bibliothèque et Archives Canada de reproduire, publier, archiver, sauvegarder, conserver, transmettre au public par télécommunication ou par l'Internet, prêter, distribuer et vendre des thèses partout dans le monde, à des fins commerciales ou autres, sur support microforme, papier, électronique et/ou autres formats.

L'auteur conserve la propriété du droit d'auteur et des droits moraux qui protègent cette thèse. Ni la thèse ni des extraits substantiels de celle-ci ne doivent être imprimés ou autrement reproduits sans son autorisation.

In compliance with the Canadian Privacy Act some supporting forms may have been removed from this thesis.

Conformément à la loi canadienne sur la protection de la vie privée, quelques formulaires secondaires ont été enlevés de cette thèse.

While these forms may be included in the document page count, their removal does not represent any loss of content from the thesis.

Bien que ces formulaires aient inclus dans la pagination, il n'y aura aucun contenu manquant.


Canada

Abstract

The gas flare process is the most common process used to dispose of waste gas generated in oil and gas operations. However, waste gas incineration has been suggested as a better alternative to gas flaring. There have been no published studies completed to assess the emissions associated with waste gas incineration or a comparison to flaring. Thus, this study has attempted to determine the emissions of waste gas incineration, particularly during well testing operations of sour gas, and make a qualitative comparison to flaring.

Thermodynamic properties combined with kinetic data were used to simulate a detailed model that examined the likely routes of formation of several toxic species during sour gas incineration. Reactions involving oxidation products, light hydrocarbons, complex sulphur species, aromatic hydrocarbons, and poly-aromatic hydrocarbons were studied. In addition, the effects of varying inlet oxygen, flow rate, and temperature on species formation in the combustion chamber and incinerator stack were also determined. A qualitative comparison was then performed on the simulated emission results and experimental measurements of emissions from a sour gas flare.

Acknowledgements

There are so many people that I would like to thank that have helped me through this entire process. First of all, I have much gratitude and appreciation for my supervisor, Dr. Kelly Hawboldt. She has given me the support and knowledge that I needed. Thank you for your patience and advice, along with the financial support from NSERC. I would also like to thank the Faculty of Engineering and Applied Science for giving me the opportunity of teaching assistantships and completing this research. To other faculty and staff, including Moya Crocker, Dr. Faisal Khan, Dr. Tahir Hussain, and Dr. Leonard Lye. You have taught me so much during my degree program.

I would like to thank the staff from Questor Incineration Technologies for providing me with parameters of their product. As well, to my co-workers at College of the North Atlantic, namely Dr. Barry Hicks and Dr. K.S. Ramadurai.

Finally, I would like to thank my mom and dad, and boyfriend Darryl. You have been able to cope with me through this long and stressful process. Your patience and humor have been greatly appreciated. Thanks everyone.

Table of Contents

Abstract.....	ii
Acknowledgements.....	iii
Table of Contents.....	iv
List of Tables.....	ix
List of Figures.....	xvii
List of Symbols.....	xxii
List of Appendices.....	xxiv
Chapter 1. Introduction.....	1
1.1. Gas Flare Process.....	1
1.2. Incineration Process.....	3
1.3. Environmental Effects.....	6
1.4. Study Objectives.....	7
Chapter 2. Literature Review.....	9
2.1. Gas Flare Studies.....	9
2.2. Incineration Studies.....	13
2.3. Kinetic Studies.....	15
2.3.1. Hydrocarbon Oxidation and Pyrolysis Reactions.....	15
2.3.1.1. Methane Reactions.....	15
2.3.1.2. Ethane Reactions.....	16
2.3.1.3. Propane Reactions.....	18
2.3.1.4. Butane Reactions.....	18
2.3.1.5. Aromatic Hydrocarbon Reactions.....	23
2.3.2. Hydrogen Sulphide Oxidation and Pyrolysis Reactions.....	25
2.4. Summary.....	28
Chapter 3. Simulation and Modeling Study.....	30
3.1. Equilibrium Study.....	30
3.1.1. Introduction.....	30

3.1.2. Equilibrium Calculations.....	31
3.1.3. Thermodynamic Data.....	31
3.1.3.1. Sources of Data.....	31
3.1.3.2. Data Calculations.....	33
3.1.4. Gibbs Free Energy Minimization Model.....	35
3.2. Kinetic Study.....	36
3.2.1. Introduction.....	36
3.2.2. Sources of Data.....	37
3.2.3. Reactor Model.....	38
3.2.3.1. Model Assumptions.....	38
3.2.3.2. Reactor Parameters.....	38
3.2.3.3. Reactor Calculations.....	39
3.2.3.4. Model Requirements.....	41
3.2.4. Kinetic Calculations.....	42
3.2.4.1. Combustion Chamber Model Calculations.....	42
3.2.4.2. Incinerator Stack Model Calculations.....	44
3.3. Summary.....	45
 Chapter 4. Equilibrium Model Results and Analysis.....	 46
4.1. Excess Oxygen Combustion Results.....	47
4.1.1. Introduction.....	47
4.1.2. Equilibrium Predictions for Oxidation Products and Light Hydrocarbon Species.....	47
4.1.3. Equilibrium Predictions for Sulphur-Containing Compounds.....	48
4.1.4. Equilibrium Predictions for Aromatic Species.....	49
4.2. Decreasing Oxygen Combustion Results.....	50
4.2.1. Introduction.....	50
4.2.2. Equilibrium Predictions for Oxidation Products and Light Hydrocarbon Species.....	51
4.2.3. Equilibrium Predictions for Sulphur-Containing Compounds.....	54
4.2.4. Equilibrium Predictions for Aromatic Species.....	56
4.3. Pyrolysis Combustion Results.....	57
4.3.1. Introduction.....	57
4.3.2. Equilibrium Predictions for Oxidation Products and Light Hydrocarbon Species.....	58
4.3.3. Equilibrium Predictions for Sulphur-Containing Compounds.....	61
4.3.4. Equilibrium Predictions for Aromatic Species.....	62
4.4. Stoichiometric Air Combustion Results.....	66
4.4.1. Introduction.....	66
4.4.2. Equilibrium Predictions for Oxidation Products and Light Hydrocarbon Species.....	67
4.4.3. Equilibrium Predictions for Sulphur-Containing Compounds.....	67
4.4.4. Equilibrium Predictions for Aromatic Species.....	69
4.5. Summary.....	70

Chapter 5. Kinetic Model Results and Analysis.....	72
5.1. Combustion Chamber Calculations.....	72
5.1.1. Case A: 14:1 Air to Fuel Ratio Results.....	72
5.1.1.1. Introduction.....	72
5.1.1.2. Kinetic Predictions for Oxidation Products and Light Hydrocarbon Species.....	73
5.1.1.3. Kinetic Predictions for Sulphur-Containing Compounds...	75
5.1.1.4. Kinetic Predictions for Aromatic Species.....	78
5.1.2. Case B: 17:1 Air to Fuel Ratio Results.....	83
5.1.2.1. Introduction.....	83
5.1.2.2. Kinetic Predictions for Oxidation Products and Light Hydrocarbon Species.....	83
5.1.2.3. Kinetic Predictions for Sulphur-Containing Compounds...	84
5.1.2.4. Kinetic Predictions for Aromatic Species.....	85
5.1.3. Case C: 21:1 Air to Fuel Ratio Results.....	87
5.1.3.1. Introduction.....	87
5.1.3.2. Kinetic Predictions for Oxidation Products and Light Hydrocarbon Species.....	87
5.1.3.3. Kinetic Predictions for Sulphur-Containing Compounds...	88
5.1.3.4. Kinetic Predictions for Aromatic Species.....	89
5.2. Incinerator Stack Calculations.....	93
5.2.1. Case A: 14:1 Air to Fuel Ratio Results.....	93
5.2.1.1. Introduction.....	93
5.2.1.2. Oxidation Products and Light Hydrocarbon Species Results.....	94
5.2.1.2.1. Kinetic Results for 1000 K Temperature Profile..	94
5.2.1.2.2. Kinetic Results for 1400 K Temperature Profile..	98
5.2.1.2.3. Kinetic Results for 1623 K Temperature Profile..	101
5.2.1.3. Sulphur-Containing Species Results.....	103
5.2.1.3.1. Kinetic Results for 1000 K Temperature Profile..	103
5.2.1.3.2. Kinetic Results for 1400 K Temperature Profile..	105
5.2.1.3.3. Kinetic Results for 1623 K Temperature Profile..	105
5.2.1.4. Aromatic and Poly-Aromatic Hydrocarbon Results.....	107
5.2.1.4.1. Kinetic Results for 1000 K Temperature Profile..	107
5.2.1.4.2. Kinetic Results for 1400 K Temperature Profile..	121
5.2.1.4.3. Kinetic Results for 1623 K Temperature Profile..	128
5.2.2. Case B: 17:1 Air to Fuel Ratio Results.....	140
5.2.2.1. Introduction.....	140
5.2.2.2. Oxidation Products and Light Hydrocarbon Species Results.....	140
5.2.2.2.1. Kinetic Results for 1000 K Temperature Profile..	140
5.2.2.2.2. Kinetic Results for 1400 K Temperature Profile..	142
5.2.2.2.3. Kinetic Results for 1623 K Temperature Profile..	144
5.2.2.3. Sulphur-Containing Species Results.....	146
5.2.2.3.1. Kinetic Results for 1000 K Temperature Profile..	146

5.2.2.3.2. Kinetic Results for 1400 K Temperature Profile..	147
5.2.2.3.3. Kinetic Results for 1623 K Temperature Profile..	147
5.2.2.4. Aromatic and Poly-Aromatic Hydrocarbon Results.....	148
5.2.2.4.1. Kinetic Results for 1000 K Temperature Profile..	148
5.2.2.4.2. Kinetic Results for 1400 K Temperature Profile..	152
5.2.2.4.3. Kinetic Results for 1623 K Temperature Profile..	155
5.2.3. Case C: 21:1 Air to Fuel Ratio Results.....	159
5.2.3.1. Introduction.....	159
5.2.3.2. Oxidation Products and Light Hydrocarbon Species Results.....	160
5.2.3.2.1. Kinetic Results for 1000 K Temperature Profile..	160
5.2.3.2.2. Kinetic Results for 1400 K Temperature Profile..	161
5.2.3.2.3. Kinetic Results for 1623 K Temperature Profile..	163
5.2.3.3. Sulphur-Containing Species Results.....	165
5.2.3.3.1. Kinetic Results for 1000 K Temperature Profile..	165
5.2.3.3.2. Kinetic Results for 1400 K Temperature Profile..	166
5.2.3.3.3. Kinetic Results for 1623 K Temperature Profile..	166
5.2.3.4. Aromatic and Poly-Aromatic Hydrocarbon Results.....	167
5.2.3.4.1. Kinetic Results for 1000 K Temperature Profile..	167
5.2.3.4.2. Kinetic Results for 1400 K Temperature Profile..	170
5.2.3.4.3. Kinetic Results for 1623 K Temperature Profile..	174
5.3. Summary.....	181
Chapter 6. Discussion.....	183
6.1. Introduction.....	183
6.2. Equilibrium Model.....	183
6.2.1. Excess Oxygen Combustion Results.....	183
6.2.2. Decreasing Oxygen Combustion Results.....	184
6.2.3. Pyrolysis Results.....	185
6.2.4. Stoichiometric Air Combustion Results.....	187
6.3. Kinetic Model.....	188
6.3.1. Combustion Chamber Model.....	188
6.3.2. Incineration Stack Model	190
6.4. Comparison Between Equilibrium Model and Kinetic Model Results.....	191
6.4.1. Combustion Chamber Comparison.....	191
6.4.2. Incineration Stack Comparison.....	195
6.5. Comparison to Gas Flaring.....	197
6.6. Summary.....	200
Chapter 7. Conclusions and Recommendations.....	202
7.1. Reactor Model Verification.....	202
7.2. Equilibrium Model.....	202

7.3. Kinetic Model.....	204
7.3.1. Combustion Chamber Calculations.....	204
7.3.2. Incineration Stack Calculations.....	205
7.4. General Recommendations.....	208
7.5. Summary.....	209
References.....	211
Appendix 1. Chemkin Input File.....	215
Appendix 2.1 Equilibrium Input File for Excess Oxygen Combustion.....	216
Appendix 2.2. Equilibrium Input File for 20% Decreasing Oxygen Combustion.....	217
Appendix 2.3. Equilibrium Input File for Pyrolysis.....	218
Appendix 2.4. Equilibrium Input File for Stoichiometric Air Combustion.....	219
Appendix 3.1. Plug Input File for Combustion Chamber Calculations under the Conditions of a 14:1 Air to Fuel Ratio and Flow Rate of $3.28 \times 10^5 \text{ cm}^3/\text{s}$	220
Appendix 3.2. Plug Input File for Incinerator Stack Calculations under the Conditions of a 1623 K Temperature Profile, Flow Rate of $1.64 \times 10^6 \text{ cm}^3/\text{s}$, and a 14:1 air to fuel ratio.....	221

List of Tables

Table 2.1. Characterization of hydrocarbon emissions from a sweet oil-field battery flare containing different levels of liquid hydrocarbon in mg/m^3	10
Table 2.2. Hydrocarbons and sulphur compounds identified in emissions and their relative concentrations in mg/m^3 from a sour oilfield battery flare in Alberta.....	11
Table 2.3. Estimated combustion efficiencies for indicated gas flames as functions of stack exit velocity V (m/sec) and wind speed U (m/sec).....	12
Table 2.4. Concentrations of compounds detected in a solid-waste incinerator stack during start-up conditions.....	14
Table 3.1. Sour gas composition and input mole fraction compositions for equilibrium model.....	32
Table 3.2. Summary of combustion chamber model parameters.....	43
Table 3.3. Temperature profiles at different lengths inside the stack.....	44
Table 4.1. Experimental input mole fraction compositions used under excess oxygen conditions.....	47
Table 4.2. Input mole fraction compositions for the decreasing oxygen content equilibrium simulations.....	51
Table 4.3. Percent increases in composition for oxidation products under equilibrium conditions while decreasing the oxygen content by 20 %, 40 %, 60 %, and 80 %.....	52
Table 4.4. Percent increases in composition for sulphur-containing species under equilibrium conditions while decreasing the oxygen content by 20 %, 40 %, 60 %, and 80 %.....	54
Table 4.5. Equilibrium input mole fraction compositions used for combustion pyrolysis.....	58
Table 4.6. Equilibrium input mole fraction compositions used for stoichiometric combustion of sour gas.....	66
Table 4.7. Chemical species predicted to form under equilibrium conditions but have no kinetic data published.....	71

Table 5.1. Kinetically predicted changes in composition (%) for lower weight hydrocarbons and oxidation products at entry of the combustion chamber under the 14:1 air to fuel ratio with increasing flow rate from $3.28 \times 10^5 \text{ cm}^3/\text{s}$ to $1.64 \times 10^6 \text{ cm}^3/\text{s}$ and a temperature of 800 K.....	76
Table 5.2. Kinetically predicted reductions in composition (%) for aromatic and poly-aromatic species at entry of the combustion chamber under the 14:1 air to fuel ratio with increasing flow rate from $3.28 \times 10^5 \text{ cm}^3/\text{s}$ to $1.64 \times 10^6 \text{ cm}^3/\text{s}$, and temperature of 800 K.....	82
Table 5.3. Kinetically predicted changes in composition (%) for lower weight hydrocarbons and oxidation products at entry of the combustion chamber under the 17:1 air to fuel ratio with increasing flow rate from $3.28 \times 10^5 \text{ cm}^3/\text{s}$ to $1.64 \times 10^6 \text{ cm}^3/\text{s}$, and a temperature of 800 K.....	84
Table 5.4. Kinetically predicted reductions in composition (%) for aromatic and poly-aromatic species at entry of the combustion chamber under the 17:1 air to fuel ratio with increasing flow rate from $3.28 \times 10^5 \text{ cm}^3/\text{s}$ to $1.64 \times 10^6 \text{ cm}^3/\text{s}$, and a temperature of 800 K.....	86
Table 5.5. Kinetically predicted changes in composition (%) for lower weight hydrocarbons and oxidation products at entry of the combustion chamber under the 21:1 air to fuel ratio with increasing flow rate from $3.28 \times 10^5 \text{ cm}^3/\text{s}$ to $1.64 \times 10^6 \text{ cm}^3/\text{s}$, and a temperature of 800 K.....	88
Table 5.6. Kinetically predicted reductions in composition (%) for aromatic and poly-aromatic species at entry of the combustion chamber under the 21:1 air to fuel ratio with increasing flow rate from $3.28 \times 10^5 \text{ cm}^3/\text{s}$ to $1.64 \times 10^6 \text{ cm}^3/\text{s}$, and a temperature of 800 K.....	90
Table 5.7. Kinetically predicted reductions in composition (%) for species at entry of the combustion chamber under three tested flow rates (a). $3.28 \times 10^5 \text{ cm}^3/\text{s}$, (b). $9.83 \times 10^5 \text{ cm}^3/\text{s}$, and (c). $1.64 \times 10^6 \text{ cm}^3/\text{s}$, when ranging air to fuel ratio from 14:1 to 21:1 and a temperature of 800 K.....	91
Table 5.8. Kinetically predicted reductions (%) in compositions from inlet lower weight hydrocarbons and oxidation products in the stack during cooling under the conditions of 14:1 air to fuel ratio, 1000 K temperature profile, and varying flow rates of (a). $3.28 \times 10^5 \text{ cm}^3/\text{s}$, (b). $9.83 \times 10^5 \text{ cm}^3/\text{s}$, and (c). $1.64 \times 10^6 \text{ cm}^3/\text{s}$	96
Table 5.9. Kinetically predicted changes in composition (%) for lower weight hydrocarbons and oxidation products within the stack under the 1000 K temperature profile, 14:1 air to fuel ratio with increasing flow rate from $3.28 \times 10^5 \text{ cm}^3/\text{s}$ to $1.64 \times 10^6 \text{ cm}^3/\text{s}$	98

Table 5.10. Kinetically predicted reductions (%) in compositions from inlet lower weight hydrocarbons and oxidation products in the stack during cooling under the conditions of 14:1 air to fuel ratio, 1400 K temperature profile, and varying flow rates of (a). $3.28 \times 10^5 \text{ cm}^3/\text{s}$, (b). $9.83 \times 10^5 \text{ cm}^3/\text{s}$, and (c). $1.64 \times 10^6 \text{ cm}^3/\text{s}$	99
Table 5.11. Kinetically predicted changes in composition (%) for lower weight hydrocarbons and oxidation products within the stack under the 1400 K temperature profile, 14:1 air to fuel ratio with increasing flow rate from $3.28 \times 10^5 \text{ cm}^3/\text{s}$ to $1.64 \times 10^6 \text{ cm}^3/\text{s}$	101
Table 5.12. Kinetically predicted reductions (%) in compositions from inlet lower weight hydrocarbons and oxidation products in the stack during cooling under the conditions of 14:1 air to fuel ratio, 1623 K temperature profile, and varying flow rates of (a). $3.28 \times 10^5 \text{ cm}^3/\text{s}$, (b). $9.83 \times 10^5 \text{ cm}^3/\text{s}$, and (c). $1.64 \times 10^6 \text{ cm}^3/\text{s}$	102
Table 5.13. Kinetically predicted changes in composition (%) for lower weight hydrocarbons and oxidation products within the stack under the 1623 K temperature profile, 14:1 air to fuel ratio with increasing flow rate from $3.28 \times 10^5 \text{ cm}^3/\text{s}$ to $1.64 \times 10^6 \text{ cm}^3/\text{s}$	103
Table 5.14. Kinetically predicted reductions (%) in compositions from inlet for single ring aromatic species in the stack during cooling under the conditions of 14:1 air to fuel ratio, 1000 K temperature profile, and varying flow rates of (a). $3.28 \times 10^5 \text{ cm}^3/\text{s}$, (b). $9.83 \times 10^5 \text{ cm}^3/\text{s}$, and (c). $1.64 \times 10^6 \text{ cm}^3/\text{s}$	108
Table 5.15. Kinetically predicted changes (%) in compositions for single ring aromatic species in the stack as inlet flow rates are increased from $3.28 \times 10^5 \text{ cm}^3/\text{s}$ to $1.64 \times 10^6 \text{ cm}^3/\text{s}$ under the 14: 1 air to fuel ratio and 1000 K temperature profile.....	112
Table 5.16. Kinetically predicted increases (%) in compositions from inlet for poly-aromatic species in the stack during cooling under the conditions of 14:1 air to fuel ratio, 1000 K temperature profile, and varying flow rates of (a). $3.28 \times 10^5 \text{ cm}^3/\text{s}$, (b). $9.83 \times 10^5 \text{ cm}^3/\text{s}$, and (c). $1.64 \times 10^6 \text{ cm}^3/\text{s}$	119
Table 5.17. Kinetically predicted changes (%) in compositions for poly-aromatic species in the stack as inlet flow rates are increased from $3.28 \times 10^5 \text{ cm}^3/\text{s}$ to $1.64 \times 10^6 \text{ cm}^3/\text{s}$ under the 14:1 air to fuel ratio and 1000 K temperature profile.....	120
Table 5.18. Kinetically predicted reductions (%) in compositions from inlet for single ring aromatic species in the stack during cooling under the conditions of 14:1 air to fuel ratio, 1400 K temperature profile, and varying flow rates of (a). $3.28 \times 10^5 \text{ cm}^3/\text{s}$, (b). $9.83 \times 10^5 \text{ cm}^3/\text{s}$, and (c). $1.64 \times 10^6 \text{ cm}^3/\text{s}$	121

Table 5.19. Kinetically predicted changes (%) in compositions for single ring aromatic species in the stack as inlet flow rates are increased from $3.28 \times 10^5 \text{ cm}^3/\text{s}$ to $1.64 \times 10^6 \text{ cm}^3/\text{s}$ under the 14:1 air to fuel ratio and 1400 K temperature profile.....	125
Table 5.20. Kinetically predicted increases (%) in compositions for poly-aromatic species in the stack during cooling under the conditions of 14:1 air to fuel ratio, 1400 K temperature profile, and varying flow rates of (a). $3.28 \times 10^5 \text{ cm}^3/\text{s}$, (b). $9.83 \times 10^5 \text{ cm}^3/\text{s}$, and (c). $1.64 \times 10^6 \text{ cm}^3/\text{s}$	127
Table 5.21. Kinetically predicted changes (%) in compositions for poly-aromatic species in the stack as inlet flow rates are increased from $3.28 \times 10^5 \text{ cm}^3/\text{s}$ to $1.64 \times 10^6 \text{ cm}^3/\text{s}$ under the 14:1 air to fuel ratio and 1400 K temperature profile.....	128
Table 5.22. Kinetically predicted reductions (%) in compositions for single ring aromatic species in the stack during cooling under the conditions of 14:1 air to fuel ratio, 1623 K temperature profile, and varying flow rates of (a). $3.28 \times 10^5 \text{ cm}^3/\text{s}$, (b). $9.83 \times 10^5 \text{ cm}^3/\text{s}$, and (c). $1.64 \times 10^6 \text{ cm}^3/\text{s}$	129
Table 5.23. Kinetically predicted changes (%) in compositions for single ring aromatic species in the stack as inlet flow rates are increased from $3.28 \times 10^5 \text{ cm}^3/\text{s}$ to $1.64 \times 10^6 \text{ cm}^3/\text{s}$ under the 14:1 air to fuel ratio and 1623 K temperature profile.....	130
Table 5.24. Kinetically predicted increases (%) in compositions for poly-aromatic species in the stack during cooling under the conditions of 14:1 air to fuel ratio, 1623 K temperature profile, and varying flow rates of (a). $3.28 \times 10^5 \text{ cm}^3/\text{s}$, (b). $9.83 \times 10^5 \text{ cm}^3/\text{s}$, and (c). $1.64 \times 10^6 \text{ cm}^3/\text{s}$	131
Table 5.25. Kinetically predicted changes (%) in compositions for poly-aromatic species in the stack as inlet flow rates are increased from $3.28 \times 10^5 \text{ cm}^3/\text{s}$ to $1.64 \times 10^6 \text{ cm}^3/\text{s}$ under the 14:1 air to fuel ratio and 1623 K temperature profile.....	139
Table 5.26. Kinetically predicted reductions (%) in compositions for lower weight hydrocarbons and oxidation products in the stack during cooling under the conditions of 17:1 air to fuel ratio, 1000 K temperature profile, and varying flow rates of (a). $3.28 \times 10^5 \text{ cm}^3/\text{s}$, (b). $9.83 \times 10^5 \text{ cm}^3/\text{s}$, and (c). $1.64 \times 10^6 \text{ cm}^3/\text{s}$	141
Table 5.27. Kinetically predicted changes in composition (%) for lower weight hydrocarbons and oxidation products within the stack under the 1000 K temperature profile, 17:1 air to fuel ratio with increasing flow rate from $3.28 \times 10^5 \text{ cm}^3/\text{s}$ to $1.64 \times 10^6 \text{ cm}^3/\text{s}$	142
Table 5.28. Kinetically predicted reductions (%) in compositions from inlet lower weight hydrocarbons and oxidation products in the stack during cooling under the conditions of 17:1 air to fuel ratio, 1400 K temperature profile, and varying flow rates of (a). $3.28 \times 10^5 \text{ cm}^3/\text{s}$, (b). $9.83 \times 10^5 \text{ cm}^3/\text{s}$, and (c). $1.64 \times 10^6 \text{ cm}^3/\text{s}$	143

Table 5.29. Kinetically predicted changes in composition (%) for lower weight hydrocarbons and oxidation products within the stack under the 1400 K temperature profile, 17:1 air to fuel ratio with increasing flow rate from $3.28 \times 10^5 \text{ cm}^3/\text{s}$ to $1.64 \times 10^6 \text{ cm}^3/\text{s}$	144
Table 5.30. Kinetically predicted reductions (%) in compositions from inlet lower weight hydrocarbons and oxidation products in the stack during cooling under the conditions of 17:1 air to fuel ratio, 1623 K temperature profile, and varying flow rates of (a). $3.28 \times 10^5 \text{ cm}^3/\text{s}$, (b). $9.83 \times 10^5 \text{ cm}^3/\text{s}$, and (c). $1.64 \times 10^6 \text{ cm}^3/\text{s}$	145
Table 5.31. Kinetically predicted changes in composition (%) for lower weight hydrocarbons and oxidation products within the stack under the 1623 K temperature profile, 17:1 air to fuel ratio with increasing flow rate from $3.28 \times 10^5 \text{ cm}^3/\text{s}$ to $1.64 \times 10^6 \text{ cm}^3/\text{s}$	146
Table 5.32. Kinetically predicted reductions (%) in compositions for single ring aromatic species in the stack under the conditions of 17:1 air to fuel ratio, 1000 K temperature profile, and varying flow rates of (a). $3.28 \times 10^5 \text{ cm}^3/\text{s}$, (b). $9.83 \times 10^5 \text{ cm}^3/\text{s}$, and (c). $1.64 \times 10^6 \text{ cm}^3/\text{s}$	149
Table 5.33. Kinetically predicted increases (%) in compositions for poly-aromatic species in the stack under the conditions of 17:1 air to fuel ratio, 1000 K temperature profile, and varying flow rates of (a). $3.28 \times 10^5 \text{ cm}^3/\text{s}$, (b). $9.83 \times 10^5 \text{ cm}^3/\text{s}$, and (c). $1.64 \times 10^6 \text{ cm}^3/\text{s}$	150
Table 5.34. Kinetically predicted changes (%) in compositions for single ring aromatic species in the stack as inlet flow rates are increased from $3.28 \times 10^5 \text{ cm}^3/\text{s}$ to $1.64 \times 10^6 \text{ cm}^3/\text{s}$ under the 17:1 air to fuel ratio and 1000 K temperature profile.....	151
Table 5.35. Kinetically predicted changes (%) in compositions for poly-aromatic species in the stack as inlet flow rates are increased from $3.28 \times 10^5 \text{ cm}^3/\text{s}$ to $1.64 \times 10^6 \text{ cm}^3/\text{s}$ under the 17:1 air to fuel ratio and 1000 K temperature profile.....	151
Table 5.36. Kinetically predicted reductions (%) in compositions for single ring aromatic species in the stack under the conditions of 17:1 air to fuel ratio, 1400 K temperature profile, and varying flow rates of (a). $3.28 \times 10^5 \text{ cm}^3/\text{s}$, (b). $9.83 \times 10^5 \text{ cm}^3/\text{s}$, and (c). $1.64 \times 10^6 \text{ cm}^3/\text{s}$	152
Table 5.37. Kinetically predicted increases (%) in compositions for poly-aromatic species in the stack under the conditions of 17:1 air to fuel ratio, 1400 K temperature profile, and varying flow rates of (a). $3.28 \times 10^5 \text{ cm}^3/\text{s}$, (b). $9.83 \times 10^5 \text{ cm}^3/\text{s}$, and (c). $1.64 \times 10^6 \text{ cm}^3/\text{s}$	153

Table 5.38. Kinetically predicted changes (%) in compositions for single ring aromatic species in the stack as inlet flow rates are increased from $3.28 \times 10^5 \text{ cm}^3/\text{s}$ to $1.64 \times 10^6 \text{ cm}^3/\text{s}$ under the 17:1 air to fuel ratio and 1400 K temperature profile.....	154
Table 5.39. Kinetically predicted changes (%) in compositions for poly-aromatic species in the stack as inlet flow rates are increased from $3.28 \times 10^5 \text{ cm}^3/\text{s}$ to $1.64 \times 10^6 \text{ cm}^3/\text{s}$ under the 17:1 air to fuel ratio and 1400 K temperature profile.....	155
Table 5.40. Kinetically predicted reductions (%) in compositions for single ring aromatic species in the stack under the conditions of 17:1 air to fuel ratio, 1623 K temperature profile, and varying flow rates of (a). $3.28 \times 10^5 \text{ cm}^3/\text{s}$, (b). $9.83 \times 10^5 \text{ cm}^3/\text{s}$, and (c). $1.64 \times 10^6 \text{ cm}^3/\text{s}$	156
Table 5.41. Kinetically predicted increases (%) in compositions for poly-aromatic species in the stack under the conditions of 17:1 air to fuel ratio, 1623 K temperature profile, and varying flow rates of (a). $3.28 \times 10^5 \text{ cm}^3/\text{s}$, (b). $9.83 \times 10^5 \text{ cm}^3/\text{s}$, and (c). $1.64 \times 10^6 \text{ cm}^3/\text{s}$	157
Table 5.42. Kinetically predicted changes (%) in compositions for single ring aromatic species in the stack as inlet flow rates are increased from $3.28 \times 10^5 \text{ cm}^3/\text{s}$ to $1.64 \times 10^6 \text{ cm}^3/\text{s}$ under the 17:1 air to fuel ratio and 1623 K temperature profile.....	158
Table 5.43. Kinetically predicted changes (%) in compositions for poly-aromatic species in the stack as inlet flow rates are increased from $3.28 \times 10^5 \text{ cm}^3/\text{s}$ to $1.64 \times 10^6 \text{ cm}^3/\text{s}$ under the 17:1 air to fuel ratio and 1623 K temperature profile.....	159
Table 5.44. Kinetically predicted reductions (%) in compositions from inlet lower weight hydrocarbons and oxidation products in the stack during cooling under the conditions of 21:1 air to fuel ratio, 1000 K temperature profile, and varying flow rates of (a). $3.28 \times 10^5 \text{ cm}^3/\text{s}$, (b). $9.83 \times 10^5 \text{ cm}^3/\text{s}$, and (c). $1.64 \times 10^6 \text{ cm}^3/\text{s}$	160
Table 5.45. Kinetically predicted changes in composition (%) for lower weight hydrocarbons and oxidation products within the stack under the 1000 K temperature profile, 21:1 air to fuel ratio with increasing flow rate from $3.28 \times 10^5 \text{ cm}^3/\text{s}$ to $1.64 \times 10^6 \text{ cm}^3/\text{s}$	161
Table 5.46. Kinetically predicted reductions (%) in compositions from inlet lower weight hydrocarbons and oxidation products in the stack during cooling under the conditions of 21:1 air to fuel ratio, 1400 K temperature profile, and varying flow rates of (a). $3.28 \times 10^5 \text{ cm}^3/\text{s}$, (b). $9.83 \times 10^5 \text{ cm}^3/\text{s}$, and (c). $1.64 \times 10^6 \text{ cm}^3/\text{s}$	162

Table 5.47. Kinetically predicted changes in composition (%) for lower weight hydrocarbons and oxidation products within the stack under the 1400 K temperature profile, 21:1 air to fuel ratio with increasing flow rate from $3.28 \times 10^5 \text{ cm}^3/\text{s}$ to $1.64 \times 10^6 \text{ cm}^3/\text{s}$ 163

Table 5.48. Kinetically predicted reductions (%) in compositions from inlet lower weight hydrocarbons and oxidation products in the stack during cooling under the conditions of 21:1 air to fuel ratio, 1623 K temperature profile, and varying flow rates of (a). $3.28 \times 10^5 \text{ cm}^3/\text{s}$, (b). $9.83 \times 10^5 \text{ cm}^3/\text{s}$, and (c). $1.64 \times 10^6 \text{ cm}^3/\text{s}$ 164

Table 5.49. Kinetically predicted changes in composition (%) for lower weight hydrocarbons and oxidation products within the stack under the 1623 K temperature profile, 21:1 air to fuel ratio with increasing flow rate from $3.28 \times 10^5 \text{ cm}^3/\text{s}$ to $1.64 \times 10^6 \text{ cm}^3/\text{s}$ 165

Table 5.50. Kinetically predicted reductions (%) in compositions for single ring aromatic species in the stack under the conditions of 21:1 air to fuel ratio, 1000 K temperature profile, and varying flow rates of (a). $3.28 \times 10^5 \text{ cm}^3/\text{s}$, (b). $9.83 \times 10^5 \text{ cm}^3/\text{s}$, and (c). $1.64 \times 10^6 \text{ cm}^3/\text{s}$ 167

Table 5.51. Kinetically predicted increases (%) in compositions for poly-aromatic species in the stack under the conditions of 21:1 air to fuel ratio, 1000 K temperature profile, and varying flow rates of (a). $3.28 \times 10^5 \text{ cm}^3/\text{s}$, (b). $9.83 \times 10^5 \text{ cm}^3/\text{s}$, and (c). $1.64 \times 10^6 \text{ cm}^3/\text{s}$ 168

Table 5.52. Kinetically predicted changes (%) in compositions for single ring aromatic species in the stack as inlet flow rates are increased from $3.28 \times 10^5 \text{ cm}^3/\text{s}$ to $1.64 \times 10^6 \text{ cm}^3/\text{s}$ under the 21:1 air to fuel ratio and 1000 K temperature profile... 169

Table 5.53. Kinetically predicted changes (%) in compositions for poly-aromatic species in the stack as inlet flow rates are increased from $3.28 \times 10^5 \text{ cm}^3/\text{s}$ to $1.64 \times 10^6 \text{ cm}^3/\text{s}$ under the 21:1 air to fuel ratio and 1000 K temperature profile..... 170

Table 5.54. Kinetically predicted reductions (%) in compositions for single ring aromatic species in the stack under the conditions of 21:1 air to fuel ratio, 1400 K temperature profile, and varying flow rates of (a). $3.28 \times 10^5 \text{ cm}^3/\text{s}$, (b). $9.83 \times 10^5 \text{ cm}^3/\text{s}$, and (c). $1.64 \times 10^6 \text{ cm}^3/\text{s}$ 171

Table 5.55. Kinetically predicted increases (%) in compositions for poly-aromatic species in the stack under the conditions of 21:1 air to fuel ratio, 1400 K temperature profile, and varying flow rates of (a). $3.28 \times 10^5 \text{ cm}^3/\text{s}$, (b). $9.83 \times 10^5 \text{ cm}^3/\text{s}$, and (c). $1.64 \times 10^6 \text{ cm}^3/\text{s}$ 172

Table 5.56. Kinetically predicted changes (%) in compositions for single ring aromatic species in the stack as inlet flow rates are increased from $3.28 \times 10^5 \text{ cm}^3/\text{s}$ to $1.64 \times 10^6 \text{ cm}^3/\text{s}$ under the 21:1 air to fuel ratio and 1400 K temperature profile... 173

Table 5.57. Kinetically predicted changes (%) in compositions for poly-aromatic species in the stack as inlet flow rates are increased from $3.28 \times 10^5 \text{ cm}^3/\text{s}$ to $1.64 \times 10^6 \text{ cm}^3/\text{s}$ under the 21:1 air to fuel ratio and 1400 K temperature profile.....	174
Table 5.58. Kinetically predicted reductions (%) in compositions for single ring aromatic species in the stack under the conditions of 21:1 air to fuel ratio, 1623 K temperature profile, and varying flow rates of (a). $3.28 \times 10^5 \text{ cm}^3/\text{s}$, (b). $9.83 \times 10^5 \text{ cm}^3/\text{s}$, and (c). $1.64 \times 10^6 \text{ cm}^3/\text{s}$	175
Table 5.59. Kinetically predicted increases (%) in compositions for poly-aromatic species in the stack under the conditions of 21:1 air to fuel ratio, 1623 K temperature profile, and varying flow rates of (a). $3.28 \times 10^5 \text{ cm}^3/\text{s}$, (b). $9.83 \times 10^5 \text{ cm}^3/\text{s}$, and (c). $1.64 \times 10^6 \text{ cm}^3/\text{s}$	176
Table 5.60. Kinetically predicted changes (%) in compositions for single ring aromatic species in the stack as inlet flow rates are increased from $3.28 \times 10^5 \text{ cm}^3/\text{s}$ to $1.64 \times 10^6 \text{ cm}^3/\text{s}$ under the 21:1 air to fuel ratio and 1623 K temperature profile...	177
Table 5.61. Kinetically predicted changes (%) in compositions for poly-aromatic species in the stack as inlet flow rates are increased from $3.28 \times 10^5 \text{ cm}^3/\text{s}$ to $1.64 \times 10^6 \text{ cm}^3/\text{s}$ under the 21:1 air to fuel ratio and 1623 K temperature profile.....	178
Table 5.62. Kinetically predicted changes (ie: ↑ for increase and ↓ for decrease) in composition (%) for species at entry of the incinerator stack, when ranging air to fuel ratio from 14:1 to 21:1 and three temperature profiles with initial internal combustion temperatures of 1000 K, 1400 K, and 1623 K.....	179
Table 6.1. Hydrocarbons and sulphur compounds identified in emissions from a sour oilfield battery flare (25% hydrogen sulphide) in Alberta and a direct comparison to this study.....	199

List of Figures

Figure 1.1. Typical Gas Flare Stack.....	3
Figure 1.2. Typical Waste Gas Incinerator.....	4
Figure 2.1. Reactions involving methane in hydrocarbon fuel combustion.....	16
Figure 2.2. Reactions involving ethane in hydrocarbon fuel combustion.....	17
Figure 2.3. Reactions involving propane in hydrocarbon fuel combustion.....	19
Figure 2.4. Reactions involving butane in hydrocarbon fuel combustion.....	21
Figure 2.5. Reaction scheme for the formation of poly-aromatic hydrocarbons in combustion flames.....	24
Figure 2.6. Experimental aromatic concentration profiles during methane flame combustion.....	25
Figure 2.7. Reactions involving hydrogen sulphide in sour gas fuel combustion.....	27
Figure 3.1. Thermodynamic data for methane in the Chemkin format.....	34
Figure 3.2. Tubular Flow Reactor.....	39
Figure 4.1. Equilibrium predictions for oxidation products under excess oxygen conditions of sour gas combustion.....	48
Figure 4.2. Equilibrium predictions for sulphur-containing compounds under excess oxygen conditions of sour gas combustion.....	49
Figure 4.3. Equilibrium predictions for aromatic hydrocarbon compounds under excess oxygen conditions of sour gas combustion.....	50
Figure 4.4. Equilibrium predictions for water under decreasing oxygen conditions of sour gas combustion.....	52
Figure 4.5. Equilibrium predictions for carbon dioxide under decreasing oxygen conditions of sour gas combustion.....	53
Figure 4.6. Equilibrium predictions for carbon monoxide under decreasing oxygen conditions of sour gas combustion.....	53

Figure 4.7. Equilibrium predictions for hydrogen sulphide under decreasing oxygen conditions of sour gas combustion.....	55
Figure 4.8. Equilibrium predictions for sulphur dioxide under decreasing oxygen conditions of sour gas combustion.....	55
Figure 4.9. Equilibrium predictions for carbonyl sulphide under decreasing oxygen conditions of sour gas combustion.....	56
Figure 4.10. Equilibrium predictions for 2-methyl naphthalene under decreasing oxygen conditions of sour gas combustion.....	57
Figure 4.11. Equilibrium predictions for light hydrocarbon species under pyrolytic conditions of sour gas combustion.....	59
Figure 4.12. Equilibrium predictions for oxidation species under pyrolytic conditions of sour gas combustion.....	60
Figure 4.13. Equilibrium predictions for sulphur-containing compounds under pyrolytic conditions of sour gas combustion.....	62
Figure 4.14. Equilibrium predictions for the formation of benzene under pyrolytic conditions of sour gas combustion.....	63
Figure 4.15. Equilibrium predictions for light aromatic hydrocarbons under pyrolytic conditions of sour gas combustion.....	64
Figure 4.16. Equilibrium predictions for poly-aromatic hydrocarbons under pyrolysis conditions of sour gas combustion.....	65
Figure 4.17. Equilibrium predictions for complete combustion products and methane under conditions of stoichiometric sour gas combustion.....	68
Figure 4.18. Equilibrium predictions for sulphur-containing compounds under conditions of stoichiometric sour gas combustion.....	69
Figure 4.19. Equilibrium predictions for aromatic hydrocarbon compounds under conditions of stoichiometric sour gas combustion.....	70
Figure 5.1. Kinetic predictions of concentrations of lower weight hydrocarbon products formed for 14:1 air to fuel ratio, an inlet flow rate of $3.28 \times 10^5 \text{ cm}^3/\text{s}$, and a temperature range of 800 K to 1800 K inside the combustion chamber during sour gas incineration.....	74

- Figure 5.2.** Kinetic predictions of concentrations of oxidation products formed for 14:1 air to fuel ratio, inlet flow rate of $3.28 \times 10^5 \text{ cm}^3/\text{s}$, and a temperature range of 800 K to 1800 K inside the combustion chamber during sour gas incineration..... 74
- Figure 5.3.** Kinetically predicted decrease in composition (%) butadiene within the combustion chamber under the 14:1 air to fuel ratio with increasing flow rate from (a). Inlet flow rate = $3.28 \times 10^5 \text{ cm}^3/\text{s}$, (b). Inlet flow rate = $9.83 \times 10^5 \text{ cm}^3/\text{s}$, (c). Inlet flow rate = $1.64 \times 10^6 \text{ cm}^3/\text{s}$, and a temperature range of 800 K to 1800 K..... 76
- Figure 5.4.** Kinetic predictions of concentrations of sulphur containing products formed for 14:1 air to fuel ratio, flow rate of $3.28 \times 10^5 \text{ cm}^3/\text{s}$, and a temperature range of 800 K to 1800 K inside the combustion chamber during sour gas incineration..... 77
- Figure 5.5.** Kinetic predictions of concentrations of radicals that aid in the formation of benzene for 14:1 air to fuel ratio, inlet flow rate of $3.28 \times 10^5 \text{ cm}^3/\text{s}$ and a temperature range of 800 K to 1800 K inside the combustion chamber during sour gas incineration..... 79
- Figure 5.6.** Kinetic predictions of concentrations of lower weight aromatic products for 14:1 air to fuel ratio, inlet flow rate of $3.28 \times 10^5 \text{ cm}^3/\text{s}$, and a temperature of 800 K to 1800 K inside the combustion chamber during sour gas incineration..... 80
- Figure 5.7.** Kinetic predictions of concentrations of poly-aromatic hydrocarbon products for 14:1 air to fuel ratio, inlet flow rate of $3.28 \times 10^5 \text{ cm}^3/\text{s}$, and a temperature range of 800 K to 1800 K inside the combustion chamber during sour gas incineration..... 80
- Figure 5.8.** Kinetic predictions of concentrations of poly-aromatic hydrocarbon products for 14:1 air to fuel ratio, inlet flow rate of $3.28 \times 10^5 \text{ cm}^3/\text{s}$, and a temperature range of 800 K to 1800 K inside the combustion chamber during sour gas incineration..... 81
- Figure 5.9.** Temperature profiles as a function of distance (cm) up the stack used in incineration stack calculations..... 94
- Figure 5.10.** Kinetic predictions of concentrations of lower weight hydrocarbon products for 14:1 air to fuel ratio, 1000 K temperature profile, and an inlet flow rate of $3.28 \times 10^5 \text{ cm}^3/\text{s}$ inside the incinerator stack during sour gas incineration..... 95
- Figure 5.11.** Kinetic predictions of concentrations of oxidation products for 14:1 air to fuel ratio, 1000 K temperature profile, and an inlet flow rate of $3.28 \times 10^5 \text{ cm}^3/\text{s}$ inside the incinerator stack during sour gas incineration..... 97

- Figure 5.12.** Kinetic predictions of concentrations of lower weight hydrocarbon products for 14:1 air to fuel ratio, 1400 K temperature profile, and an inlet flow rate of $3.28 \times 10^5 \text{ cm}^3/\text{s}$ inside the incinerator stack during sour gas incineration..... 100
- Figure 5.13.** Kinetic predictions of concentrations of sulphur dioxide for 14:1 air to fuel ratio, 1000 K temperature profile, and varying inlet flow rates inside the incinerator stack during sour gas incineration. (a). Inlet flow rate $=3.28 \times 10^5 \text{ cm}^3/\text{s}$, (b). Inlet flow rate $=9.83 \times 10^5 \text{ cm}^3/\text{s}$ (c). Inlet flow rate $=1.64 \times 10^6 \text{ cm}^3/\text{s}$ 104
- Figure 5.14.** Kinetic predictions of concentrations of sulphur-containing species for 14:1 air to fuel ratio, 1000 K temperature profile, and an inlet flow rate of $3.28 \times 10^5 \text{ cm}^3/\text{s}$ inside the incinerator stack during sour gas incineration..... 105
- Figure 5.15.** Kinetic predictions of concentrations of sulphur dioxide for 14:1 air to fuel ratio, 1623 K temperature profile, and varying inlet flow rates inside the incinerator stack during sour gas incineration. (a). Inlet flow rate $=3.28 \times 10^5 \text{ cm}^3/\text{s}$, (b). Inlet flow rate $=9.83 \times 10^5 \text{ cm}^3/\text{s}$ (c). Inlet flow rate $=1.64 \times 10^6 \text{ cm}^3/\text{s}$ 106
- Figure 5.16.** Kinetic predictions of concentrations of sulphur-containing species for 14:1 air to fuel ratio, 1623 K temperature profile, and an inlet flow rate of $3.28 \times 10^5 \text{ cm}^3/\text{s}$ inside the incinerator stack during sour gas incineration..... 107
- Figure 5.17.** Kinetic predictions of concentrations of single ring aromatic species for 14:1 air to fuel ratio, 1000 K temperature profile, and varying inlet flow rates inside the incinerator stack during sour gas incineration. (a). Inlet flow rate $=3.28 \times 10^5 \text{ cm}^3/\text{s}$, (b). Inlet flow rate $=9.83 \times 10^5 \text{ cm}^3/\text{s}$ (c). Inlet flow rate $=1.64 \times 10^6 \text{ cm}^3/\text{s}$ 109
- Figure 5.18.** Kinetic predictions of concentrations of poly-aromatic hydrocarbon species for 14:1 air to fuel ratio, 1000 K temperature profile, and varying inlet flow rates inside the incinerator stack during sour gas incineration. (a). Inlet flow rate $=3.28 \times 10^5 \text{ cm}^3/\text{s}$, (b). Inlet flow rate $=9.83 \times 10^5 \text{ cm}^3/\text{s}$ (c). Inlet flow rate $=1.64 \times 10^6 \text{ cm}^3/\text{s}$ 113
- Figure 5.19.** Kinetic predictions of concentrations of single ring aromatic species for 14:1 air to fuel ratio, 1400 K temperature profile, and varying inlet flow rates inside the incinerator stack during sour gas incineration. (a). Inlet flow rate $=3.28 \times 10^5 \text{ cm}^3/\text{s}$, (b). Inlet flow rate $=9.83 \times 10^5 \text{ cm}^3/\text{s}$ (c). Inlet flow rate $=1.64 \times 10^6 \text{ cm}^3/\text{s}$ 122
- Figure 5.20.** Kinetic predictions of concentrations of poly-aromatic species for 14:1 air to fuel ratio, 1623 K temperature profile, and varying inlet flow rates inside the incinerator stack during sour gas incineration. (a). Inlet flow rate $=3.28 \times 10^5 \text{ cm}^3/\text{s}$, (b). Inlet flow rate $=9.83 \times 10^5 \text{ cm}^3/\text{s}$ (c). Inlet flow rate $=1.64 \times 10^6 \text{ cm}^3/\text{s}$ 133

- Figure 6.1.** Comparison for oxidation product trends of excess oxygen equilibrium conditions and combustion chamber kinetic conditions of 14:1 air to fuel ratio and a flow rate of $3.28 \times 10^5 \text{ cm}^3/\text{s}$ 193
- Figure 6.2.** Comparison for sulphur-containing species product trends of excess oxygen equilibrium conditions and combustion chamber kinetic conditions of 14:1 air to fuel ratio and a flow rate of $3.28 \times 10^5 \text{ cm}^3/\text{s}$ 193

List of Symbols

m, n	reaction coefficients
η_C	carbon conversion efficiency (%)
η_S	sulphur conversion efficiency (%)
V	exit velocity (m/sec)
U	wind speed (m/sec)
M	molecule
C_p	heat capacity (J/K mol)
R	universal gas constant (8.314 J/mol K) (p. 33)
$a_1, a_2, a_3, a_4, a_5, a_6, a_7$	polynomial coefficients
T	temperature (K)
H^0	enthalpy (J/mol)
S^0	entropy (J/K mol)
G	Gibb's free energy of a system (J/mol)
\bar{g}_k	partial molal Gibb's function
N_k	number of moles of each reacting species k
K	total number of species
$g_k(T,P)$	Gibb's function for the pure species k , at system temperature and pressure
X_k	mole fraction of the k^{th} species
n_{jk}	number of j^{th} atoms in the k^{th} molecule
p_j	total population in moles of j^{th} atom in the system
E_a	activation energy (kJ/mol)

A	collision factor (p. 37)
Q_{in}	incoming flow rate (cm^3/s)
Q_{out}	outgoing flow rate (cm^3/s)
dV	reactor volume (cm^3)
dL	reactor length (cm)
ρ	mass density (g/m^3)
u	axial velocity of gas (m/s)
W_k	molecular weight of species k (g/mol)
A	cross-sectional flow area (m^2) (p. 37)
h_k	specific enthalpy of species k (J/mol)
$\overline{C_p}$	mean heat capacity per unit mass of gas (J/K mol)
Q_e	heat flux (W/m^2)
P	absolute pressure (atm)
F	drag force (N)
R	radius of the combustion chamber (m) (p. 41)
D	species diffusivity (m^2/s)
α_{td}	thermal diffusivity coefficient (m^2/s)
L	combustion chamber length (m) (p. 41)
Pe	Peclet number
L	stack length (cm) (p. 44)

List of Appendices

Appendix 1. Chemkin Input File.....	215
Appendix 2.1 Equilibrium Input File for Excess Oxygen Combustion.....	216
Appendix 2.2. Equilibrium Input File for 20% Decreasing Oxygen Combustion.....	217
Appendix 2.3. Equilibrium Input File for Pyrolysis.....	218
Appendix 2.4. Equilibrium Input File for Stoichiometric Air Combustion.....	219
Appendix 3.1. Plug Input File for Combustion Chamber Calculations under the Conditions of a 14:1 Air to Fuel Ratio and Flow Rate of $3.28 \times 10^5 \text{ cm}^3/\text{s}$	220
Appendix 3.2. Plug Input File for Incinerator Stack Calculations under the Conditions of a 1623 K Temperature Profile, Flow Rate of $1.64 \times 10^6 \text{ cm}^3/\text{s}$, and a 14:1 air to fuel ratio.....	221

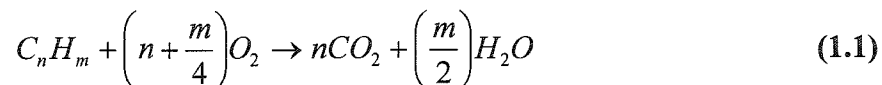
Chapter 1. Introduction

The gas flare process is the most common process used in the petroleum industry to dispose of waste gas generated in oil and gas operations, particularly during well testing. A typical gas flare is a high-temperature oxidation process used to burn waste combustible fuel with an open-flame at the top of a stack. Incineration is suggested as a better alternative to gas flaring. However, there have been no published studies completed to assess the emissions associated with waste gas incineration or a comparison to flaring. Thus, this study attempts to determine these emissions and make a qualitative comparison to flaring.

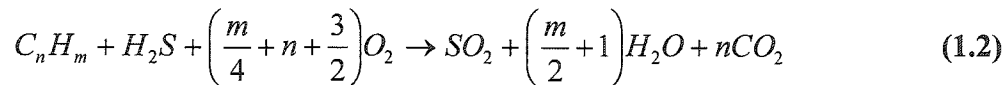
1.1. Gas Flare Process

The purpose of gas flaring is to dispose of any flammable waste gases and vapors from oil and gas operations in a safe, reliable, and efficient manner. The gases and vapors are converted, through high-temperature oxidation, to a more desirable emission than simply venting the gases into the atmosphere.

Under ideal conditions of perfect mixing between the gas and oxygen, sufficient residence time for a reaction to occur, and optimum temperature, complete combustion of hydrocarbons proceed through the following reaction:



If the hydrocarbon stream contains contaminants such as sulphur, the reaction is:

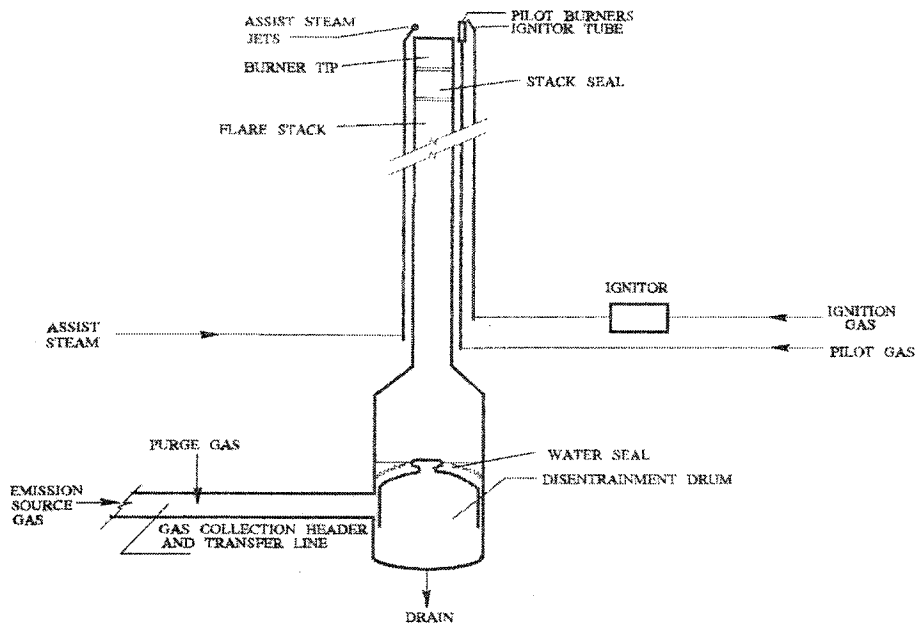


where m and n are reaction coefficients. However, complete gas combustion rarely ever takes place. Rather due to insufficient mixing, temperature and residence time, incomplete combustion and pyrolysis occurs. This results in products such as poly-aromatic hydrocarbons, olefins, soot, nitrous oxides, and sulphur compounds (Stroscher, 2000).

Figure 1.1 details a typical gas flare. Source gas from the collection units is directed to the liquid knockout drum where any condensable and entrained liquids are removed. The source gas is then forced through a water seal and directed to the top of the stack to an ignitor. The source gas is mixed with air, combusted, and the products are released into the atmosphere (Stone *et al*, 1995).

Gas flaring is used for emergency use during operational upsets, during production and processing, and for analysis in production characteristics (U.S. Department of Energy, 2000). Emergency flaring occurs at larger facilities such as gas plants and refineries where large amounts of gas may be flared off in very short periods of time if an emergency occurs (Johnson *et al*, 2001). Process flaring occurs at refineries, petrochemical plants, and sour gas plants, when gases leak past relief valves and are generally flared off at continuous low flow rates (Johnson *et al*, 2001). Production flaring refers to all types of flaring that take place during exploration and production in oil and gas fields, beginning with well development (Johnson *et al*, 2001). In well testing, a slip-stream of the gas from the reservoir is tested for properties and the bulk of the gas is flared, as there is no infrastructure for gas recovery.

Figure 1.1. Typical Gas Flare Stack (United States Environmental Protection Agency, 1983).



The disadvantage to flaring is the inability to control oxygen levels, which results in lower combustion efficiencies and incomplete combustion. This is why incineration is suggested as a better choice.

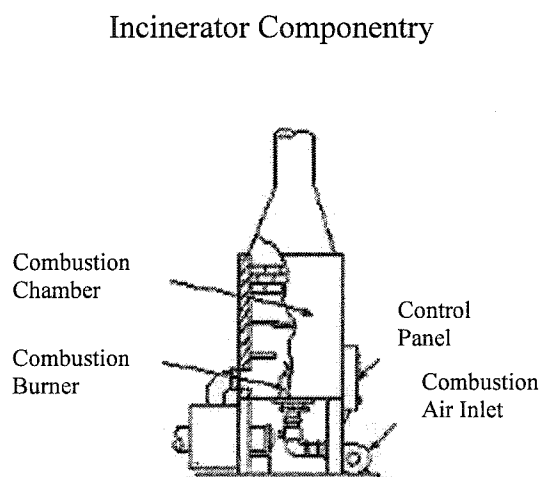
1.2. Incineration Process

Waste gas incineration has been used in the petroleum industry as an alternative to gas flaring. Typically, more than 90% of original waste gas is combusted during incineration (U.S. Department of Energy, 2000). The purpose is to convert the gas to carbon dioxide and water, which is less hazardous to human health and the environment.

In the oil and gas industry, incineration is used to manage the disposal of waste hydrocarbon products from production processes, for emergency use during operational upsets, and for analysis in production characteristics (U.S. Department of Energy, 2000). They are used in gas plants, refineries, pipelines, compressor stations, and during well-test development. Well-test incinerators are designed to efficiently incinerate waste gas containing hydrocarbons, hydrogen sulphide, and water vapor. Its features include over 99% combustion efficiency, no visible flame, no black smoke, and a stable pilot system (Delta Combustion Solutions, 2003).

Figure 1.2 details a typical waste gas incinerator. The four key components are (i) combustion air inlet, (ii) combustion burners, (iii) combustion chamber, and (iv) a stack (Motyka *et al*, 2002).

Figure 1.2. Typical Waste Gas Incinerator (modified from Meridian Engineering and Technology, 1997).



The combustion air inlet provides sufficient oxygen to the combustion chamber to complete the burning of all combustibles in the incinerator. It controls the flow rates and

provides excess air that is used to cool and quench the high flame temperatures back down to the acceptable operating temperature (Motyka *et al*, 2002). The combustion burners are able to control and maintain the release of gases into the combustion chamber and promote the proper air mixing with the gases prior to ignition (Motyka *et al*, 2002). The fuel gas enters the combustion chamber through specially configured and sized nozzles, which helps a vigorous vortex to be developed. This results in a thorough mixing of the hydrocarbon fuel and oxygen, maximizing combustion. As well, the combustion chamber provides sufficient residence time for combustion. Residence time depends on the composition of the gas and length of the hydrocarbon chain (*i.e.* molecular weight). For example, the residence time required for theoretical complete combustion is at least 0.23 seconds for lighter hydrocarbons, and can be up to 0.5 seconds for heavier hydrocarbons (Delta Combustion Solutions, 2003). The height of the incinerator stack is designed based on the residence time in the stack and emission dispersion. At the appropriate stack height, emissions would disperse in a manner that minimize or eliminate environmental hazard (Motyka *et al*, 2002). This is particularly important when sour gas is being disposed of.

The primary difference between a waste gas incinerator and a flare stack is that a flare stack results in uncontrolled combustion of gases at the flare tip, whereas incineration takes place in an enclosed combustion chamber. As a result, the energy is released and the light from the combustion process is visible when using a flare stack. As well, flame speed, flame temperature, and air mixing affect the process of combustion during flaring. These are difficult to control and therefore complete combustion cannot be

guaranteed with acceptable ranges under all conditions with a flare (Delta Combustion Solutions, 2003).

1.3. Environmental Effects

Emissions from flaring result in an atmospheric, terrestrial, and aquatic toxicity impact. This impact is generally described in terms of the flame's combustion efficiency and emissions.

Flame efficiency is the effectiveness of a combustion process in fully oxidizing the fuel into its primary combustion products. These products include carbon dioxide, water, and sulphur dioxide (if hydrogen sulphide is present). Two different efficiencies are important in terms of flame combustion. The first is carbon conversion efficiency:

$$\eta_c = \frac{\text{Mass Rate of Carbon in the Form of CO}_2 \text{ Produced by the Flame}}{\text{Mass Rate of Carbon in Form of Hydrocarbon Fuel Entering the Flame}} \quad (1.3)$$

This measures the flame's ability to fully convert all hydrocarbons to CO₂. The second sulphur conversion efficiency:

$$\eta_s = \frac{\text{Mass Rate of Sulphur in the Form of SO}_2 \text{ Produced by the Flame}}{\text{Mass Rate of Sulphur in Form of Sulphur Based Fuel Entering the Flame}} \quad (1.4)$$

This measures the flame's ability to convert H₂S to SO₂ (Stroscher, 2000).

When inefficiencies occur, unburned fuel, carbon monoxide, volatile organic compounds, poly-aromatic hydrocarbons, soot, and sulphur compounds are emitted into the atmosphere. These compounds enhance the formation of smog, acid rain, ozone, and carcinogens (U.S. Department of Energy, 2000). If the gas stream that is being burned

contains CH₄, the unburned fuel represents an increase in greenhouse gas emissions, since the global warming potential is 21 times greater than that of CO₂ (U.S. Department of Energy, 2000). If the gas stream being burned contains H₂S, the unburned fuel that is emitted is considered to be toxic. As well, any products emitted from incomplete combustion cause a potential health risk to all animals and humans. This may occur through exposure routes such as inhalation, dermal, and ingestion, where inhalation is the predominant one. Thus, the critical issue is to quantify this potential risk and to determine methods to minimize or eliminate it.

1.4. Study Objectives

Previous studies completed by the Alberta Research Council indicate that a variety of complex chemical species are produced and emitted through the gas flaring process (Stroscher, 1996). As a result, there is increasing pressure to minimize or eliminate flaring, particularly in sour gas well testing operations. As previously mentioned, incineration is suggested as an alternative to gas flaring. However, there is no scientific evidence to conclude that emissions from incineration procedures are an improvement in comparison to flaring. Thus, this study focuses on the prediction of emissions from waste gas incineration and the comparison with experimental flare emission data.

The objective of this study is to simulate the combustion of gas in an incinerator in well testing operations. The model is used to predict unburned constituents, products of combustion, and factors / procedures that contribute to complete and incomplete combustion in oil wells. In particular, sour gas has been studied.

Combustion mechanisms for sour waste gas incineration have been developed through detailed literature reviews. The necessary thermodynamic and kinetic data have been collected for these mechanisms in order to perform the proper equilibrium and kinetic simulations. Equilibrium simulations are carried out on the gas streams to determine hydrocarbon concentrations where kinetic data is not available. The incinerator is modeled as a plug flow reactor and simulations are performed on sour gas streams. The simulations determine output temperatures and species mole fractions inside the incinerator combustion chamber and during the cooling process as species exit at the top of the stack.

Chapter 2. Literature Review

Studies on combustion of waste gas have been divided into two categories, (1) overall flaring and incineration studies, and (2) individual kinetic studies. The overall flaring and incineration studies have been subcategorized into studies of the gas flare process and studies of the waste gas incineration process. This section focuses on the general processes and factors that have an effect on the flame's efficiency. The kinetic studies section focuses on modeling studies of detailed chemical reactions.

2.1. Gas Flare Studies

Emissions from flaring operations are complex and their composition is influenced by the composition of feed gas, flare design, and operating conditions (Stroscher, 1996).

Studies have shown that gas streams with low heating values do not have the ability to maintain a stable flame, therefore resulting in a reduction of the overall combustion flame efficiency (McCrillis, 1988). As well, gas streams containing varying amounts of liquid hydrocarbons, nitrogen, carbon dioxide, and/or sulphur compounds reduce the overall combustion efficiency, as well as produce some undesirable emissions (Pohl and Soelberg, 1985; 1986; and 1986a). It has been shown that a decrease in the level of liquid hydrocarbons can reduce undesirable emissions coming out of the flare by as much as 25 to 50% (Stroscher, 2000).

The majority of flare systems used in the upstream oil and gas industry are diffusion flames, where the fuel and the air are not premixed (Stroscher, 1996). If

sufficient amounts of fuel and oxygen are used, solely carbon dioxide, water, and heat will be produced. When insufficient oxygen is supplied to the mixture, the flame often becomes smoky as a result of incomplete combustion (Stroscher, 1996). Studies completed by the Alberta Research Council conclude that diffusion flames are extremely difficult to operate with exactly the correct proportions of fuel and oxygen to give complete combustion. In addition, it concludes that efficiencies in these flames range from 62% to 84%, which is relatively low and that they emit pyrolytic products such as poly-aromatic hydrocarbons and volatile organics (Stroscher, 2000). Table 2.1 show results taken from a sweet oil-field battery site gas flame in Alberta.

Table 2.1. Characterization of hydrocarbon emissions from a sweet oil-field battery flare containing different levels of liquid hydrocarbon in mg/m³ (Stroscher, 2000).

Chemical Components	High	Medium	Low
O ₂ (%)	20.4	20.8	20.8
N ₂ (%)	78.2	77.9	78.4
H ₂	15	20	10
CO	18	16	10
CO ₂	5050	4890	4720
Carbon	58	54	32
Hydrocarbon Gases	224	215	168
Volatile Hydrocarbons	340	320	215
Semi-volatile Hydrocarbons	235	206	170
Combustion Efficiency (%)	64	65	71

As previously mentioned, poly-aromatic hydrocarbons and volatile organic compounds are emitted into the atmosphere during incomplete combustion processes.

Studies completed by the Alberta Research Council have identified many of these species during sour oilfield battery flaring. Table 2.2 shows a summary of species and their relative concentrations from a sour gas flare with 23% hydrogen sulphide in the gas.

Table 2.2. Hydrocarbons and sulphur compounds identified in emissions and their relative concentrations in mg/m³ from a sour oilfield battery flare in Alberta (Stroscher, 1996).

Compound	Concentration (mg/m³)
Sulphur Dioxide	6910
Hydrogen Sulphide	126.0
Carbonyl Sulphide	64.00
Carbon Disulphide	482.0
Thiophene	179.2
Benzene	64.30
Methyl Benzene	20.5
Benzo(b)thiophene	156.6
Naphthalene	77.11
Biphenyl	77.99
Pyrene	83.26
Phenanthrene	34.09
Fluorene	54.21
Fluoranthene	157.35
Combustion Efficiency (%)	82.4%

Another factor that influences a flare's ability to perform properly are its operating conditions. Some of these operating conditions include wind speed, stack exit velocity, and stoichiometric mixing ratios.

Studies completed by Leahey *et al* (2001) suggest that the flame size is largely affected by wind speed, stack exit velocities, and stoichiometric mixing ratios, which in turn, affects a flame's combustion efficiency. Results from this study indicate that combustion efficiencies typically are around 70% at low wind speeds and less at higher wind speeds. A decrease in flame size occurs with increasing stoichiometric mixing ratio,

wind speed, and stack exit velocities, and a decrease in flame size causes a decrease in a flame's combustion efficiency (Leahey *et al.*, 2001). Table 2.3 give some estimated combustion efficiencies at varying stack exit velocities and wind speeds.

Table 2.3. Estimated combustion efficiencies for indicated gas flames as functions of stack exit velocity V (m/sec) and wind speed U (m/sec) (Leahey *et al.*, 2001).

U (m/sec)	Methane Flame	Hydrogen Sulphide Flame
	$V=2.5$ m/sec	
2	52.7	50.3
5	28.3	27.6
10	17.6	17.7
15	13.7	14.1
20	11.7	12.2
	$V=10$ m/sec	
2	30.4	29.6
5	21.4	21.2
10	15.3	15.6
15	12.5	13.0
20	11.0	11.5
	$V=20$ m/sec	
2	20.7	20.6
5	16.7	16.9
10	13.3	13.7
15	11.4	11.9
20	10.2	10.9

In summary, there are several factors that affect a flare's combustion efficiency. Although much is known qualitatively with respect to flaring, more research is needed in order to deal with the growing concern of its emissions.

2.2. Incineration Studies

Incineration of waste gases is not widely studied, since most incineration studies have focused on municipal waste and coal combustion. Traditionally, incinerators have been used for the destruction of waste gases from sulphur recovery plants. However, they are now being used more often in the oil and gas industry for well testing purposes, acid gas and tail gas elimination, and tank vapour recovery (Questor Incineration Technologies, 2003).

Questor Incineration Technologies performed a comparison case study between a 300 ft flare stack and an 82 ft incinerator. It concluded that the flare stack produced an on-site visible flame, smoke, and odour, whereas the incinerator produced no visible flame, no smoke, and no odour. In addition, a study completed by Shell Canada (2000) indicates that incineration of waste gases is a better alternative to flaring. It produces high combustion efficiency, no ground level detection of hydrogen sulphide or sulphur dioxide, no visible flame, and reduces the relative magnitude of greenhouse gas emissions by converting virtually all methane to carbon dioxide (Questor Incineration Technologies, 2003).

Other studies have indicated that toxic compounds such as poly-aromatic hydrocarbons (PAH) and volatile organic compounds (VOC) are produced during incineration processes (Zhang, 1998; Anders *et al*, 1986; Yasuda *et* Takahashi, 1998). Table 2.4 gives concentrations of some compounds that were detected in a solid-waste incinerator stack during start-up conditions.

Table 2.4. Concentrations of compounds detected in a solid-waste incinerator stack during start-up conditions (Anders *et al*, 1986).

Compound	Concentration ($\mu\text{g}/\text{m}^3$)
Naphthalene	114.0
Methylnaphthalene	40.0
Biphenyl	2.3
Fluorene	12.0
Phenanthrene	43.0
Anthracene	3.7

Chagger and co-workers (1997) studied the nature of hydrocarbon emissions formed from a propane flame during waste gas incineration at a series of temperatures (773 K to 1923 K) and residence times using a composition of 0.70 propane and 0.30 air. They also studied the emissions of the flame species subjected to a cooling process. Results indicated suggest that the majority of the PAH and VOC are formed from hydrocarbon radicals in the flame and that their concentrations change during start-up, burning, and burnout of the flame. PAH levels are high during start-up inside the combustion chamber because incomplete combustion occurs at relatively low temperatures. As well, this study indicates PAH exist in the stack because of post-combustion gas temperature and residence time in the stack (Chagger *et al*, 1997).

There are no studies published on incineration as an alternative to flaring. This is why it is important to focus on the kinetic studies of oxidation and pyrolysis of these waste gases, from an incineration point of view.

2.3. Kinetic Studies

Previous kinetic studies on the oxidation and pyrolysis of sour gas are limited. Researchers suggest that since its composition primarily consists of methane, ethane, propane, butane, and hydrogen sulphide, the combustion is similar to that of hydrocarbons, with the addition of hydrogen sulphide reactions. Thus, this section focuses on the high temperature oxidation and pyrolysis reactions of hydrocarbons and hydrogen sulphide contained in sour gas.

2.3.1. Hydrocarbon Oxidation and Pyrolysis Reactions

2.3.1.1. Methane Reactions

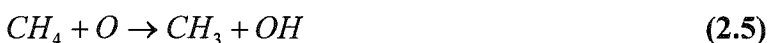
More modeling work have been devoted to methane oxidation than to all other hydrocarbon fuels combined (Westbrook and Dryer, 1984). Methane has often been used in mechanistic studies because of its apparent simplicity. Westbrook and co-workers (1984) indicate that during oxidation and pyrolysis, initial methane molecules undergo fast initiations reactions, which break down molecules into simplified species. The simplified species tend to go through a step of hydrogen abstraction to produce hydrocarbon radicals. Once these radicals have formed, they undergo radical recombination reactions to produce relatively stable larger hydrocarbons. These hydrocarbons include ethane, ethylene, and acetylene (Westbrook *et al*, 1977; Warnatz, 1981, Olsen *et al*, 1977). Figure 2.1 gives this reaction scheme for methane combustion.

Figure 2.1. Reactions involving methane in hydrocarbon fuel combustion (Westbrook et al, 1984).

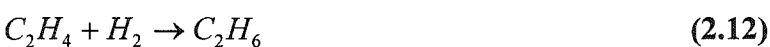
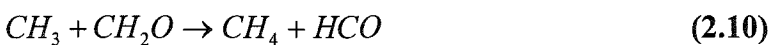
Initiation Steps



Hydrogen Abstraction Steps



Radical Recombination Steps



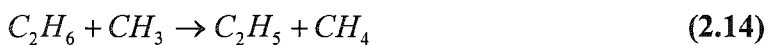
2.3.1.2. Ethane Reactions

Studies have shown that the ethane combustion reaction scheme is similar to that of methane (Westbrook et al, 1984; Olsen *et al*, 1977). It undergoes fast initiation

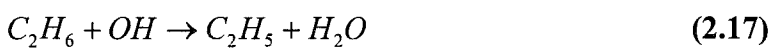
reactions, followed by hydrogen abstraction, and finally radical recombination to produce relative stable, larger hydrocarbons. Reaction scheme for ethane is shown in Figure 2.2.

Figure 2.2. Reactions involving ethane in hydrocarbon fuel combustion (Westbrook et al, 1984).

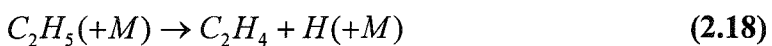
Initiation Steps



Hydrogen Abstraction Steps



Radical Recombination Steps



2.3.1.3. Propane Reactions

As already seen, the construction of a detailed reaction mechanism is a sequential process that begins with the simplest species (i.e.: methane) and building up to include larger and more complex species, such as propane and butane. A propane reaction scheme in this combustion process is similar to that of methane and ethane, but is a little more complex. Propane molecules undergo fast initiation reactions, followed by hydrogen abstraction to produce radical isomers. These radical isomers undergo thermal decomposition reactions to produce more stable molecules such as propene. These molecules can undergo initiation steps, hydrogen abstraction, and radical recombination to produce stable hydrocarbons (Westbrook et al, 1984; Olsen *et al*, 1977). Reactions involving propane are shown in Figure 2.3. Note that iC_3H_7 and nC_3H_7 are isomer propyl radicals.

2.3.1.4. Butane Reactions

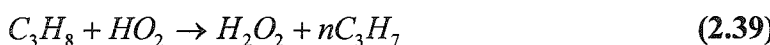
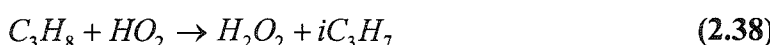
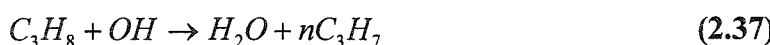
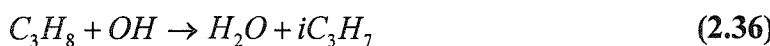
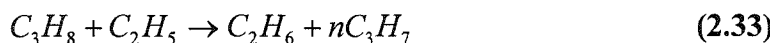
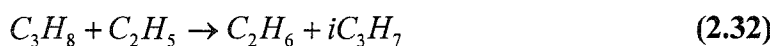
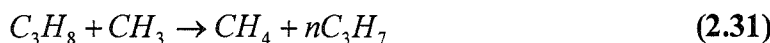
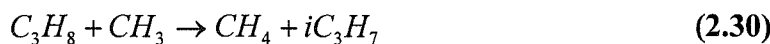
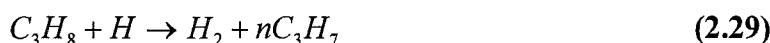
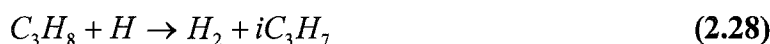
The level of complexity of butane combustion reactions is comparable to that of propane. Butane molecules undergo fast initiation reactions, followed by hydrogen abstraction to produce butyl radical isomers. These radical isomers undergo thermal decomposition reactions to produce more stable molecules such as butene. These molecules can undergo hydrogen abstraction and radical recombination to produce stable hydrocarbons (Westbrook et al, 1984; Olsen *et al*, 1977). Reactions involving butane are shown in Figure 2.4. Note that pC_4H_9 and sC_4H_9 are isomer butyl radicals.

Figure 2.3. Reactions involving propane in hydrocarbon fuel combustion (Westbrook et al, 1984).

Initiation Steps for Propane



Hydrogen Abstraction Steps for Propane



(Figure 2.3 continued)

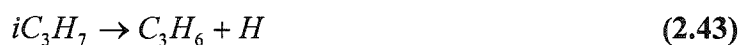
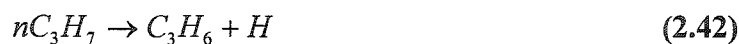
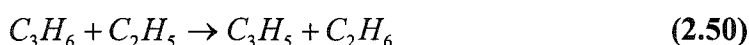
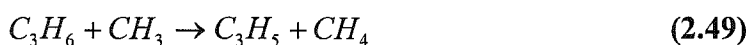
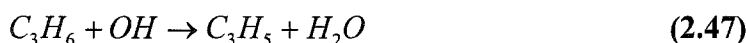
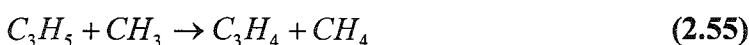
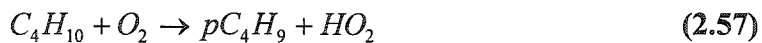
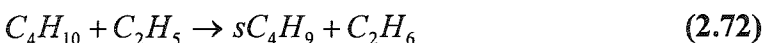
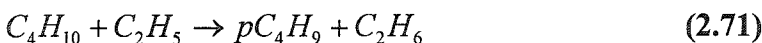
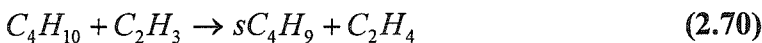
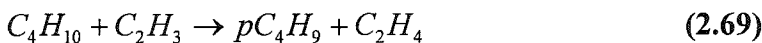
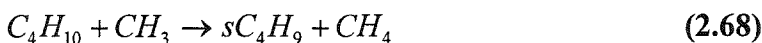
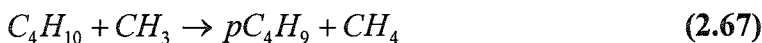
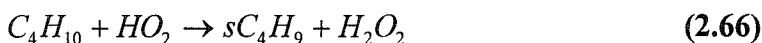
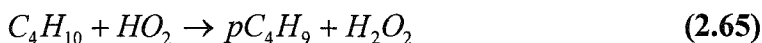
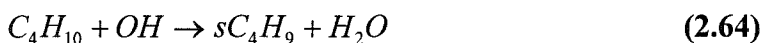
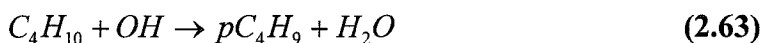
Thermal Decomposition Reactions for Propyl Radicals**Initiation Steps of Propene****Hydrogen Abstraction Steps of Propene****Radical Recombination Steps**

Figure 2.4. Reactions involving butane in hydrocarbon fuel combustion (Westbrook et al, 1984).

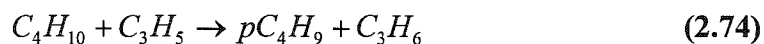
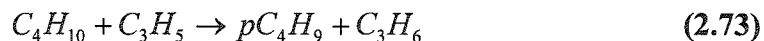
Initiation Steps for Butane



Hydrogen Abstraction Steps for Butane



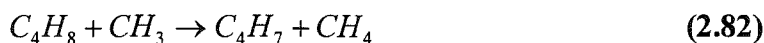
(Figure 2.4 continued)



Thermal Decomposition Reactions for Butyl Radicals



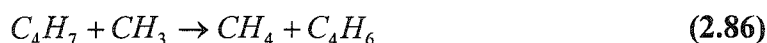
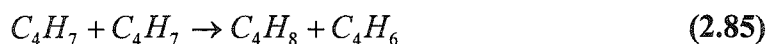
Hydrogen Abstraction Steps for Butene



Thermal Decomposition Reactions for Butenyl Radicals



Radical Recombination Steps



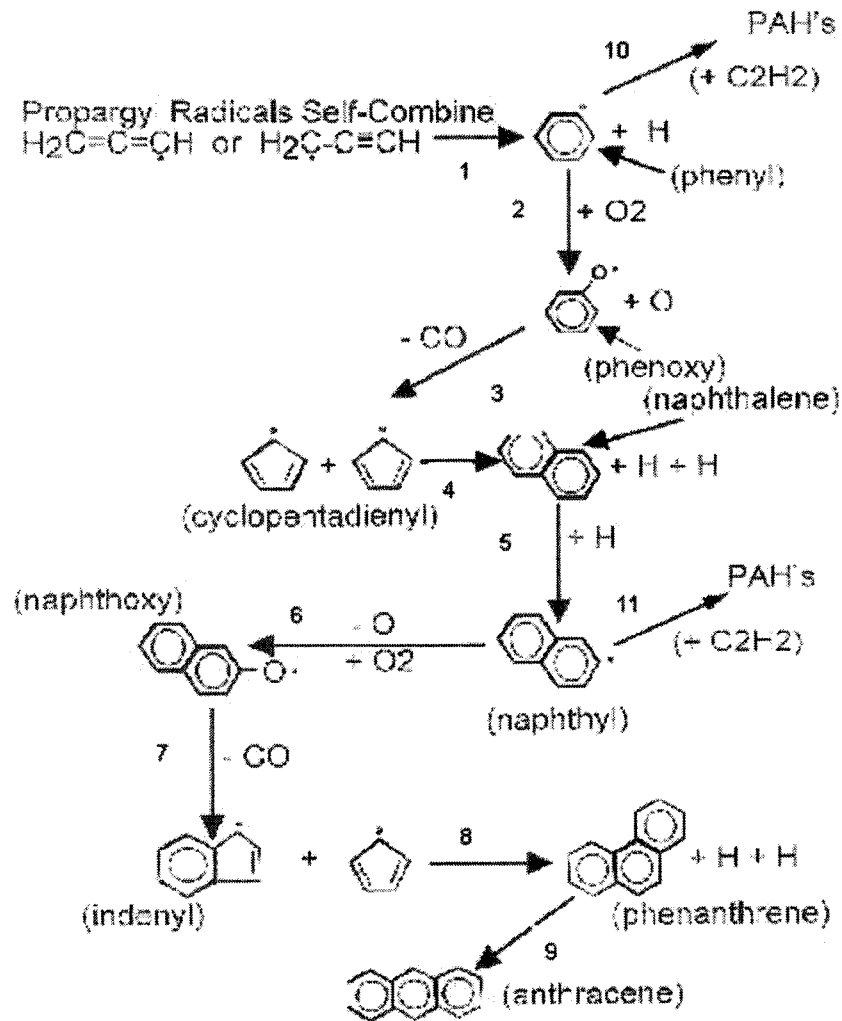
2.3.1.5. Aromatic Hydrocarbon Reactions

As previously mentioned, reactions involving hydrocarbons during combustion go through a series of elementary steps involving recombination reactions of radicals to form relatively stable hydrocarbons. Marinov and co-workers (1996) modeled premixed methane and ethane flames at atmospheric pressure and at an equivalence ratio of 2.5 and indicated that the relatively stable hydrocarbons are the precursors to aromatic formation pathways. They are proposed to react with carbon-3 radicals in recombination reactions, which are then followed by multiple isomerizations involving hydrogen atom shifts. Several concerted cyclization steps follow leading to the phenyl radical and H-atom. A reaction is thought to take place between the phenyl radical and H-atom, which in turn, leads to benzene formation (Marinov *et al*, 1996).

Frenklach and co-workers (1985 and 1987) have suggested that PAH growth in hydrocarbon pyrolysis and oxidation begins after the formation of the first aromatic ring (Frenklach *et al*, 1985; 1987). A detailed schematic diagram and explanation for this mechanism is given in Figure 2.5.

As shown in Figure 2.5, the first aromatic ring is activated by hydrogen abstraction followed by acetylene addition. Experiments show that cyclization occurs and forms the next highest order ring, and so on. The sequence goes as benzene (1 fused ring) to naphthalene (2 fused rings) to phenanthrene (3 fused rings) to pyrene (4 fused rings) to higher order aromatics (Marinov *et al*, 1996). This trend is represented by experimental evidence in Figure 2.6.

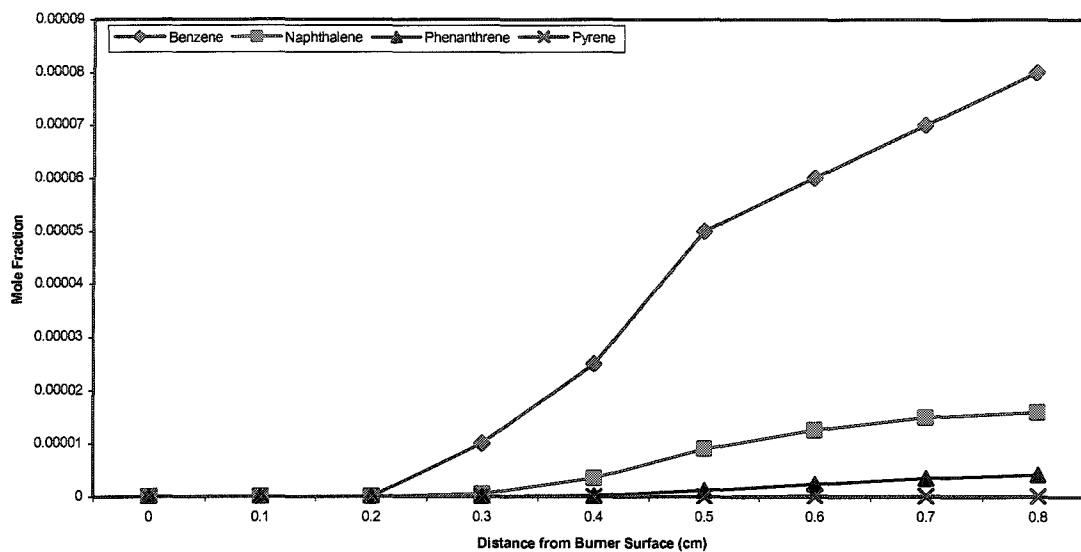
Figure 2.5. Reaction scheme for the formation of poly-aromatic hydrocarbons in combustion flames (<http://combustion-net.com>, 2003).



When an oxygen molecule and the phenyl radical combine, the result is a cyclopentadienyl radical and a CO-anion. Following is the formation of naphthalene by two cyclopentadienyl radicals combining (Pathways # 1-4). Naphthalene then loses a hydrogen atom to form a naphthyl radical (Pathway # 5). The indenyl radical forms by successive combinations with oxygen (Pathways # 6,7). The indenyl radical then reacts with a cyclopentadiene radical to produce phenanthrene, which isomerizes into anthracene (Pathways # 8, 9).

An indenyl radical has the ability to self-combine, or combine with other structures having cyclopentadienyl moiety to form still larger polycyclic aromatic hydrocarbons. As well, the reaction between acetylene and a benzyl radical (from toluene) can produce an indenyl radical. The other cyclopentadienyl radicals must still successfully compete with oxygen in order to form anthracene, despite the fact that this process is independent of oxygen, (<http://combustion-net.com>, 2003).

Figure 2.6. Experimental aromatic concentration profiles during methane flame combustion (Marinov *et al*, 1996).



From the above figure, it is obvious that the formation of the first aromatic fused ring triggers the formation of the next higher order aromatic fused ring and so on. Aromatic derivatives are formed as a result of addition reactions from radical species.

2.3.2. Hydrogen Sulphide Oxidation and Pyrolysis Reactions

Several research groups have investigated the high-temperature oxidation and pyrolysis processes of sulphur containing fuels. Many carbon-sulphur species and aromatic species have been identified during the combustion of sour gas.

The University of Leeds (1998) indicate that the combustion of hydrogen sulphide in fuel decomposes in simple initiation reactions involving an S-H bond fusion. This reaction is then followed by a number of hydrogen abstraction steps where radical species are formed. Some radical species react and recombine to produce relatively stable

molecules (Figure 2.7). This group also indicated that species such as carbon sulphide, carbonyl sulphide, and carbon disulphide are formed at specific temperature profiles, but tend to react with oxygen species to produce carbon oxides and sulphur oxides (University of Leeds, 1998).

Studies completed by the Alberta Research Council (ARC) have identified these carbon-sulphur species, as well as aromatic species that have formed during the combustion of sour gas. They identified abundant amounts of sulphur dioxide and carbon disulfide, as well as thiophenes, carbonyl sulphide, and larger aromatic compounds. The most abundant aromatic compounds are benzene, naphthalene, pyrene, 1,1-biphenyl, and fluorene (Stroscher, 1996).

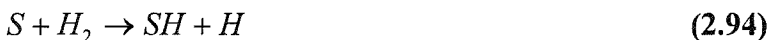
Unfortunately, the reaction pathway for larger aromatic species formation in sour gas combustion is unclear. Researchers believe that the formation of aromatic species occurs in a similar manner as they do form during hydrocarbon combustion (Woiki and Roth, 1994). It is proposed that the stable species formed during recombination reactions react with carbon-3 radicals, which is followed by a number of isomerizations and cyclization steps, and eventually resulting in the formation of benzene. The formation of larger aromatic species occurs after the formation of the first aromatic ring, as indicated in Figure 2.5.

Figure 2.7. Reactions involving hydrogen sulphide in sour gas fuel combustion (University of Leeds, 1998).

Initiation Steps

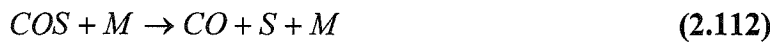
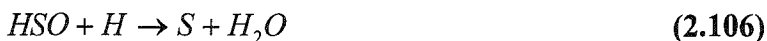
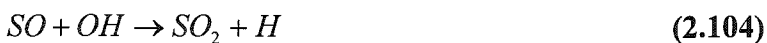


Hydrogen Abstraction Steps



(Figure 2.7 continued)

Radical Recombination Steps



2.4. Summary

The main concern with gas flaring and waste gas incineration is the release of toxic compounds into the atmosphere. Since there are only limited published data resources available on these toxic compounds, it is important to study the kinetic reaction mechanisms of combustion from which these compounds are produced. Many studies

have focused on the kinetic modeling of hydrocarbon combustion. However, much more research is needed to order to understand the behavior of chemical reactions taking place during gas flaring and waste gas incineration. This study focuses on the modeling of chemical reactions taking place inside the incinerator combustion chamber and during the cooling process as the chemical species are exiting the stack. The modeling study procedures are discussed in Chapter 3.

Chapter 3. Simulation and Modeling Study

In this study, equilibrium and kinetic simulations are carried out for incineration combustion reactions. These reactions include the oxidation and pyrolysis of sour gas. Kinetics is used to model the combustion reactions taking place inside the combustion chamber and during the cooling process. In this chapter, the detailed procedures used for the modeling simulations are discussed for both chemical equilibrium and reaction kinetics.

3.1. Equilibrium Study

3.1.1. Introduction

By definition, a system is in chemical equilibrium with its surroundings if the system's measurable properties, such as concentration, temperature and pressure, do not change with time on a macroscopic scale (Atkins, 1999). The state of chemical equilibrium in a reacting system depends on the reacting species and system conditions such as temperature and pressure. Equilibrium studies are typically performed to determine if reactions occur at a specified temperature and/or pressure and to aid in determining species composition at temperature and pressure where kinetic data is not available.

In this study, a number of equilibrium simulations are carried out at constant temperature and pressure for excess oxygen combustion, decreasing oxygen combustion, pyrolytic conditions, and stoichiometric oxygen combustion of a sour gas flame. These simulations are performed by using the Gibbs Free Energy Minimization method.

3.1.2. Equilibrium Calculations

Equilibrium simulations are performed on sour gas flame combustion reactions. These simulations are carried out at constant temperatures ranging from 300 K to 2000 K and constant pressure of 1.0 atm. Input mole fraction compositions for excess oxygen combustion, decreasing oxygen combustion, and pyrolysis are calculated based on a sour gas composition measured by the Alberta Research Council and on the air and fuel flow rates measured in the Alberta Research Council report in 1996. As well, input mole fraction compositions for stoichiometric oxygen combustion are calculated by using the same sour gas composition. See Appendices 1 and 2 for equilibrium input files. Note that for decreasing oxygen content combustion, equilibrium simulations are carried out by decreasing the oxygen content of the excess oxygen compositions by 20%. All normalised input compositions are shown in Table 3.1.

3.1.3. Thermodynamic Data

The Gibbs Free Energy Minimization method is used to calculate equilibrium compositions of reactants and products. Thermodynamic properties for each species are required, including heat capacity, enthalpy, and entropy, to calculate equilibrium concentrations.

3.1.3.1. Sources of Data

The specific formatted thermodynamic data to calculate the three gas properties outlined previously are taken from the thermodynamic database within the Chemkin collection software, thermodynamic databases from previous studies including Konnov (1997), University of Leeds (1998), Burcat (2001), Marinov *et al* (1996), and

Table 3.1. Sour gas composition and normalised input mole fraction compositions for equilibrium model.

Chemical Species	Composition in sour gas (%)	Excess O ₂	20% O ₂ Reduction	40% O ₂ Reduction	60% O ₂ Reduction	80% O ₂ Reduction	Pyrolysis O ₂	Stoichiom. O ₂
CH ₄	45.4	1.6964×10^{-3}	1.7703×10^{-3}	1.8509×10^{-3}	1.9392×10^{-3}	2.0364×10^{-3}	2.1439×10^{-3}	3.6879×10^{-2}
C ₂ H ₆	10.7	3.9980×10^{-4}	4.1722×10^{-4}	4.3623×10^{-4}	4.5704×10^{-4}	4.7995×10^{-4}	5.0527×10^{-4}	8.6918×10^{-3}
C ₃ H ₈	5.7	2.1298×10^{-4}	2.2226×10^{-4}	2.3238×10^{-4}	2.4347×10^{-4}	2.5567×10^{-4}	2.6917×10^{-4}	4.6302×10^{-3}
C ₄ H ₁₀	2.4	8.9675×10^{-5}	9.3582×10^{-5}	9.7845×10^{-5}	1.0251×10^{-4}	1.0765×10^{-4}	1.1333×10^{-4}	1.9496×10^{-3}
H ₂ S	22.8	8.5191×10^{-4}	8.8903×10^{-4}	9.2953×10^{-4}	9.7389×10^{-4}	1.0227×10^{-3}	1.0767×10^{-3}	1.8521×10^{-2}
H ₂	0.2	7.4729×10^{-6}	7.7985×10^{-6}	8.1537×10^{-6}	8.5429×10^{-6}	8.9711×10^{-6}	9.4444×10^{-6}	1.6246×10^{-4}
O ₂	0.0	2.0874×10^{-1}	1.7427×10^{-1}	1.3666×10^{-1}	9.5453×10^{-2}	5.0118×10^{-2}	0.0000×10^0	1.9292×10^{-1}
CO ₂	2.0	4.0354×10^{-4}	4.2112×10^{-4}	4.4030×10^{-4}	4.6132×10^{-4}	4.8444×10^{-4}	5.1000×10^{-4}	1.9577×10^{-3}
N ₂	8.2	7.7829×10^{-1}	8.1220×10^{-1}	8.4919×10^{-1}	8.8972×10^{-1}	9.3431×10^{-1}	9.8361×10^{-1}	7.2572×10^{-1}
Ar	0.0	9.3063×10^{-3}	9.7117×10^{-3}	1.0154×10^{-2}	1.0639×10^{-2}	1.1172×10^{-2}	1.1761×10^{-2}	8.5618×10^{-3}

Howard (2001), NIST Database (2003), and Thermodynamics Research Center Tables (1982). The previous studies contained data formatted in the form required for the Chemkin simulations. However, data in the NIST database and the Thermodynamic Research Center tables are not in the Chemkin format. This format and parameter calculation is discussed in the next section.

3.1.3.2. Data Calculations

The thermodynamic parameters, within Chemkin, are calculated using polynomial equations. The polynomial equations are shown in equations 3.1, 3.2, and 3.3 (Chemkin Collection 3.7 User Manuel, 2003).

$$\frac{C_p}{R} = a_1 + a_2T + a_3T^2 + a_4T^3 + a_5T^4 \quad (3.1)$$

$$\frac{H^0}{RT} = a_1 + \frac{a_2}{2}T + \frac{a_3}{3}T^2 + \frac{a_4}{4}T^3 + \frac{a_5}{5}T^4 + \frac{a_6}{T} \quad (3.2)$$

$$\frac{S^0}{R} = a_1 \ln T + a_2T + \frac{a_3}{2}T^2 + \frac{a_4}{3}T^3 + \frac{a_5}{4}T^4 + a_7 \quad (3.3)$$

where C_p is heat capacity in $J/K \text{ mol}$, H^0 is enthalpy in J/mol , S^0 is entropy in $J/K \text{ mol}$, T is temperature in *Kelvins*, R is the universal gas constant of $8.314 J/mol \text{ K}$, and a_1 through to a_7 are coefficients.

For each chemical species there exists seven coefficients for each of two different temperature ranges, resulting 14 coefficients in total. In addition to the polynomial coefficients for each species, the thermodynamic database provides the species name, its elemental makeup, and the temperature ranges over which the fits are valid. Generally, the common temperature connecting the two ranges is 1000 K, but this differs in some

cases (Chemkin Collection 3.7 User Manual, 2003). Figure 3.1 shows an example of the specified format for thermodynamics that is recognized by the Chemkin software.

Figure 3.1. Thermodynamic data for methane in the Chemkin format.

```

CH4      C 1H 4   G           0300.00 5000.00 1000.00  1
0.01683478E+02 0.10237236E-01 -0.03875128E-04 0.06785585E-08 -0.04503423E-12 2
-0.10080787E+05 0.09623395E+02 0.07787415E+01 0.01747668E+00 -0.02783409E-03 3
0.03049708E-06 -0.12239307E-10 -0.09825229E+05 0.13722195E+02 4

```

In the above figure, line 1 gives the species name (ie: CH₄), its elemental makeup which is 1 carbon atom and 4 hydrogen atoms, the phase (gas), and the two temperature ranges used. In this case, the two temperature ranges are 300 K to 1000 K and 1000 K to 5000 K. Line 2, 3, and 4 give the polynomial coefficients used by Chemkin to calculate equilibrium. The first seven coefficients represent the higher temperature range of 1000 K to 5000 K and the second seven coefficients represent the lower temperature range of 300 K to 1000 K.

Data for specific heat, enthalpy, and entropy as a function of temperature is needed to perform these calculations. Generally, the linear least squares fitting procedure is used. In this case, a software package called DATAFIT is used to perform the fitting procedure. The first step is to fit specific heat data, C_p/R , for both temperature ranges to a fourth order polynomial to determine a_1 through a_5 . A constraint is made on the common temperature so that the specific heat and its first derivative are equal (Chemkin Collection 3.7 User Manual, 2003). Secondly, a_6 is determined by fitting the enthalpy data, H^0/RT . In this step, a_1 through a_5 are held constant, and as in the specific heat fit, the enthalpy and its first derivative are equal at the common temperature. In the third step, a_7 is

determined by fitting the entropy data, S^0/R , and a_1 through a_5 are held constant (Collection 3.7 User Manuel, 2003).

3.1.4. Gibbs Free Energy Minimization Model

There are various ways in which chemical equilibrium compositions can be calculated for a reacting system. Chemkin uses the Gibbs Free Energy Minimization Model. The requirement that the Gibbs free energy (G) of a system at a fixed temperature and pressure be a minimum at equilibrium is applied to determine the equilibrium composition of the reacting species.

This model is based on the Gibbs free energy function of a system:

$$G = \sum_{k=1}^K \bar{g}_k N_k \quad (3.4)$$

where \bar{g}_k is the partial molal Gibbs function and N_k is the number of moles of each reacting species k in the system. K is the total number of species (Chemkin Collection 3.7 User Manuel, 2003).

For ideal gas mixtures and ideal solutions, the partial molal Gibbs functions are given by

$$\bar{g}_k = g_k(T, P) + RT \ln X_k \quad (3.5)$$

where $g_k(T, P)$ is the Gibbs function for the pure species k , evaluated at the system temperature and pressure; R is the universal gas constant in $J/mol K$; and X_k is the mole fraction of the k^{th} species (Chemkin Collection 3.7 User Manuel, 2003).

The equilibrium solution at a fixed temperature and pressure is the distribution of N_k that minimizes the system Gibbs function, G , subject to the total quantities of individual chemical elements. These constraints are represented by equation (3.6).

$$\sum_{k=1}^K n_{jk} N_k = p_j \quad \text{where } j = 1, \dots, M \quad (3.6)$$

where n_{jk} is the number of j^{th} atoms in the k^{th} molecule, p_j is the total population in moles of the j^{th} atom in the system, and M is the total number of different elements that are present in the system (Chemkin Collection 3.7 User Manual, 2003).

3.2. Kinetic Study

3.2.1. Introduction

Chemical kinetics is the primary step in understanding reaction rates, mechanisms of reactions and their analysis into a sequence of elementary steps. Kinetics largely depends on variables such as pressure, temperature, and initial concentrations (Atkins, 1999).

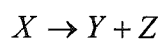
In this study, kinetic simulations are performed using chemical reaction mechanisms for the incineration of sour gas from well testing. A plug-flow reactor is used to model the incineration at high temperatures and atmospheric pressure. Simulations are performed to determine the gas composition in the combustion chamber and in the incinerator stack.

The sources of data used, kinetic calculations, and the reactor model are discussed in this section.

3.2.2. Sources of Data

A proposed chemical reaction mechanism is developed through detailed literature reviews on the incineration of sour gas. This mechanism and its data are compiled from previous sources that are discussed in Chapter 2. They include: Konnov (1997), University of Leeds (1998), Burcat (2001), Marinov *et al* (1996), and Howard (2001).

The formulation of data used in the chemical kinetic calculations deal with the variation of reaction rates with temperature. In this study, data is expressed in modified Arrhenius form. Therefore, the given irreversible reaction,



has a rate expressed as

$$Rate = AT^n e^{-\frac{E_a}{RT}} \quad (3.7)$$

where the rate depends on the temperature T in *Kelvins* and activation energy E_a , in *kJ/mole* with a pre-exponential collision factor A where units are a function of reaction (Westbrook *et al*, 1984). In many cases all of the dependence is incorporated into a single exponential term where $n=0$, since many elementary reactions portray classical Arrhenius behaviour. However, elementary reactions that occur in combustion processes portray significant non-Arrhenius behaviour over wide temperature ranges (Westbrook *et al*, 1984).

The thermodynamic data originates from the thermodynamic database as outlined in Section 3.1.2.

3.2.3. Reactor Model

3.2.3.1. Model Assumptions

In the reactor model, a series of ordinary differential equations are solved in order to determine the distribution of products. The main assumptions taken in this model are:

- (1). Plug Flow Reactor
- (2). Steady-State Condition
- (3). Ideal Gas Behaviour

The plug flow reactor model in Chemkin is designed to model non-dispersive, one-dimensional flow of a chemically reacting, ideal gas mixture. It considers a tube flow gradient (ie: plug flow) in which there is no mixing in the axial flow direction, but perfect mixing in the transverse direction (Chemkin Collection 3.7 User Manual, 2003). The requirements for a plug flow reactor are discussed in Section 3.2.3.4.

The model also assumes steady state conditions. This condition eases the complexity of the reactor model calculations because it makes an approximation that during which the reaction takes place the rate of change of concentrations of all intermediate species is negligibly small (Atkins, 1999).

Since the simulations are performed under high temperature and constant atmospheric pressure, the ideal gas behaviour assumption is acceptable.

3.2.3.2. Reactor Parameters

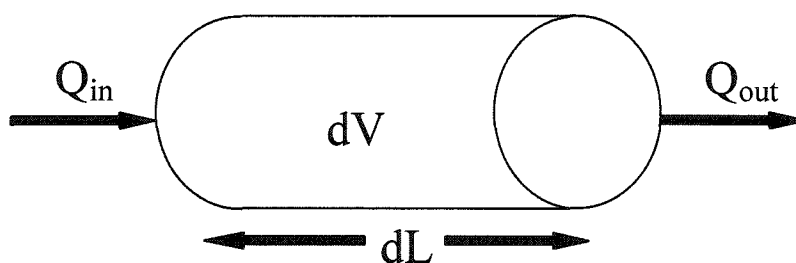
As previously mentioned, the incinerator being modeled in this study is that of Questor Technologies. The air and fuel flow rates are calculated based on fuel flow rates of $3.28 \times 10^5 \text{ cm}^3/\text{s}$, $9.83 \times 10^5 \text{ cm}^3/\text{s}$, and $1.64 \times 10^6 \text{ cm}^3/\text{s}$ at standard temperature and pressure, used by Questor Technologies. As well, three air to fuel ratios are used,

including 14:1, 17:1, and 21:1. The combustion chamber of this incinerator has dimensions of 243 cm in length and 338 cm in diameter. Mole fraction compositions inside the incinerator are calculated for a range of temperatures between 800 and 1800 K. Heat transfer modeling is required to determine a temperature profile for the incinerator stack. However, it is beyond the scope of this study. For the present study, the stack is modeled by using a linear temperature profile along the entire length of the stack with dimensions of 338 cm in diameter and 975 cm in length. This is done to avoid any unnecessary complications.

3.2.3.3. Reactor Calculations

The equations governing the behaviour of the plug flow reactor are derived from a tubular reactor. Figure 3.2 shows a typical example of a tubular flow reactor.

Figure 3.2. Tubular Flow Reactor.



where Q_{in} and Q_{out} are the incoming and outgoing flow rates in cm^3 / s , dV is the reactor volume in cm^3 , and dL is the reactor length in cm.

The model consists of equations that calculate conservation of mass, energy, and momentum for the gas flow taking place inside the tubular flow reactor.

Conservation of mass simply states that for homogenous gas reactions the total mass of the gas cannot change, but its composition can be altered. This may be calculated by the overall mass balance continuity equation.

$$\rho u \frac{dA}{dx} + \rho A \frac{du}{dx} + uA \frac{d\rho}{dx} = \sum_{k=1}^{K_g} W_k \quad (3.8)$$

where ρ is the mass density, u is the axial velocity of the gas which consists of K_g species, W_k is the molecular weight of species k , and A is the cross-sectional flow area (Chemkin Collection 3.7 User Manuel, 2003).

Conservation of energy states that the total energy of the flowing gas changes due to the heat flux from the surroundings to the outer tube wall. This is calculated by

$$\rho u A \left(\sum_{k=1}^{K_g} h_k \frac{dY_k}{dx} + \bar{C}_p \frac{dT}{dx} + u \frac{du}{dx} \right) + \left(\sum_{k=1}^{K_g} h_k Y_k + \frac{1}{2} u^2 \right) a_i \sum_{k=1}^{K_g} W_k = a_e Q_e - a_i \sum_{k=K_b'}^{K_b} W_k h_k \quad (3.9)$$

where h_k is the specific enthalpy of species k , \bar{C}_p is the mean heat capacity per unit mass of gas, T is the temperature, and Q_e is the heat flux (Chemkin Collection 3.7 User Manuel, 2003).

Conservation of momentum equation for gases includes a balance between pressure forces, inertia, and viscous drag (Chemkin Collection User Manuel, 2003).

This may be calculated by the equation:

$$A \frac{dP}{dx} + \rho u A \frac{du}{dx} + \frac{dF}{dx} = 0 \quad (3.10)$$

where P is the absolute pressure and F is the drag force exerted on the gas by the tube wall.

3.2.3.4. Model Requirements

In this study, three requirements are used in order to ensure that the reactor may be approximated in plug flow. They are taken from a paper by Cutler *et al* (1988).

(1). Constant Temperature

It is assumed that constant temperature is maintained in the radial direction of the combustion chamber. This requirement can be estimated by the following equation:

$$\frac{Ru}{D} \ll 3.7 \quad (3.11)$$

where R is the radius of the combustion chamber (m), u is the average gas velocity (m/s), and D is the species diffusivity (m^2/s) (Cutler *et al*, 1988). Calculations based on the Questor incineration results in values between 3.85 to 4.01, slightly above the limit.

(2). Negligible Variation in the Transverse Direction

Plug flow assumes that there is no mixing of flow in the axial direction, but perfect mixing in the transverse direction. This parameter is estimated by the following equation:

$$\frac{R^2u}{\alpha_{td}L} < 0.5 \quad (3.12)$$

where α_{td} is the thermal diffusivity coefficient (m^2/s), and L is the combustion chamber length (m) (Cutler *et al*, 1988). Based on the Questor incinerator, this requirement is met with values 0.035 to 0.047.

(3). Negligible Axial Diffusion

Again plug flow assumes no mixing in the axial direction of flow, thus no axial diffusion. This requirement can be estimated by the following equation:

$$\frac{1}{Pe} \ll 0.02 \quad (3.13)$$

where Pe is the Peclet number (Cutler *et al*, 1988). In this study, values for this requirement ranged from 0.012 to 0.015, thus this requirement is met.

Although the constant temperature requirement slightly exceeds the required value, the plug flow reactor model is still used for the kinetic simulations. This study's objective is to provide qualitative data on the exit gas compositions of incineration. To correct for the non-ideal flow, characteristic mixing times and temperatures within the combustion chamber and the stack are required. However, this data is not available and determination of these parameters is outside the scope of this study.

3.2.4. Kinetic Calculations

Kinetic simulations are performed on sour gas incineration. An incinerator designed by Questor Technologies is modeled in this study. See Appendices 1 and 3 for kinetic input files of the combustion chamber and incineration stack.

3.2.4.1. Combustion Chamber Model Calculations

The simulations are carried out at isothermal temperatures ranging from 800 K to 1800 K, constant pressure of 1.0 atm, air to fuel mixing ratios of 14:1, 17:1, 21:1, and three flow rates used by Questor Technologies. Input mole fraction compositions are calculated based on a sour gas composition given from Strosher (1996). Each air to fuel flow rate is calculated at internal combustion chamber temperatures ranging from 800 K to 1800 K and for each air to fuel mixing ratio accordingly. Table 3.2 gives a summary of input mole fraction compositions and flow rates used for these simulations.

Concentrations for chemical species are calculated over the entire reactor length of 244 cm.

Table 3.2. Summary of combustion chamber model parameters.

Chemical Species	% Composition	Case A: 14 Air : 1 Fuel Composition	Case B: 17 Air : 1 Fuel Composition	Case C: 21 Air : 1 Fuel Composition
CH ₄	45.4	0.03046	0.02539	0.02078
C ₂ H ₆	10.7	0.00731	0.00610	0.00499
C ₃ H ₈	5.7	0.00398	0.00332	0.00272
C ₄ H ₁₀	2.4	0.00178	0.00146	0.00122
H ₂ S	22.8	0.01538	0.01283	0.01049
H ₂	0.2	0.00031	0.00026	0.00021
O ₂	0.0	0.19570	0.19800	0.20009
CO ₂	2.0	0.00185	0.00161	0.00138
N ₂	8.2	0.73437	0.74210	0.74912
Ar	0.0	0.00886	0.00893	0.00900
Fuel Flow Rate of 3.28 x 10⁵ cm³/s				
Air/Fuel Flow Rate @ 800 K(cm ³ /s)	-	1.37 x 10 ⁷	1.64 x 10 ⁷	2.00 x 10 ⁷
Air/Fuel Flow Rate @ 1000 K(cm ³ /s)	-	1.71 x 10 ⁷	2.05 x 10 ⁷	2.50 x 10 ⁷
Air/Fuel Flow Rate @ 1200 K(cm ³ /s)	-	2.05 x 10 ⁷	2.46 x 10 ⁷	3.00 x 10 ⁷
Air/Fuel Flow Rate @ 1400 K(cm ³ /s)	-	2.39 x 10 ⁷	2.87 x 10 ⁷	3.51 x 10 ⁷
Air/Fuel Flow Rate @ 1623 K(cm ³ /s)	-	2.77 x 10 ⁷	3.32 x 10 ⁷	4.06 x 10 ⁷
Air/Fuel Flow Rate @ 1800 K(cm ³ /s)	-	3.07 x 10 ⁷	3.69 x 10 ⁷	4.51 x 10 ⁷
Fuel Flow Rate of 9.83 x 10⁵ cm³/s				
Air/Fuel Flow Rate @ 800 K(cm ³ /s)	-	4.10 x 10 ⁷	4.92 x 10 ⁷	6.01 x 10 ⁷
Air/Fuel Flow Rate @ 1000 K(cm ³ /s)	-	5.12 x 10 ⁷	6.15 x 10 ⁷	7.51 x 10 ⁷
Air/Fuel Flow Rate @ 1200 K(cm ³ /s)	-	6.15 x 10 ⁷	7.37 x 10 ⁷	9.01 x 10 ⁷
Air/Fuel Flow Rate @ 1400 K(cm ³ /s)	-	7.17 x 10 ⁷	8.60 x 10 ⁷	1.05 x 10 ⁸
Air/Fuel Flow Rate @ 1623 K(cm ³ /s)	-	8.31 x 10 ⁷	9.97 x 10 ⁷	1.22 x 10 ⁸
Air/Fuel Flow Rate @ 1800 K(cm ³ /s)	-	9.22 x 10 ⁷	1.11 x 10 ⁸	1.35 x 10 ⁸
Fuel Flow Rate of 1.64 x 10⁶ cm³/s				
Air/Fuel Flow Rate @ 800 K(cm ³ /s)	-	6.83 x 10 ⁷	8.19 x 10 ⁷	1.00 x 10 ⁸
Air/Fuel Flow Rate @ 1000 K(cm ³ /s)	-	8.53 x 10 ⁷	1.02 x 10 ⁸	1.25 x 10 ⁸
Air/Fuel Flow Rate @ 1200 K(cm ³ /s)	-	1.02 x 10 ⁸	1.23 x 10 ⁸	1.50 x 10 ⁸
Air/Fuel Flow Rate @ 1400 K(cm ³ /s)	-	1.19 x 10 ⁸	1.43 x 10 ⁸	1.75 x 10 ⁸
Air/Fuel Flow Rate @ 1623 K(cm ³ /s)	-	1.39 x 10 ⁸	1.66 x 10 ⁸	2.03 x 10 ⁸
Air/Fuel Flow Rate @ 1800 K(cm ³ /s)	-	1.54 x 10 ⁸	1.84 x 10 ⁸	2.25 x 10 ⁸

3.2.4.2. Incinerator Stack Model Calculations

The stack of the incinerator is modeled by using a linear temperature profile along the entire length of the stack with dimensions of 338 cm in diameter and 975 cm in length. The temperature is calculated using three different exit temperatures from the combustion chamber of 1623 K, 1400 K, and 1000 K. The gas temperature at the stack exit is set at 200 K below the entrance temperature. This 200 K drop is based on actual incinerator operating data from Questor Technologies and approximate heat transfer calculations. The equations for the temperature profiles are as follows

$$T = -0.20513L + 1623 \quad (3.14)$$

$$T = -0.20513L + 1400 \quad (3.15)$$

$$T = -0.20513L + 1000 \quad (3.16)$$

where T is the temperature in kelvins and L is the length of the stack ranging from 0 to 975 cm at the top of the stack. Thus, temperature inside the stack decreases toward the top as L reaches 975 cm. Table 3.3 shows the temperature profiles as a function of length of the stack.

Table 3.3. Temperature profiles at different lengths inside the stack.

T_{internal} (K)	Length = 0 cm	Length = 500 cm	Length = 975 cm
1623	T=1623 K	T=1520 K	T=1423 K
1400	T=1400 K	T=1297 K	T=1200 K
1000	T=1000 K	T=897 K	T=800 K

The simulations are also carried out at a pressure of 1.0 atm, air to fuel mixing ratios of 14:1, 17:1, and 21:1. The inlet air to fuel flow rates used for the stack simulations are the calculated flow rate values from the combustion chamber simulations at each fuel flow rate used

by Questor Technologies. The input mole fractions for these simulations are the output mole fractions that are exiting the combustion chamber at the specified temperatures, flow rate, and air to fuel mixing ratios. The purpose of this phase is to model the formation of aromatic species as they form during cooling processes.

3.3. Summary

Thermodynamics are used to calculate equilibrium and kinetic concentrations of species in reaction during combustion of sour gas. The plug flow reactor is appropriate to use for the kinetic modeling procedures. Kinetically modeling the consumption of reactants and formation of products within the combustion chamber and during the cooling process is necessary in order to get a complete understanding of the reactions and products formed.

The proceeding chapters discuss the results and analysis for these modeling simulations.

Chapter 4. Equilibrium Model Results and Analysis

The primary purpose of performing equilibrium calculations on products of sour gas combustion is to determine equilibrium compositions for those chemical species for which there is no kinetic data available. Thus, these species can be included in the analysis, although they have not been studied kinetically.

Under incineration conditions of sweet and sour gas, the temperatures of the combustion chamber can rise as high as 1800 K, while stack exit gas temperature may be as low as 800 K. As such, the equilibrium concentrations of products are computed over a temperature range of 800 – 2000 K, using a computer program (Chemkin 3.7). The Chemkin program uses the minimization of Gibbs Free Energy (refer to Section 3.1.4) to determine equilibrium concentrations. The sour gas inlet compositions used in these simulations are taken from a study completed by Strosher in 1996. In the Strosher (1996) study, several aromatic and complex sulphur compounds are formed which cannot be predicted through kinetics due to lack of published data. In this study, simulations are performed under excess oxygen conditions, decreasing oxygen conditions to pyrolysis, and stoichiometric oxygen conditions. Equilibrium predictions for complete combustion products, light hydrocarbon species, sulphur-containing compounds, and aromatic hydrocarbons under all sets of conditions are discussed in detail.

4.1. Excess Oxygen Combustion Results

4.1.1. Introduction

Input mole fraction compositions for excess oxygen conditions are shown in

Table 4.1.

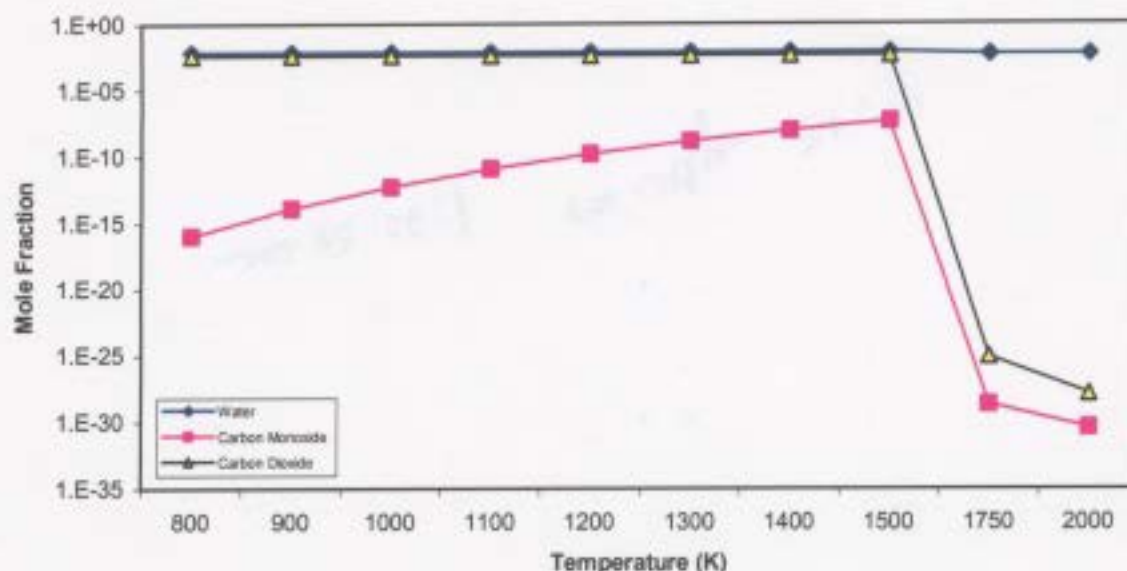
Table 4.1. Experimental input mole fraction compositions used under excess oxygen conditions.

Chemical Species	Mole Fraction
CH ₄	1.6964 x 10 ⁻³
C ₂ H ₆	3.9980 x 10 ⁻⁴
C ₃ H ₈	2.1298 x 10 ⁻⁴
C ₄ H ₁₀	8.9675 x 10 ⁻⁵
H ₂ S	8.5191 x 10 ⁻⁴
H ₂	7.4729 x 10 ⁻⁶
O ₂	2.0874 x 10 ⁻¹
CO ₂	4.0354 x 10 ⁻⁴
N ₂	7.7829 x 10 ⁻¹
Ar	9.3063 x 10 ⁻³

4.1.2. Equilibrium Predictions for Oxidation Products and Light Hydrocarbon Species

The key to 100% complete combustion where carbon dioxide, sulphur dioxide, and water are produced is to use the proper oxygen content and to have relatively stable temperature conditions (Chagger *et al*, 1997). Under excess oxygen conditions, equilibrium predicts the formation of oxidation products, but no light hydrocarbon species. Figure 4.1 indicates that relatively large concentrations are predicted for carbon dioxide, carbon monoxide, and water. Trends for sulphur dioxide are discussed in section 4.1.3.

Figure 4.1. Equilibrium predictions for oxidation products under excess oxygen conditions of sour gas combustion.



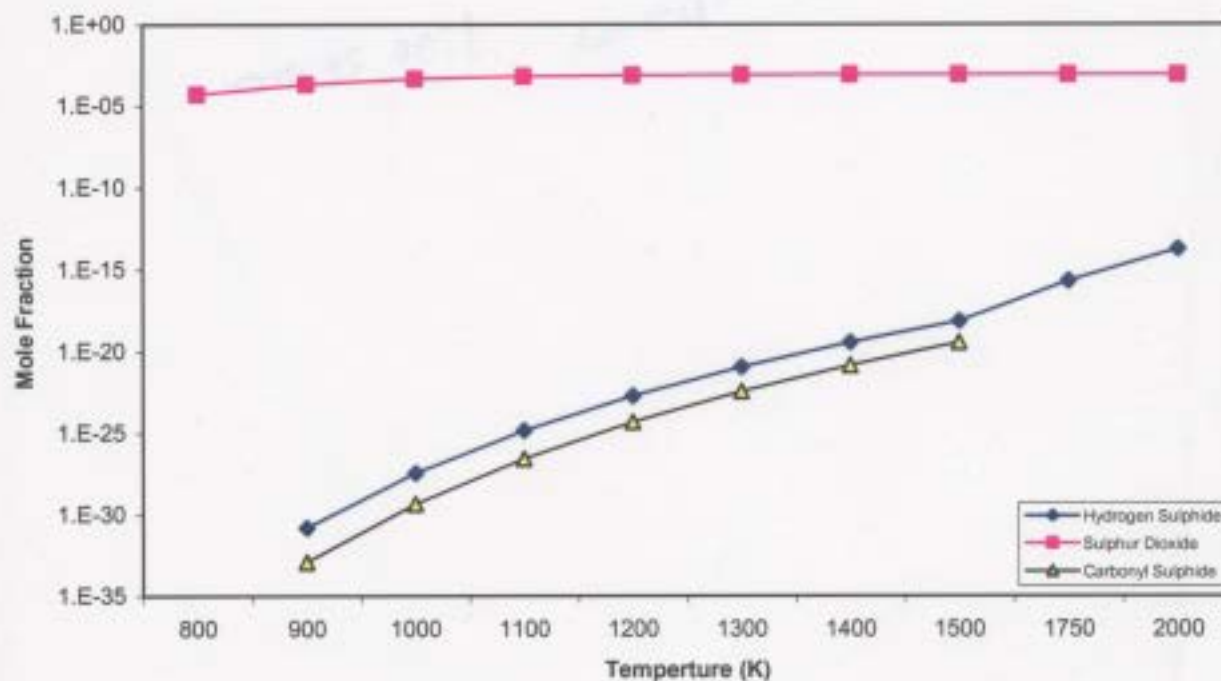
Predictions for water show relatively constant concentrations over the temperature range, but concentrations slightly decrease at 1500 K. Predictions for carbon monoxide increase until 1500 K and then decrease dramatically. As well, predictions for carbon dioxide are high and constant until 1500 K and decrease toward the higher temperatures. These results are expected to occur as a result of complete combustion conditions with the exception of a decrease in composition at 1500 K. Aromatics form above 1500 K (See section 4.1.4.).

4.1.3. Equilibrium Predictions for Sulphur-Containing Compounds

Three sulphur-containing species are produced under equilibrium conditions of excess oxygen (See Figure 4.2). Hydrogen sulphide concentrations are not predicted until 900 K and gradually increase to 2000 K. Sulphur dioxide concentrations increase to 1300 K and remain constant at higher temperatures. Finally, concentrations for carbonyl

sulphide are essentially zero until 900 K, increase to 1500 K, and do not exist after 1500 K.

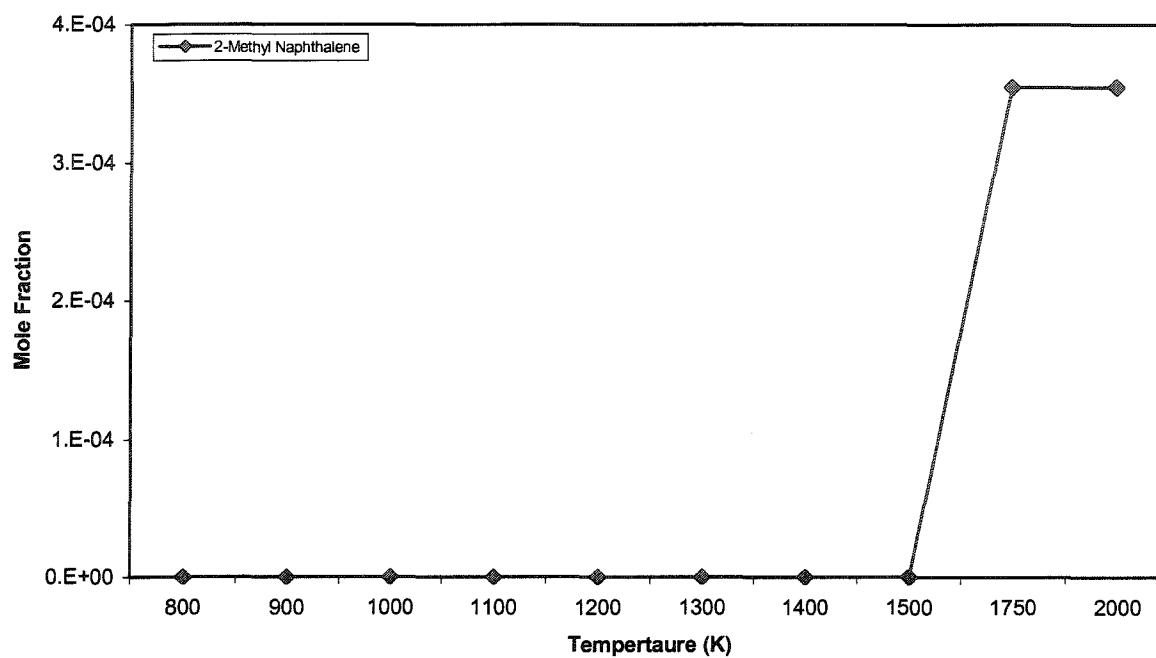
Figure 4.2. Equilibrium predictions for sulphur-containing compounds under excess oxygen conditions of sour gas combustion.



4.1.4. Equilibrium Predictions for Aromatic Species

Under equilibrium excess oxygen conditions, the only aromatic species formed is 2-methyl naphthalene. Figure 4.3 shows that concentrations are zero at the lower temperatures, an increase from 1500 K to 1750 K, and are relatively constant at higher temperatures. These results are in agreement with the fact that poly-aromatic hydrocarbon formation is strongly dependent upon reactor temperature.

Figure 4.3. Equilibrium predictions for aromatic hydrocarbon compounds under excess oxygen conditions of sour gas combustion.



4.2. Decreasing Oxygen Combustion Results

4.2.1. Introduction

In order to determine the effect of insufficient oxygen conditions, oxygen content was decreased by 20%, 40% 60%, and 80% from the previous runs. The input mole fraction compositions are shown in Table 4.2. It should be noted that all of the oxygen levels are still in excess of stoichiometric oxygen required for complete combustion.

Table 4.2. Input mole fraction compositions for the decreasing oxygen content equilibrium simulations.

Chemical Species	20%	40%	60%	80%
	Reduction	Reduction	Reduction	Reduction
CH ₄	1.770×10^{-3}	1.851×10^{-3}	1.939×10^{-3}	2.036×10^{-3}
C ₂ H ₆	4.172×10^{-4}	4.362×10^{-4}	4.570×10^{-4}	4.800×10^{-4}
C ₃ H ₈	2.223×10^{-4}	2.324×10^{-4}	2.435×10^{-4}	2.557×10^{-4}
C ₄ H ₁₀	9.358×10^{-5}	9.785×10^{-5}	1.025×10^{-4}	1.077×10^{-4}
H ₂ S	8.890×10^{-4}	9.295×10^{-4}	9.739×10^{-4}	1.023×10^{-3}
H ₂	7.799×10^{-6}	8.154×10^{-6}	8.543×10^{-6}	8.971×10^{-6}
O ₂	1.743×10^{-1}	1.367×10^{-1}	9.545×10^{-2}	5.011×10^{-2}
CO ₂	4.211×10^{-4}	4.403×10^{-4}	4.613×10^{-4}	4.844×10^{-4}
N ₂	8.122×10^{-1}	8.492×10^{-1}	8.897×10^{-1}	9.343×10^{-1}
Ar	9.712×10^{-3}	1.015×10^{-2}	1.064×10^{-2}	1.117×10^{-2}

4.2.2. Equilibrium Predictions for Oxidation Products and Light Hydrocarbon Species

The results for 20 %, 40 %, 60 %, and 80 % decrease in oxygen content are generally the same as excess oxygen results. However, relatively larger equilibrium concentrations are predicted for H₂O, CO₂, and CO as oxygen content decreases. This is due to the fact that relative concentrations of hydrocarbons in the input were increased to compensate for the decrease in O₂ content. Thus, more H₂O, CO₂, and CO are produced as a result of more hydrocarbons in the feed.

Table 4.3 gives the percent increase for each of these species between each run and overall as the O₂ content is decreased by a factor of 20 %. Carbon monoxide has the most significant increase in composition by 62.6 % overall.

Table 4.3. Percent increases in composition for oxidation products under equilibrium conditions while decreasing the oxygen content by 20 %, 40 %, 60 %, and 80 %.

Species	0-20 % O ₂ Reduction	20-40 % O ₂ Reduction	40-60 % O ₂ Reduction	60-80 % O ₂ Reduction	0-80 % O ₂ Reduction
Water	4.18	4.36	4.56	4.77	16.7
Carbon Dioxide	4.18	4.36	4.56	4.77	16.7
Carbon Monoxide	12.5	16.1	21.9	34.9	62.6

Predictions for H₂O show that its concentration stays constant in the temperature range of 800 to 1500 K, and decreases at this point. Predictions for CO₂ indicate large constant concentrations, but a dramatic decrease at 1500 K. CO concentrations show a constant increase of equilibrium concentrations in the temperature range of 800 to 1500 K and a dramatic decrease toward the higher temperatures. These results are shown in Figures 4.4, 4.5, and 4.6.

Figure 4.4. Equilibrium predictions for water under decreasing oxygen conditions of sour gas combustion.

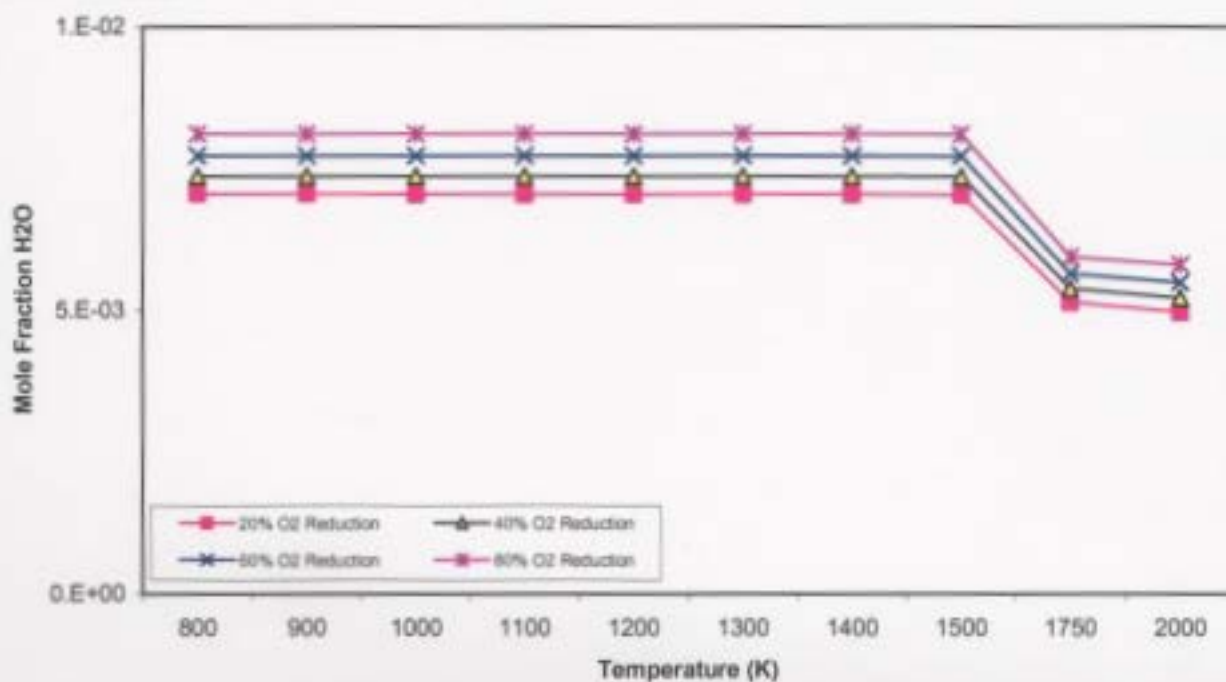


Figure 4.5. Equilibrium predictions for carbon dioxide under decreasing oxygen conditions of sour gas combustion.

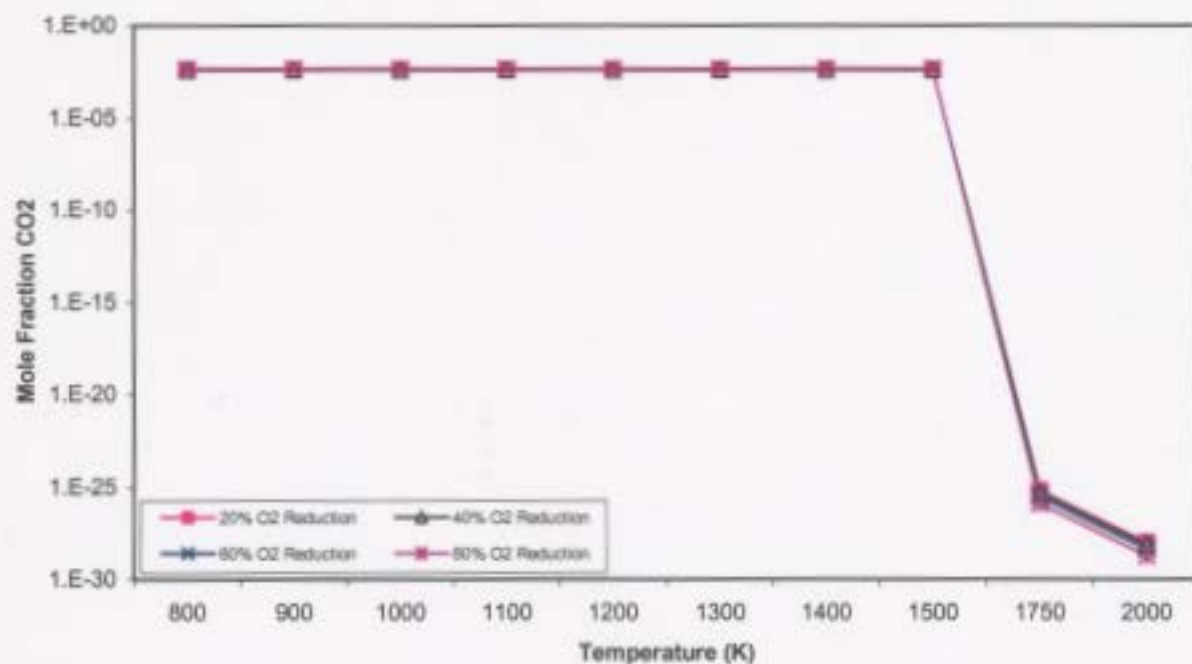
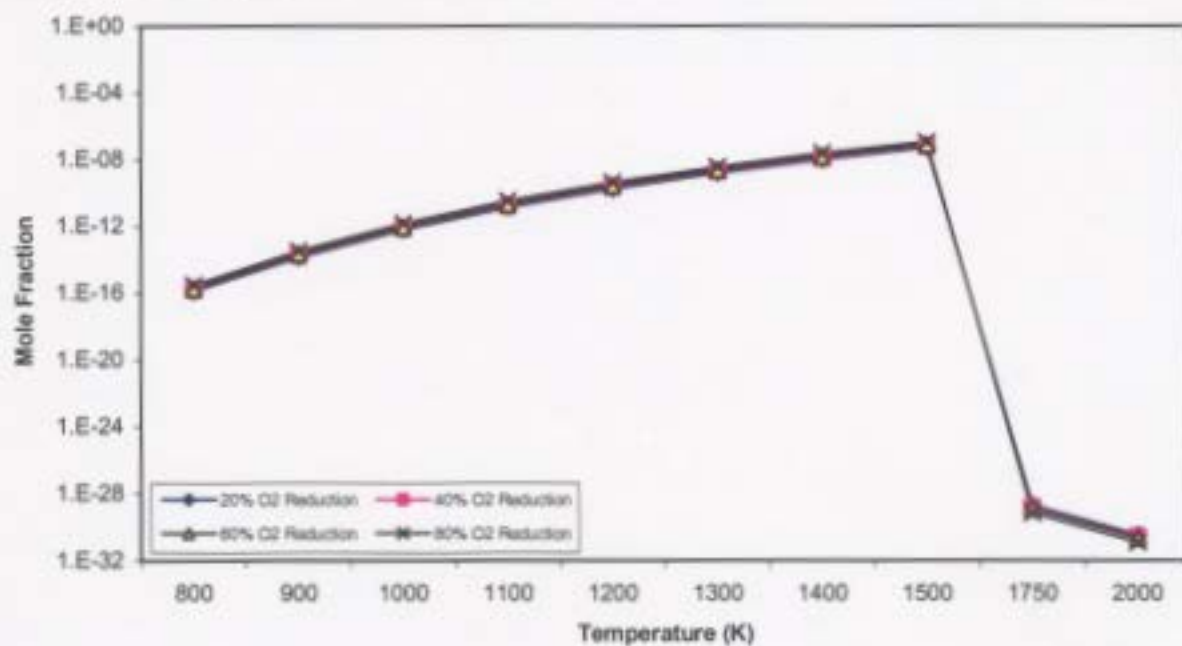


Figure 4.6. Equilibrium predictions for carbon monoxide under decreasing oxygen conditions of sour gas combustion.



4.2.3. Equilibrium Predictions for Sulphur-Containing Compounds

Several sulphur-containing compounds are predicted to form under equilibrium conditions when decreasing the oxygen content. These results are generally the same as the results for the excess oxygen conditions. In this case, larger concentrations are predicted for hydrogen sulphide, sulphur dioxide, and carbonyl sulphide as oxygen content decreases. This is again as a result of higher input mole fractions of sulphur containing species.

Table 4.4 gives the percent increases for sulphur-containing species between each run and overall.

Table 4.4. Percent increases in composition for sulphur-containing species under equilibrium conditions while decreasing the oxygen content by 20 %, 40 %, 60 %, and 80 %.

Species	0-20 % O ₂ Reduction	20-40 % O ₂ Reduction	40-60 % O ₂ Reduction	60-80 % O ₂ Reduction	0-80 % O ₂ Reduction
Hydrogen Sulphide	35.7	43.6	55.9	76.9	96.3
Sulphur Dioxide	12.3	15.3	20.3	32.1	59.8
Carbonyl Sulphide	35.6	43.5	55.9	76.9	96.3

Figure 4.7 show that hydrogen sulphide has a zero concentration below 900 K and a constant increase between 900 K and 2000 K. Figure 4.8 show a constant increase in sulphur dioxide concentrations between 800 K and 1000 K and leveling off at the higher temperatures. As well, Figure 4.9 show that carbonyl sulphide has a zero concentration below 900 K and above 1500 K, but a constant increase from 900 K to 1500 K.

Figure 4.7. Equilibrium predictions for hydrogen sulphide under decreasing oxygen conditions of sour gas combustion.

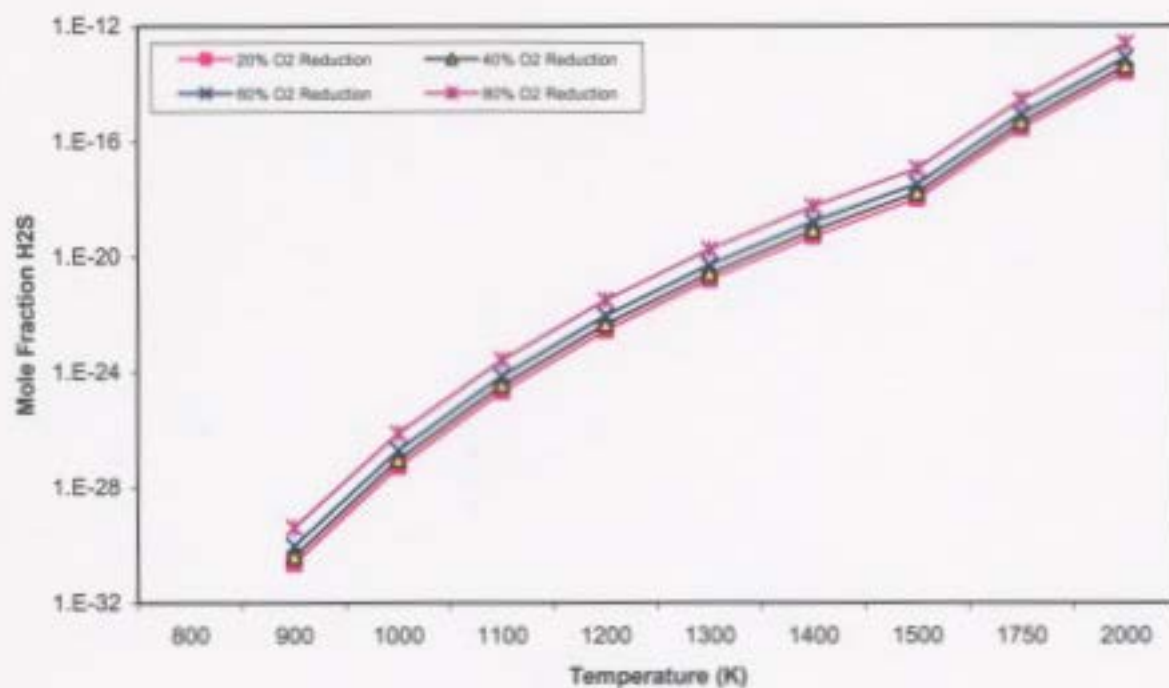


Figure 4.8. Equilibrium predictions for sulphur dioxide under decreasing oxygen conditions of sour gas combustion.

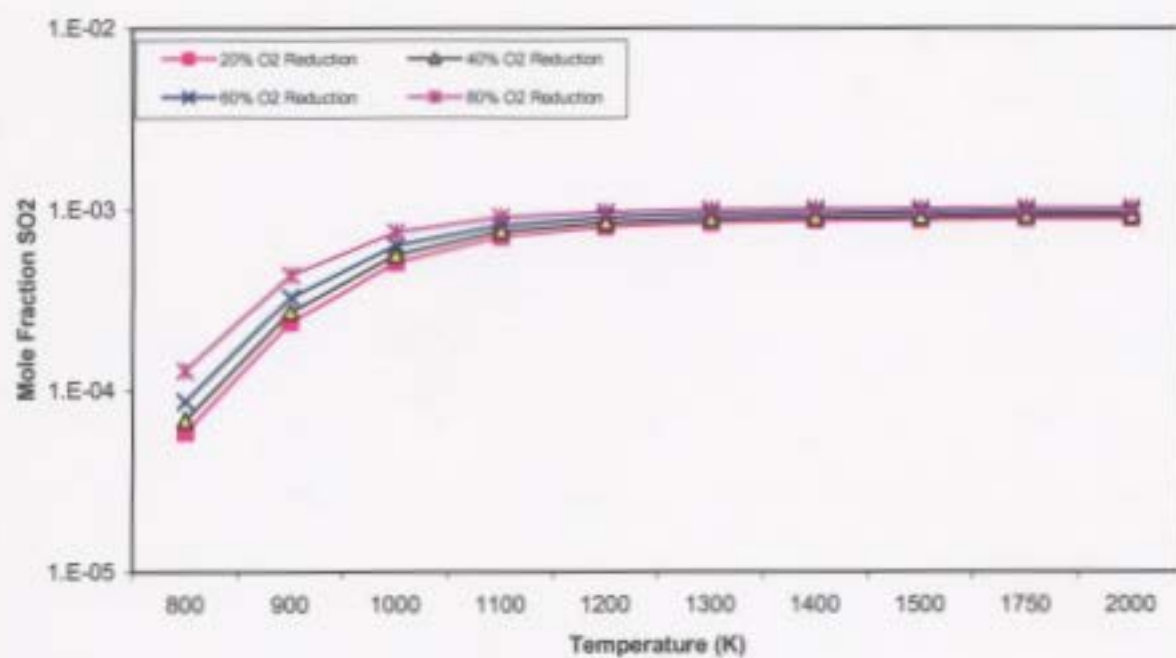
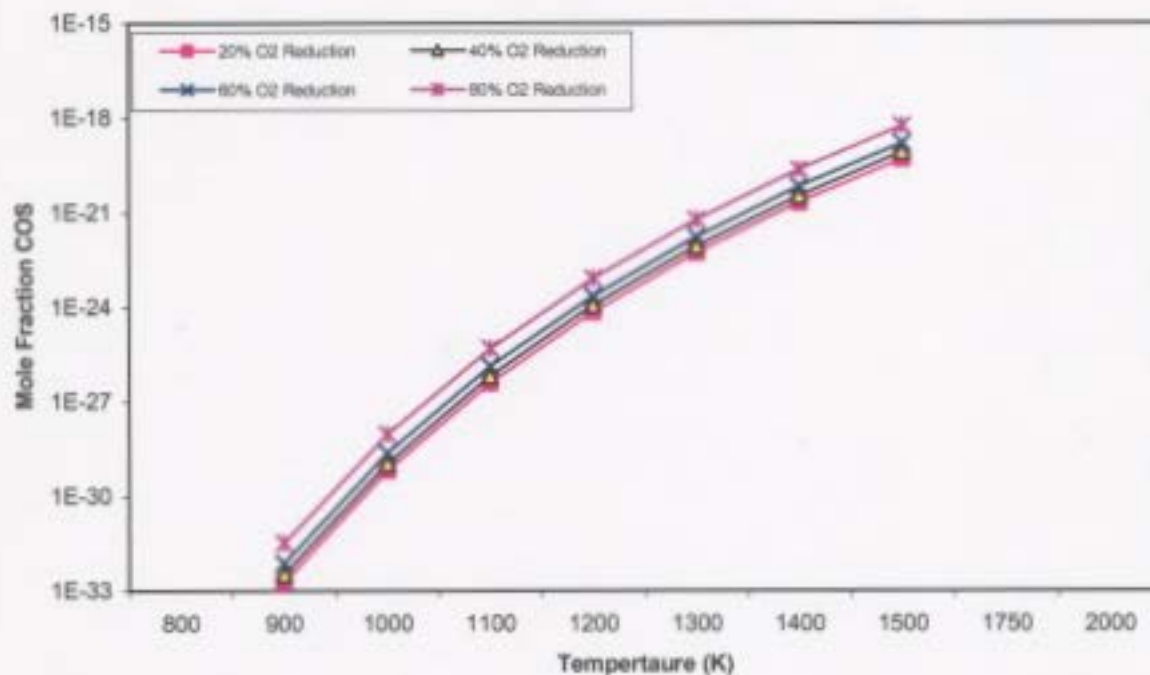


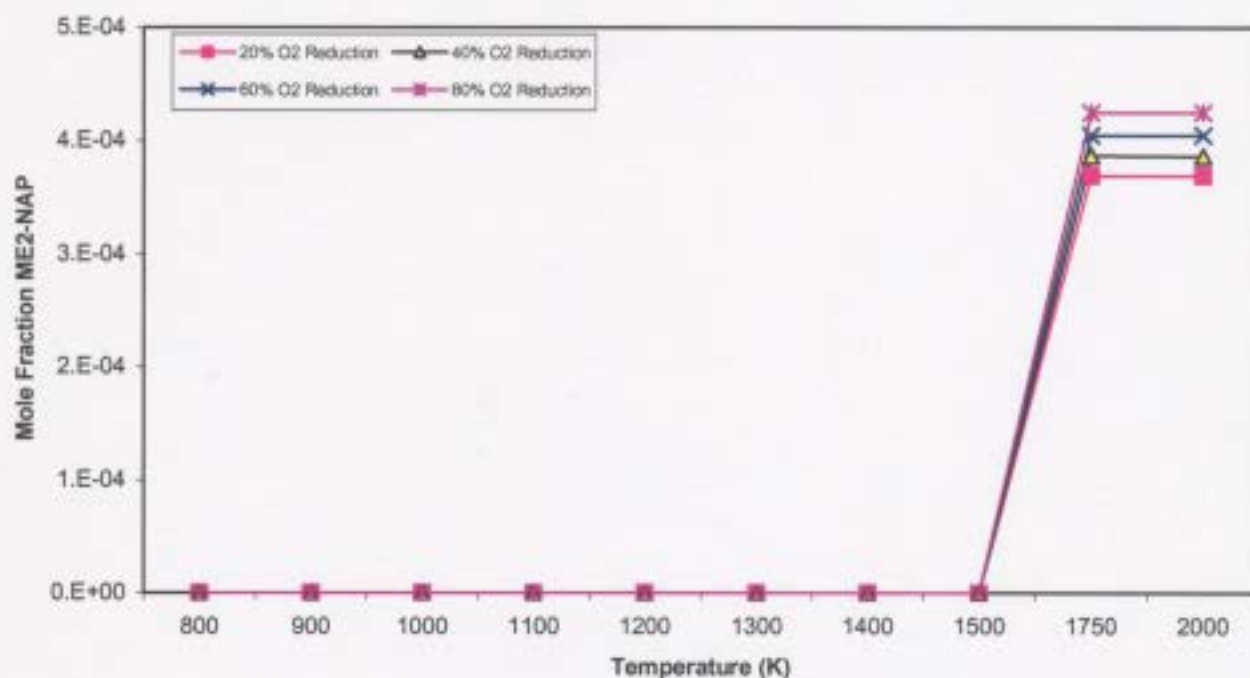
Figure 4.9. Equilibrium predictions for carbonyl sulphide under decreasing oxygen conditions of sour gas combustion.



4.2.4. Equilibrium Predictions for Aromatic Species

The sole aromatic species predicted to form in equilibrium when reducing the oxygen content by 20%, 40%, 60% and 80% is 2-methyl naphthalene. Figure 4.10 shows that concentrations are zero at the lower temperatures, a dramatic increase from 1500 K to 1750 K, and a constant concentration at higher temperatures. In addition, these results yield an increasing concentration with decreasing oxygen content trend. Compositions increase by 4.18 % between 0 – 20 % O₂ reduction, 4.36 % between 20 – 40 % O₂ reduction, 4.56 % between 40 – 60 % O₂ reduction, 4.78 % between 60 – 80 % O₂ reduction, and 16.7 % overall between 0 – 80 % O₂ reduction. This is due to the fact that there is more carbon and other species in the input and less oxygen.

Figure 4.10. Equilibrium predictions for 2-methyl naphthalene under decreasing oxygen conditions of sour gas combustion.



4.3. Pyrolysis Combustion Results

4.3.1. Introduction

Lack of oxygen plays a large role in the formation and behaviour of many complex chemical species, particularly poly-aromatic hydrocarbons and soot precursors. The input mole fractions compositions used in this case are shown in Table 4.5. Nitrogen is kept in the simulation so comparisons can be made to previous simulations. Nitrogen acts as an inert gas, but does affect the partial pressures of the system.

Table 4.5. Equilibrium input mole fraction compositions used for combustion pyrolysis.

Chemical Species	Mole Fraction
CH ₄	2.144 x 10 ⁻³
C ₂ H ₆	5.053 x 10 ⁻⁴
C ₃ H ₈	2.692 x 10 ⁻⁴
C ₄ H ₁₀	1.133 x 10 ⁻⁴
H ₂ S	1.077 x 10 ⁻³
H ₂	9.444 x 10 ⁻⁶
CO ₂	5.100 x 10 ⁻⁴
N ₂	9.836 x 10 ⁻¹
Ar	1.176 x 10 ⁻²

4.3.2. Equilibrium Predictions for Oxidation Products and Light Hydrocarbon Species

Species predicted include lighter hydrocarbons and oxidation products including carbon dioxide, carbon monoxide, and water. The oxygen contained in these species is likely supplied by the input carbon dioxide.

Several lighter hydrocarbon species are predicted under pyrolysis conditions. Figure 4.11 show that methane, ethane, propane, and butane predictions indicate a slight decrease in concentration from 800 K to 1500 K, and zero concentration above 1500 K. The remaining hydrocarbons including ethene, propene, propyne, butene, butyne, butadiene, and butadiyne have similar trends where equilibrium concentrations increase from 800 K to 1000 K, gradually decrease to 1500 K, and go to zero above 1500 K. However, ethyne concentrations are predicted to increase up to 1000 K, level off until 1500 K, and go to zero above 1500 K. The most abundant species present are methane and ethyne. In addition, it can be noted that equilibrium pyrolysis predictions indicate larger concentrations for smaller hydrocarbons (*i.e.* methane has a larger concentrations compared to ethane).

Figure 4.11. Equilibrium predictions for light hydrocarbon species under pyrolytic conditions of sour gas combustion.

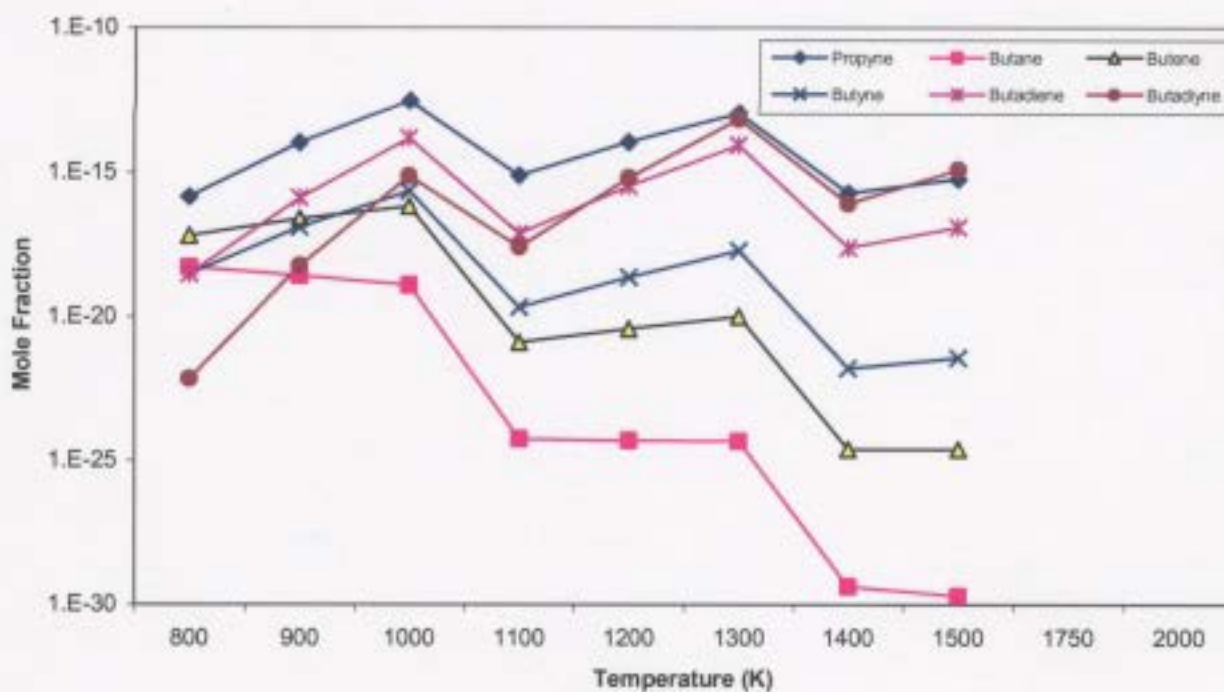
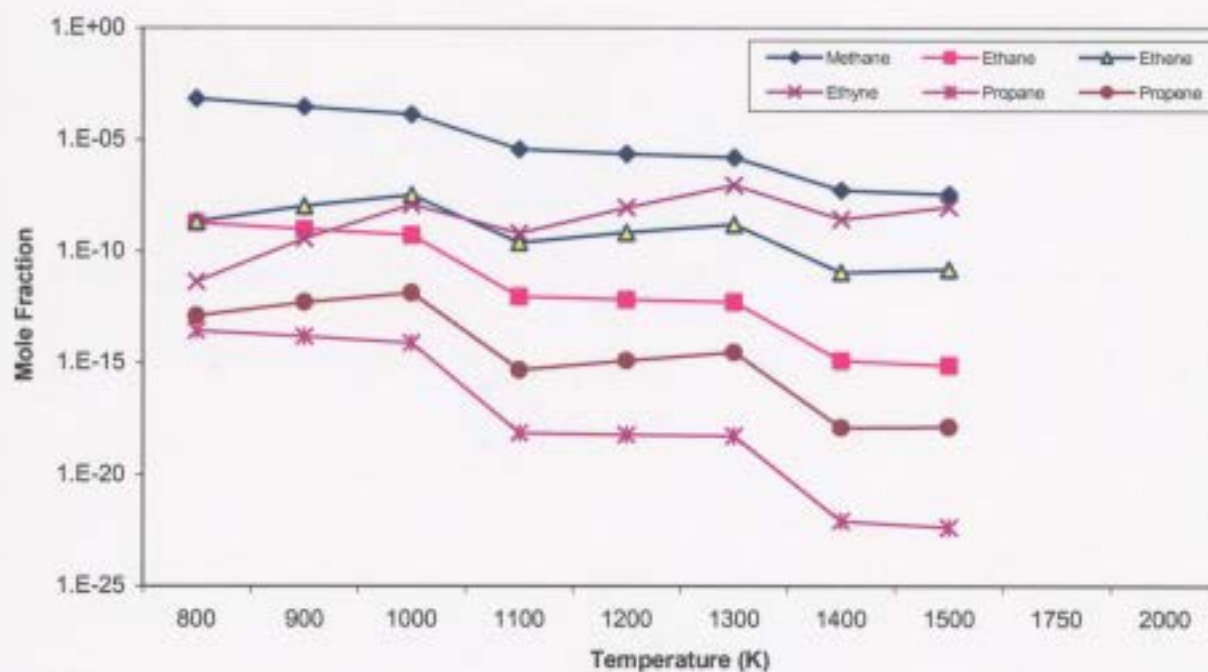
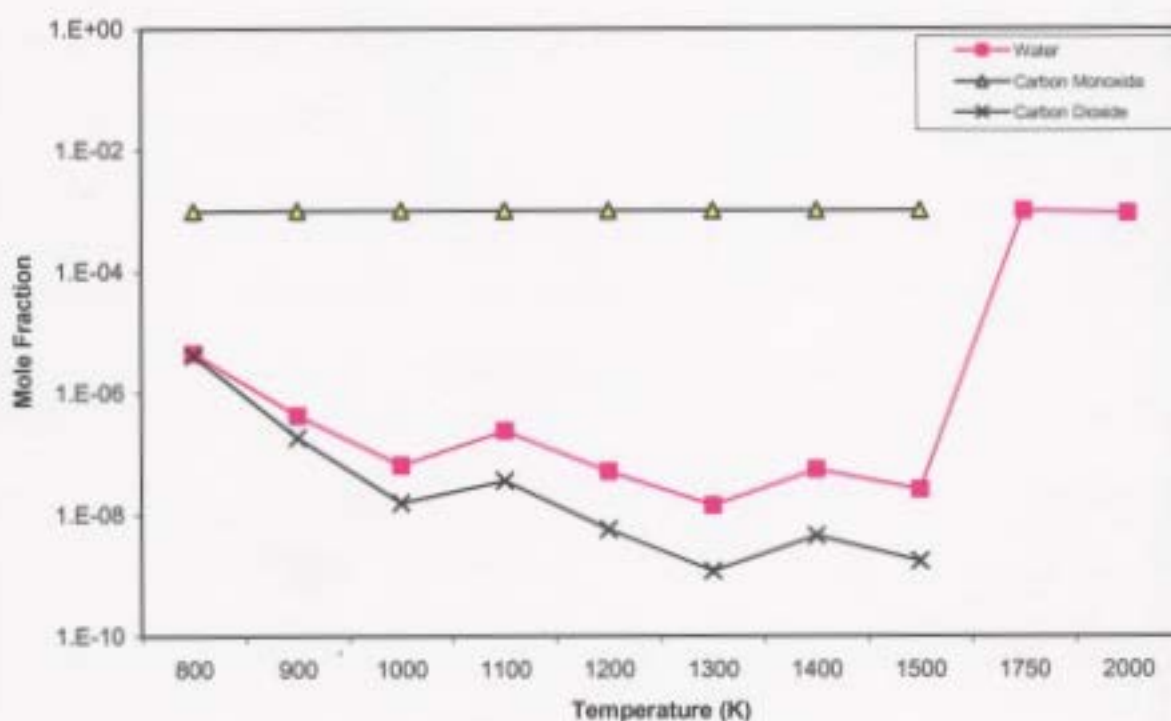


Figure 4.12 show that other species are predicted under pyrolysis equilibrium conditions. These include carbon dioxide, carbon monoxide, and water. The species are predicted at relatively lower concentrations compared to the corresponding results of excess oxygen and decreasing oxygen. Predictions for carbon dioxide concentrations are at maximum at 800 K, decrease until 1500 K, and goes to zero above 1500 K. Water concentrations decrease to 1500 K, and start to increase again. Predictions for carbon monoxide show a constant trend in concentration up to 1500 K, and zero concentration above 1500 K.

Figure 4.12. Equilibrium predictions for oxidation species under pyrolytic conditions of sour gas combustion.

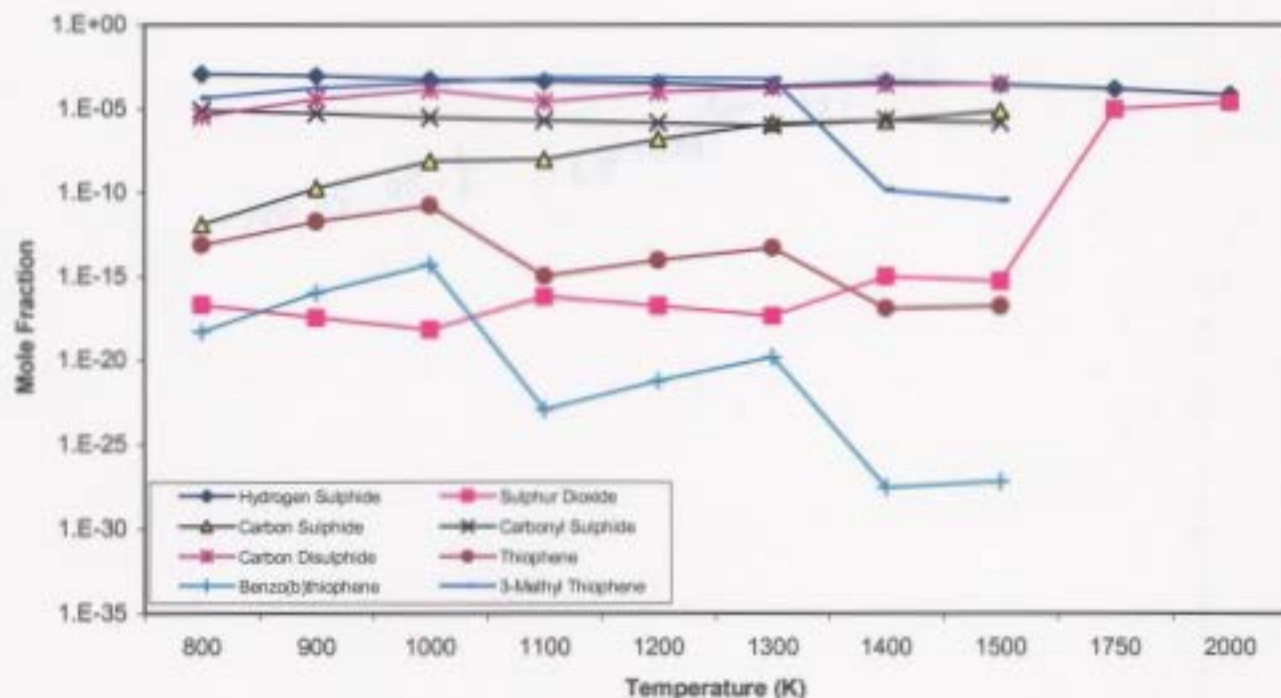


4.3.3. Equilibrium Predictions for Sulphur-Containing Compounds

Several sulphur-containing compounds are predicted to form under equilibrium pyrolysis conditions. These include hydrogen sulphide, sulphur dioxide, carbon sulphide, carbonyl sulphide, carbon disulphide, thiophene, 3-methyl thiophene, and benzo(b)thiophene.

Figure 4.13 shows the equilibrium predictions for these species. Predictions for hydrogen sulphide show relatively large constant concentrations, with a slight decrease between 1000 K and 2000 K. Carbon sulphide and carbon disulphide increase in concentration up to 1500 K, and go to zero above this temperature. Sulphur dioxide slightly increases in concentration up to 1500 K, and dramatically increases to 2000 K. Predictions for carbonyl sulphide show slight decreases to 1500 K, and go to zero above 1500 K. Thiophene and benzo(b)thiophene results increase in concentration to 1000 K, decrease to 1500 K, and a zero concentration above 1500 K. Finally, 3-methyl thiophene concentrations increase to 1300 K, decrease to 1500 K, and zero concentration above 1500 K. The most abundant sulphur species in this study are hydrogen sulphide, 3-methyl thiophene, and carbonyl sulphide at the lower temperatures and hydrogen sulphide, carbon disulphide, and sulphur dioxide at the higher temperatures.

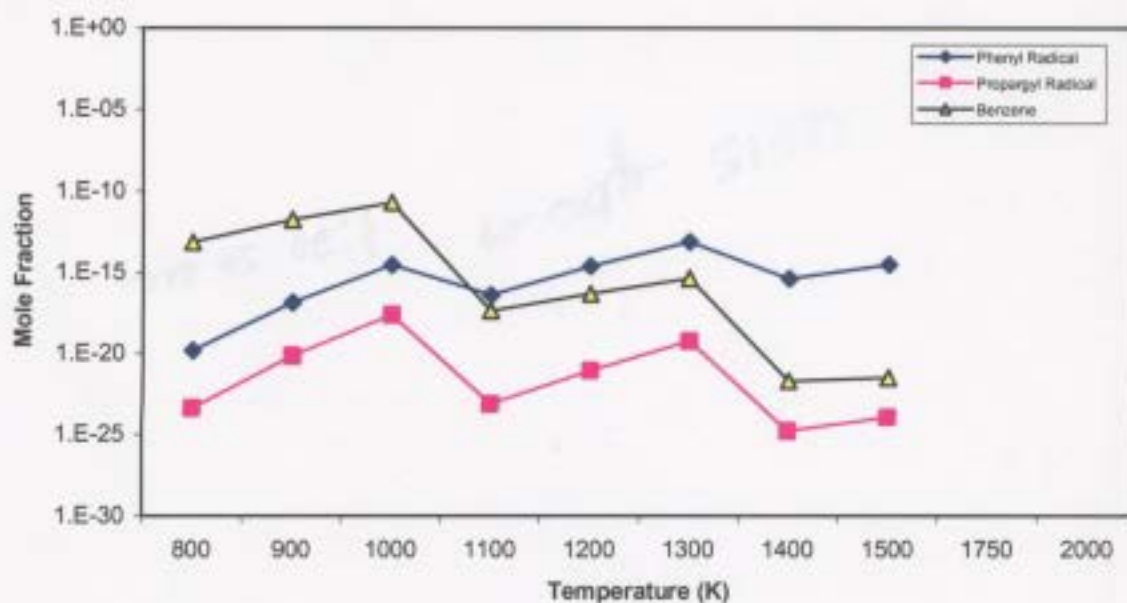
Figure 4.13. Equilibrium predictions for sulphur-containing compounds under pyrolytic conditions of sour gas combustion.



4.3.4. Equilibrium Predictions for Aromatic Species

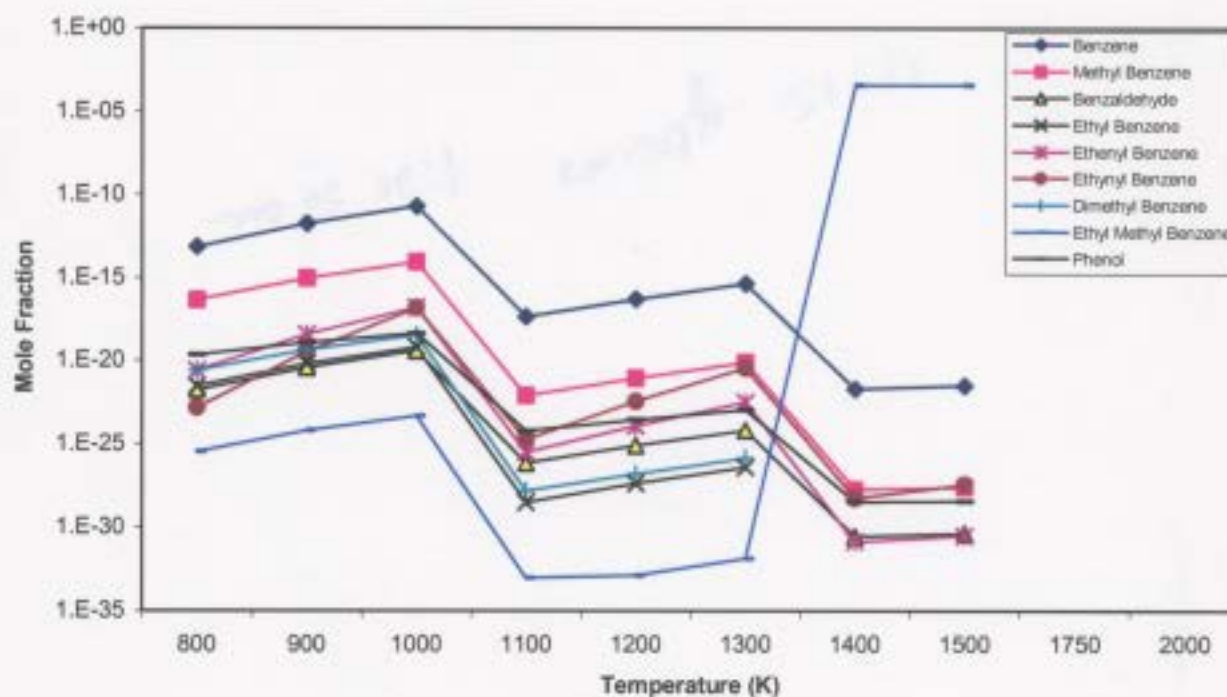
Equilibrium predictions for pyrolysis indicate the formation of numerous aromatic and poly-aromatic hydrocarbons. The formation of the simplest aromatic species, benzene, is a result of recombination reactions between carbon-3 radicals, which form the phenyl radical, and then benzene (Marinov *et al*, 1996). Figure 4.14 shows evidence of this where propargyl (carbon-3) radicals appear to recombine to produce larger amounts of phenyl radicals, and later benzene.

Figure 4.14. Equilibrium predictions for the formation of benzene under pyrolytic conditions of sour gas combustion.



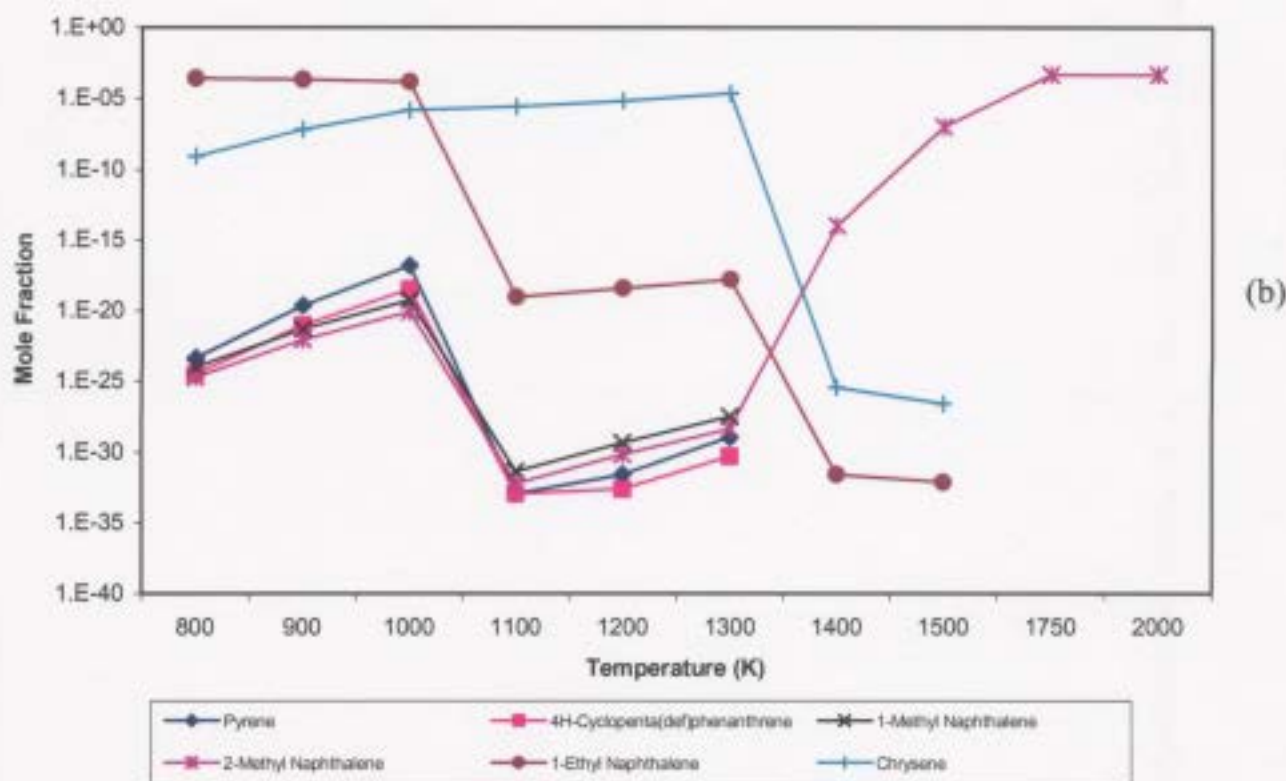
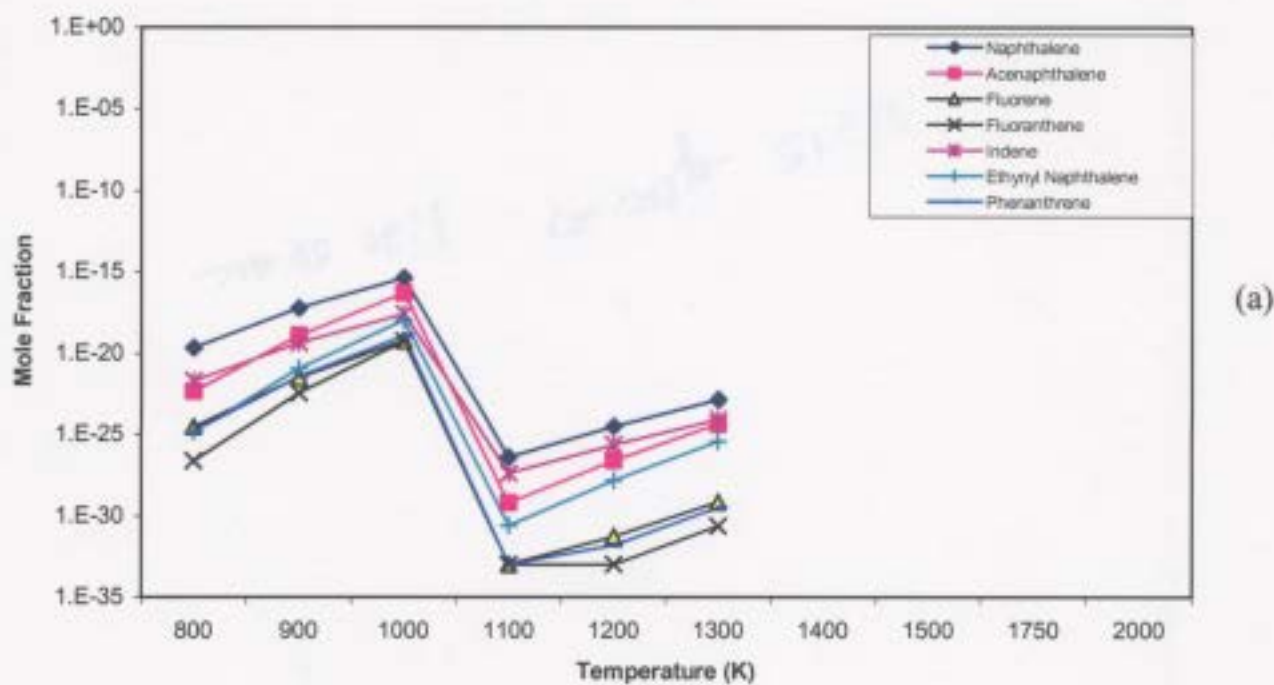
Once benzene is formed, many other light aromatic species are formed. In this case the most abundant aromatic species include methylbenzene and phenol at the lower temperatures and ethyl methylbenzene at the higher temperatures. Figure 4.15 shows that with the exception of ethyl methyl benzene, the general trend for these species concentrations is an increase up to 1000 K and an overall decrease at higher temperatures. However, ethyl methyl benzene predictions show an increase in concentration up to 1000 K, a decrease to 1100 K, and an increase to maximum concentration at 1400 K. The change in composition trend between 1000 K and 1100 K may be a result of a thermodynamic transition between the higher and lower temperature correlations. All aromatic species compositions appear to go to zero above 1500 K. However, there is an overall decreasing trend for aromatic species.

Figure 4.15. Equilibrium predictions for light aromatic hydrocarbons under pyrolytic conditions of sour gas combustion.



Several poly-aromatic hydrocarbons are predicted to form under equilibrium pyrolysis conditions. With the exception of 1-ethyl naphthalene, 2-methyl naphthalene, and chrysene, Figure 4.16 shows that concentrations for the poly-aromatic species generally increase up to 1000 K, decrease to 1100 K, increase to 1300 K, and go to zero above 1300 K. 1-ethyl naphthalene concentrations are relatively large and constant at the lower temperatures and begin to decrease at 1000 K, and go to zero above 1500 K. The composition for 2-methyl naphthalene increases to 1000 K, decreases to 1100 K, and increases to 2000 K. As well, chrysene predictions show a constant increase in concentration until 1300 K and a dramatic decrease to 1500 K, and zero beyond this temperature. The most abundant species are 1-ethyl naphthalene and chrysene at the lower temperatures and 2-methyl naphthalene at the higher temperatures.

Figure 4.16. Equilibrium predictions for poly-aromatic hydrocarbons under pyrolysis conditions of sour gas combustion.



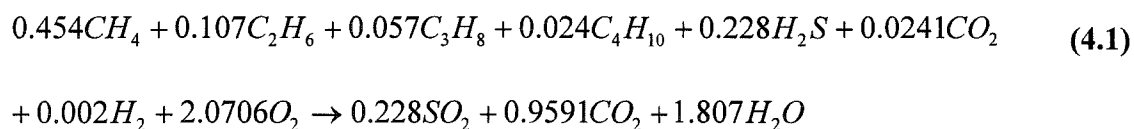
Once again, the change in composition trend between 1000 K and 1100 K may be a result of a thermodynamic transition between the higher and lower temperature correlations.

There is an overall increase in composition trend for poly-aromatic species.

4.4. Stoichiometric Air Combustion Results

4.4.1. Introduction

The input mole fraction compositions for stoichiometric air combustion simulations are calculated by using the stoichiometric ratio for sour gas combustion. The ratio is determined by using a sour gas feed composition used by Strosher (1996) in the balanced chemical reaction:



This chemical reaction yields an air to fuel ratio of 11.080 air : 1.000 fuel. Thus the input mole fraction compositions are calculated and are shown in Table 4.6.

Table 4.6. Equilibrium input mole fraction compositions used for stoichiometric combustion of sour gas.

Chemical Species	Mole Fraction
CH ₄	3.688 x 10 ⁻²
C ₂ H ₆	8.692 x 10 ⁻³
C ₃ H ₈	4.630 x 10 ⁻³
C ₄ H ₁₀	1.9506 x 10 ⁻³
H ₂ S	1.852 x 10 ⁻²
H ₂	1.625 x 10 ⁻⁴
O ₂	1.929 x 10 ⁻¹
CO ₂	1.958 x 10 ⁻³
N ₂	7.257 x 10 ⁻¹
Ar	8.562 x 10 ⁻³

4.4.2. Equilibrium Predictions for Oxidation Products and Light Hydrocarbon Species

Under stoichiometric oxygen conditions, equilibrium predicts the formation of several oxidation products and methane as the single light hydrocarbon species. Figure 4.17 indicates that large concentrations of these species are formed under equilibrium conditions.

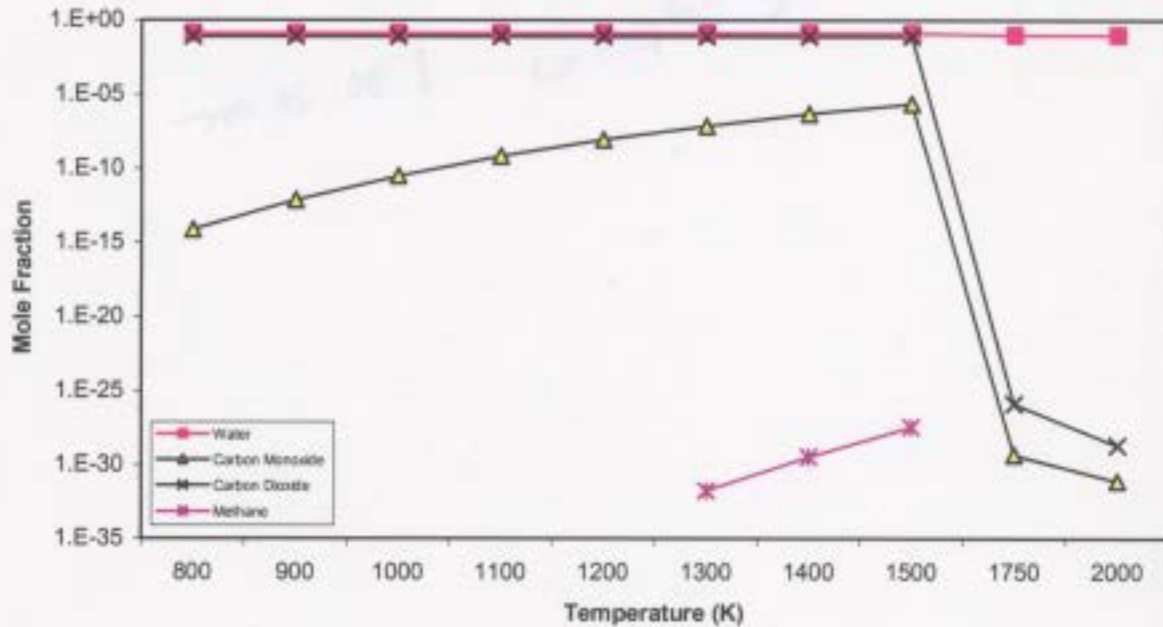
Predictions for water show relatively constant concentrations over the temperature range, but concentrations slightly decrease at 1500 K. Predictions for carbon monoxide are increasing constantly until 1500 K and decreases dramatically at this temperature. As well, predictions for carbon dioxide remain large and constant up to 1500 K and decrease toward the higher temperatures. This decrease in composition for oxidation species at 1500 K appears to be a result of the formation of carbon disulphide and aromatic formation (see sections 4.4.3. and 4.4.4.). In addition, methane is also predicted to form under equilibrium conditions. These predictions indicate that methane only exists between 1300 and 1500 K.

4.4.3. Equilibrium Predictions for Sulphur-Containing Compounds

Equilibrium calculations predict the formation of numerous sulphur-containing compounds under stoichiometric reaction conditions. Figure 4.18 shows the predictions for these species.

Predictions for sulphur dioxide indicate concentrations constantly increase up to 1000 K and beginning to level off at the higher temperatures. Concentrations of hydrogen sulphide start increasing at 800 K and are at maximum at 2000 K. Carbonyl sulphide compositions increase from 800 K to 1500 K and go to zero above 1500 K.

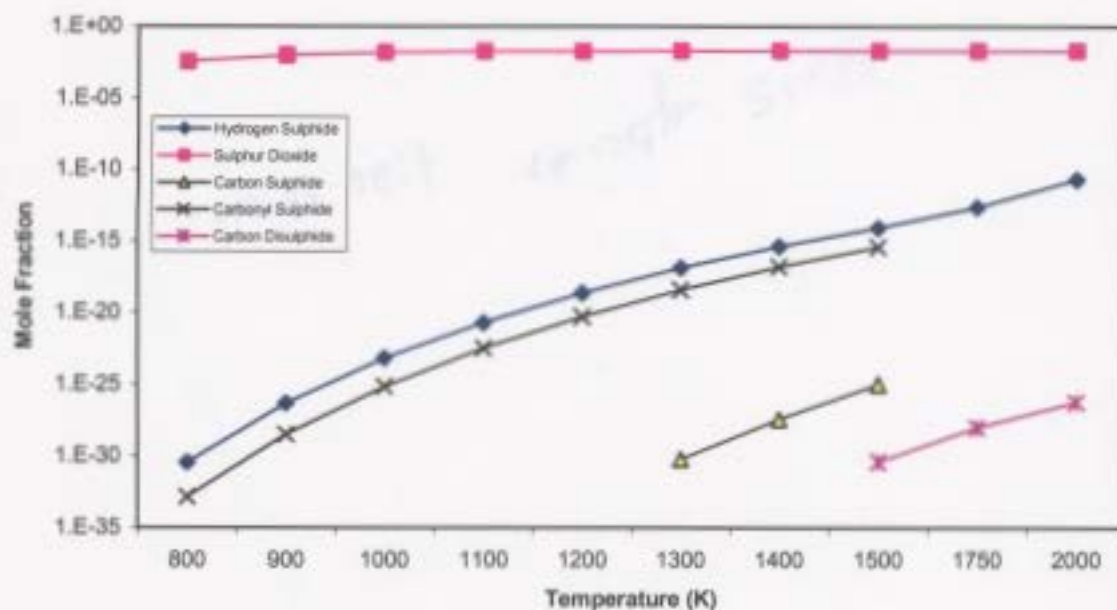
Figure 4.17. Equilibrium predictions for complete combustion products and methane under conditions of stoichiometric sour gas combustion.



Carbon sulphide concentrations are zero up to 1300 K, increase from 1300 K to 1500 K and go to zero above 1500 K. Lastly, carbon disulphide does not exist up to 1500 K and then increases from 1500 K to 2000 K.

Figure 4.18 shows that concentrations for hydrogen sulphide, sulphur dioxide and carbonyl sulphide are effectively the same as previous predictions. However, the results for carbon sulphide and carbon disulphide are different, where excess oxygen conditions show no presence of these species and pyrolysis predictions show large amounts of these species. Thus, the lack of oxygen causes these species to form.

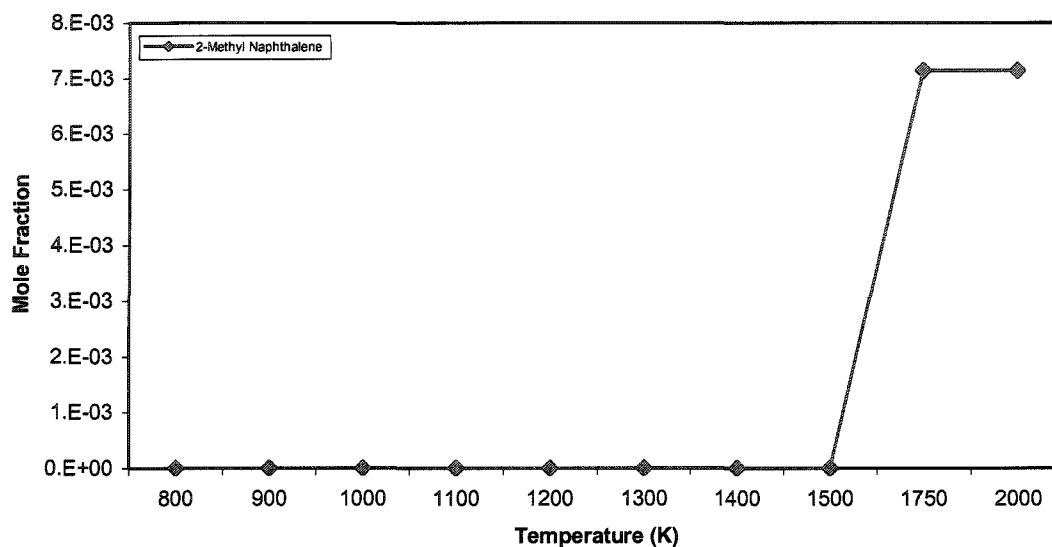
Figure 4.18. Equilibrium predictions for sulphur-containing compounds under conditions of stoichiometric sour gas combustion.



4.4.4. Equilibrium Predictions for Aromatic Species

Similar to the results of excess oxygen and decreasing oxygen conditions, the sole aromatic species that is predicted to form under equilibrium conditions is 2-methyl naphthalene. Figure 4.19 indicates that concentrations are zero at the lower temperatures, dramatically increase from 1500 K to 1750 K, and constant at higher temperatures.

Figure 4.19. Equilibrium predictions for aromatic hydrocarbon compounds under conditions of stoichiometric sour gas combustion.



4.5. Summary

Equilibrium results under excess oxygen conditions, decreasing oxygen, and stoichiometric oxygen conditions give similar results. The oxidation products are shown to have large concentrations at lower temperatures and to decrease with increasing oxygen content. Many of the smaller hydrocarbons produced under pyrolysis conditions increase to 1000 K and methane and ethyne are the most abundant at the higher temperatures. The formation of complex sulphur-containing compounds and aromatic hydrocarbons occur especially under pyrolysis conditions. In addition, the composition transition between 1000 K and 1100 K for aromatic and poly-aromatic species under pyrolysis conditions may be a result of a thermodynamic transition between the higher and lower temperature ranges.

As previously mentioned, the primary purpose of performing equilibrium calculations in this study is to determine equilibrium data for chemical species in which there is no kinetic data available. Data for many of the complex sulphur compounds and aromatic hydrocarbons have been obtained. Table 4.7 gives a list of these species.

Table 4.7. Chemical species predicted to form under equilibrium conditions but have no kinetic data published.

Chemical Species
2-Methyl Naphthalene
Carbon Disulphide
Thiophene
3-Methyl Thiophene
Benzo(b)thiophene
1-Ethyl Naphthalene
1-Methyl Naphthalene
Chrysene

Therefore, the chemical behaviours of species in Table 4.7 during sour gas incineration are predicted based on their equilibrium results. In addition, equilibrium calculations for other species can now be used as a comparison tool for kinetic calculations.

Chapter 5. Kinetic Model Results and Analysis

Under incineration conditions the temperatures in the combustion chamber can rise as high as 1800 K and drop as low as 800 K. As such, the concentrations of products inside the combustion chamber are computed over a temperature range of 800 to 1800 K with three regions. These regions include a reaction zone (approximately above 1600 K), a post combustion zone (approximately 1200 K – 1600 K), and a quenching zone (approximately up to 1200 K). After the combustion chamber, the gases enter a stack in which cooling takes place. The cooling is simulated by modeling the stack as a plug flow reactor with a decreasing linear temperature profile. Three temperature profiles with initial temperatures of 1623 K, 1400 K, and 1000 K are used to compute kinetic concentrations of products during the cooling process. In order to approximate actual incineration conditions, calculations are performed on air to fuel ratios and flow rates that are used by Questor Technologies.

5.1. Combustion Chamber Calculations

5.1.1. Case A: 14:1 Air to Fuel Ratio Results

5.1.1.1 Introduction

The input mole fraction compositions used in these simulations are calculated based on a sour gas composition taken from Strosher (1996). With a 14 air : 1 fuel ratio, the input composition is 0.03046 CH₄, 0.00731 C₂H₆, 0.00398 C₃H₈, 0.00178 C₄H₁₀, 0.01538 H₂S, 0.00031 H₂, 0.19570 O₂, 0.00185 CO₂, 0.73437 N₂, and 0.00886 Ar.

The air flow rates are based on the actual fuel rates used by Questor Incineration Technologies, which are $3.28 \times 10^5 \text{ cm}^3/\text{s}$, $9.83 \times 10^5 \text{ cm}^3/\text{s}$, and $1.64 \times 10^6 \text{ cm}^3/\text{s}$. The simulated temperature ranges from 800 to 1800 K (See Table 3.2). Results of primary combustion products, lower weight hydrocarbons, sulphur compounds, and aromatic species are discussed in this section.

5.1.1.2. Kinetic Predictions for Oxidation Products and Light Hydrocarbon Species

Many of the oxidation and light hydrocarbon kinetic predictions are similar to equilibrium predictions. This is especially true at the higher temperatures where reaction rates are fast. Composition trends from three different flow rates are similar, but differ in magnitude.

As shown in Figure 5.1 with the exception of butane, three temperature regions can be identified based on composition trends. These regions are approximately up to 1200 K, 1200 K to 1600 K, and up to 1800 K. Concentrations for lower weight hydrocarbons are at maximum at the lower temperatures where methane is the most abundant species. These concentrations tend to decrease with increasing temperature and gradually level off at the higher temperatures, where ethyne is the abundant species and it appears that methane is being consumed. Butane concentrations remain relatively constant over the entire temperature range.

Figure 5.2 shows that oxygen is consumed by the formation of other oxidation products including carbon monoxide, carbon dioxide, and water at the lower temperatures. Concentrations for carbon dioxide and water increase up to 1000 K and remain constant at the higher temperatures. Carbon monoxide concentrations decrease at

Figure 5.1. Kinetic predictions of concentrations of lower weight hydrocarbon products formed for 14:1 air to fuel ratio, an inlet flow rate of $3.28 \times 10^5 \text{ cm}^3/\text{s}$, and a temperature range of 800 K to 1800 K inside the combustion chamber during sour gas incineration.

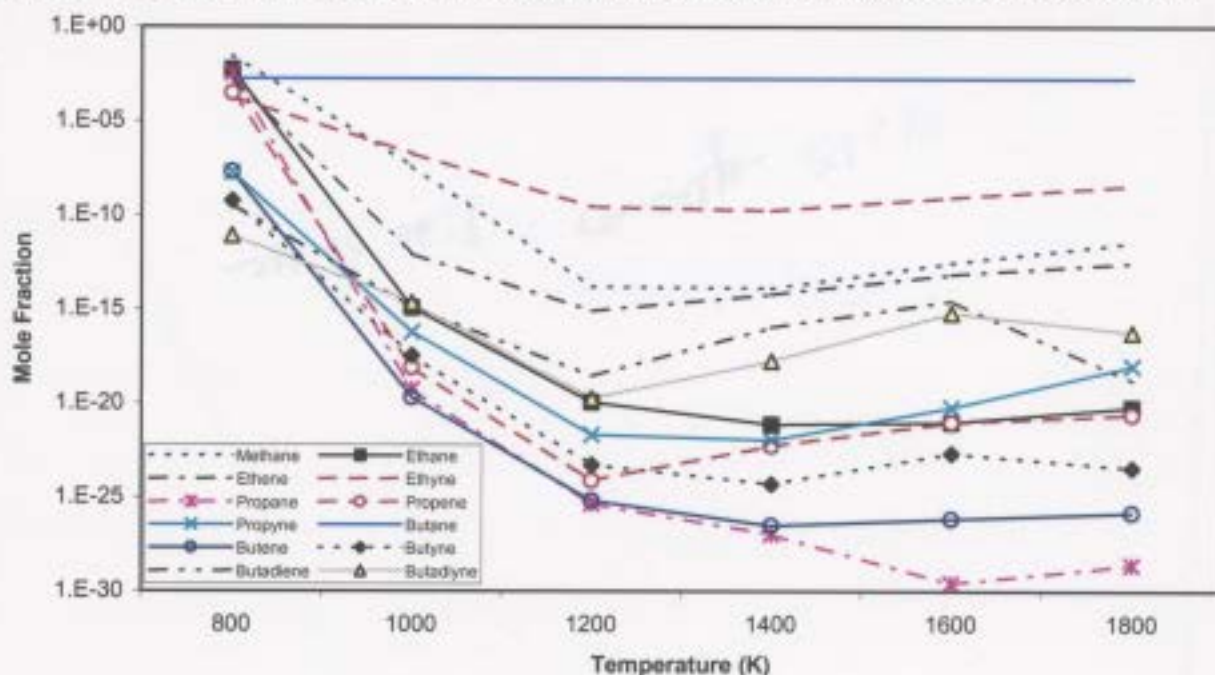
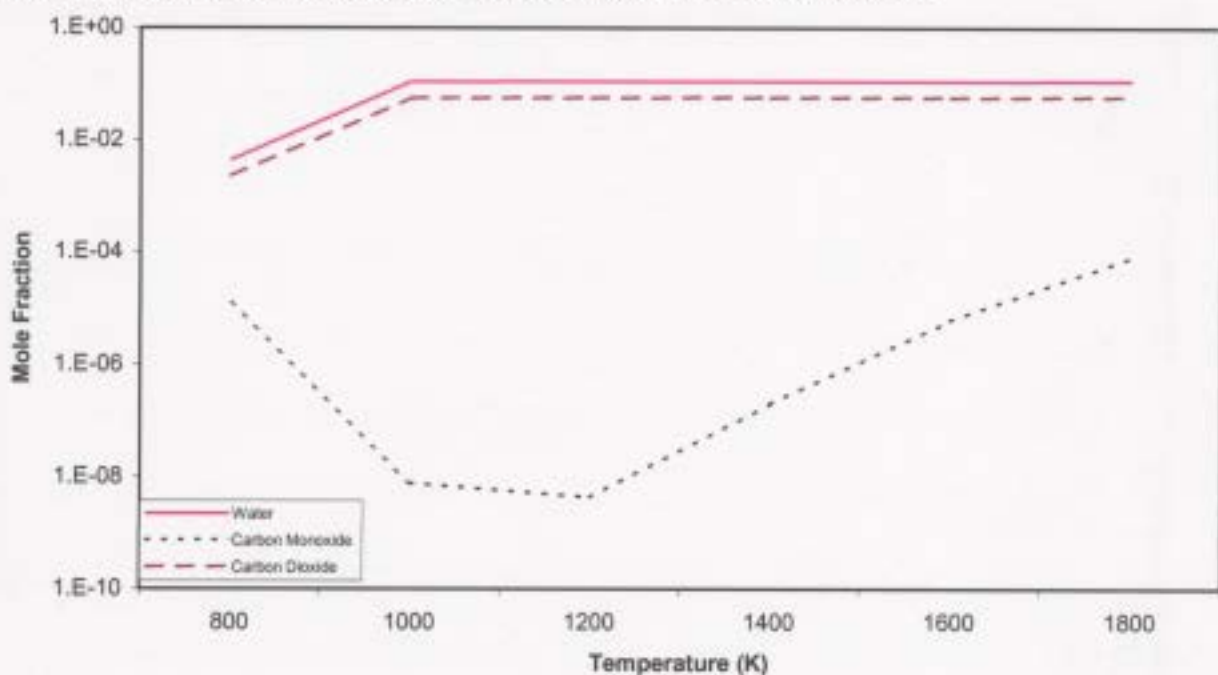


Figure 5.2. Kinetic predictions of concentrations of oxidation products formed for 14:1 air to fuel ratio, inlet flow rate of $3.28 \times 10^5 \text{ cm}^3/\text{s}$, and a temperature range of 800 K to 1800 K inside the combustion chamber during sour gas incineration.



the lower temperatures and increase at the higher temperatures. However, carbon dioxide and water are highest in terms of concentration, while carbon monoxide concentrations increase dramatically at the higher temperatures.

Kinetic compositions for light hydrocarbons and oxidation products change in magnitude with varying flow rates, but give the same overall trend. Species that increase in magnitude with increasing flow rates include ethane and propane. Species that decrease in magnitude with increasing flow rates include ethene, ethyne, propene, propyne, butene, butyne, butadiene, butadiyne, water, carbon monoxide, and carbon dioxide. Table 5.1 gives the percent change in composition for lower weight hydrocarbons and oxidation products under varying flow rate. Note that there is no change for methane and butane. In addition, Figure 5.3 shows the most significant decrease in composition for butadiene as the flow rate ranges from $3.28 \times 10^5 \text{ cm}^3/\text{s}$ to $1.64 \times 10^6 \text{ cm}^3/\text{s}$.

As flow rates increase, oxygen compositions increase and possibly react with the unsaturated hydrocarbons (*i.e.* ethene) to produce more saturated hydrocarbons (*i.e.* ethane).

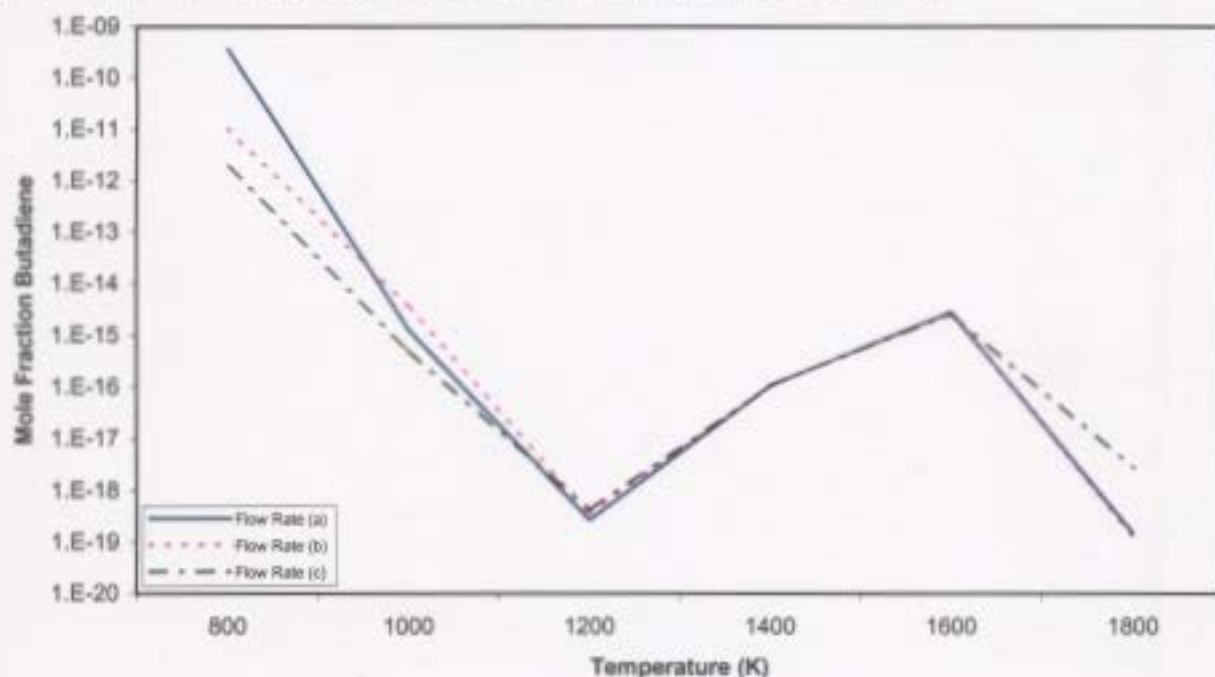
5.1.1.3. Kinetic Predictions for Sulphur-Containing Compounds

Several sulphur containing species are predicted to form during the combustion of sour gas. Kinetic and equilibrium calculations are similar, especially at the higher temperatures. As well, the three different flow rates show similar overall trends, but slight changes in magnitude. Kinetic calculations for sulphur dioxide concentrations are similar to equilibrium values over the entire temperature range of 800 K to 1800 K. Calculations

Table 5.1. Kinetically predicted changes in composition (%) for lower weight hydrocarbons and oxidation products at entry of the combustion chamber under the 14:1 air to fuel ratio with increasing flow rate from $3.28 \times 10^5 \text{ cm}^3/\text{s}$ to $1.64 \times 10^6 \text{ cm}^3/\text{s}$ and a temperature of 800 K.

Species	Increase (%)	Decrease (%)
Methane	-	-
Ethane	22.3	-
Ethene	-	79.6
Ethyne	-	82.8
Propane	9.63	-
Propene	-	85.3
Propyne	-	97.8
Butane	-	-
Butene	-	98.0
Butyne	-	99.0
Butadiene	-	99.5
Butadiyne	-	99.5
Water	-	86.0
Carbon Monoxide	-	8.33
Carbon Dioxide	-	15.8

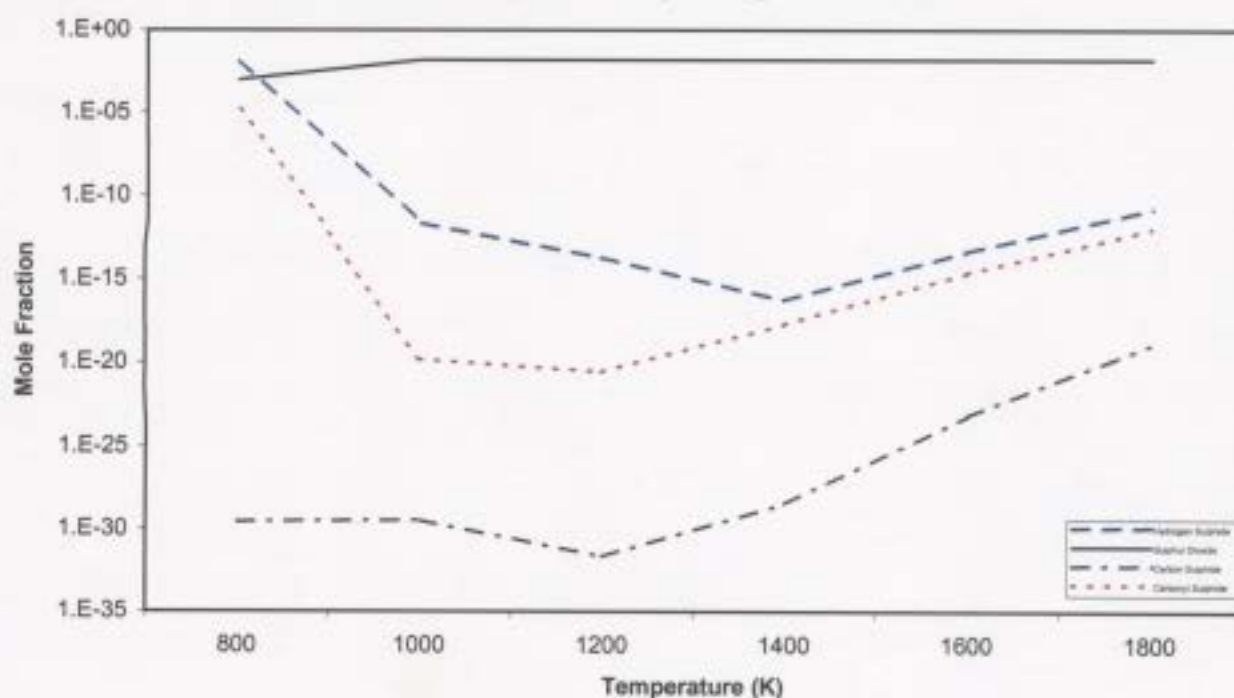
Figure 5.3. Kinetically predicted decrease in composition (%) butadiene within the combustion chamber under the 14:1 air to fuel ratio with increasing flow rate from (a). Inlet flow rate = $3.28 \times 10^5 \text{ cm}^3/\text{s}$, (b). Inlet flow rate = $9.83 \times 10^5 \text{ cm}^3/\text{s}$, (c). Inlet flow rate = $1.64 \times 10^6 \text{ cm}^3/\text{s}$, and a temperature range of 800 K to 1800 K.



for hydrogen sulphide, carbon sulphide and carbonyl sulphide are similar to equilibrium values only at higher temperatures, starting at 1200 K.

Figure 5.4 show that composition trends for sulphur containing species show similar distinct temperature regions as in the previous sections. Hydrogen sulphide and carbonyl sulphide show the same pattern as the lower weight hydrocarbons. Their concentrations drastically decrease up to approximately 1200 K and then gradually increase with increasing temperature. Sulphur dioxide, an oxidation product of sour gas combustion, appears to have a similar pattern as carbon dioxide and water, where levels increase to 1000 K and plateau off at the higher temperatures. Carbon sulphide yields a similar trend over the temperature range as carbon monoxide, where concentrations slightly increase up to 1000 K and decrease up to 1200 K and then increase at the higher temperatures.

Figure 5.4. Kinetic predictions of concentrations of sulphur containing products formed for 14:1 air to fuel ratio, flow rate of $3.28 \times 10^5 \text{ cm}^3/\text{s}$, and a temperature range of 800 K to 1800 K inside the combustion chamber during sour gas incineration.



Predictions for hydrogen sulphide increase by 7.2 % with increasing flow rate, and decrease for sulphur dioxide by 81.3%, carbon sulphide by 83.4 %, and carbonyl sulphide by 17.2 %.

5.1.1.4. Kinetic Predictions for Aromatic Species

Aromatics predicted to occur under both equilibrium and kinetic simulations show similar trends at the same temperatures. The most abundant aromatic species predicted under both equilibrium and kinetic conditions are benzene, phenol, ethynyl benzene, and methyl benzene.

As mentioned in section 2.3.1.5, the formation of benzene occurs in a series of radical recombination steps of propargyl radicals, leading to the reaction between the phenyl radical and the hydrogen atom, which produces the benzene molecule. Figure 5.5 gives evidence to prove this theory and that there are the same three temperature regions identified earlier. The propargyl radical is predicted to have a maximum initial concentration at 800 K where it starts to decrease until 1200 K and then starts to increase at the higher temperatures. The concentration of the phenyl radical increases continuously until it reaches a temperature of 1600 K and gradually starts to decrease. This may be a result of increasing concentrations of propargyl radicals recombining and producing increasing concentrations of the phenyl radical. Benzene has a larger concentration than the phenyl radical, but has the same trend over the entire temperature range. Benzene and the phenyl radical decrease above 1600 K, which may be a result of the propargyl radical taking part in the formation of other species or benzene and the phenyl radical may be consumed in the formation of larger poly-aromatic species.

Figure 5.5. Kinetic predictions of concentrations of radicals that aid in the formation of benzene for 14:1 air to fuel ratio, inlet flow rate of $3.28 \times 10^5 \text{ cm}^3/\text{s}$ and a temperature range of 800 K to 1800 K inside the combustion chamber during sour gas incineration.

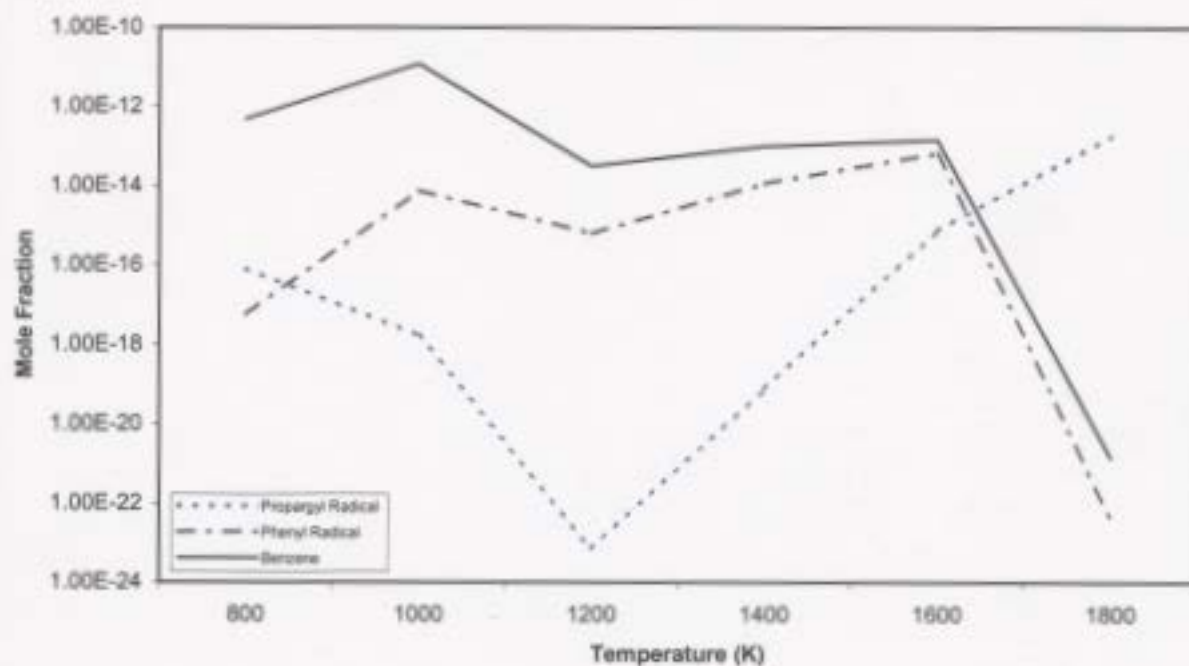


Figure 5.6 indicates that lower weight aromatic hydrocarbons are formed at the low temperatures, then level off, and finally decrease at the high temperatures. In addition, Figure 5.7 and 5.8 show that poly-aromatic hydrocarbons are formed at temperatures just slightly higher than those of lower weight aromatic species. This suggests that lower weight aromatics are precursors in the formation of larger poly-aromatic hydrocarbons. The most abundant poly-aromatic species in this case are naphthalene, methyl indene, biphenyl, and biphenylene.

Figure 5.6. Kinetic predictions of concentrations of lower weight aromatic products for 14:1 air to fuel ratio, inlet flow rate of $3.28 \times 10^5 \text{ cm}^3/\text{s}$, and a temperature of 800 K to 1800 K inside the combustion chamber during sour gas incineration.

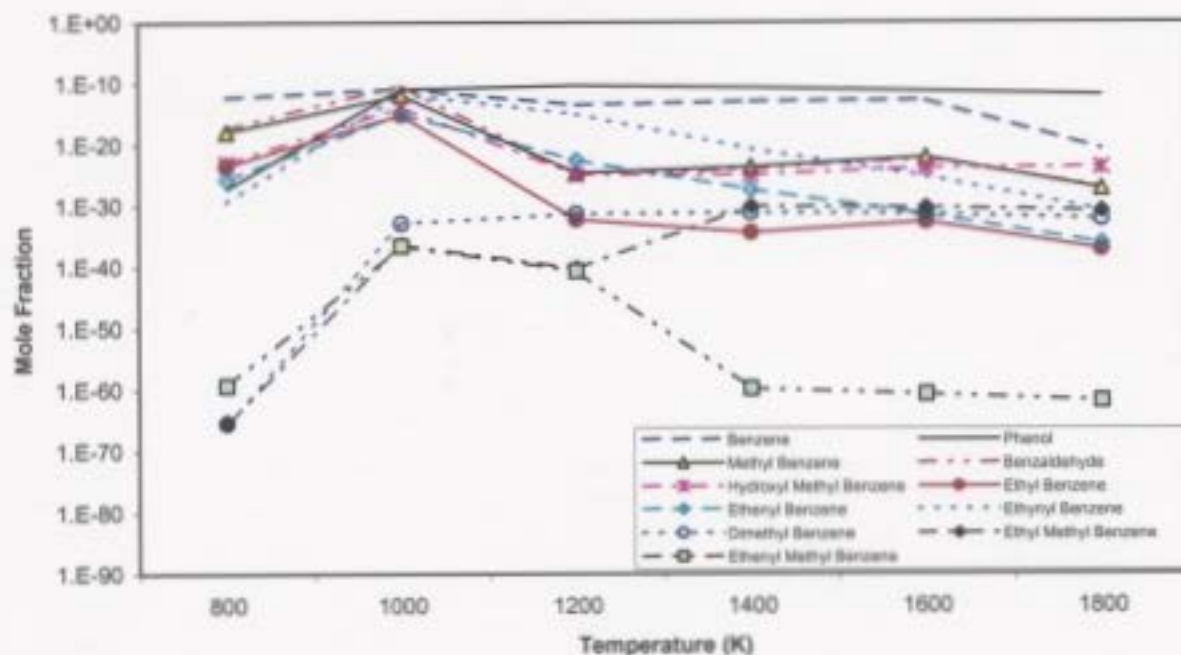


Figure 5.7. Kinetic predictions of concentrations of poly-aromatic hydrocarbon products for 14:1 air to fuel ratio, inlet flow rate of $3.28 \times 10^5 \text{ cm}^3/\text{s}$, and a temperature range of 800 K to 1800 K inside the combustion chamber during sour gas incineration.

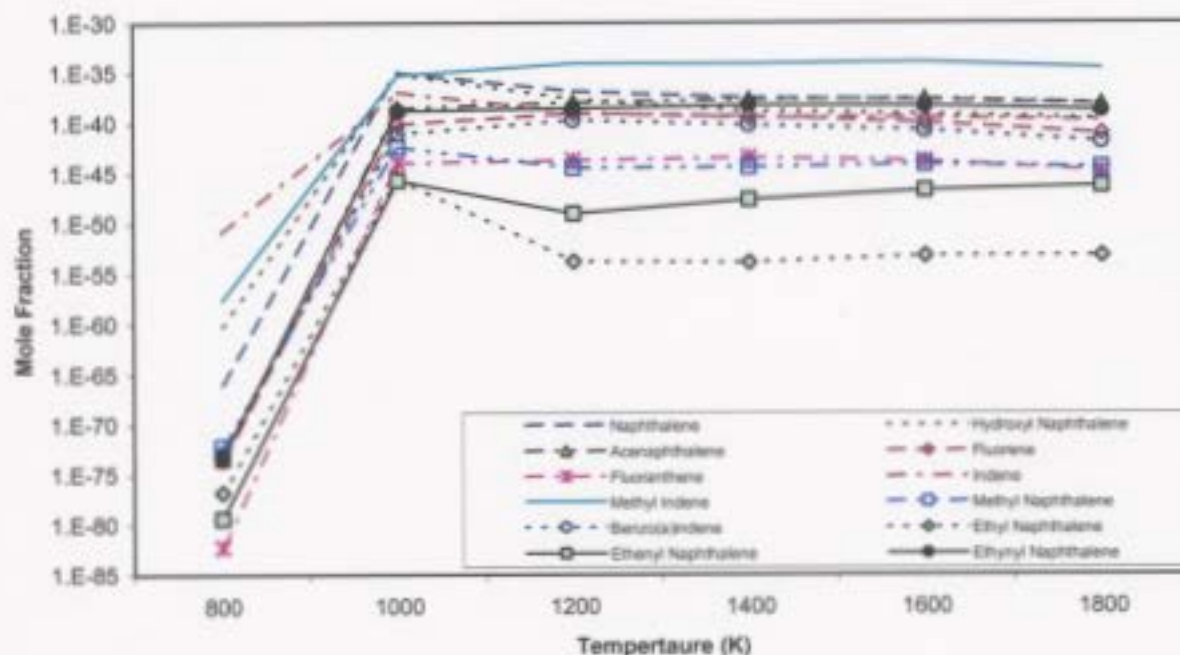
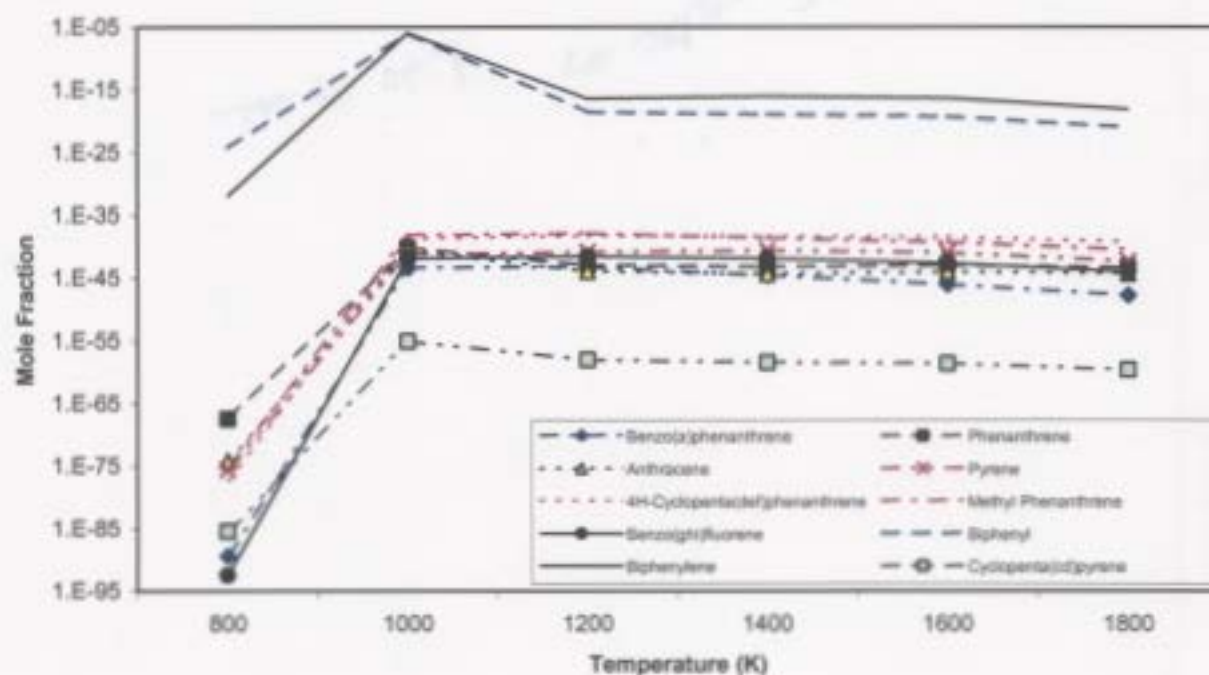


Figure 5.8. Kinetic predictions of concentrations of poly-aromatic hydrocarbon products for 14:1 air to fuel ratio, inlet flow rate of $3.28 \times 10^5 \text{ cm}^3/\text{s}$, and a temperature range of 800 K to 1800 K inside the combustion chamber during sour gas incineration.



Aromatic and poly-aromatic compounds show similar trends for increasing flow rate over the temperature of 800 K to 1800 K, but decrease in magnitude with increasing inlet flow rate. Percent reductions in composition for aromatic and poly-aromatic species with increasing flow rate are given in Table 5.2.

Table 5.2. Kinetically predicted reductions in composition (%) for aromatic and poly-aromatic species at entry of the combustion chamber under the 14:1 air to fuel ratio with increasing flow rate from $3.28 \times 10^5 \text{ cm}^3/\text{s}$ to $1.64 \times 10^6 \text{ cm}^3/\text{s}$, and temperature of 800 K.

Species	% Reduction
Benzene	99.9
Phenol	99.9
Methyl Benzene	99.9
Benzaldehyde	99.9
Hydroxyl Methyl Benzene	99.9
Ethyl Benzene	99.9
Ethenyl Benzene	99.9
Ethynyl Benzene	99.9
Dimethyl Benzene	99.9
Ethyl Methyl Benzene	99.9
Ethenyl Methyl Benzene	99.9
Naphthalene	100.0
Hydroxyl Naphthalene	99.9
Acenaphthalene	99.9
Fluorene	100.0
Fluoranthene	100.0
Indene	99.9
Methyl Indene	99.9
Methyl Naphthalene	100.0
Benzo(a)indene	100.0
Ethyl Naphthalene	99.9
Ethenyl Naphthalene	99.9
Ethynyl Naphthalene	99.9
Benzo(a)phenanthrene	100.0
Phenanthrene	100.0
Anthracene	100.0
Pyrene	100.0
4H-cylopenta(def)phenanthrene	100.0
Methyl Phenanthrene	100.0
Benzo(ghi)fluorene	100.0
Biphenyl	99.9
Biphenylene	99.9
Cyclopenta(cd)pyrene	100.0

5.1.2. Case B: 17:1 Air to Fuel Ratio Results

5.1.2.1. Introduction

The input mole fraction composition for Case B is 0.02539 CH₄, 0.00610 C₂H₆, 0.00332 C₃H₈, 0.00146 C₄H₁₀, 0.01283 H₂S, 0.00026 H₂, 0.19800 O₂, 0.00161 CO₂, 0.74210 N₂, and 0.00893 Ar. Fuel flow rates of 3.28 x 10⁵ cm³/s, 9.83 x 10⁵ cm³/s, and 1.64 x 10⁶ cm³/s are used and temperatures ranging from 800 K to 1800 K (See Table 3.2). The results from these simulations are discussed in this section.

5.1.2.2. Kinetic Predictions for Oxidation Products and Light Hydrocarbon Species

As in the results for the 14:1 air to fuel ratio, several lower weight hydrocarbons and oxidation products are predicted to form and show similar results as equilibrium predictions at the same temperature. All three flow rates yield similar trends, but slight changes in composition.

Predictions show the same temperature regions and the same product composition trends, as well as the same trends with increasing flow rates as in Case A. Table 5.3 gives the percent changes in composition for lower weight hydrocarbons and oxidation products under these conditions. Note that once again there is no change in methane and butane.

However, a decrease in composition for lower weight hydrocarbons and oxidation products is predicted as the ratio is changed from 14:1 to 17:1. Refer to Table 5.7.

Table 5.3. Kinetically predicted changes in composition (%) for lower weight hydrocarbons and oxidation products at entry of the combustion chamber under the 17:1 air to fuel ratio with increasing flow rate from $3.28 \times 10^5 \text{ cm}^3/\text{s}$ to $1.64 \times 10^6 \text{ cm}^3/\text{s}$, and a temperature of 800 K.

Species	Increase (%)	Decrease (%)
Methane	-	-
Ethane	19.4	-
Ethene	-	80.8
Ethyne	-	83.5
Propane	8.28	-
Propene	-	87.0
Propyne	-	98.4
Butane	-	-
Butene	-	98.4
Butyne	-	98.8
Butadiene	-	99.5
Butadiyne	-	99.5
Water	-	87.6
Carbon Monoxide	-	5.03
Carbon Dioxide	-	13.4

5.1.2.3. Kinetic Predictions for Sulphur-Containing Compounds

As in Case A, kinetic predictions for sulphur-containing species are similar to equilibrium predictions at the same temperature. The three flow rates tested all produce the same trends, but slight differences in magnitude. Predictions for sulphur dioxide are similar to equilibrium values over the temperature range of 800 K to 1800 K. Predictions for hydrogen sulphide, carbon sulphide and carbonyl sulphide are similar at the higher temperature levels.

Results indicate the same temperature trends, product composition trends, and varying flow rate trends. Increasing flow rate trends are somewhat different. Hydrogen sulphide increases by 6.32 %, sulphur dioxide decreases by 82.3 %, carbon sulphide

decreases by 82.8%, and carbonyl sulphide decreases by 13.4 %. As well, a decrease in magnitude for sulphur-containing species is predicted as the air to fuel ratio is increased from 14:1 to 17:1. Refer is Table 5.7.

5.1.2.4. Kinetic Predictions for Aromatic Species

As in the results for the 14:1 air to fuel ratio, many aromatic species that are predicted under equilibrium conditions are also predicted under kinetic conditions. As well, there are aromatic species predicted under kinetic conditions that were not predicted by equilibrium.

Kinetic predictions for aromatic hydrocarbons for 17:1 air to fuel ratio show the same trends as those obtained from the 14:1 air to fuel ratio. The three different flow rates tested yield the same trends, but slight changes in magnitude as in the results for Case A. Trends for initial formation of benzene, product composition, temperature region trends, poly-aromatic formation, and decreasing compositions with increasing flow rates are similar to the 14:1 air to fuel results. Percent changes in composition for aromatic and poly-aromatic species under increasing flow rate and 17:1 air to fuel conditions are given in Table 5.4. The only difference is that changing the air to fuel ratio from 14:1 to 17:1 shows a decrease in magnitude for aromatic species (See Table 5.7).

Table 5.4. Kinetically predicted reductions in composition (%) for aromatic and poly-aromatic species at entry of the combustion chamber under the 17:1 air to fuel ratio with increasing flow rate from $3.28 \times 10^5 \text{ cm}^3/\text{s}$ to $1.64 \times 10^6 \text{ cm}^3/\text{s}$, and a temperature of 800 K.

Species	% Reduction
Benzene	99.9
Phenol	99.9
Methyl Benzene	99.9
Benzaldehyde	99.9
Hydroxyl Methyl Benzene	99.9
Ethyl Benzene	99.9
Ethenyl Benzene	99.9
Ethynyl Benzene	100.0
Dimethyl Benzene	99.9
Ethyl Methyl Benzene	99.9
Ethenyl Methyl Benzene	99.9
Naphthalene	100.0
Hydroxyl Naphthalene	99.9
Acenaphthalene	99.9
Fluorene	100.0
Fluoranthene	100.0
Indene	99.9
Methyl Indene	99.9
Methyl Naphthalene	100.0
Benzo(a)indene	100.0
Ethyl Naphthalene	99.9
Ethenyl Naphthalene	99.9
Ethynyl Naphthalene	99.9
Benzo(a)phenanthrene	100.0
Phenanthrene	100.0
Anthracene	100.0
Pyrene	100.0
4H-cylopenta(def)phenanthrene	100.0
Methyl Phenanthrene	100.0
Benzo(ghi)fluorene	100.0
Biphenyl	99.9
Biphenylene	99.9
Cyclopenta(cd)pyrene	100.0

5.1.3. Case C: 21:1 Air to Fuel Ratio Results

5.1.3.1. Introduction

The input mole fraction composition for the 21:1 air to fuel ratio is 0.02078 CH₄, 0.00499 C₂H₆, 0.00272 C₃H₈, 0.00122 C₄H₁₀, 0.01049 H₂S, 0.00021 H₂, 0.20009 O₂, 0.00138 CO₂, 0.74912 N₂, and 0.00900 Ar. As before, air to fuel flow rates are calculated based on fuel flow rates of 3.28×10^5 cm³/s, 9.83×10^5 cm³/s, and 1.64×10^6 cm³/s and temperatures ranging from 800 to 1800 K (See Table 3.2).

5.1.3.2. Kinetic Predictions for Oxidation Products and Light Hydrocarbon Species

As in the results from case A and case B, many light hydrocarbon species and oxidation products are predicted to form. Several of these species yield similar results as equilibrium predictions at the same temperatures. As well, all three flow rates yield similar trends, but slightly different changes in species composition.

Predictions for lower weight hydrocarbons and oxidation products under these conditions show no distinct difference from those results of the previous two ratios. Lower weight hydrocarbon and oxidation product compositions decrease when changing the air to fuel ratio from 14:1 to 21:1 (See Table 5.7). Percent changes in composition for lower weight hydrocarbons and oxidation products under increasing flow rate are given in Table 5.5. Note that there is no change for methane and butane.

Table 5.5. Kinetically predicted changes in composition (%) for lower weight hydrocarbons and oxidation products at entry of the combustion chamber under the 21:1 air to fuel ratio with increasing flow rate from $3.28 \times 10^5 \text{ cm}^3/\text{s}$ to $1.64 \times 10^6 \text{ cm}^3/\text{s}$, and a temperature of 800 K.

Species	Increase (%)	Decrease (%)
Methane	-	-
Ethane	6.14	-
Ethene	-	84.1
Ethyne	-	87.0
Propane	-	5.26
Propene	-	93.3
Propyne	-	99.7
Butane	-	-
Butene	-	99.4
Butyne	-	98.2
Butadiene	-	99.6
Butadiyne	-	99.4
Water	-	93.3
Carbon Monoxide	-	3.70
Carbon Dioxide	-	3.74

5.1.3.3. Kinetic Predictions for Sulphur-Containing Compounds

Kinetic predictions for sulphur-containing species are much the same as equilibrium predictions at the same temperature. As well, the three flow rates tested all produce the same overall trends, but slight differences in magnitude. These predictions are the same as those from case A and B in terms of comparison between kinetic and equilibrium results, temperature regions, flow rate trends, and product composition trends. Increasing the flow rate results in 2.09 % increase for hydrogen sulphide, 82.1 % decrease for sulphur dioxide, 85.0 % decrease for carbon sulphide, and 34.7 % decrease for carbonyl sulphide. In addition, Table 5.7 shows a decreasing trend for all major sulphur-containing species, including hydrogen sulphide, sulphur dioxide, carbon sulphide, and carbonyl sulphide, when as the air to fuel ratio is increased.

5.1.3.4. Kinetic Predictions for Aromatic Species

As in the results from case A and B, many aromatic species that are predicted under equilibrium conditions are predicted under kinetic conditions and aromatic species form under kinetic conditions, but not under equilibrium.

Kinetic predictions for aromatic hydrocarbons are similar to equilibrium predictions for those species, especially at higher temperatures. As well, the three flow rates tested all yield similar trends, but slight changes in composition. Trends for the initial formation of benzene, poly-aromatic formation, product composition trends, temperature trends, and inlet flow rate trends are similar to those obtained from 14:1 and 17:1 air to fuel ratios. However, the percent reductions in composition for increasing flow rates are slightly different than previous results. These results are shown in Table 5.6. The trend of decreasing species composition for aromatic species when changing the air to fuel ratio from 14:1 to 21:1 is the same as previous results. The most significant reductions are found amongst aromatic species. See Table 5.7.

Table 5.6. Kinetically predicted reductions in composition (%) for aromatic and poly-aromatic species at entry of the combustion chamber under the 21:1 air to fuel ratio with increasing flow rate from $3.28 \times 10^5 \text{ cm}^3/\text{s}$ to $1.64 \times 10^6 \text{ cm}^3/\text{s}$, and a temperature of 800 K.

Species	% Reduction
Benzene	99.9
Phenol	99.9
Methyl Benzene	99.9
Benzaldehyde	99.9
Hydroxyl Methyl Benzene	99.9
Ethyl Benzene	99.9
Ethenyl Benzene	99.9
Ethynyl Benzene	99.9
Dimethyl Benzene	100.0
Ethyl Methyl Benzene	100.0
Ethenyl Methyl Benzene	100.0
Naphthalene	100.0
Hydroxyl Naphthalene	100.0
Acenaphthalene	100.0
Fluorene	100.0
Fluoranthene	100.0
Indene	100.0
Methyl Indene	100.0
Methyl Naphthalene	100.0
Benzo(a)indene	100.0
Ethyl Naphthalene	100.0
Ethenyl Naphthalene	100.0
Ethynyl Naphthalene	100.0
Benzo(a)phenanthrene	100.0
Phenanthrene	100.0
Anthracene	100.0
Pyrene	100.0
4H-cylopenta(def)phenanthrene	100.0
Methyl Phenanthrene	100.0
Benzo(ghi)fluorene	100.0
Biphenyl	99.9
Biphenylene	99.9
Cyclopenta(cd)pyrene	100.0

Table 5.7. Kinetically predicted reductions in composition (%) for species at entry of the combustion chamber under three tested flow rates (a). $3.28 \times 10^5 \text{ cm}^3/\text{s}$, (b). $9.83 \times 10^5 \text{ cm}^3/\text{s}$, and (c). $1.64 \times 10^6 \text{ cm}^3/\text{s}$, when ranging air to fuel ratio from 14:1 to 21:1 and a temperature of 800 K.

Species	Flow Rate (a)	Flow Rate (b)	Flow Rate (c)
Methane	31.2	31.6	31.6
Ethane	13.8	26.2	28.7
Ethene	81.1	84.9	85.3
Ethyne	91.1	93.6	93.3
Propane	24.5	29.6	30.6
Propene	87.8	93.7	94.4
Propyne	99.1	99.8	99.9
Butane	31.4	31.4	31.5
Butene	99.2	99.7	99.8
Butyne	98.9	98.1	98.0
Butadiene	99.9	99.9	99.9
Butadiyne	99.8	99.8	99.7
Water	89.4	94.3	94.9
Carbon Monoxide	64.0	55.1	59.3
Carbon Dioxide	36.9	29.5	27.9
Hydrogen Sulphide	26.3	30.1	30.8
Sulphur Dioxide	89.1	89.6	89.5
Carbon Sulphide	99.7	99.7	99.8
Carbonyl Sulphide	53.4	54.0	63.3
Benzene	99.9	99.9	99.9
Phenol	99.9	99.9	99.9
Methyl Benzene	99.9	99.9	99.9
Benzaldehyde	99.9	99.9	99.9
Hydroxyl Methyl Benzene	99.9	99.9	99.9
Ethyl Benzene	99.9	99.9	99.9
Ethenyl Benzene	99.9	99.9	99.9

Table 5.7 (Continued)

Species	Flow Rate (a)	Flow Rate (b)	Flow Rate (c)
Ethynyl Benzene	99.9	99.9	99.9
Dimethyl Benzene	100.0	100.0	100.0
Ethyl Methyl Benzene	100.0	100.0	100.0
Ethenyl Methyl Benzene	100.0	100.0	100.0
Naphthalene	100.0	100.0	100.0
Hydroxyl Naphthalene	100.0	100.0	100.0
Acenaphthalene	100.0	100.0	100.0
Fluorene	100.0	100.0	100.0
Fluoranthene	100.0	100.0	100.0
Indene	99.9	100.0	100.0
Methyl Indene	100.0	100.0	100.0
Methyl Naphthalene	100.0	100.0	100.0
Benzo(a)indene	100.0	100.0	100.0
Ethyl Naphthalene	100.0	100.0	100.0
Ethenyl Naphthalene	100.0	100.0	100.0
Ethynyl Naphthalene	100.0	100.0	100.0
Benzo(a)phenanthrene	100.0	100.0	100.0
Phenanthrene	100.0	100.0	100.0
Anthracene	100.0	100.0	100.0
Pyrene	100.0	100.0	100.0
4H-cylopenta(def)phenanthrene	100.0	100.0	100.0
Methyl Phenanthrene	100.0	100.0	100.0
Benzo(ghi)fluorene	100.0	100.0	100.0
Biphenyl	99.9	99.9	99.9
Biphenylene	99.9	99.9	99.9
Cyclopenta(cd)pyrene	100.0	100.0	100.0

5.2. *Incinerator Stack Calculations*

5.2.1. **Case A: 14:1 Air to Fuel Ratio Results**

5.2.1.1. **Introduction**

The input mole fractions used in these simulations are the output mole fractions of combustion chamber calculations. The output of the combustion chamber were based on results of the 14:1 air to fuel ratio and the three flow rates outlined in previous sections. In this phase, three linear temperature profiles with initial input temperatures of 1623 K, 1400 K, and 1000 K at entry of stack are used to calculate mole fraction compositions of species at varying locations within the stack. The linear temperature profile is based on approximate heat transfer calculations and data from Questor Incineration Technologies. The temperature profiles are outlined below:

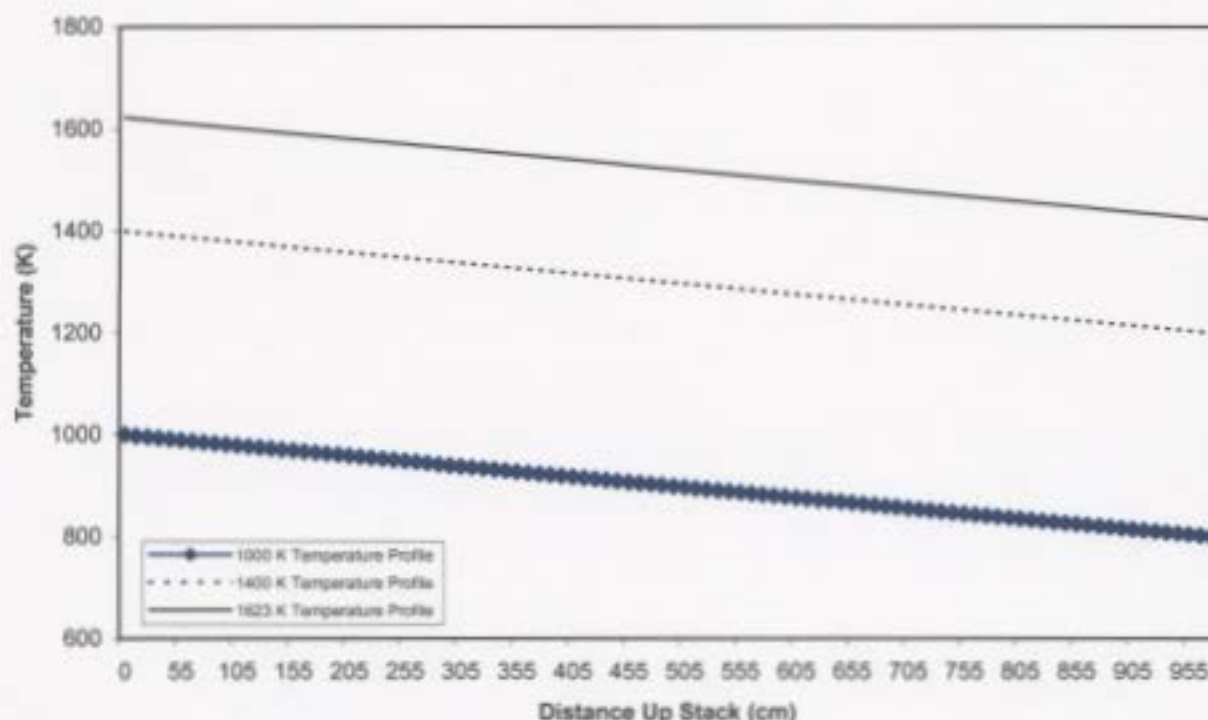
$$T = -0.20513L + 1623 \quad (5.1)$$

$$T = -0.20513L + 1400 \quad (5.2)$$

$$T = -0.20513L + 1000 \quad (5.3)$$

where T is the temperature in kelvins and L is the length of the stack ranging from 0 to 975 cm at the top of the stack. Figure 5.9 represents the temperature profiles as a function as distance up the stack.

Figure 5.9. Temperature profiles as a function of distance (cm) up the stack used in incineration stack calculations.



5.2.1.2. Oxidation Products and Light Hydrocarbon Species Results

5.2.1.2.1. Kinetic Results for 1000 K Temperature Profile

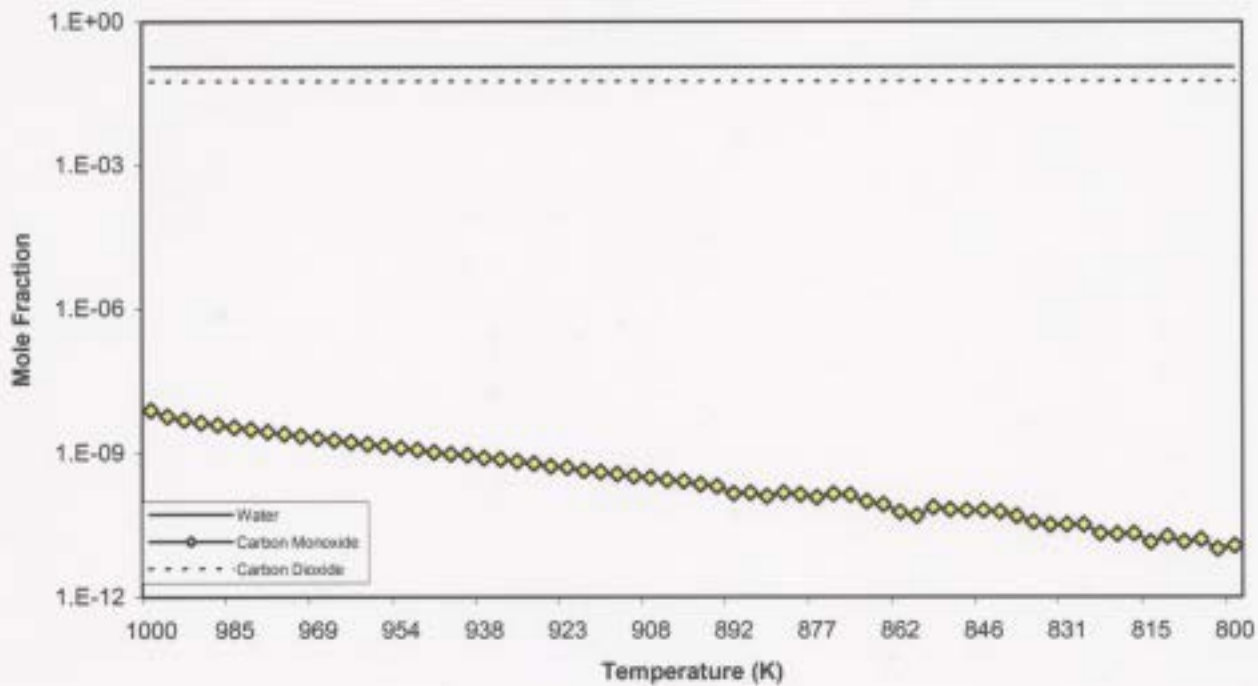
Kinetic predictions show compositions for oxidation products and light hydrocarbon species within the stack have similar trends for varying flow rates, but differences in magnitude as the inlet flow rate is increased. Figure 5.10 indicates that lower weight hydrocarbon species decrease during the cooling process. As well, all lower weight hydrocarbons are reduced as the inlet flow rate is increased. As in the combustion chamber, the most abundant light hydrocarbons present are butane, ethyne, and methane. Methane has the most significant average decrease in composition by over

99.4 % as the gases are cooled, whereas compositions for butane, water, and carbon dioxide decreased insignificantly. Figure 5.11 show that compositions of carbon monoxide decreased by an average significant amount of 99 % as the temperature decreased toward the top of the stack. Kinetically predicted reductions for lower weight hydrocarbons and oxidation products during cooling are shown in Table 5.8.

Table 5.8. Kinetically predicted reductions (%) in compositions from inlet lower weight hydrocarbons and oxidation products in the stack during cooling under the conditions of 14:1 air to fuel ratio, 1000 K temperature profile, and varying flow rates of (a). $3.28 \times 10^5 \text{ cm}^3/\text{s}$, (b). $9.83 \times 10^5 \text{ cm}^3/\text{s}$, and (c). $1.64 \times 10^6 \text{ cm}^3/\text{s}$.

Species	Flow Rate (a)	Flow Rate (b)	Flow Rate (c)
Methane	99.6	99.6	99.0
Ethane	96.8	94.3	57.1
Ethene	95.6	97.4	90.5
Ethyne	91.7	35.3	35.3
Propane	99.1	99.6	93.5
Propene	99.5	99.7	32.4
Propyne	99.8	99.9	92.2
Butane	-	-	-
Butene	95.5	94.5	96.3
Butyne	96.5	82.1	99.4
Butadiene	98.4	99.2	20.7
Butadiyne	98.8	99.8	89.4
Water	-	-	-
Carbon Monoxide	99.8	99.3	90.2
Carbon Dioxide	-	-	-

Figure 5.11. Kinetic predictions of concentrations of oxidation products for 14:1 air to fuel ratio, 1000 K temperature profile, and an inlet flow rate of $3.28 \times 10^5 \text{ cm}^3/\text{s}$ inside the incinerator stack during sour gas incineration.



In addition, compositions for butane, water, and carbon dioxide do not change significantly as inlet flow rates are increased, and carbon monoxide compositions increase with increasing flow rate by 2.3 %. Propane has the most significant reduction by 97.7% as inlet flow rates are increased. Percent reductions in compositions for due to increasing flow rates are shown in Table 5.9.

Table 5.9. Kinetically predicted changes in composition (%) for lower weight hydrocarbons and oxidation products within the stack under the 1000 K temperature profile, 14:1 air to fuel ratio with increasing flow rate from $3.28 \times 10^5 \text{ cm}^3/\text{s}$ to $1.64 \times 10^6 \text{ cm}^3/\text{s}$.

Species	% Increase	% Decrease
Methane	-	53.1
Ethane	-	55.7
Ethene	-	15.8
Ethyne	-	77.3
Propane	-	97.7
Propene	-	43.7
Propyne	-	90.3
Butane	-	-
Butene	-	68.4
Butyne	-	22.7
Butadiene	-	92.8
Butadiyne	-	93.5
Water	-	-
Carbon Monoxide	2.3	-
Carbon Dioxide	-	-

5.2.1.2.2. Kinetic Results for 1400 K Temperature Profile

Results with an exit combustion chamber temperature of 1400 K yield similar results as the 1000 K case. Compositions for oxidation products and light hydrocarbon species within the stack have similar trends for varying flow rates, but differences in magnitude.

Predictions indicate the same cooling trends, and the same product composition trends as the 1000 K case. Calculation results for percent reductions during cooling are given in Table 5.10. Figure 5.12 shows that butadiene and butadiyne both have the most significant reductions during cooling by 99.9 % and butane, water, and carbon dioxide have no significant reduction.

Table 5.10. Kinetically predicted reductions (%) in compositions from inlet lower weight hydrocarbons and oxidation products in the stack during cooling under the conditions of 14:1 air to fuel ratio, 1400 K temperature profile, and varying flow rates of (a). 3.28×10^5 cm³/s, (b). 9.83×10^5 cm³/s, and (c). 1.64×10^6 cm³/s.

Species	Flow Rate (a)	Flow Rate (b)	Flow Rate (c)
Methane	97.2	94.8	91.6
Ethane	78.0	99.9	91.2
Ethene	97.2	96.5	96.2
Ethyne	86.3	77.8	72.4
Propane	95.4	98.2	99.0
Propene	99.0	98.7	97.4
Propyne	98.7	95.9	97.0
Butane	-	-	-
Butene	64.9	95.0	95.7
Butyne	82.0	98.9	99.2
Butadiene	99.9	99.9	99.9
Butadiyne	99.9	99.9	99.9
Water	-	-	-
Carbon Monoxide	98.3	98.3	98.3
Carbon Dioxide	-	-	-

These results also indicate similar trends for inlet flow rate changes as the results from the 1000 K case. Most trends are the same, but in this case there is no change for butane, butadiyne, carbon monoxide, carbon dioxide, and water. Table 5.11 indicates propane has the most significant reduction by 97.3 % as inlet flow rates are increased.

Figure 5.12. Kinetic predictions of concentrations of lower weight hydrocarbon products for 14:1 air to fuel ratio, 1400 K temperature profile, and an inlet flow rate of $3.28 \times 10^5 \text{ cm}^3/\text{s}$ inside the incinerator stack during sour gas incineration.

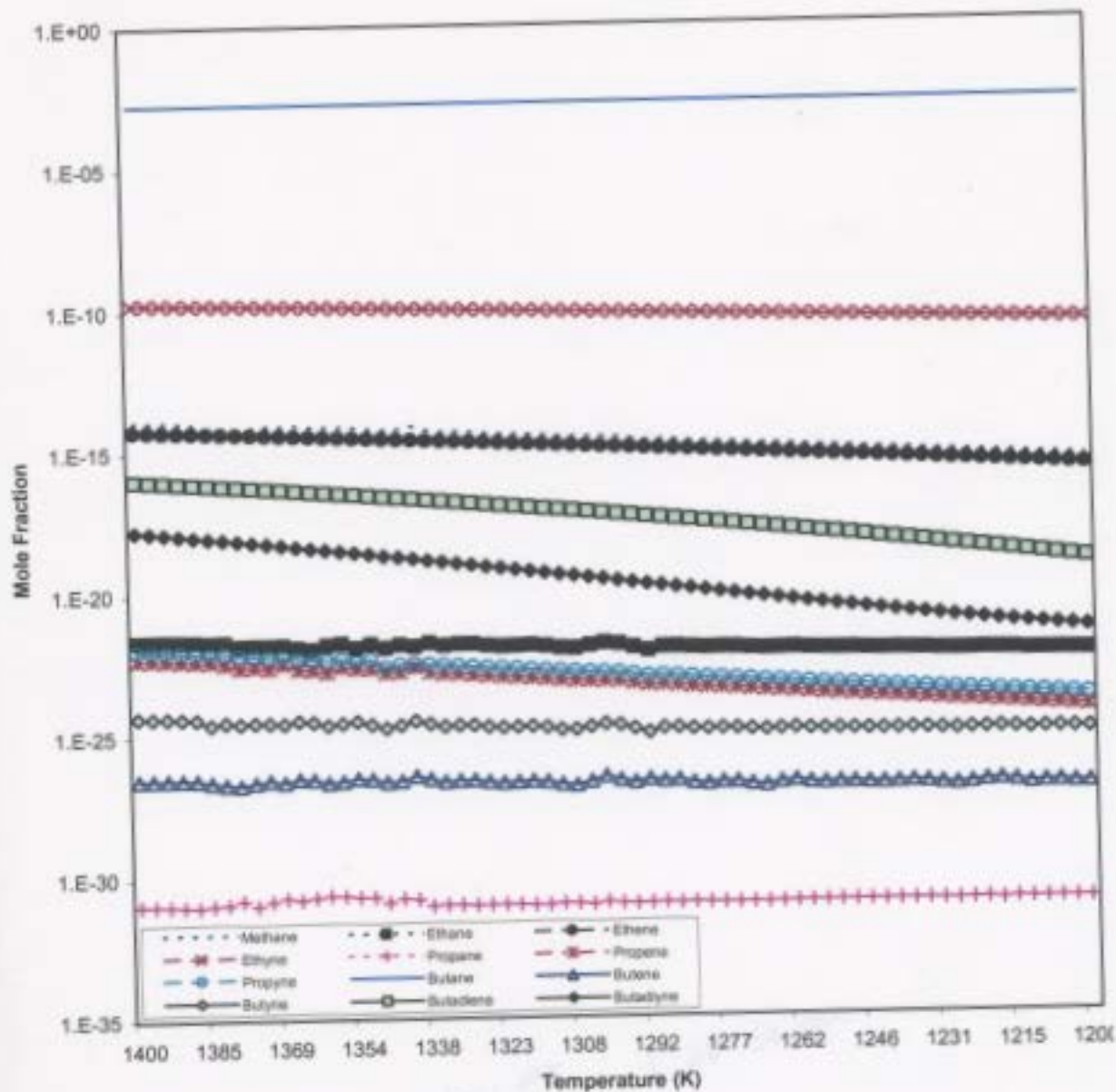


Table 5.11. Kinetically predicted changes in composition (%) for lower weight hydrocarbons and oxidation products within the stack under the 1400 K temperature profile, 14:1 air to fuel ratio with increasing flow rate from $3.28 \times 10^5 \text{ cm}^3/\text{s}$ to $1.64 \times 10^6 \text{ cm}^3/\text{s}$.

Species	% Increase	% Decrease
Methane	-	39.8
Ethane	-	22.6
Ethene	-	2.27
Ethyne	-	3.22
Propane	-	97.3
Propene	-	43.7
Propyne	-	90.3
Butane	-	-
Butene	-	39.6
Butyne	-	89.5
Butadiene	-	2.75
Butadiyne	-	-
Water	-	-
Carbon Monoxide	-	-
Carbon Dioxide	-	-

5.2.1.2.3. Kinetic Results for 1623 K Temperature Profile

As in the last two temperature profiles, compositions for oxidation products and light hydrocarbon species within the stack have similar trends for varying flow rates and changes in magnitude when flow rates are increased.

Kinetic results show similar trends when compared to temperature profiles of 1400 K and 1000 K. Table 5.12 shows that butadiyne has the most significant decrease in composition by 99.7 % during cooling, whereas the compositions for butane, water, and carbon dioxide have no significant reductions.

Table 5.12. Kinetically predicted reductions (%) in compositions from inlet lower weight hydrocarbons and oxidation products in the stack during cooling under the conditions of 14:1 air to fuel ratio, 1623 K temperature profile, and varying flow rates of (a). 3.28×10^5 cm³/s, (b). 9.83×10^5 cm³/s, and (c). 1.64×10^6 cm³/s.

Species	Flow Rate (a)	Flow Rate (b)	Flow Rate (c)
Methane	90.1	89.2	88.5
Ethane	78.9	77.9	76.4
Ethene	92.2	91.1	90.6
Ethyne	73.0	73.2	72.6
Propane	94.5	93.4	92.5
Propene	93.7	93.2	92.6
Propyne	96.6	96.6	96.4
Butane	-	-	-
Butene	70.0	69.6	67.8
Butyne	98.3	98.3	98.4
Butadiene	98.2	98.0	98.0
Butadiyne	99.7	99.7	99.7
Water	-	-	-
Carbon Monoxide	92.7	92.7	92.6
Carbon Dioxide	-	-	-

The overall composition trends when increasing the flow rate are similar to previous results for temperature profiles of 1000 K and 1400 K. The difference is that in this case, carbon monoxide decreases with increasing inlet flow rate. Table 5.13 gives the percent changes in composition with increasing flow rate for lower weight hydrocarbons and oxidation products of the temperature profile of 1623 K. Note that propane has the most significant reduction by 71.9 % as inlet flow rates are increased.

Table 5.13. Kinetically predicted changes in composition (%) for lower weight hydrocarbons and oxidation products within the stack under the 1623 K temperature profile, 14:1 air to fuel ratio with increasing flow rate from $3.28 \times 10^5 \text{ cm}^3/\text{s}$ to $1.64 \times 10^6 \text{ cm}^3/\text{s}$.

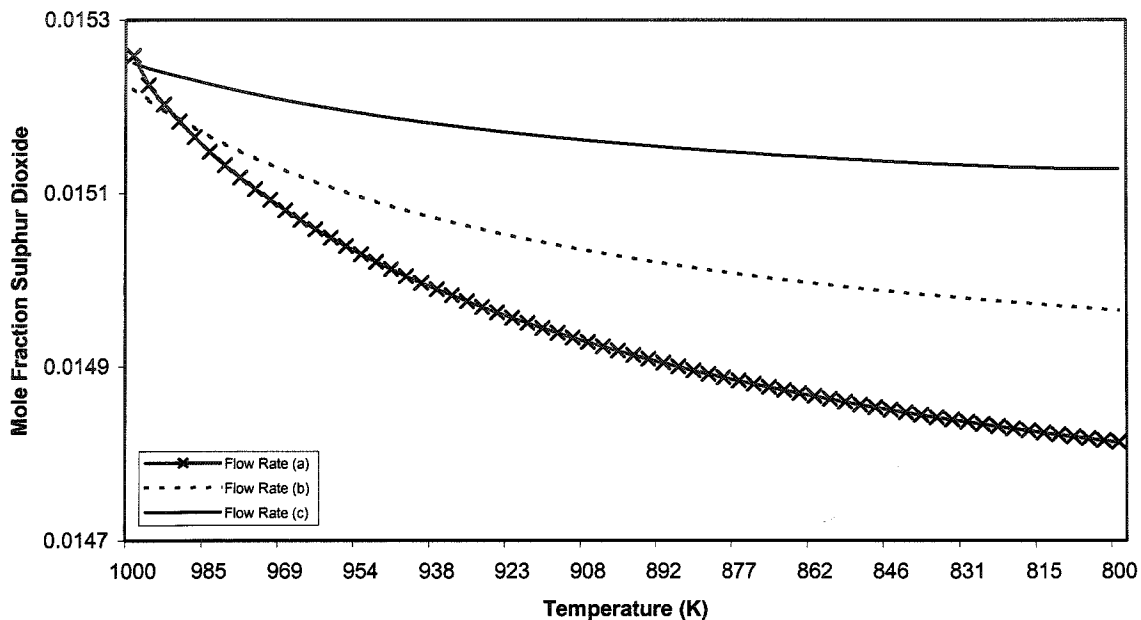
Species	% Increase	% Decrease
Methane	-	58.1
Ethane	-	50.4
Ethene	-	25.4
Ethyne	-	36.5
Propane	-	71.9
Propene	-	56.8
Propyne	-	62.9
Butane	-	-
Butene	-	48.6
Butyne	-	29.7
Butadiene	-	5.34
Butadiyne	-	20.7
Water	-	-
Carbon Monoxide	-	25.0
Carbon Dioxide	-	-

5.2.1.3. Sulphur-Containing Species Results

5.2.1.3.1. Kinetic Results for 1000 K Temperature Profile

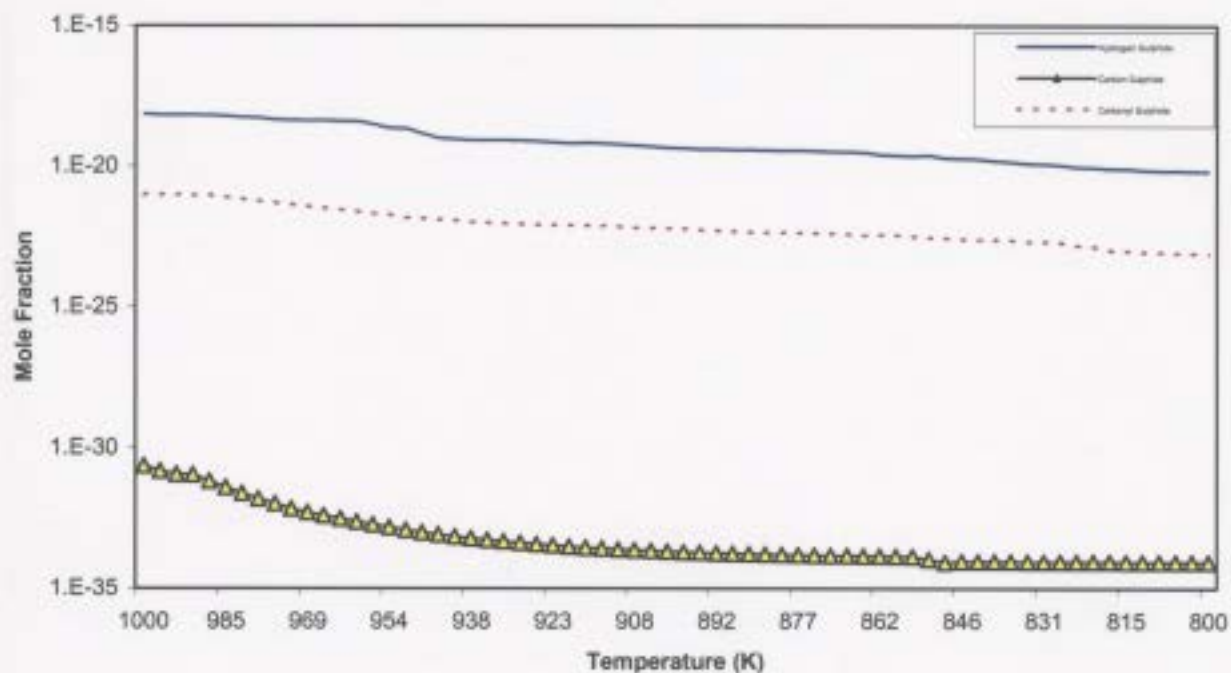
Like previous results, kinetic predictions for sulphur-containing species within the stack have similar trends for varying flow rates, and changes in composition magnitude when flow rates are increased. Predictions show that compositions for all species decrease during the cooling process and with the exception of sulphur dioxide, all species increase as the inlet flow rates are increased. This is shown in Figures 5.13 and 5.14.

Figure 5.13. Kinetic predictions of concentrations of sulphur dioxide for 14:1 air to fuel ratio, 1000 K temperature profile, and varying inlet flow rates inside the incinerator stack during sour gas incineration. **(a)**. Inlet flow rate = $3.28 \times 10^5 \text{ cm}^3/\text{s}$, **(b)**. Inlet flow rate = $9.83 \times 10^5 \text{ cm}^3/\text{s}$ **(c)**. Inlet flow rate = $1.64 \times 10^6 \text{ cm}^3/\text{s}$.



The most abundant species is sulphur dioxide and least abundant species is carbon sulphide. Carbonyl sulphide compositions decrease the most during cooling by over 98%, hydrogen sulphide decreases by 97%, carbon sulphide decreases by 95%, and sulphur dioxide decreases by 1.8 %. These results are in agreement with theory as the strongest oxidizing species (carbonyl sulphide) is consumed faster because it is the most reactive. Hydrogen sulphide and carbonyl sulphide increase by 99.9 %, carbon sulphide by 98.5 %, and sulphur dioxide did not increase significantly as the flow rate is increased.

Figure 5.14. Kinetic predictions of concentrations of sulphur-containing species for 14:1 air to fuel ratio, 1000 K temperature profile, and an inlet flow rate of $3.28 \times 10^5 \text{ cm}^3/\text{s}$ inside the incinerator stack during sour gas incineration.



5.2.1.3.2. Kinetic Results for 1400 K Temperature Profile

The results for the 1400 K temperature profile are similar to the results of the temperature profile of 1000 K. During cooling, there is a 99% decrease in composition for hydrogen sulphide, carbon sulphide, and carbonyl sulphide, and only 1.90% reduction for sulphur dioxide. The most abundant species present is sulphur dioxide. Some sulphur-containing species compositions are predicted to increase with increasing flow rate; hydrogen sulphide increases by 73.5 % and 1.44 % for carbon sulphide. Carbonyl sulphide and sulphur dioxide do not increase significantly.

5.2.1.3.3. Kinetic Results for 1623 K Temperature Profile

Kinetic predictions for the initial internal combustion temperature profile of 1623 K show similar trends for varying flow rates. Results are similar to those obtained from

the 1400 K and 1000 K temperature profiles, with the exception that sulphur-containing species compositions are predicted to decrease with increasing inlet flow rate; hydrogen sulphide decreases by 30.3 %, 29.5 % for carbonyl sulphide, 27.2 % for carbon sulphide, and no change for sulphur dioxide. Composition reductions during cooling are over 99% for hydrogen sulphide, carbon sulphide, and carbonyl sulphide, and no significant change for sulphur dioxide. The most abundant species present is sulphur dioxide. Results are shown in Figures 5.15 and 5.16.

Figure 5.15. Kinetic predictions of concentrations of sulphur dioxide for 14:1 air to fuel ratio, 1623 K temperature profile, and varying inlet flow rates inside the incinerator stack during sour gas incineration. **(a)**. Inlet flow rate = $3.28 \times 10^5 \text{ cm}^3/\text{s}$, **(b)**. Inlet flow rate = $9.83 \times 10^5 \text{ cm}^3/\text{s}$ **(c)**. Inlet flow rate = $1.64 \times 10^6 \text{ cm}^3/\text{s}$.

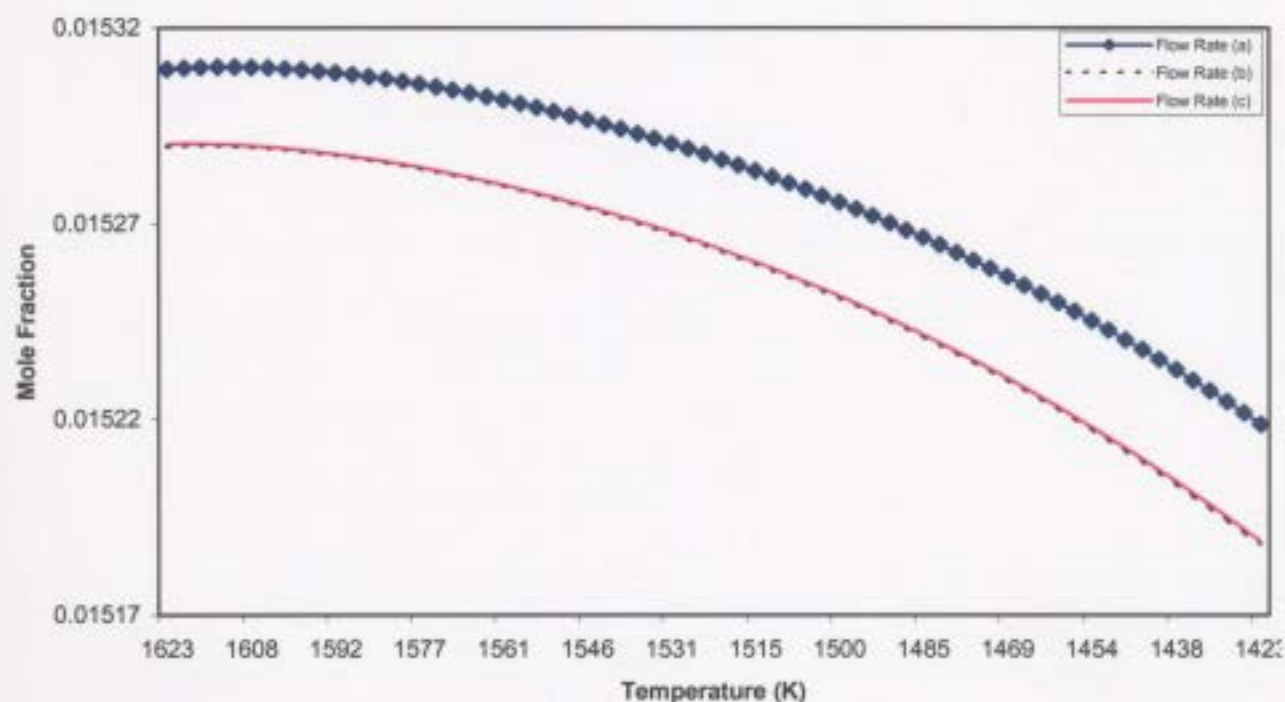
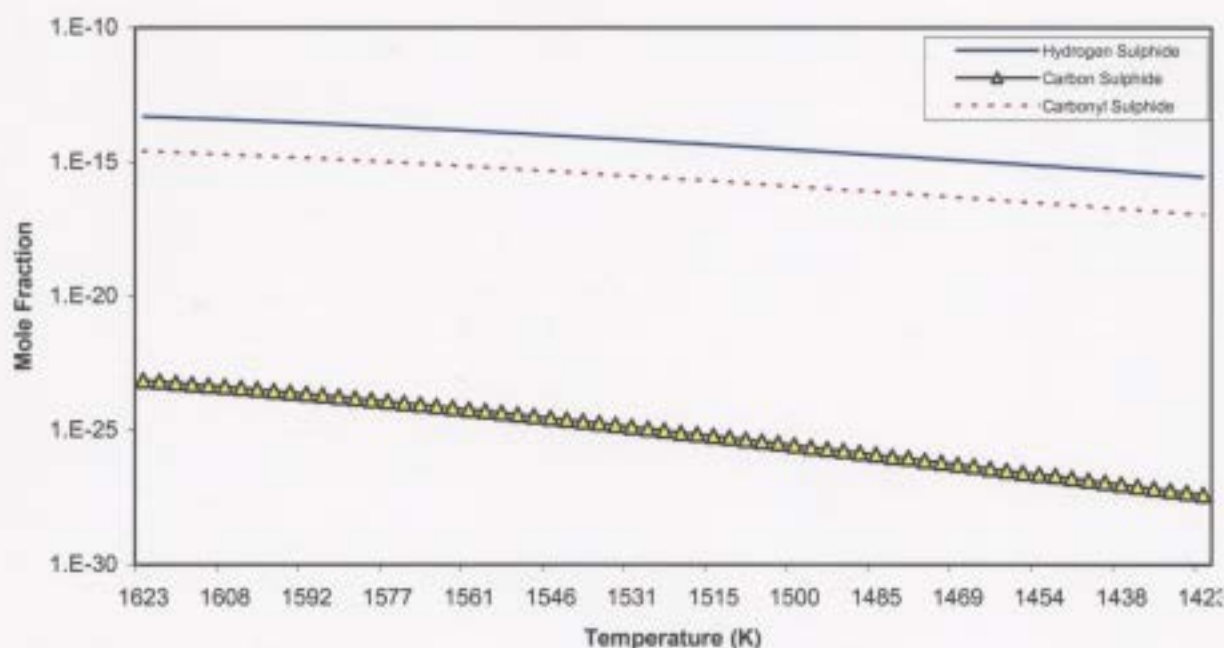


Figure 5.16. Kinetic predictions of concentrations of sulphur-containing species for 14:1 air to fuel ratio, 1623 K temperature profile, and an inlet flow rate of $3.28 \times 10^5 \text{ cm}^3/\text{s}$ inside the incinerator stack during sour gas incineration.



5.2.1.4. Aromatic and Poly-Aromatic Hydrocarbon Results

As mentioned in Chapter 2, the formation of the first aromatic ring initiates poly-aromatic formation. Previous studies have indicated that the majority of poly-aromatic species are formed during the cooling stage of gases in incineration procedures (Marinov *et al*, 1996; Chagger *et al*, 1997).

5.2.1.4.1. Kinetic Results for 1000 K Temperature Profile

Kinetic compositions for single ring aromatic species decrease during the cooling process inside the incineration stack as the temperature decreases. This is to be expected because these species are being consumed by reactions that are producing poly-aromatic species as the temperature decreases toward the top of the stack. In this case, the most abundant species present is phenol and the least abundant is ethenyl methyl benzene.

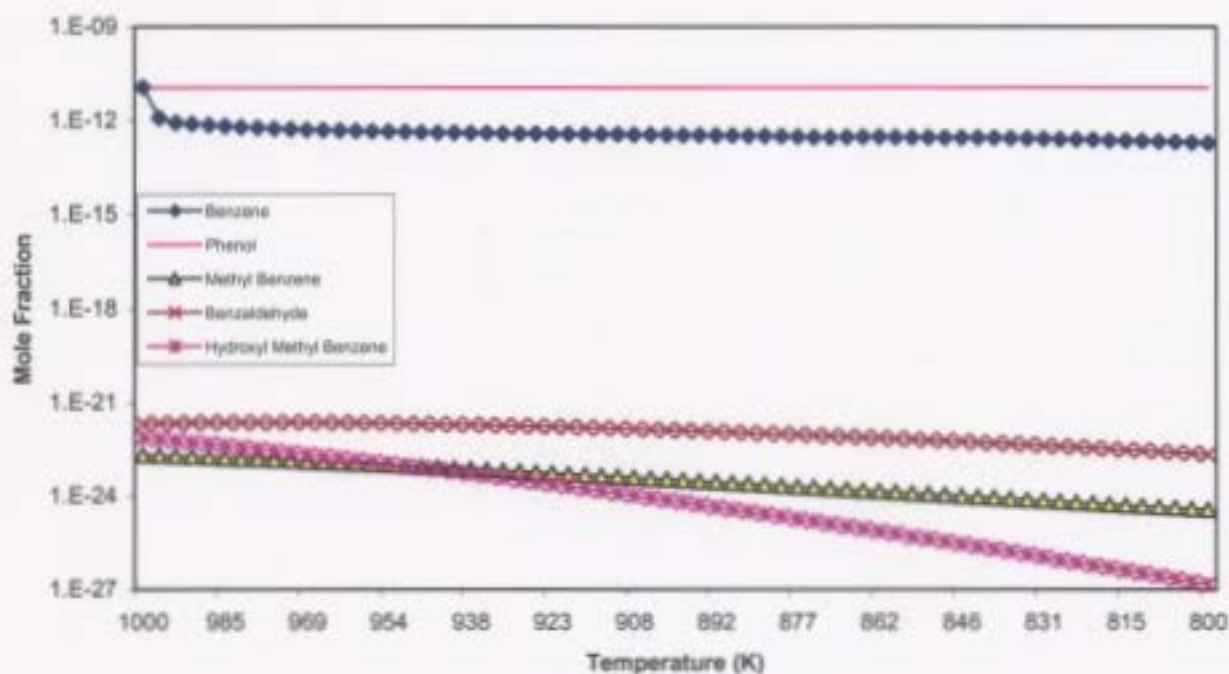
Figure 5.17 shows that majority of these species' compositions decrease significantly as the temperature is decreased. Table 5.14 shows that the most significant reduction in composition during cooling is for methyl benzene by 99.1 %. Kinetic compositions for phenol are not significantly reduced.

Table 5.14. Kinetically predicted reductions (%) in compositions from inlet for single ring aromatic species in the stack during cooling under the conditions of 14:1 air to fuel ratio, 1000 K temperature profile, and varying flow rates of (a). $3.28 \times 10^5 \text{ cm}^3/\text{s}$, (b). $9.83 \times 10^5 \text{ cm}^3/\text{s}$, and (c). $1.64 \times 10^6 \text{ cm}^3/\text{s}$.

Aromatic Species	Flow Rate (a)	Flow Rate (b)	Flow Rate (c)
Benzene	98.3	96.0	95.2
Phenol	-	-	-
Methyl Benzene	98.3	99.9	98.9
Benzaldehyde	89.4	99.9	99.9
Hydroxyl Methyl Benzene	99.9	99.5	88.7
Ethyl Benzene	98.6	94.5	95.4
Ethenyl Benzene	35.8	58.3	67.7
Ethynyl Benzene	98.9	9.06	12.6
Dimethyl Benzene	65.5	67.6	57.9
Ethyl Methyl Benzene	99.7	96.8	93.1
Ethenyl Methyl Benzene	88.4	97.8	93.3

The compositions for these species are also dependent upon inlet flow rate. Table 5.15 shows changes in composition for single ring aromatic species as inlet flow rates are increased. Ethyl methyl benzene shows the most significant reduction in composition by 100 % and ethyl benzene and ethenyl benzene shows the most significant increase in composition by 99.9 % as flow rates are increased.

Figure 5.17. Kinetic predictions of concentrations of single ring aromatic species for 14:1 air to fuel ratio, 1000 K temperature profile, and varying inlet flow rates inside the incinerator stack during sour gas incineration. **(a).** Inlet flow rate = $3.28 \times 10^5 \text{ cm}^3/\text{s}$, **(b).** Inlet flow rate = $9.83 \times 10^5 \text{ cm}^3/\text{s}$ **(c).** Inlet flow rate = $1.64 \times 10^6 \text{ cm}^3/\text{s}$.



(a)

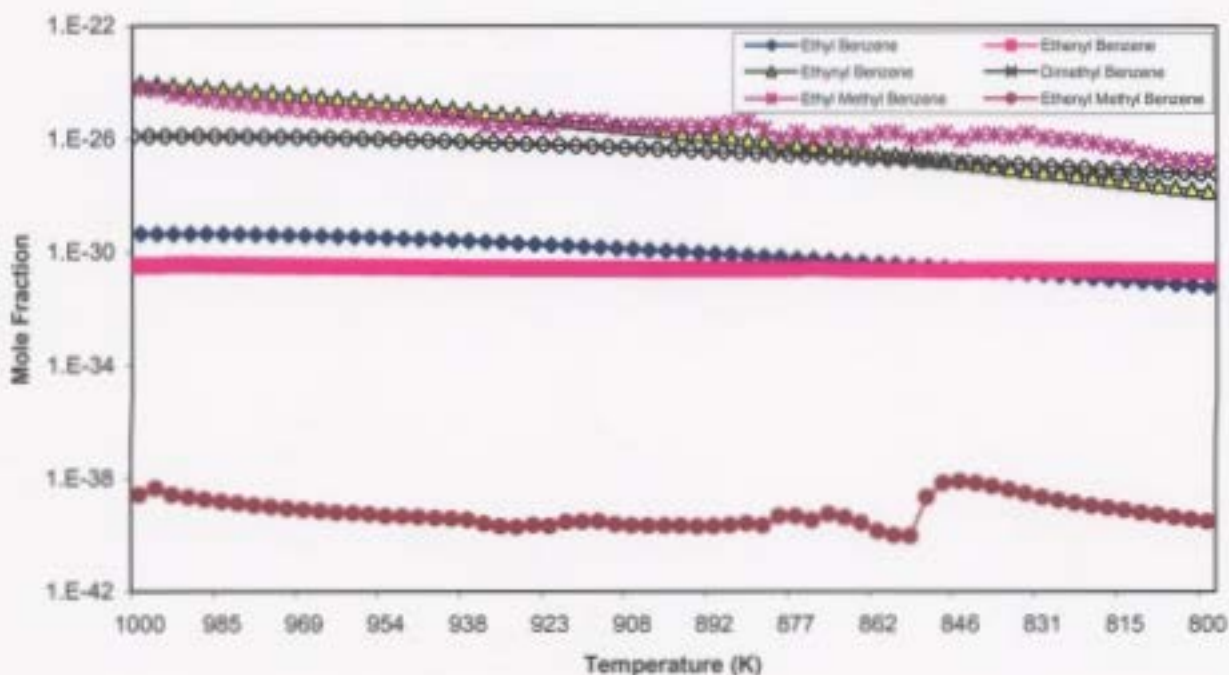
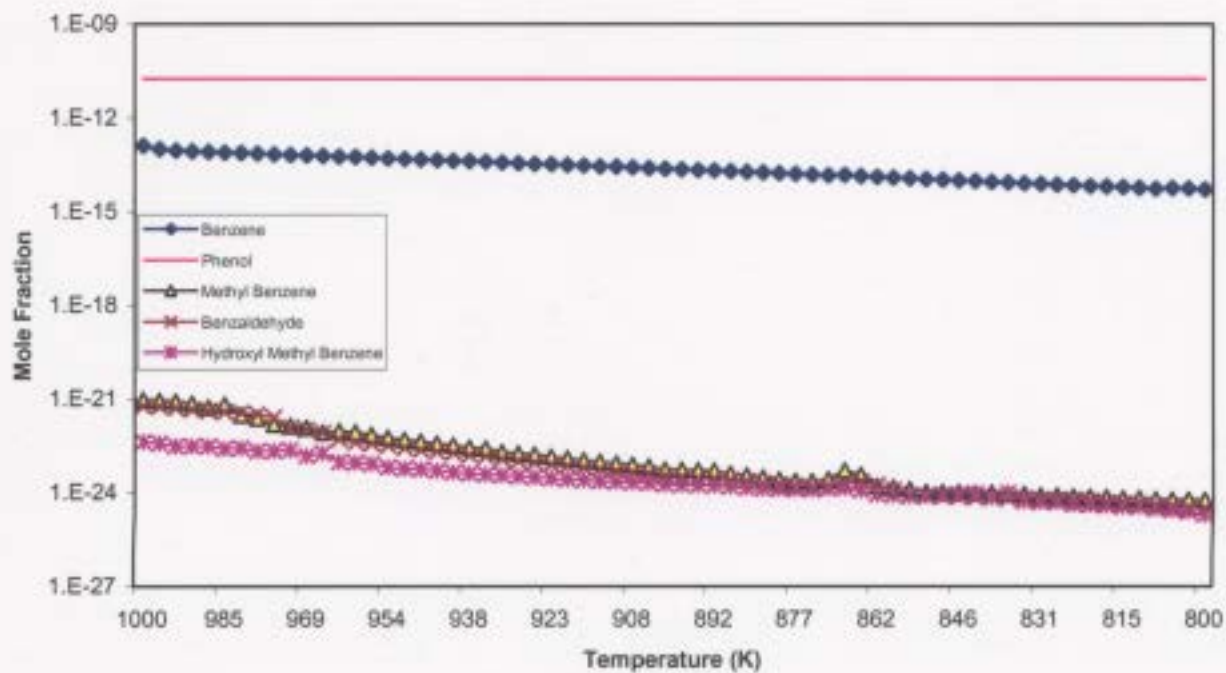


Figure 5.17 (Continued)



(b)

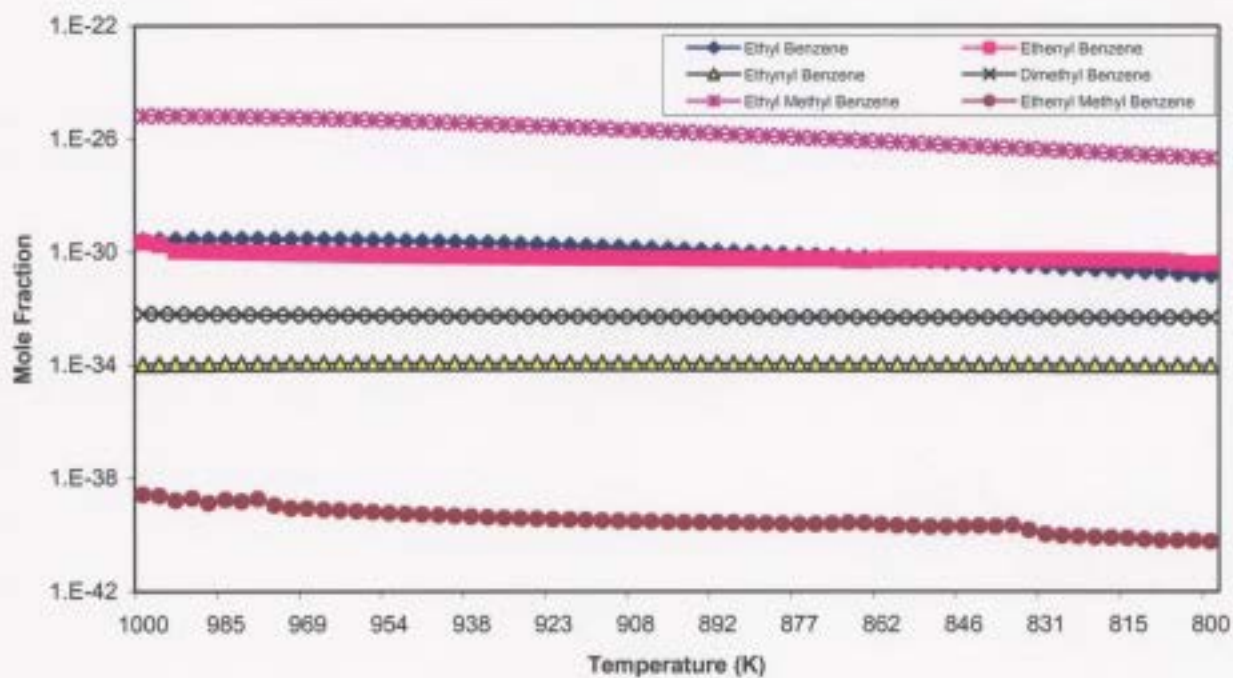
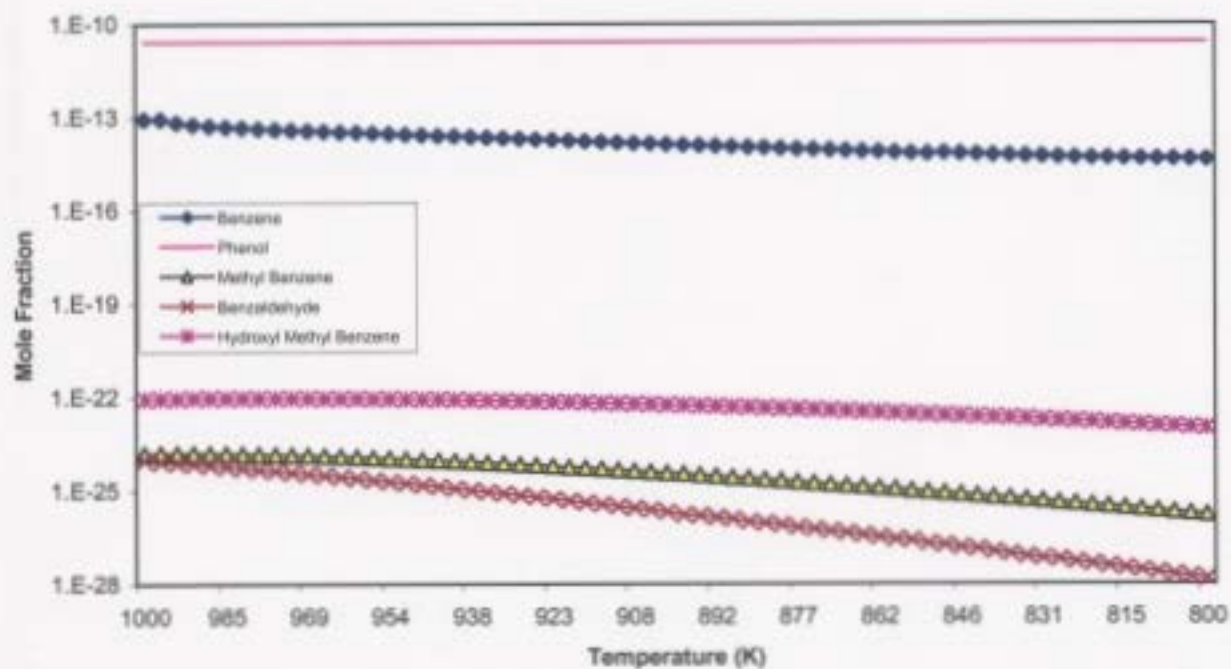


Figure 5.17 (Continued)



(c)

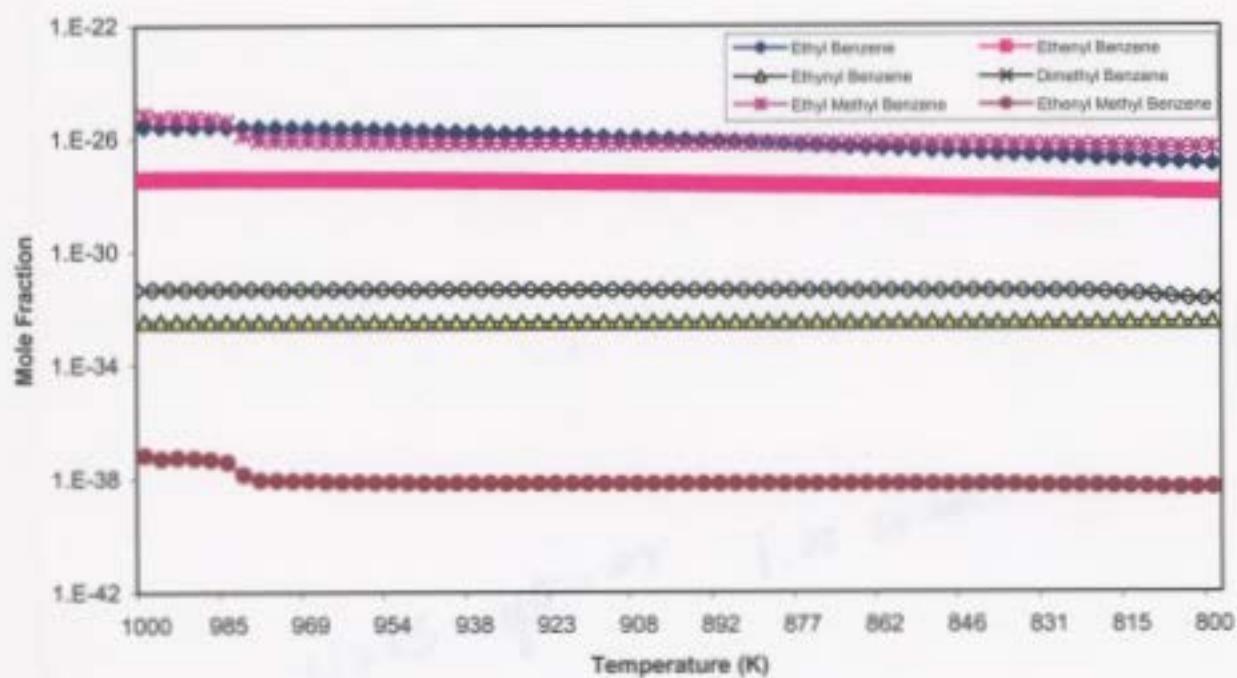


Table 5.15. Kinetically predicted changes (%) in compositions for single ring aromatic species in the stack as inlet flow rates are increased from $3.28 \times 10^5 \text{ cm}^3/\text{s}$ to $1.64 \times 10^6 \text{ cm}^3/\text{s}$ under the 14: 1 air to fuel ratio and 1000 K temperature profile.

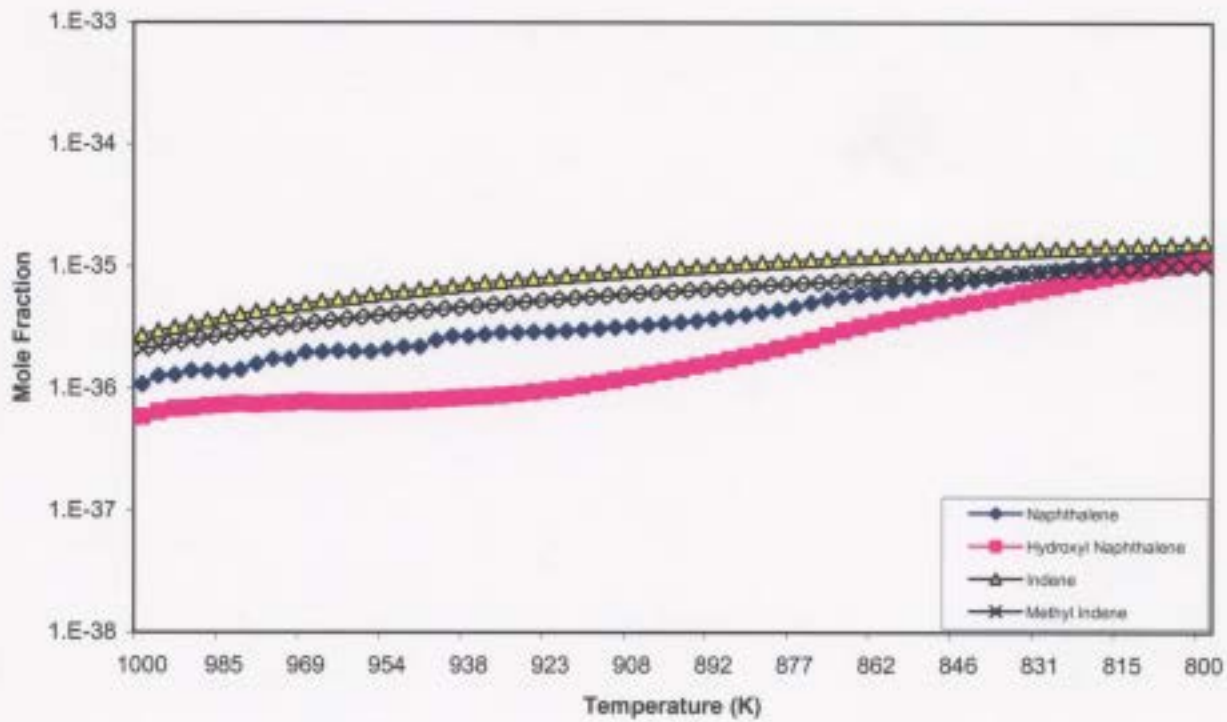
Aromatic Species	Increase (%)	Decrease (%)
Benzene	-	99.3
Phenol	54.1	-
Methyl Benzene	-	92.5
Benzaldehyde	-	99.5
Hydroxyl Methyl Benzene	14.0	-
Ethyl Benzene	99.9	-
Ethenyl Benzene	99.9	-
Ethynyl Benzene	-	99.9
Dimethyl Benzene	-	99.9
Ethyl Methyl Benzene	-	100.
Ethenyl Methyl Benzene	96.1	-

Overall, benzene, methyl benzene, benzaldehyde, ethynyl benzene, dimethyl benzene, and ethyl methyl benzene decrease with increasing flow rate (or decreasing residence time). The remaining species, including phenol, hydroxyl methyl benzene, ethyl benzene, ethenyl benzene, and ethenyl methyl benzene increase with increasing flow rate.

Figure 5.18 shows that the most abundant poly-aromatic species present are biphenylene and biphenyl over the entire temperature range. The least abundant species present is cyclopenta(cd)pyrene. Table 5.16 shows that all poly-aromatic species compositions increase as the cooling process occurs in the stack. Methyl phenanthrene compositions have the most significant increase by 96.0 %, whereas acenaphthalene, fluoranthene, ethynyl naphthalene, and pyrene do not change.

The compositions for these species are also dependent on inlet flow rate. Table 5.17 show changes in composition for poly-aromatic species as flow rates are increased. Overall, hydroxyl naphthalene, fluoranthene, indene, ethyl naphthalene,

Figure 5.18. Kinetic predictions of concentrations of poly-aromatic hydrocarbon species for 14:1 air to fuel ratio, 1000 K temperature profile, and varying inlet flow rates inside the incinerator stack during sour gas incineration. **(a).** Inlet flow rate = $3.28 \times 10^5 \text{ cm}^3/\text{s}$, **(b).** Inlet flow rate = $9.83 \times 10^5 \text{ cm}^3/\text{s}$ **(c).** Inlet flow rate = $1.64 \times 10^6 \text{ cm}^3/\text{s}$.



(a)

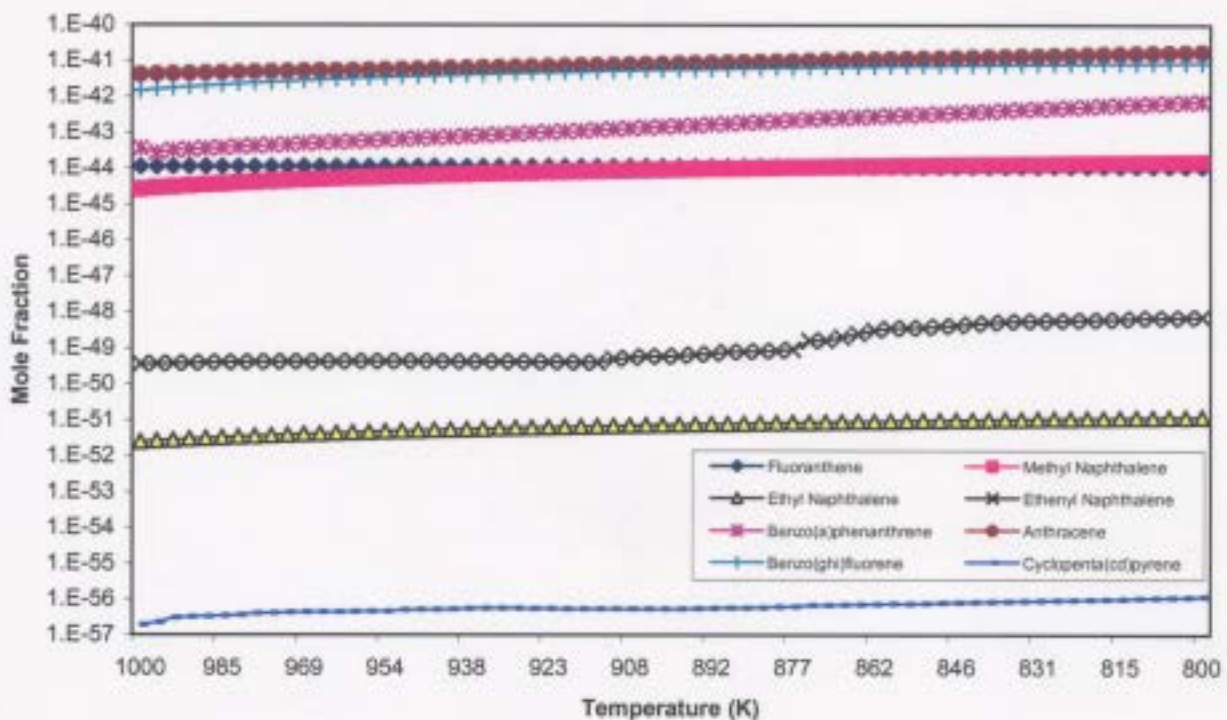
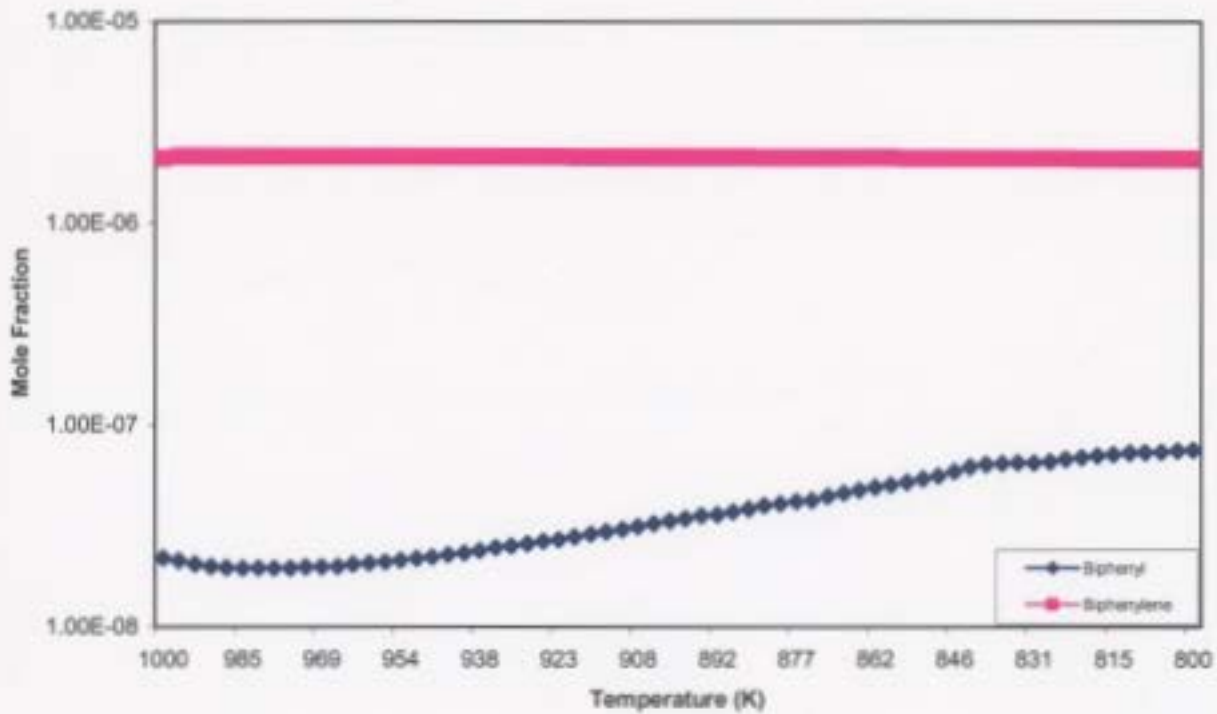


Figure 5.18 (Continued)



(a)

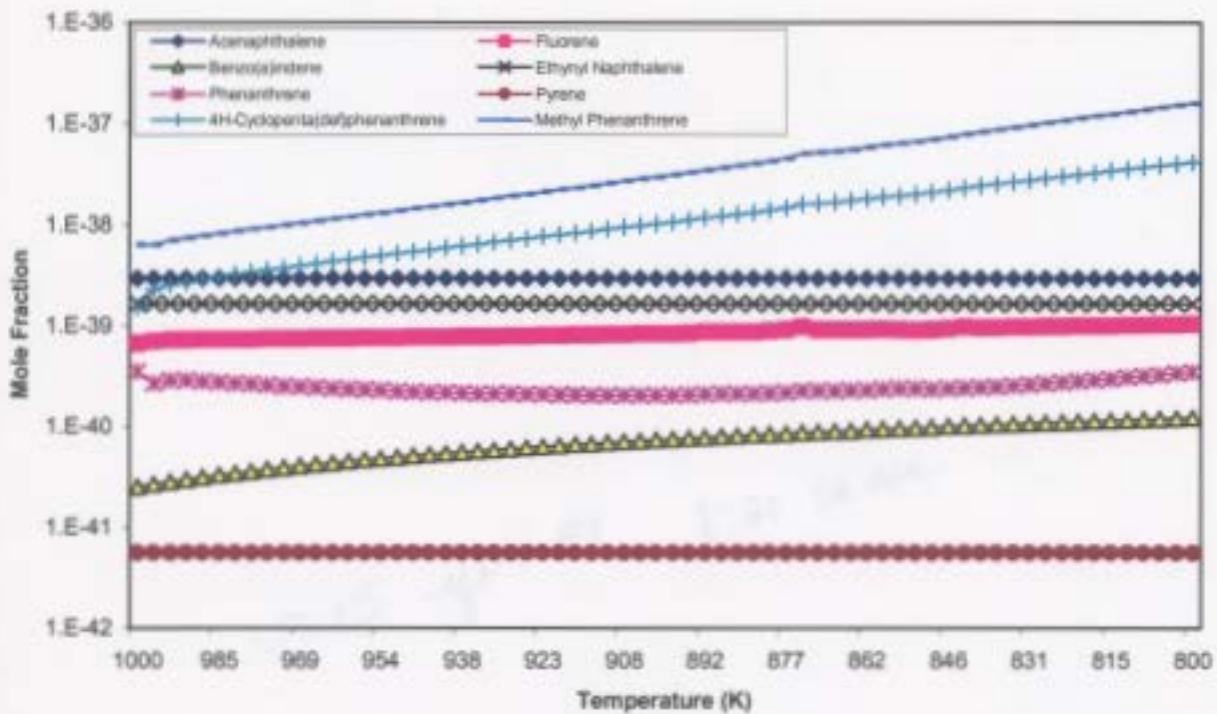
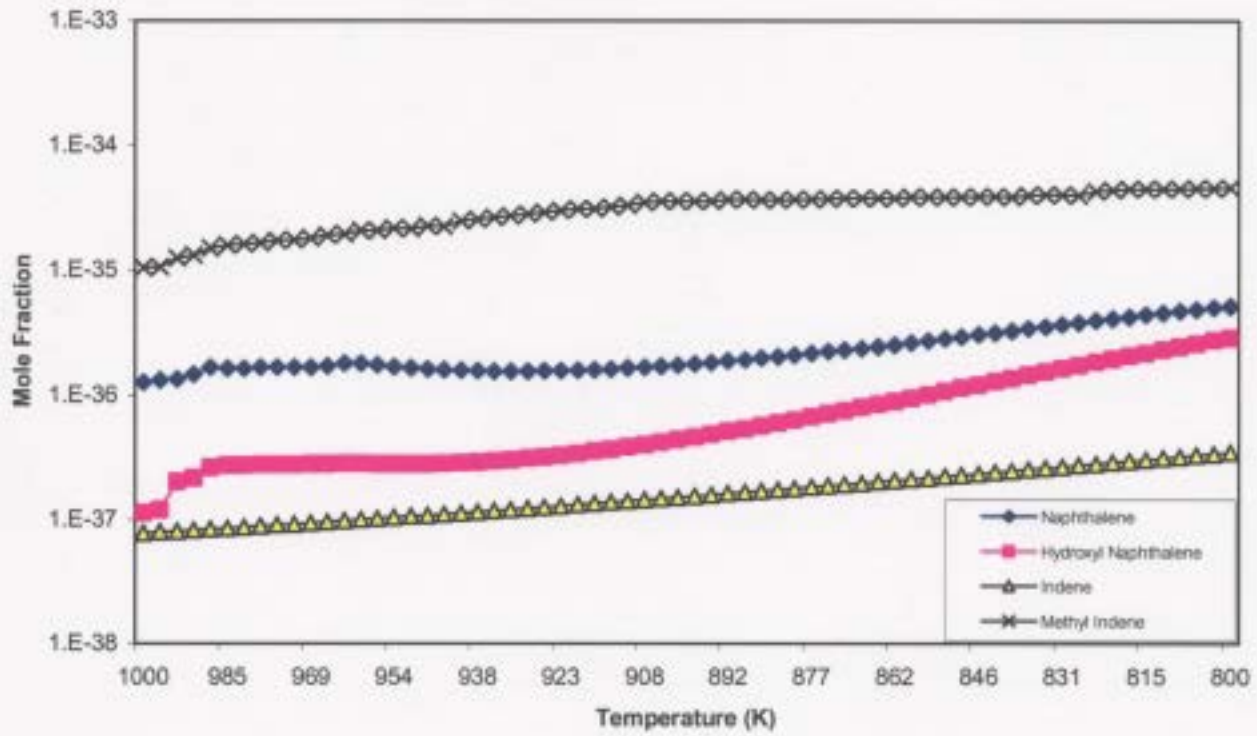


Figure 5.18 (Continued)



(b)

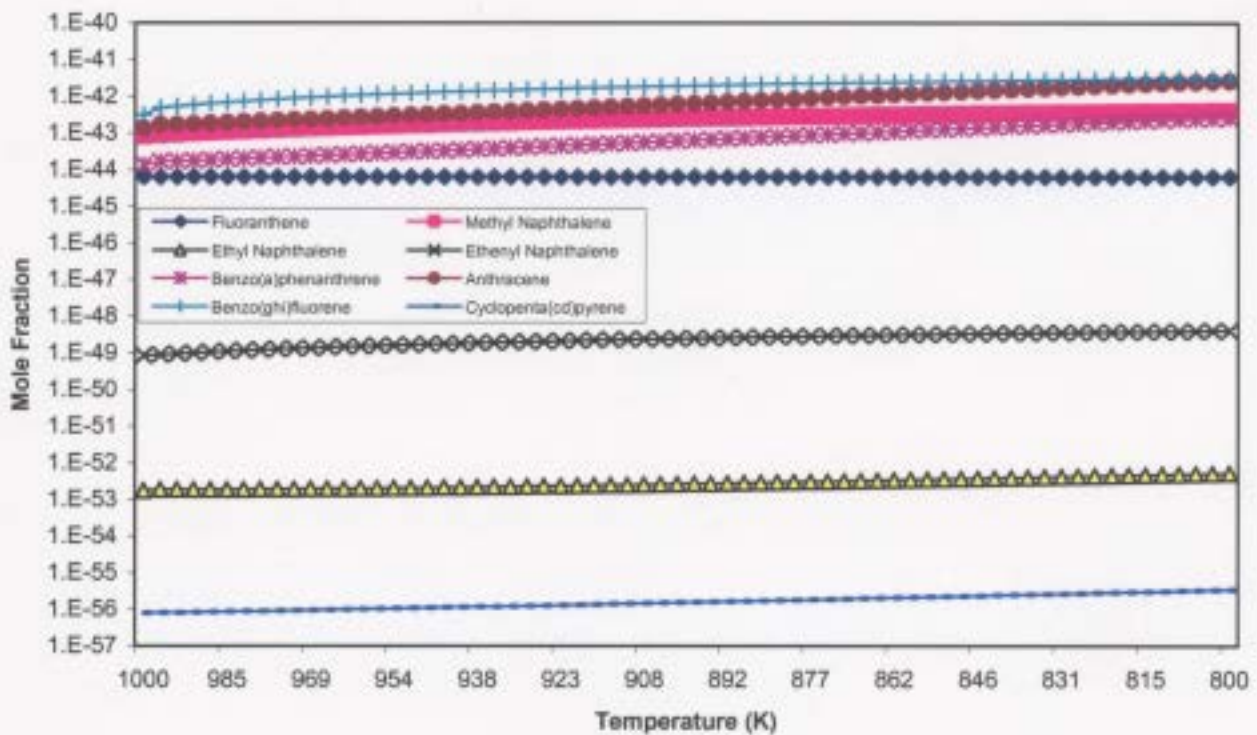
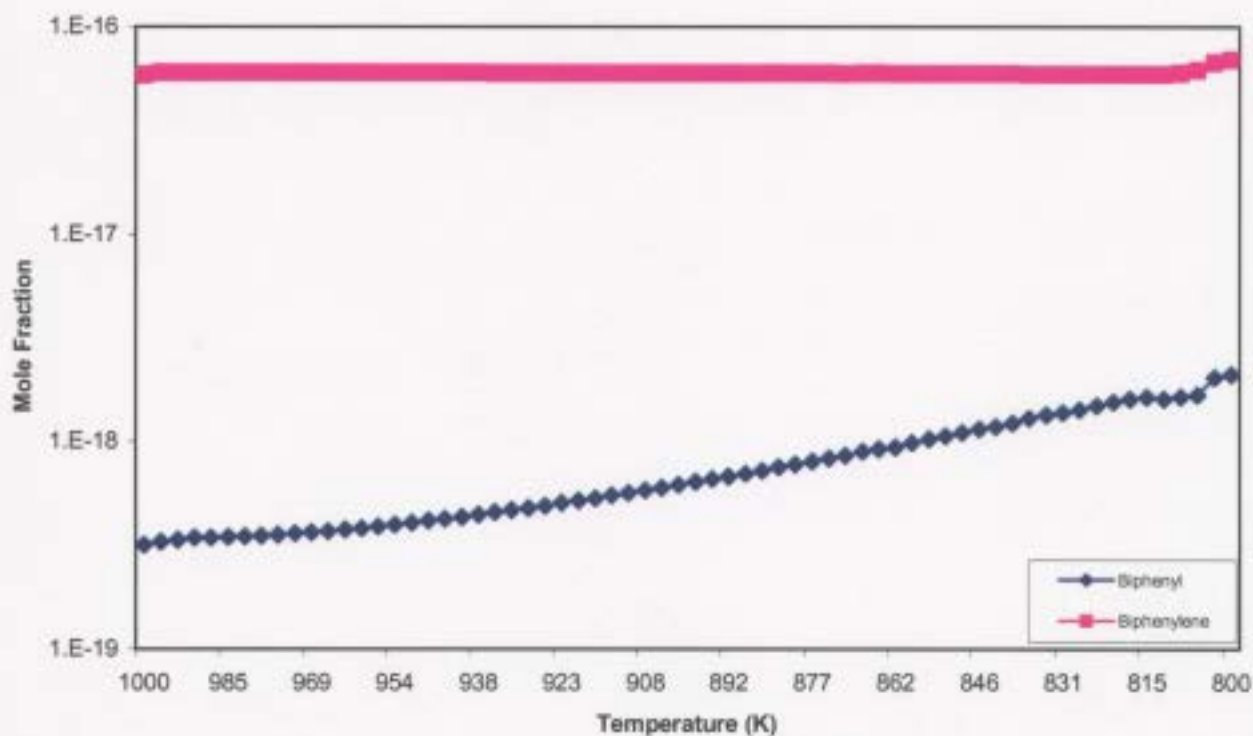


Figure 5.18 (Continued)



(b)

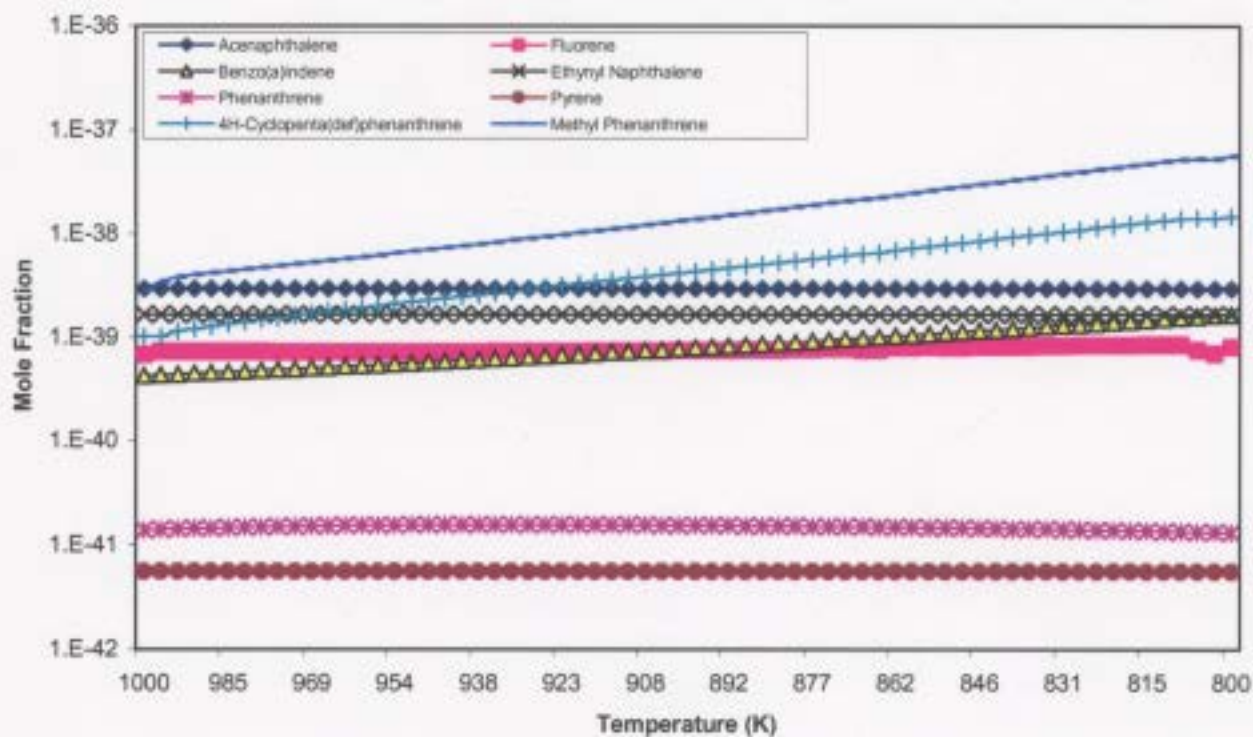
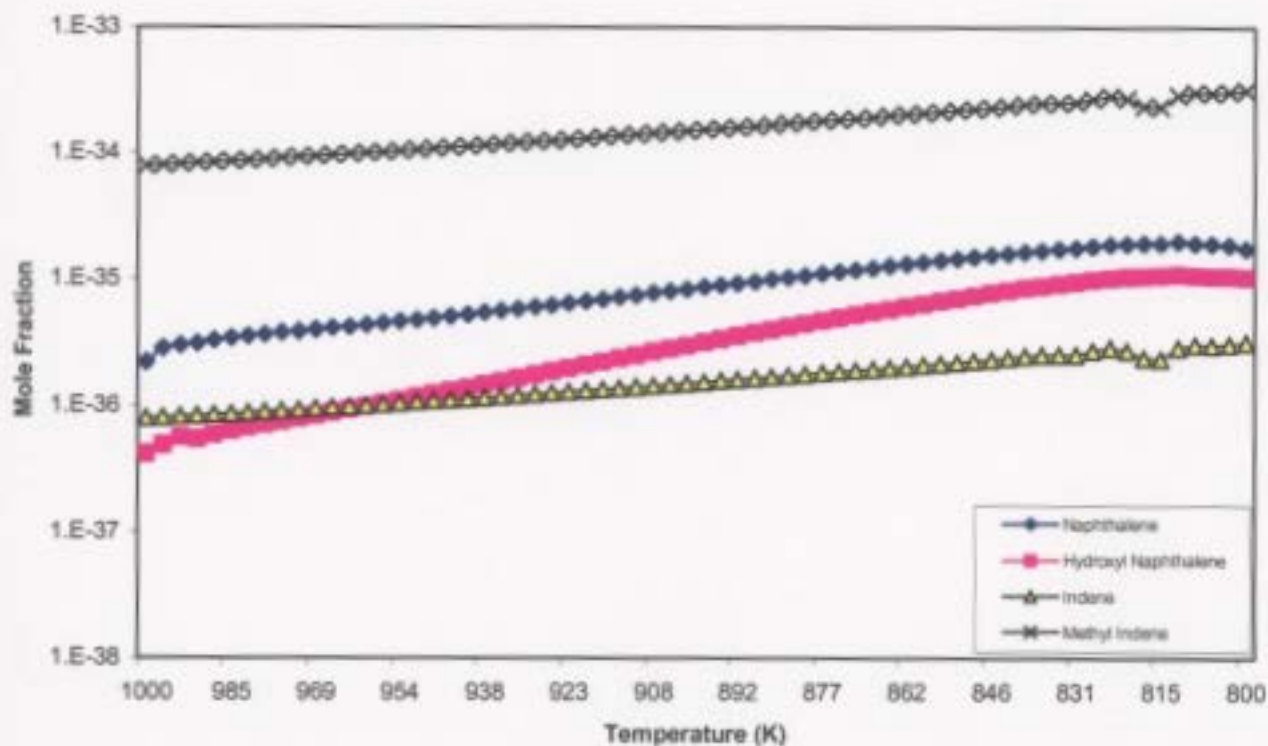


Figure 5.18 (Continued)



(c)

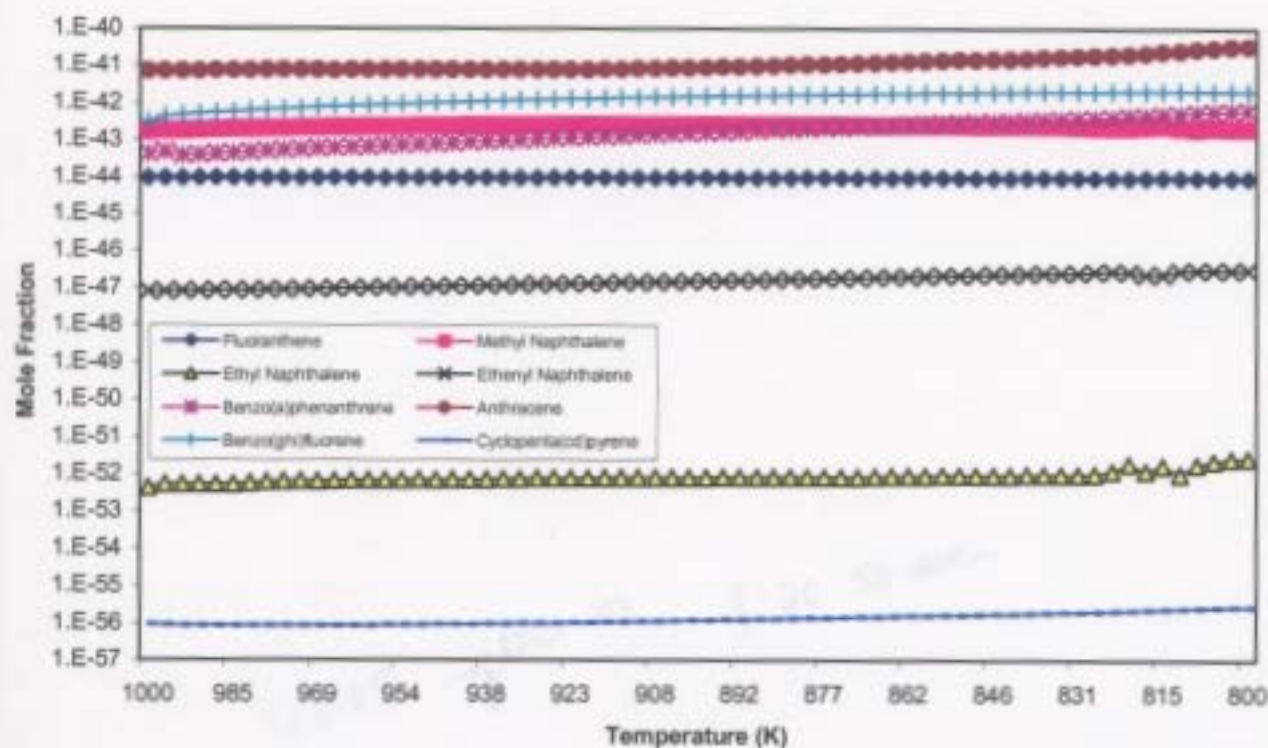
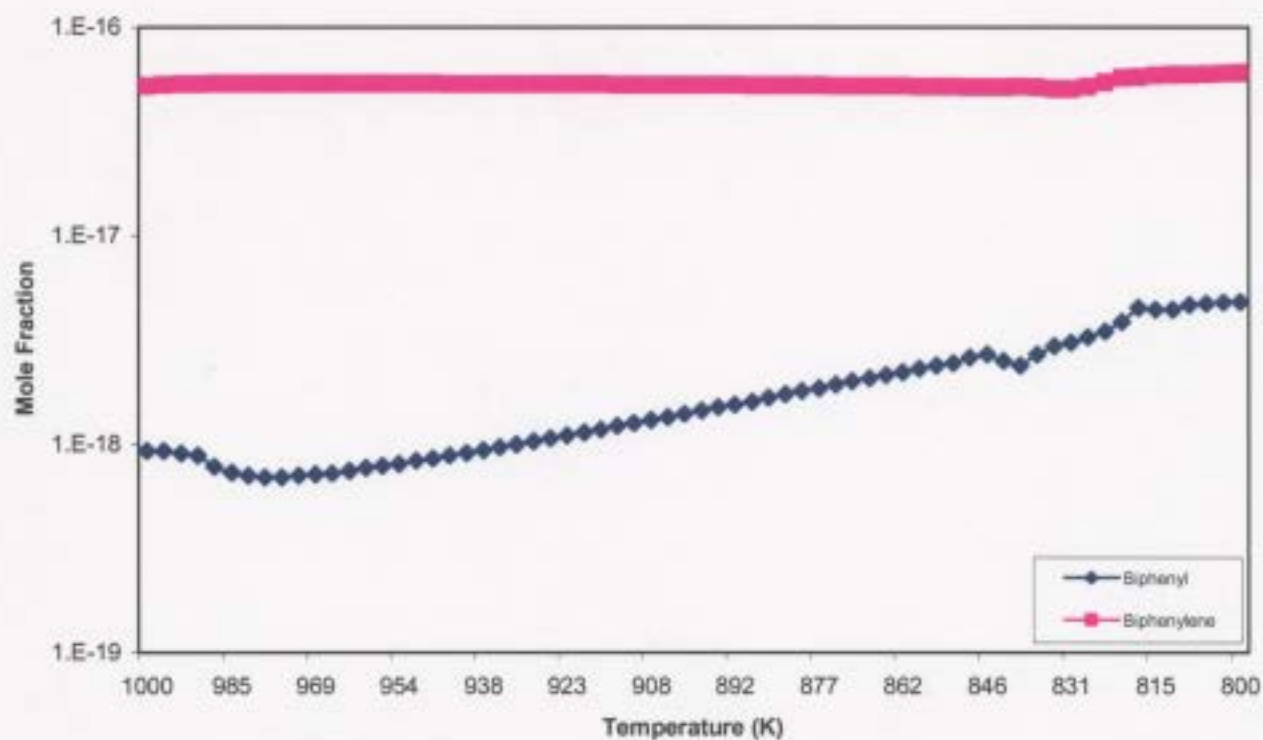


Figure 5.18 (Continued)



(c)

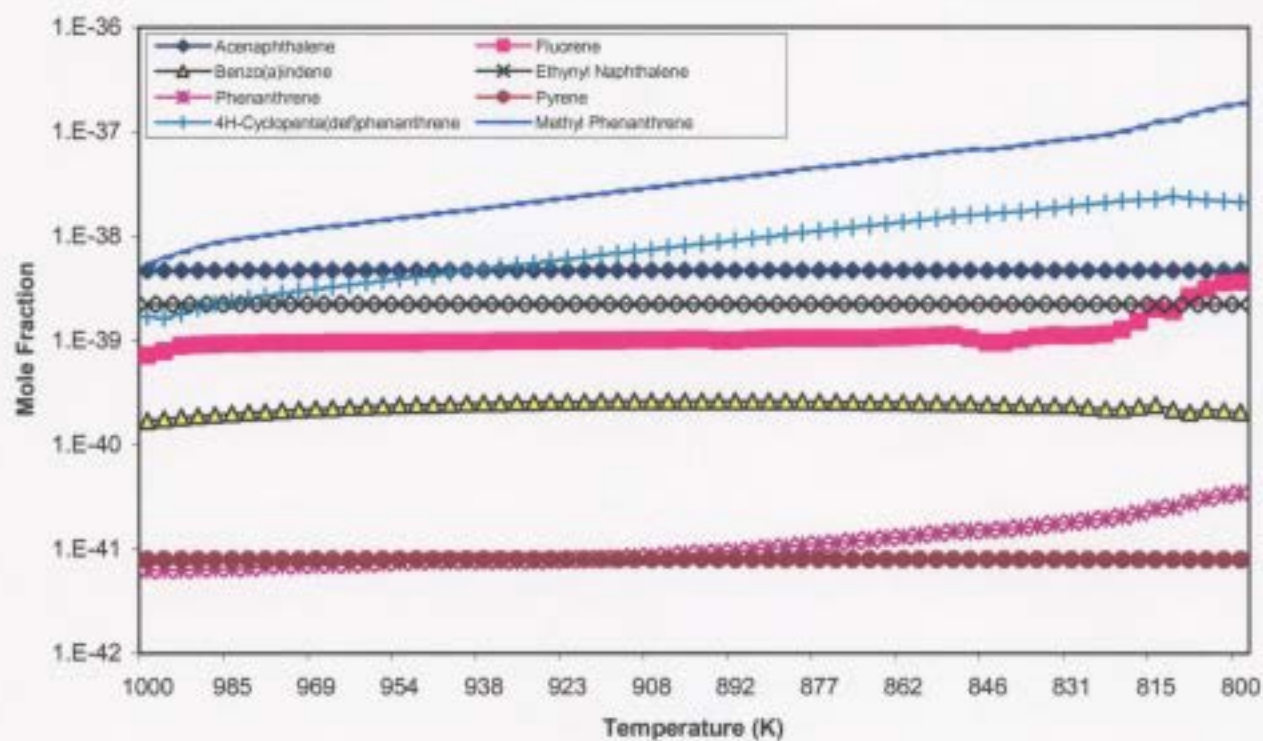


Table 5.16. Kinetically predicted increases (%) in compositions from inlet for poly-aromatic species in the stack during cooling under the conditions of 14:1 air to fuel ratio, 1000 K temperature profile, and varying flow rates of (a). $3.28 \times 10^5 \text{ cm}^3/\text{s}$, (b). $9.83 \times 10^5 \text{ cm}^3/\text{s}$, and (c). $1.64 \times 10^6 \text{ cm}^3/\text{s}$.

Poly-Aromatic Species	Flow Rate (a)	Flow Rate (b)	Flow Rate (c)
Naphthalene	91.7	75.3	87.5
Hydroxyl Naphthalene	94.7	96.0	96.0
Acenaphthalene	-	-	-
Fluorene	35.6	33.2	30.5
Fluoranthene	-	-	-
Indene	82.0	77.6	74.9
Methyl Indene	79.4	77.4	74.9
Methyl Naphthalene	82.3	79.4	78.5
Benzo(a)indene	79.4	74.3	70.2
Ethyl Naphthalene	79.6	66.9	84.0
Ethenyl Naphthalene	95.0	79.9	74.9
Ethynyl Naphthalene	-	-	-
Benzo(a)phenanthrene	95.0	94.7	93.3
Phenanthrene	5.69	8.49	82.05
Anthracene	76.2	94.7	79.1
Pyrene	-	-	-
4H-cylopenta(def)phenanthrene	96.4	93.0	92.0
Methyl Phenanthrene	96.1	94.9	97.1
Benzo(ghi)fluorene	83.4	89.9	85.3
Biphenyl	70.8	84.9	80.0
Biphenylene	1.93	2.48	13.46
Cyclopenta(cd)pyrene	83.0	78.0	66.0

Table 5.17. Kinetically predicted changes (%) in compositions for poly-aromatic species in the stack as inlet flow rates are increased from $3.28 \times 10^5 \text{ cm}^3/\text{s}$ to $1.64 \times 10^6 \text{ cm}^3/\text{s}$ under the 14:1 air to fuel ratio and 1000 K temperature profile.

Aromatic Species	Increase (%)	Decrease (%)
Naphthalene	50.2	-
Hydroxyl Naphthalene	-	30.1
Acenaphthalene	37.0	-
Fluorene	6.82	-
Fluoranthene	-	18.1
Indene	-	71.2
Methyl Indene	97.3	-
Methyl Naphthalene	98.4	-
Benzo(a)indene	85.3	-
Ethyl Naphthalene	-	83.3
Ethenyl Naphthalene	99.5	-
Ethynyl Naphthalene	25.6	-
Benzo(a)phenanthrene	-	10.8
Phenanthrene	-	98.2
Anthracene	40.9	-
Pyrene	28.2	-
4H-cyclopenta(def)phenanthrene	8.82	-
Methyl Phenanthrene	-	15.9
Benzo(ghi)fluorene	-	79.2
Biphenyl	-	99.9
Biphenylene	-	100.
Cyclopenta(cd)pyrene	79.4	-

benzo(a)phenanthrene, phenanthrene, methyl phenanthrene, benzo(ghi)fluorene, biphenyl, and biphenylene decrease with increasing flow rate. The remaining species including naphthalene, acenaphthalene, fluorene, methyl indene, methyl naphthalene, benzo(a)indene, ethenyl naphthalene, ethynyl naphthalene, anthracene, pyrene, 4H-cyclopenta(def)phenanthrene, and cyclopenta(cd)pyrene increase with increasing flow rate.

Compositions for ethenyl naphthalene has the most significant increase by 99.5 % and biphenylene has the most significant decrease by 100 % as flow rates are increased.

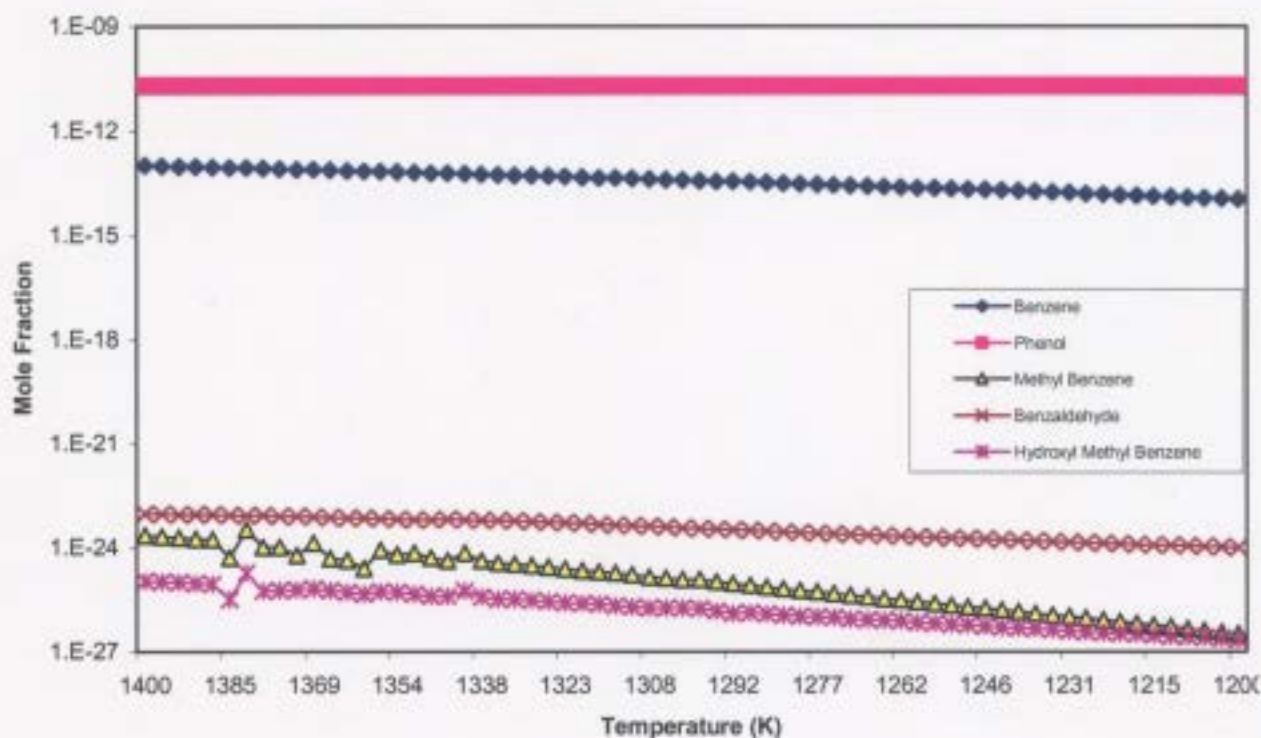
5.2.1.4.2. Kinetic Results for 1400 K Temperature Profile

As in the results from the 1000 K temperature profile, single ring aromatic species are kinetically predicted to decrease during the cooling process in the stack. Results in this case have somewhat different trends, with the exception that the most abundant species is phenol and the least abundant species is ethenyl methyl benzene. Figure 5.19 shows that majority of these species' compositions decrease significantly as the temperature is decreased during cooling. Table 5.18 indicates that the most significant average reduction in composition during cooling is for ethynyl benzene by over 99% and ethenyl benzene by over 99%. The compositions for phenol do not significantly change.

Table 5.18. Kinetically predicted reductions (%) in compositions from inlet for single ring aromatic species in the stack during cooling under the conditions of 14:1 air to fuel ratio, 1400 K temperature profile, and varying flow rates of (a). $3.28 \times 10^5 \text{ cm}^3/\text{s}$, (b). $9.83 \times 10^5 \text{ cm}^3/\text{s}$, and (c). $1.64 \times 10^6 \text{ cm}^3/\text{s}$.

Aromatic Species	Flow Rate (a)	Flow Rate (b)	Flow Rate (c)
Benzene	89.2	86.9	90.5
Phenol	-	-	-
Methyl Benzene	99.9	98.4	91.3
Benzaldehyde	89.4	98.9	99.9
Hydroxyl Methyl Benzene	97.9	89.0	98.8
Ethyl Benzene	72.9	94.5	98.6
Ethenyl Benzene	99.9	99.0	98.5
Ethynyl Benzene	99.7	99.1	99.5
Dimethyl Benzene	51.8	97.6	24.0
Ethyl Methyl Benzene	-	88.3	99.9
Ethenyl Methyl Benzene	69.3	99.0	86.8

Figure 5.19. Kinetic predictions of concentrations of single ring aromatic species for 14:1 air to fuel ratio, 1400 K temperature profile, and varying inlet flow rates inside the incinerator stack during sour gas incineration. **(a).** Inlet flow rate = $3.28 \times 10^5 \text{ cm}^3/\text{s}$, **(b).** Inlet flow rate = $9.83 \times 10^5 \text{ cm}^3/\text{s}$ **(c).** Inlet flow rate = $1.64 \times 10^6 \text{ cm}^3/\text{s}$.



(a)

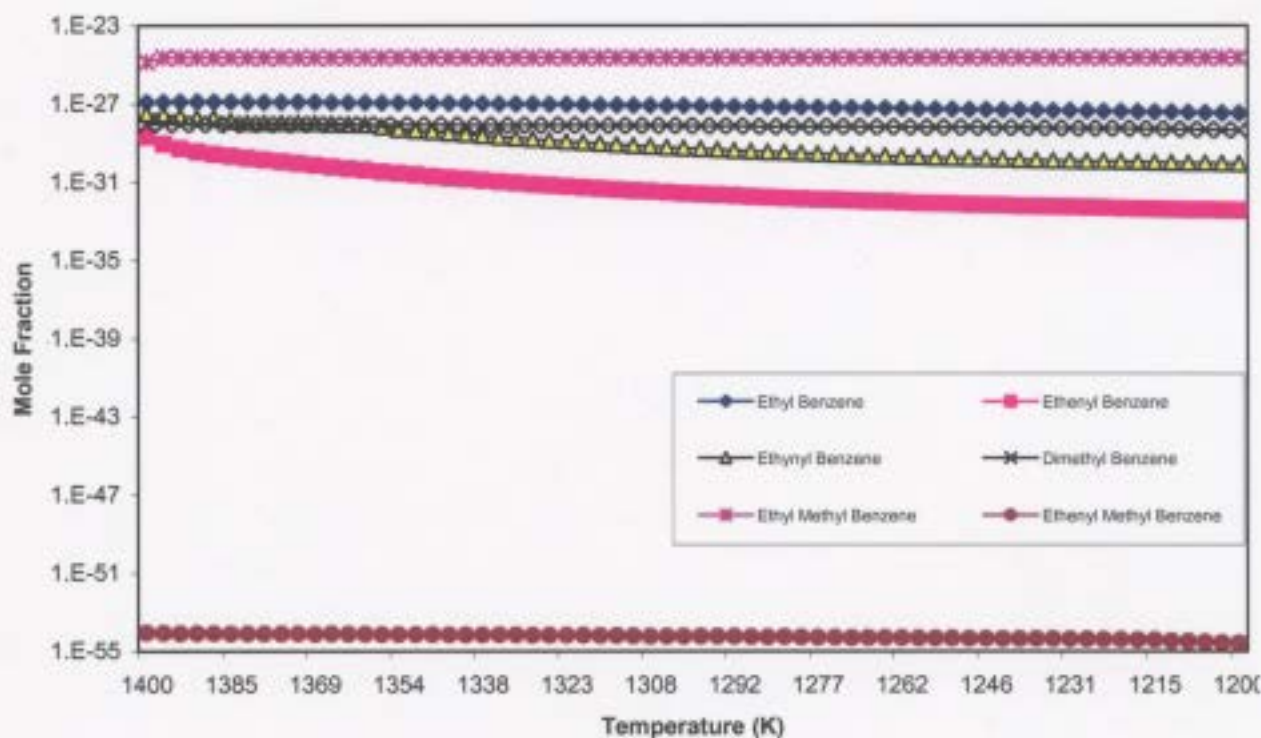
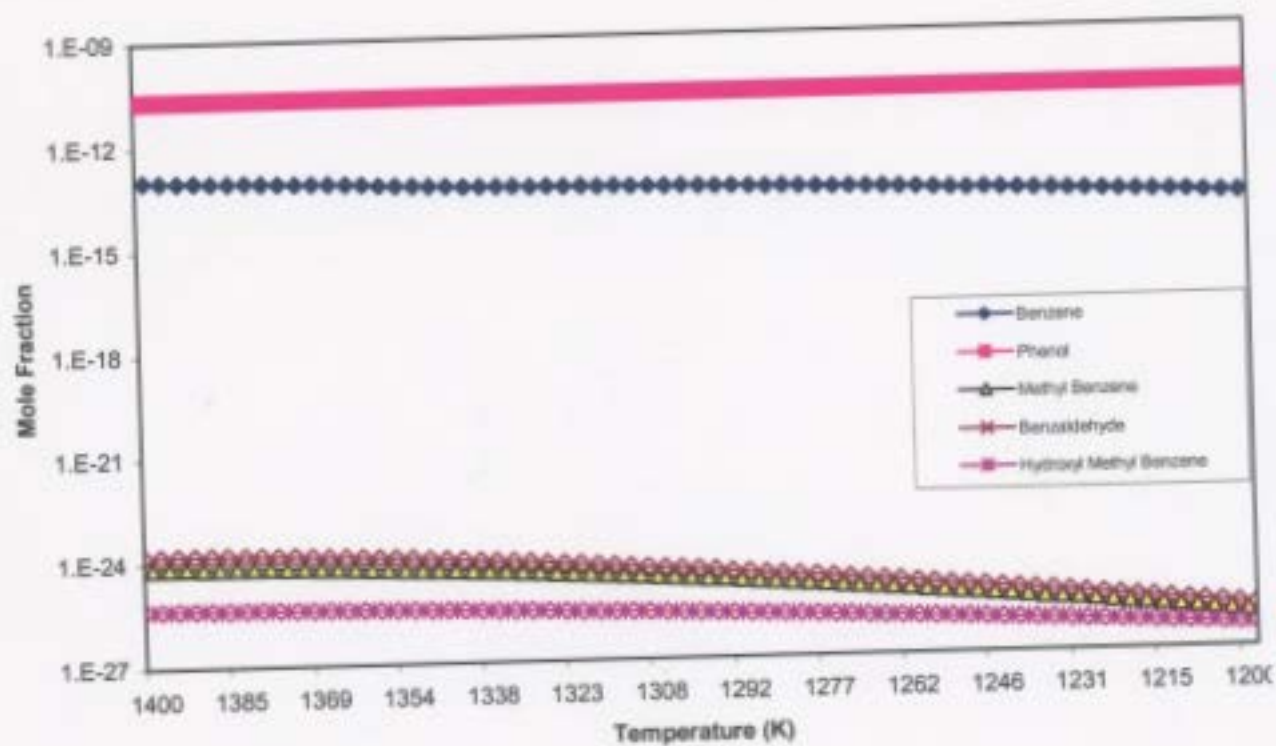


Figure 5.19 (Continued)



(b)

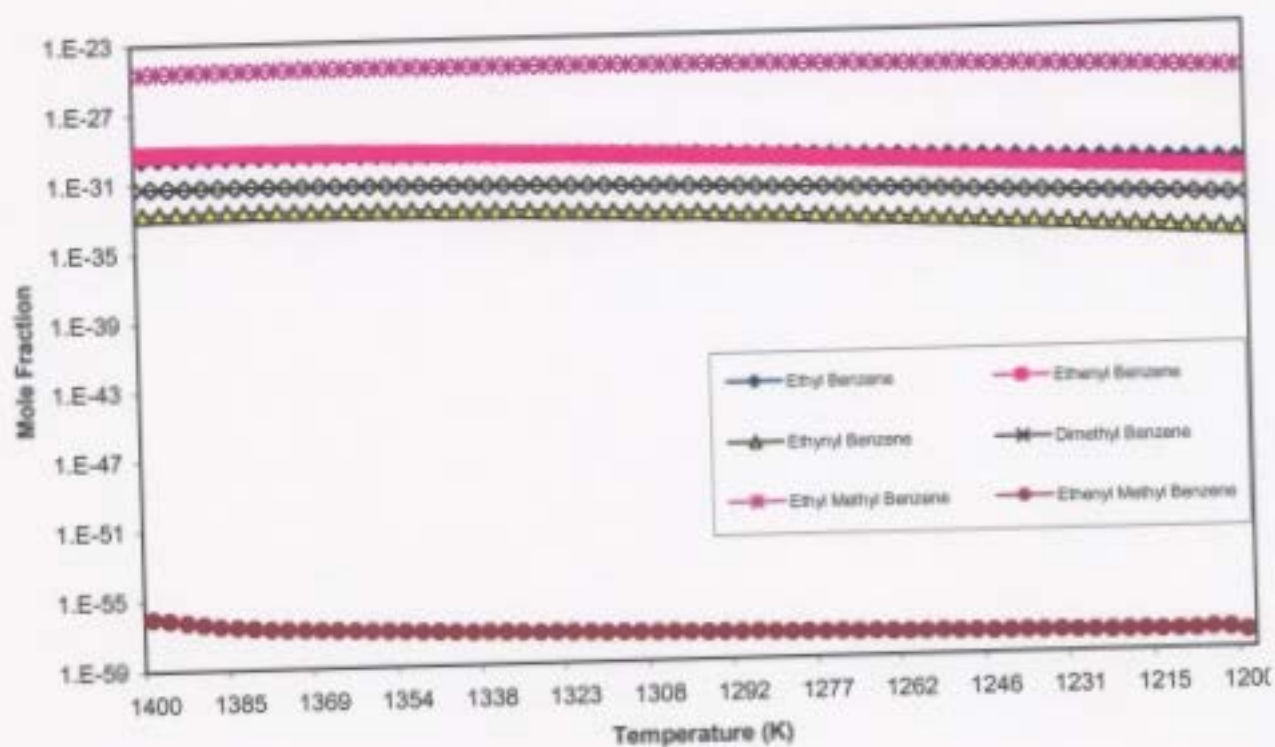
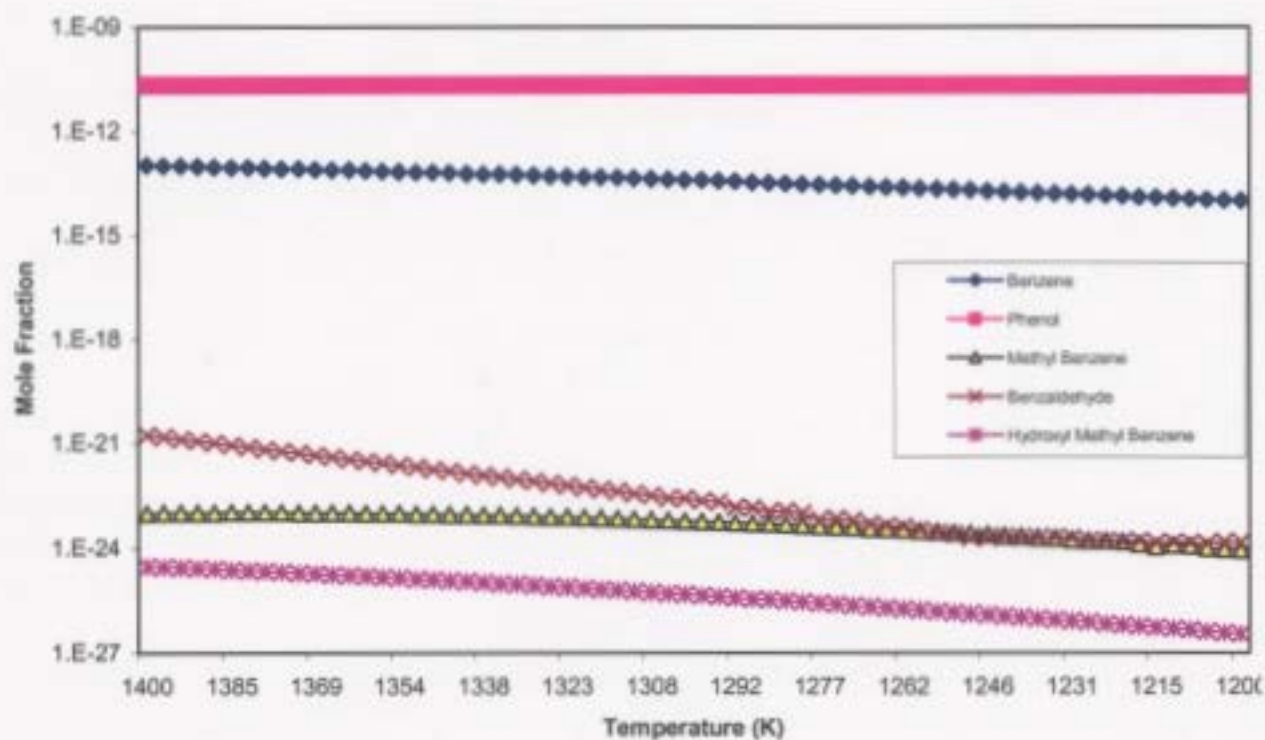


Figure 5.19 (Continued)



(c)

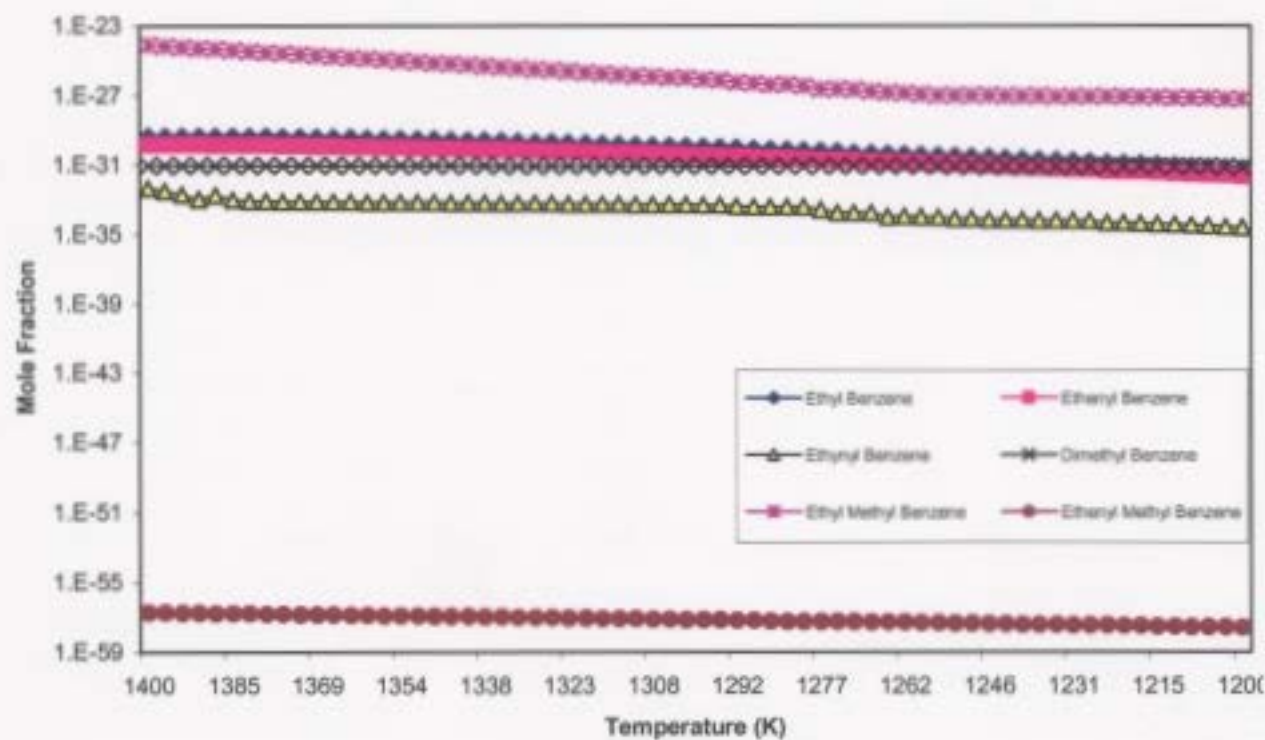


Table 5.19 shows changes in composition for single ring aromatic species that are somewhat different than results from 1000 K temperature profile. The difference is that in this case, ethyl benzene, ethenyl benzene, and ethenyl methyl benzene are decreasing; methyl benzene and benzaldehyde are increasing; and benzene and phenol have insignificant changes. Overall, the species including ethyl benzene, ethenyl benzene, ethynyl benzene, dimethyl benzene, ethyl methyl benzene, and ethenyl methyl benzene decrease with increasing flow rate. The remaining species including methyl benzene, benzaldehyde, and hydroxyl methyl benzene increase with increasing flow rate. Ethynyl benzene and dimethyl benzene have the most significant decrease in composition by 99.9 % and benzaldehyde has the most significant increase by 99.4 % as flow rates are increased.

Table 5.19. Kinetically predicted changes (%) in compositions for single ring aromatic species in the stack as inlet flow rates are increased from $3.28 \times 10^5 \text{ cm}^3/\text{s}$ to $1.64 \times 10^6 \text{ cm}^3/\text{s}$ under the 14:1 air to fuel ratio and 1400 K temperature profile.

Aromatic Species	Increase (%)	Decrease (%)
Benzene	-	-
Phenol	-	-
Methyl Benzene	77.7	-
Benzaldehyde	99.4	-
Hydroxyl Methyl Benzene	63.0	-
Ethyl Benzene	-	99.6
Ethenyl Benzene	-	93.7
Ethynyl Benzene	-	99.9
Dimethyl Benzene	-	99.9
Ethyl Methyl Benzene	-	79.9
Ethenyl Methyl Benzene	-	99.8

Results show the same trend as the 1000 K temperature profile in that the most abundant species are biphenylene and biphenyl and the least abundant species is cyclopenta(cd)pyrene. Table 5.20 shows that, as in previous results, methyl phenanthrene compositions are predicted to have the most significant average increase by 98.5% during cooling. Biphenylene is predicted to not change significantly.

Poly-aromatic species compositions are also dependent on inlet flow rate. Percent changes in compositions are given in Table 5.21. Overall, the species including hydroxyl naphthalene, acenaphthalene, indene, phenanthrene, 4H-cyclopenta(def)phenanthrene, and benzo(ghi)fluorene decrease with increasing flow rate. The remaining species including naphthalene, fluorene, fluoranthene, methyl indene, methyl naphthalene, benzo(a)indene, ethyl naphthalene, ethenyl naphthalene, ethynyl naphthalene, anthracene, pyrene, methyl phenanthrene, biphenyl, and cyclopenta(cd)pyrene increase with increasing flow rate. Ethyl naphthalene has the most significant increase by 99.8 % and benzo(ghi)fluorene has the most significant reduction by 92.0 % with increasing flow rate. Biphenylene and benzo(a)phenanthrene are predicted to have no significant change. Again, these results are somewhat different from 1000 K temperature profile. The difference is that in this case, acenaphthalene and 4H-cyclopenta(def)phenanthrene are decreasing; fluoranthene, ethyl naphthalene, methyl phenanthrene, and biphenyl are increasing with increasing flow rate; and biphenylene and benzo(a)phenanthrene change insignificantly.

Table 5.20. Kinetically predicted increases (%) in compositions for poly-aromatic species in the stack during cooling under the conditions of 14:1 air to fuel ratio, 1400 K temperature profile, and varying flow rates of (a). $3.28 \times 10^5 \text{ cm}^3/\text{s}$, (b). $9.83 \times 10^5 \text{ cm}^3/\text{s}$, and (c). $1.64 \times 10^6 \text{ cm}^3/\text{s}$.

Poly-Aromatic Species	Flow Rate (a)	Flow Rate (b)	Flow Rate (c)
Naphthalene	93.9	96.1	91.4
Hydroxyl Naphthalene	93.5	77.6	95.5
Acenaphthalene	95.6	79.4	96.1
Fluorene	86.8	75.4	79.2
Fluoranthene	96.6	71.5	90.4
Indene	6.25	20.7	17.7
Methyl Indene	82.4	99.5	89.5
Methyl Naphthalene	13.1	12.0	6.25
Benzo(a)indene	81.3	98.8	83.5
Ethyl Naphthalene	79.3	74.2	80.1
Ethenyl Naphthalene	96.6	77.7	97.6
Ethynyl Naphthalene	19.1	12.7	9.1
Benzo(a)phenanthrene	96.6	53.8	96.7
Phenanthrene	17.5	69.7	79.2
Anthracene	79.4	99.5	79.4
Pyrene	59.8	73.3	79.4
4H-cylopenta(def)phenanthrene	98.7	79.2	99.9
Methyl Phenanthrene	99.5	96.1	99.9
Benzo(ghi)fluorene	98.8	98.8	73.4
Biphenyl	59.9	67.8	70.3
Biphenylene	-	-	-
Cyclopenta(cd)pyrene	75.4	91.9	85.4

Table 5.21. Kinetically predicted changes (%) in compositions for poly-aromatic species in the stack as inlet flow rates are increased from $3.28 \times 10^5 \text{ cm}^3/\text{s}$ to $1.64 \times 10^6 \text{ cm}^3/\text{s}$ under the 14:1 air to fuel ratio and 1400 K temperature profile.

Aromatic Species	Increase (%)	Decrease (%)
Naphthalene	26.2	-
Hydroxyl Naphthalene	-	34.8
Acenaphthalene	-	33.4
Fluorene	5.21	-
Fluoranthene	20.5	-
Indene	-	57.5
Methyl Indene	50.9	-
Methyl Naphthalene	85.7	-
Benzo(a)indene	80.6	-
Ethyl Naphthalene	99.8	-
Ethenyl Naphthalene	84.1	-
Ethynyl Naphthalene	2.69	-
Benzo(a)phenanthrene	-	-
Phenanthrene	-	58.3
Anthracene	39.9	-
Pyrene	42.0	-
4H-cyclopenta(def)phenanthrene	-	42.4
Methyl Phenanthrene	92.9	-
Benzo(ghi)fluorene	-	92.0
Biphenyl	1.52	-
Biphenylene	-	-
Cyclopenta(cd)pyrene	77.5	-

5.2.1.4.3. Kinetic Results for 1623 K Temperature Profile

The predictions with a temperature profile with an initial internal combustion temperature of 1623 K are similar to 1000 K and 1400 K temperature profile results. Kinetic predictions indicate the same decreasing composition trends for single ring aromatic species during the cooling process. These results have the same trends for the most significant species. In this case, the most abundant species is phenol and the least abundant species is ethenyl methyl benzene. Table 5.22 indicates that the most significant

reduction in composition again is for ethenyl benzene and ethyl benzene by over 98%.

Compositions of phenol and ethyl methyl benzene are not significantly reduced.

Table 5.22. Kinetically predicted reductions (%) in compositions for single ring aromatic species in the stack during cooling under the conditions of 14:1 air to fuel ratio, 1623 K temperature profile, and varying flow rates of (a). $3.28 \times 10^5 \text{ cm}^3/\text{s}$, (b). $9.83 \times 10^5 \text{ cm}^3/\text{s}$, and (c). $1.64 \times 10^6 \text{ cm}^3/\text{s}$.

Aromatic Species	Flow Rate (a)	Flow Rate (b)	Flow Rate (c)
Benzene	77.7	75.8	75.7
Phenol	-	-	-
Methyl Benzene	98.2	97.7	97.5
Benzaldehyde	98.5	98.1	97.9
Hydroxyl Methyl Benzene	95.5	95.0	94.5
Ethyl Benzene	99.1	98.8	98.1
Ethenyl Benzene	97.9	99.3	99.3
Ethynyl Benzene	99.9	93.2	99.6
Dimethyl Benzene	46.5	28.5	36.1
Ethyl Methyl Benzene	-	-	-
Ethenyl Methyl Benzene	60.4	25.8	62.2

Table 5.23 shows the percent reductions and increases for each single ring aromatic species. Overall, benzene, methyl benzene, benzaldehyde, hydroxyl methyl benzene, ethyl benzene, ethyl methyl benzene, and ethenyl methyl benzene decrease with increasing flow rate. Ethenyl benzene, ethynyl benzene, and dimethyl benzene increase with increasing flow rate. Ethynyl benzene has the most significant increase in composition by 96.7 % and ethyl benzene has the most significant reduction in composition by 85.2 % as flow rates are increased. Phenol is not significantly changed. It should also be noted that these trends are completely different from those of 1400 K and 1000 K temperature profiles. The difference between these results and those of the 1000

K temperature profile is that in this case, hydroxyl methyl benzene, ethyl benzene, and ethenyl methyl benzene are decreasing; ethynyl benzene and dimethyl benzene are increasing; and phenol changes insignificantly as flow rates are increased. The difference between these results and those of the 1400 K temperature profile is that ethenyl benzene, ethynyl benzene, and dimethyl benzene are increasing, and methyl benzene, benzaldehyde, and hydroxyl methyl benzene are decreasing as flow rates are increased.

Table 5.23. Kinetically predicted changes (%) in compositions for single ring aromatic species in the stack as inlet flow rates are increased from $3.28 \times 10^5 \text{ cm}^3/\text{s}$ to $1.64 \times 10^6 \text{ cm}^3/\text{s}$ under the 14:1 air to fuel ratio and 1623 K temperature profile.

Aromatic Species	Increase (%)	Decrease (%)
Benzene	-	4.79
Phenol	-	-
Methyl Benzene	-	59.4
Benzaldehyde	-	58.3
Hydroxyl Methyl Benzene	-	58.1
Ethyl Benzene	-	85.2
Ethenyl Benzene	70.3	-
Ethynyl Benzene	96.7	-
Dimethyl Benzene	2.86	-
Ethyl Methyl Benzene	-	43.3
Ethenyl Methyl Benzene	-	85.1

Compositions for poly-aromatic species in this case have similar trends compared to the previous two temperature profiles. Results indicate the same species and the same increasing trend as cooling occurs. However, Table 5.24 show that the most significantly increased species during cooling is indene by 92.0 % and pyrene is insignificantly increased. This is not in agreement with the previous two temperature profiles since the

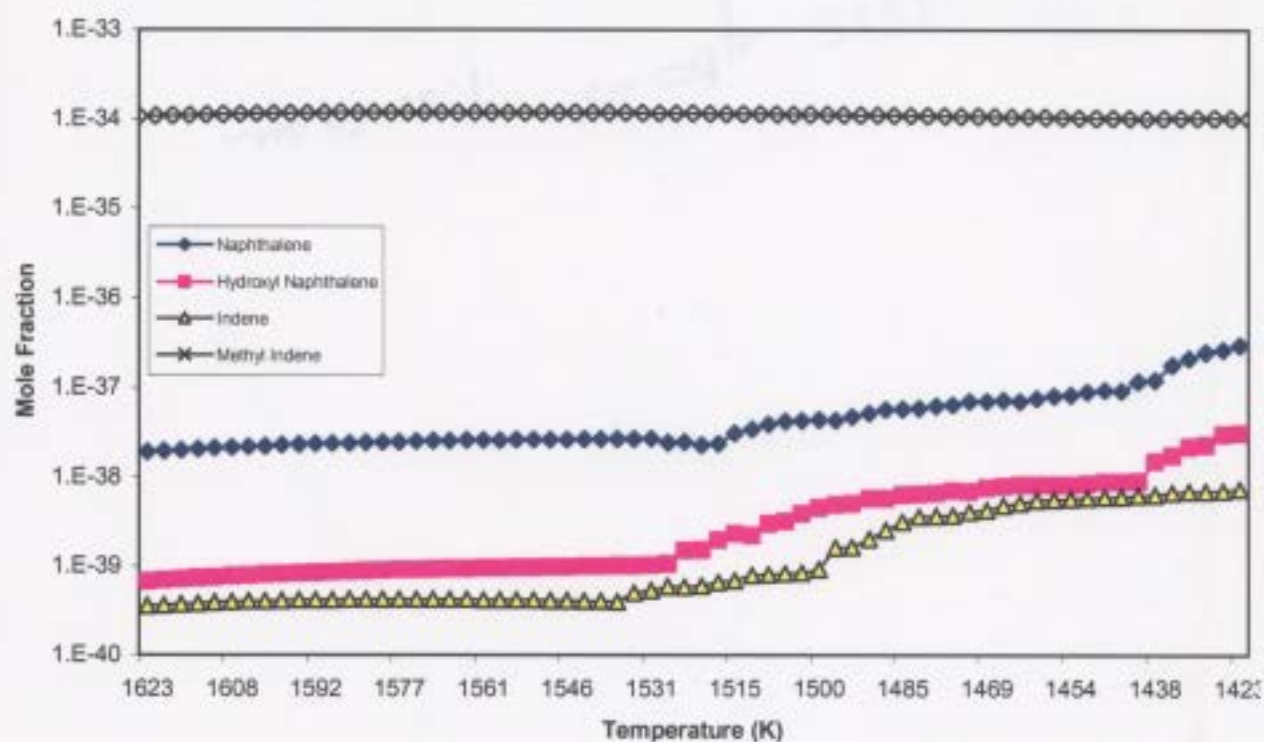
Table 5.24. Kinetically predicted increases (%) in compositions for poly-aromatic species in the stack during cooling under the conditions of 14:1 air to fuel ratio, 1623 K temperature profile, and varying flow rates of (a). $3.28 \times 10^5 \text{ cm}^3/\text{s}$, (b). $9.83 \times 10^5 \text{ cm}^3/\text{s}$, and (c). $1.64 \times 10^6 \text{ cm}^3/\text{s}$.

Poly-Aromatic Species	Flow Rate (a)	Flow Rate (b)	Flow Rate (c)
Naphthalene	93.6	88.1	86.3
Hydroxyl Naphthalene	97.9	87.2	73.6
Acenaphthalene	5.93	6.75	8.58
Fluorene	13.6	19.7	19.7
Fluoranthene	30.8	33.0	30.7
Indene	95.2	91.1	89.7
Methyl Indene	11.3	13.5	15.7
Methyl Naphthalene	72.8	43.6	19.7
Benzo(a)indene	20.5	15.2	10.5
Ethyl Naphthalene	88.3	91.9	89.0
Ethenyl Naphthalene	79.3	77.6	79.7
Ethynyl Naphthalene	16.9	23.1	25.2
Benzo(a)phenanthrene	79.3	77.6	74.9
Phenanthrene	17.5	11.6	10.5
Anthracene	44.3	53.8	34.3
Pyrene	-	-	-
4H-cylopenta(def)phenanthrene	82.3	83.9	84.7
Methyl Phenanthrene	76.2	74.2	73.4
Benzo(ghi)fluorene	79.4	79.4	79.2
Biphenyl	40.5	49.7	51.9
Biphenylene	20.5	14.9	12.7
Cyclopenta(cd)pyrene	38.6	45.4	43.1

most significantly increased species for the 1000 K and 1400 K temperature profiles is methyl phenanthrene. As well, the 1000 K temperature profile predicts that acenaphthalene, fluoranthene, ethynyl naphthalene, and pyrene do not change significantly. The 1400 K temperature profile predicts that biphenylene does not change significantly. Refer to Figure 5.20.

The trends for poly-aromatic species differ from the previous two temperature profiles. Table 5.25 shows that species including naphthalene, hydroxyl naphthalene, acenaphthalene, fluorene, indene, methyl indene, methyl naphthalene, benzo(a)indene, ethyl naphthalene, ethenyl naphthalene, phenanthrene, anthracene, 4H-cyclopenta(def)phenanthrene, benzo(ghi)fluorene, biphenyl, and cyclopenta(cd)pyrene decrease with increasing flow rate. The remaining species including ethynyl naphthalene, benzo(a)phenanthrene, methyl phenanthrene, and biphenylene increase with increasing flow rate. As well, it also shows that pyrene and fluoranthene do not change significantly. Ethynyl naphthalene is the most significantly increased by 35.0 % and phenanthrene is the most significantly reduced by 90.7 % as flow rates are increased. These trends are not comparable to those of the previous two temperature profiles. The difference between these results compared to those of the 1000 K temperature profile is that naphthalene, acenaphthalene, fluorene, methyl indene, methyl naphthalene, benzo(a)indene, ethenyl naphthalene, anthracene, 4H-cyclopenta(def)phenanthrene, and cyclopenta(cd)pyrene are decreasing; benzo(a)phenanthrene, methyl phenanthrene, and biphenylene are increasing with increasing flow rate; and pyrene and fluoranthene are not changed significantly. The difference between these results compared to those of the 1400 K temperature profile is that naphthalene, fluorene, methyl indene, methyl naphthalene, benzo(a)indene, ethyl

Figure 5.20. Kinetic predictions of concentrations of poly-aromatic species for 14:1 air to fuel ratio, 1623 K temperature profile, and varying inlet flow rates inside the incinerator stack during sour gas incineration. **(a)** Inlet flow rate = $3.28 \times 10^5 \text{ cm}^3/\text{s}$, **(b)** Inlet flow rate = $9.83 \times 10^5 \text{ cm}^3/\text{s}$ **(c)** Inlet flow rate = $1.64 \times 10^6 \text{ cm}^3/\text{s}$.



(a)

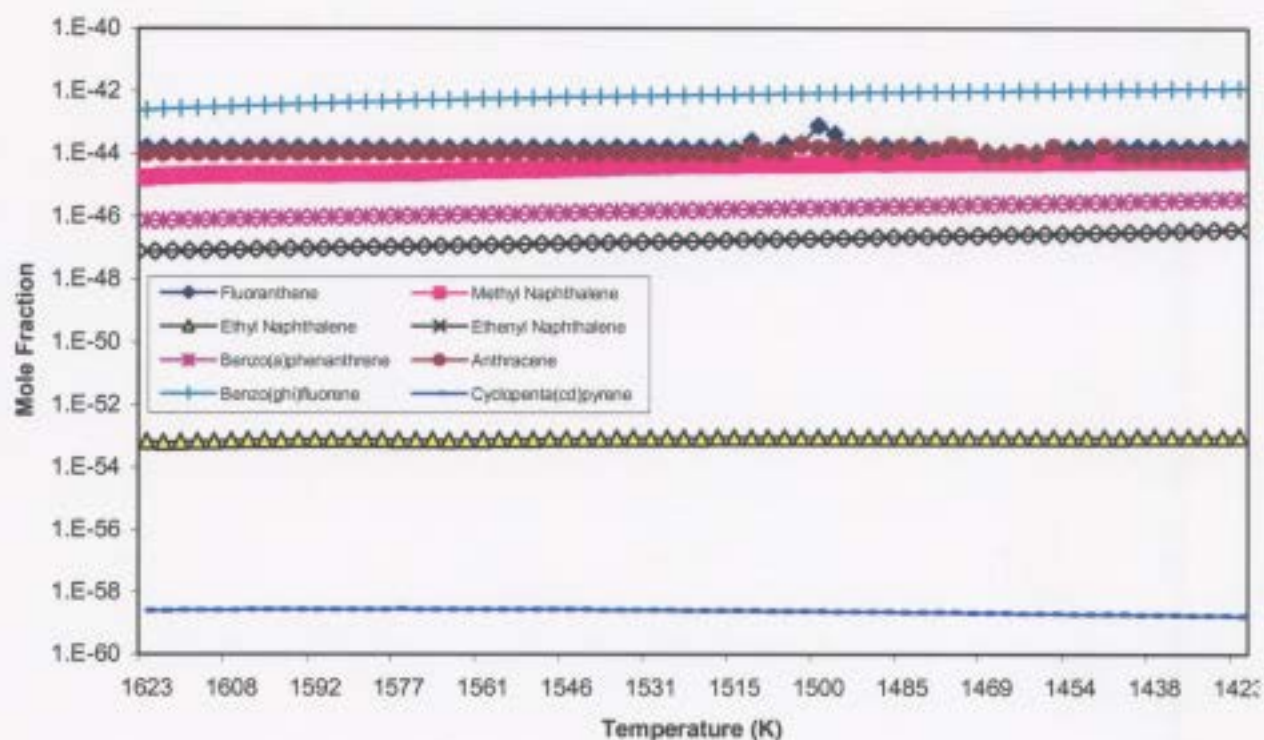
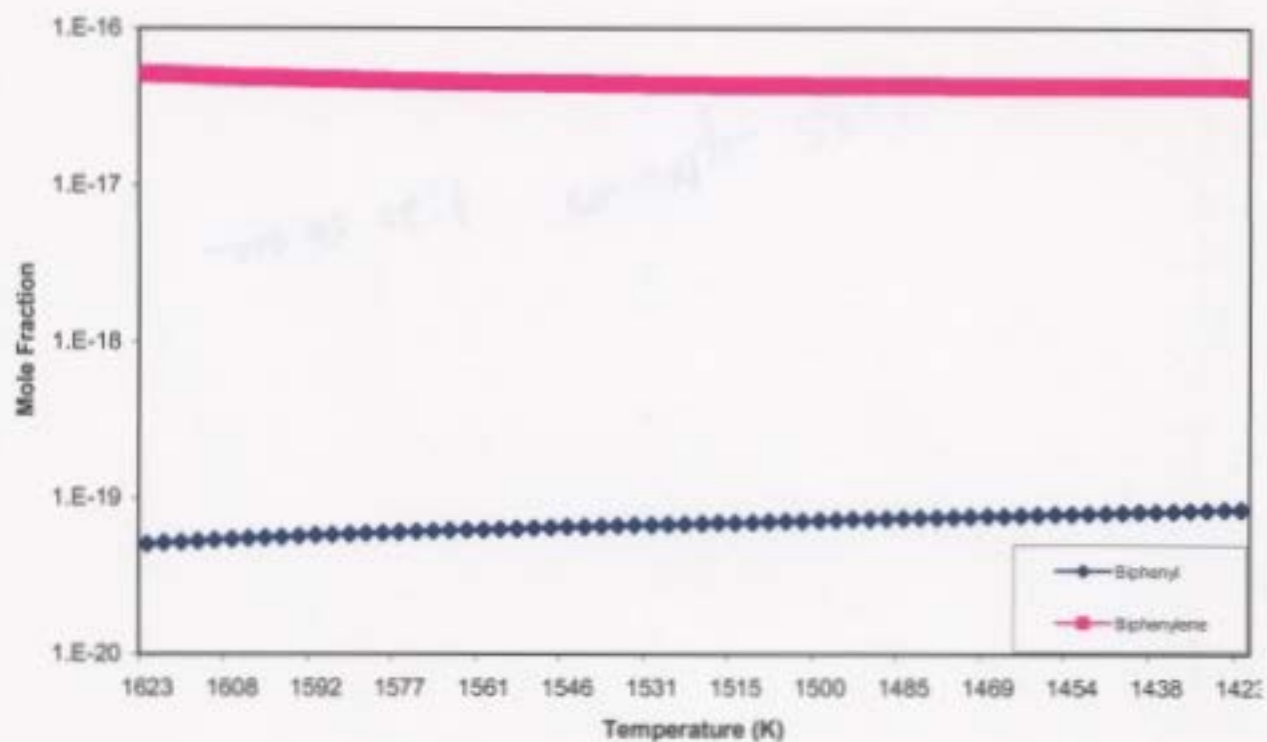


Figure 5.20 (Continued)



(a)

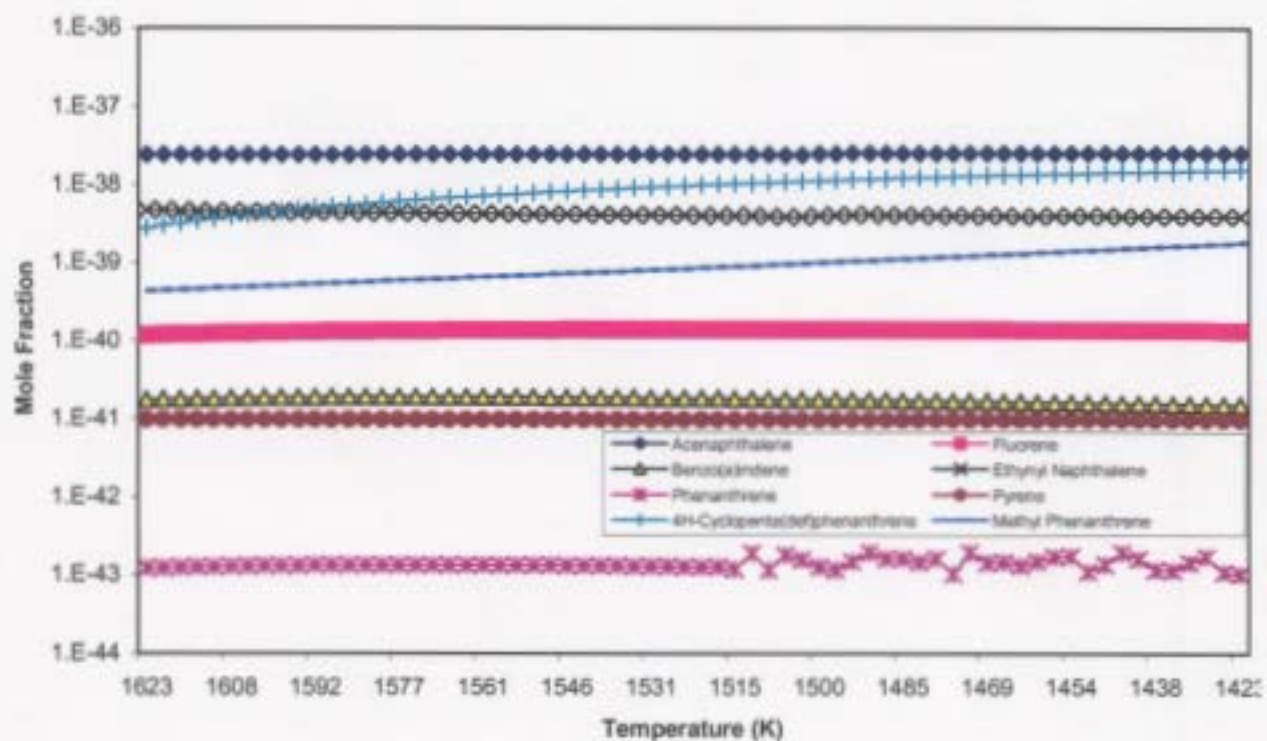
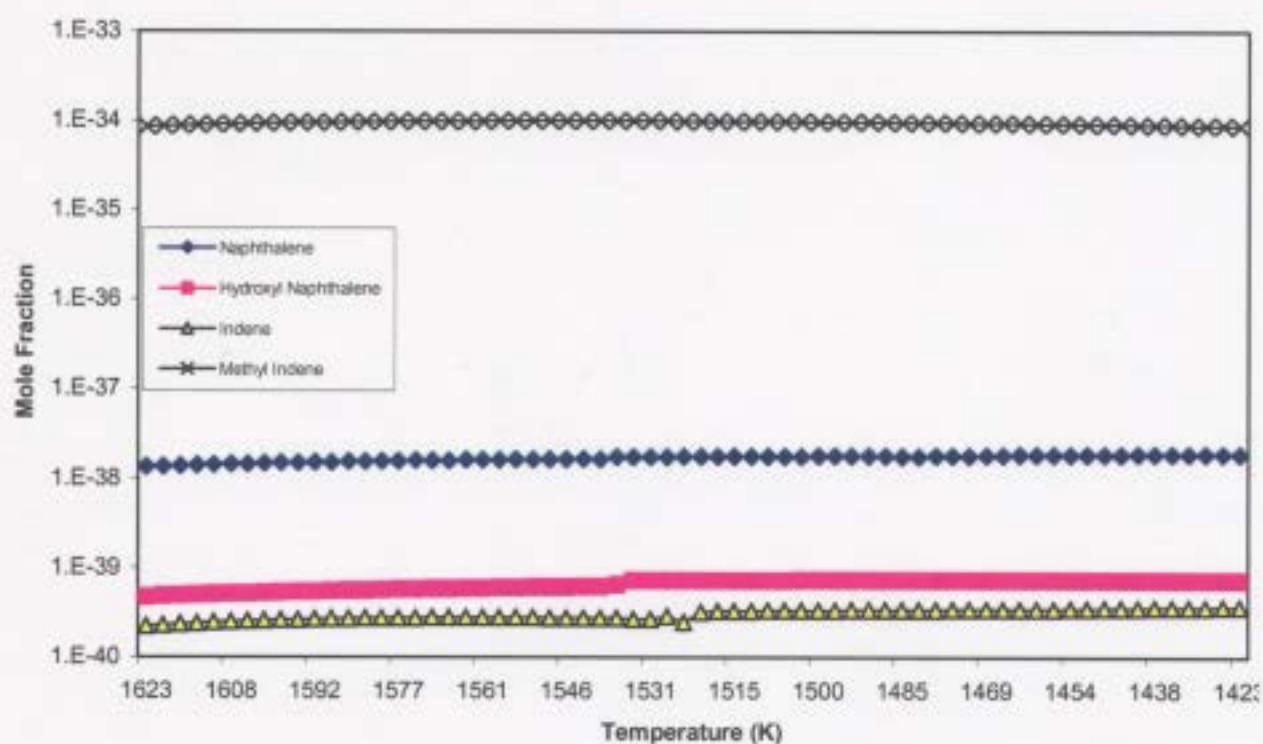


Figure 5.20 (Continued)



(b)

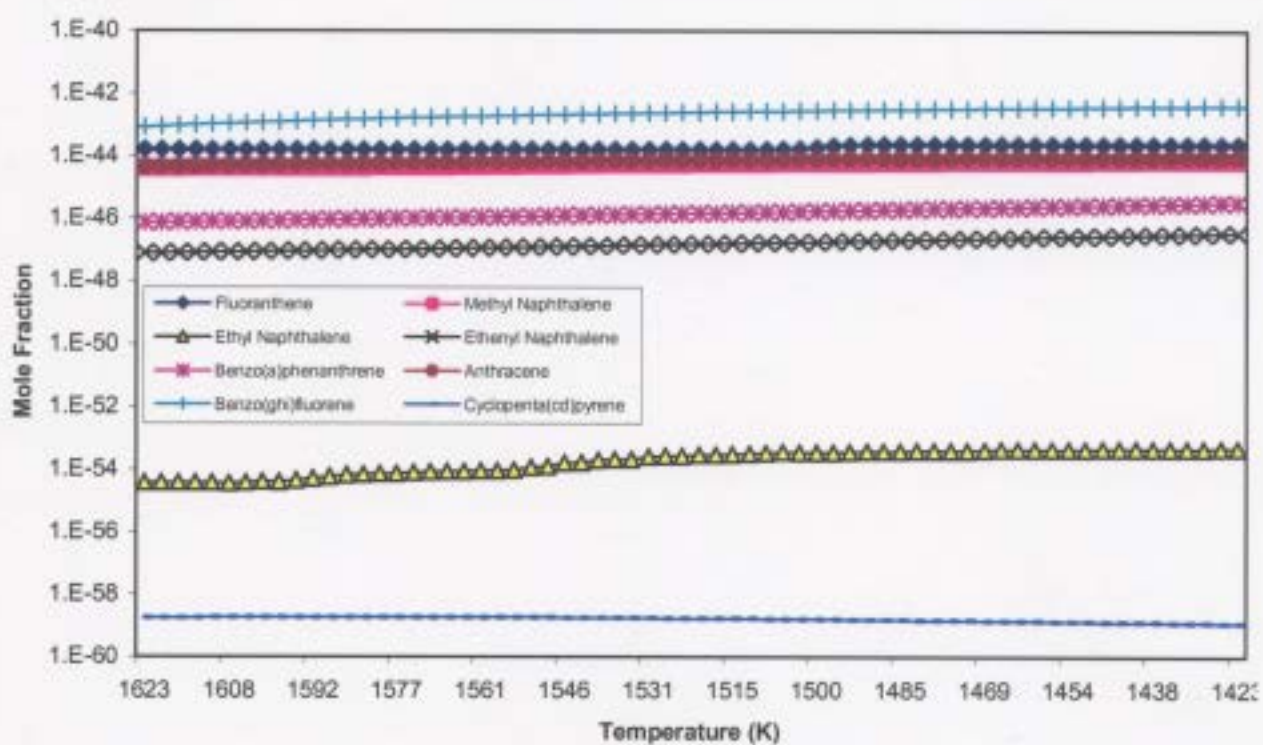
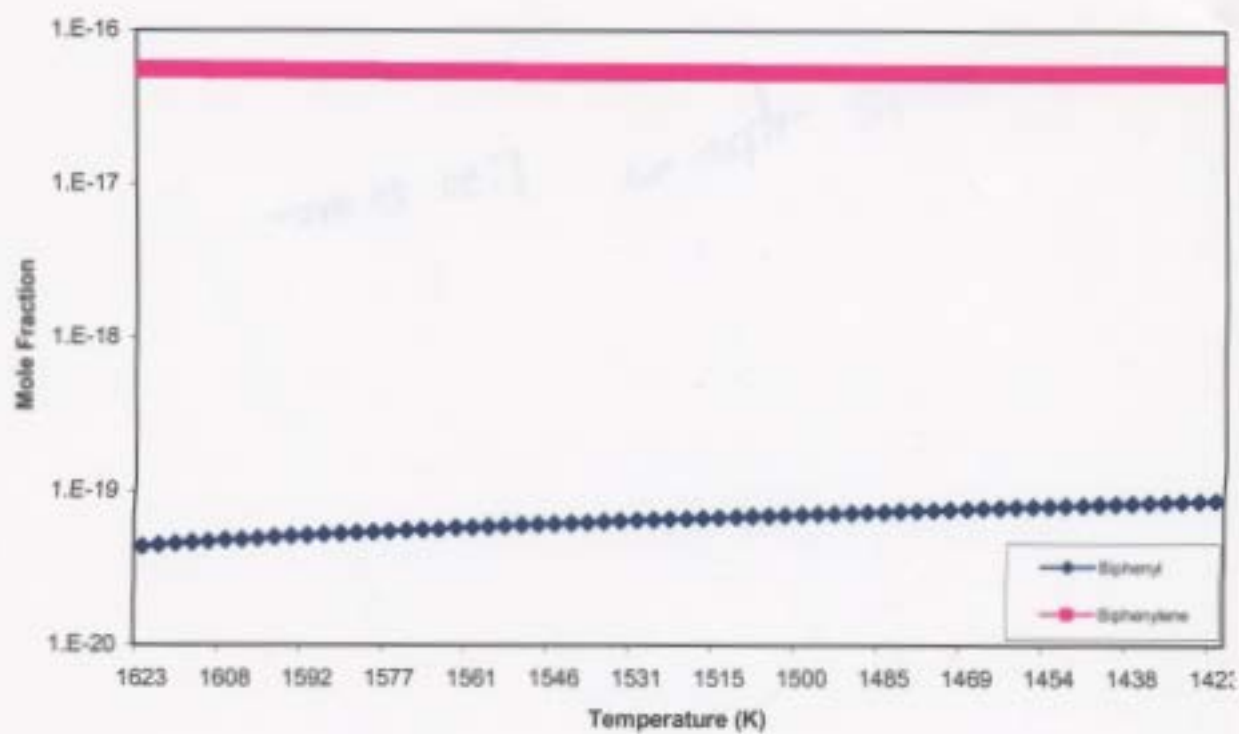


Figure 5.20 (Continued)



(b)

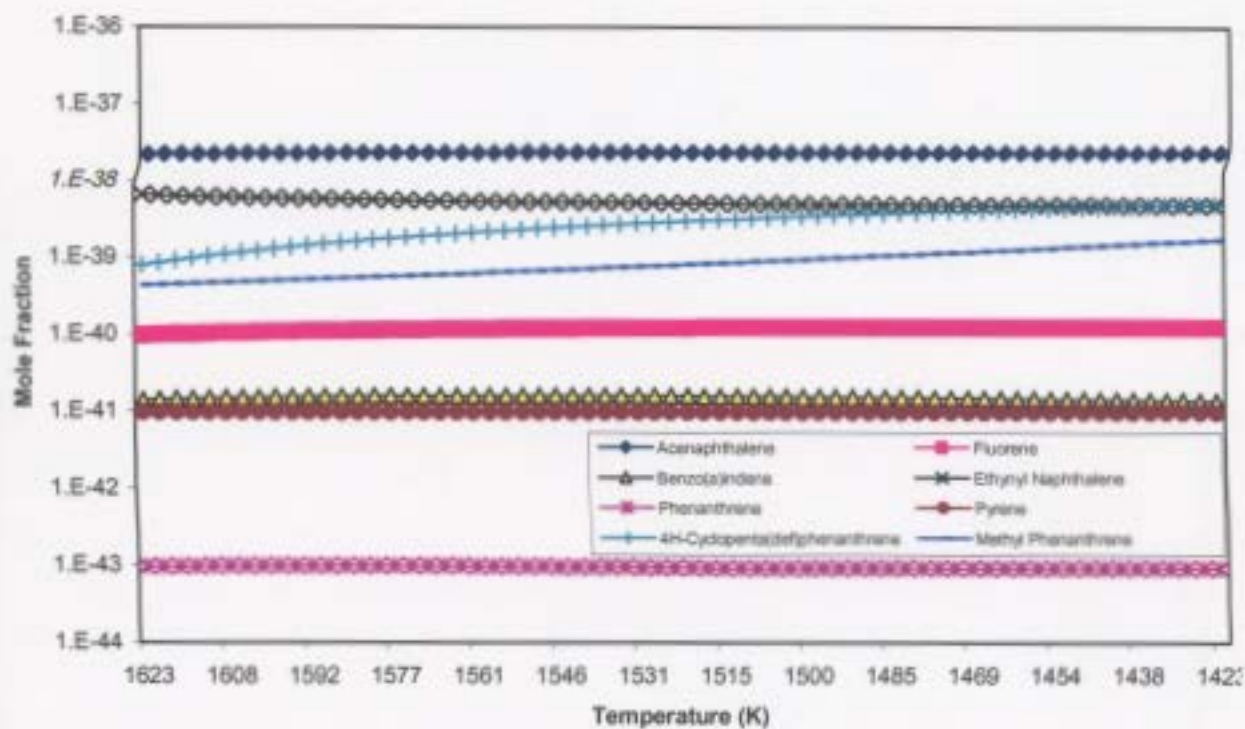
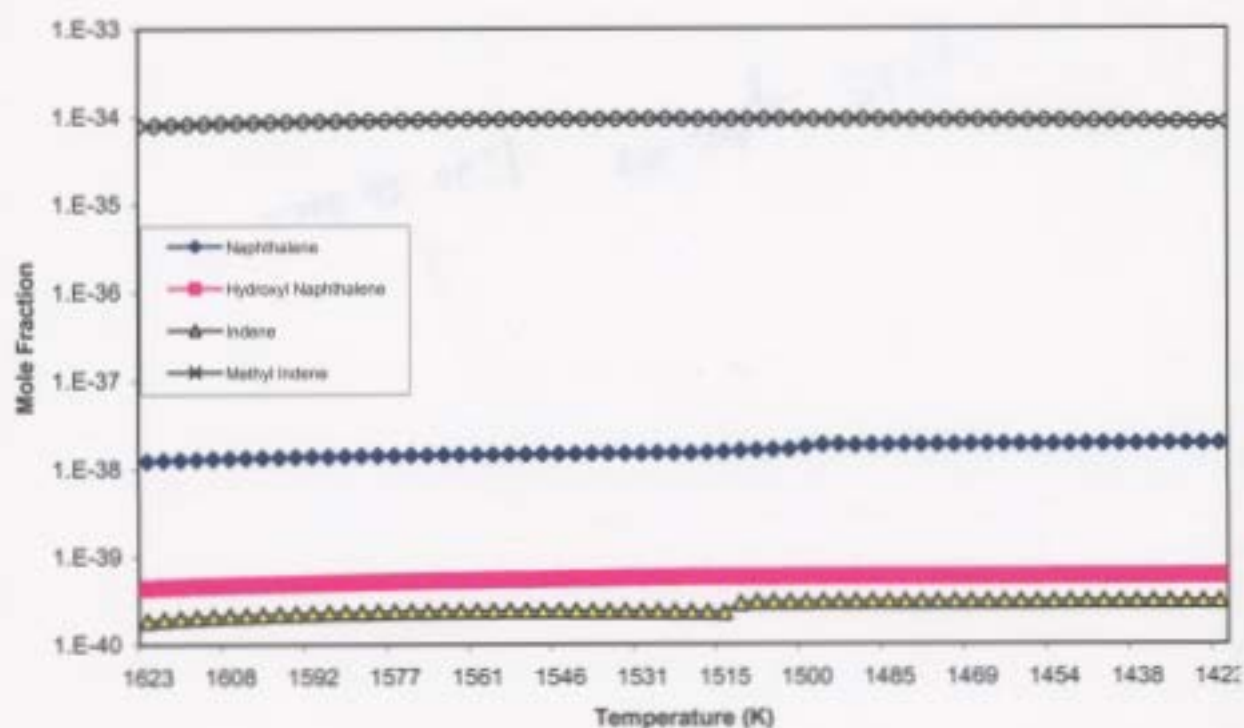


Figure 5.20 (Continued)



(c)

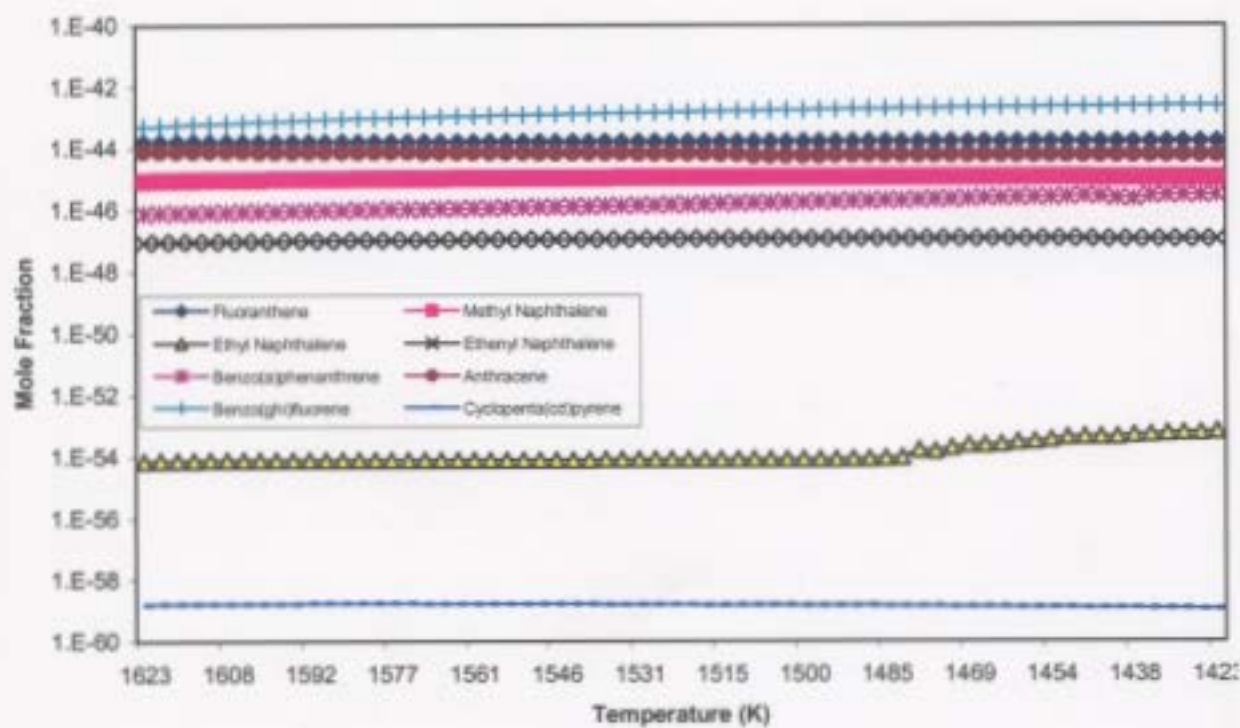
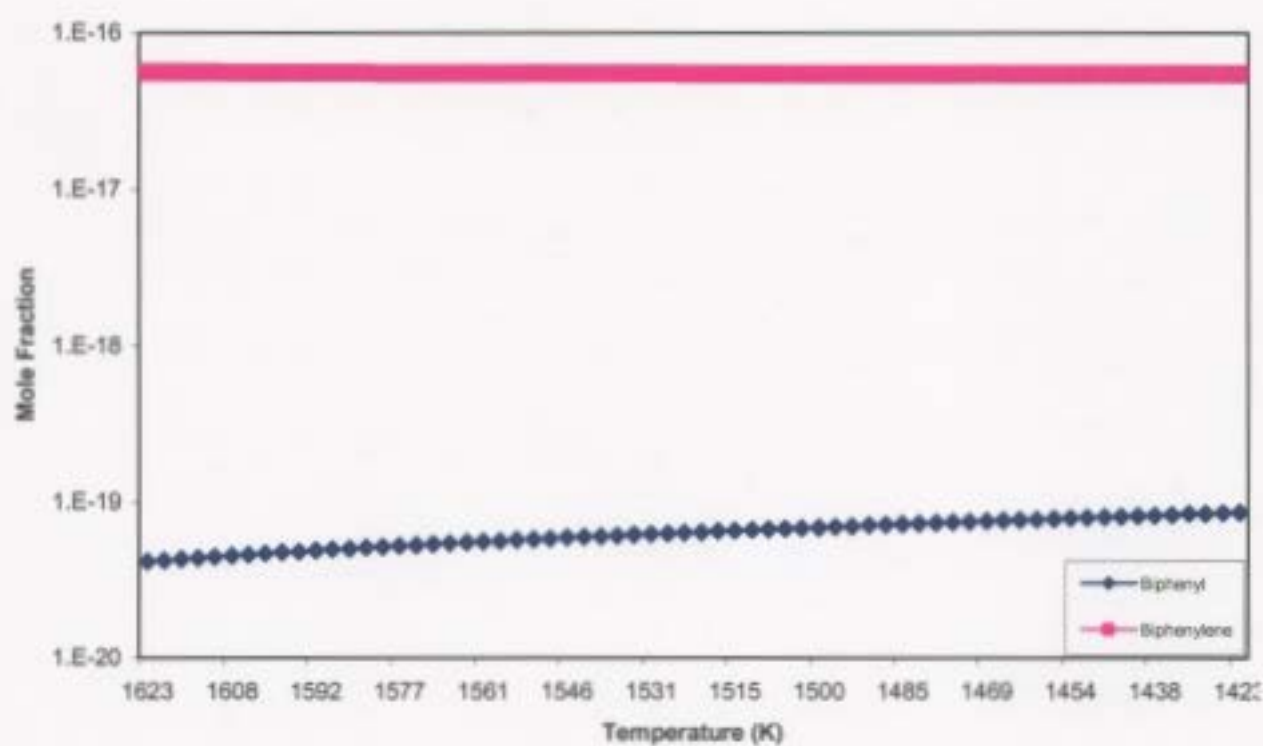
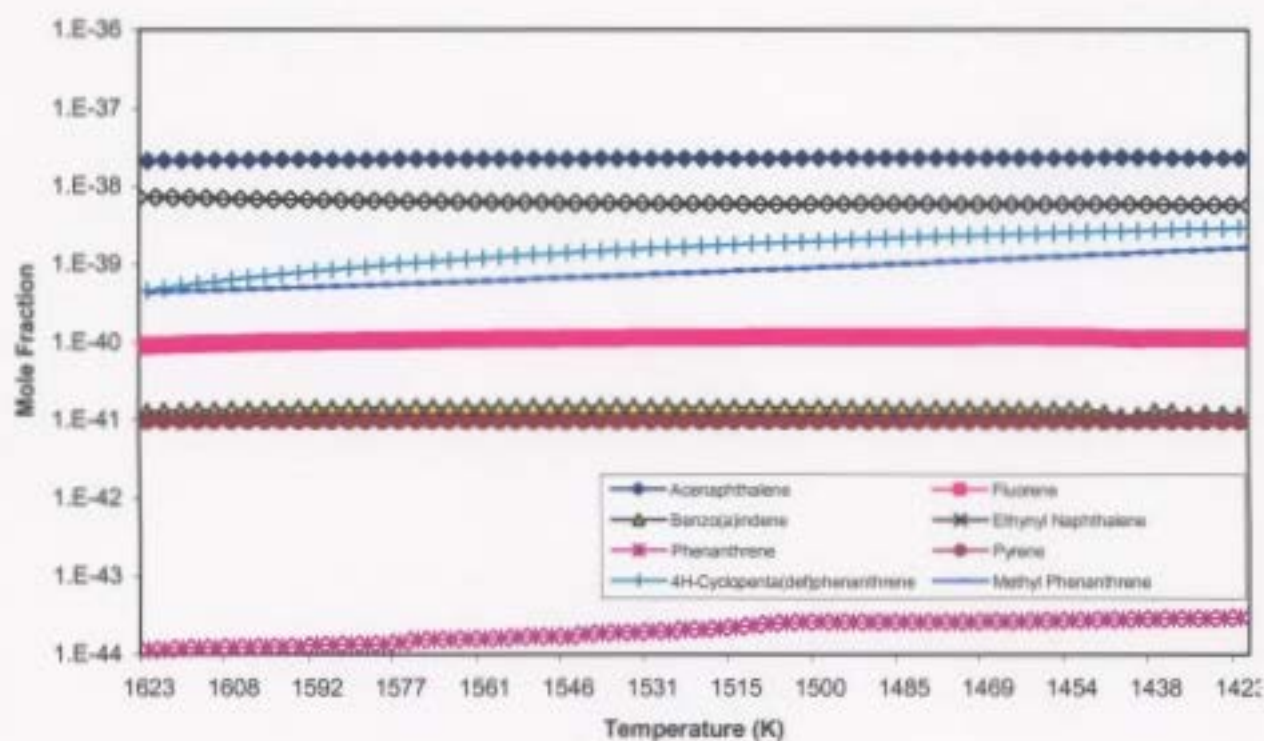


Figure 5.20 (Continued)



(c)



naphthalene, ethenyl naphthalene, anthracene, biphenyl, and cyclopenta(def)phenanthrene are decreasing; benzo(a)phenanthrene is increasing with increasing flow rate; and pyrene and fluoranthene are not changing.

Table 5.25. Kinetically predicted changes (%) in compositions for poly-aromatic species in the stack as inlet flow rates are increased from $3.28 \times 10^5 \text{ cm}^3/\text{s}$ to $1.64 \times 10^6 \text{ cm}^3/\text{s}$ under the 14:1 air to fuel ratio and 1623 K temperature profile.

Aromatic Species	Increase (%)	Decrease (%)
Naphthalene	-	35.6
Hydroxyl Naphthalene	-	35.6
Acenaphthalene	-	10.5
Fluorene	-	21.1
Fluoranthene	-	-
Indene	-	42.6
Methyl Indene	-	26.6
Methyl Naphthalene	-	51.4
Benzo(a)indene	-	26.4
Ethyl Naphthalene	-	89.3
Ethenyl Naphthalene	-	88.5
Ethynyl Naphthalene	35.0	-
Benzo(a)phenanthrene	1.52	-
Phenanthrene	-	90.7
Anthracene	-	24.3
Pyrene	-	-
4H-cyclopenta(def)phenanthrene	-	83.7
Methyl Phenanthrene	1.84	-
Benzo(ghi)fluorene	-	80.0
Biphenyl	-	17.8
Biphenylene	9.22	-
Cyclopenta(cd)pyrene	-	36.3

5.2.2. Case B: 17:1 Air to Fuel Ratio Results

5.2.2.1. Introduction

Again the input mole fraction compositions used in these simulations are output mole fraction compositions of combustion chamber calculations. The flow rates of $3.28 \times 10^5 \text{ cm}^3/\text{s}$, $9.83 \times 10^5 \text{ cm}^3/\text{s}$, and $1.64 \times 10^6 \text{ cm}^3/\text{s}$ were simulated. As in Case A, the three linear temperature profiles shown in Figure 5.8 with initial input temperatures of 1623 K, 1400 K, and 1000 K are used to calculate mole fraction compositions of species.

5.2.2.2. Oxidation Products and Light Hydrocarbon Species Results

5.2.2.2.1. Kinetic Results for 1000 K Temperature Profile

Kinetic predictions for oxidation products and light hydrocarbon species within the stack have similar trends for varying flow rates, and are similar to results from the ratio of 14:1 air to fuel with the same temperature profile. The compositions for light hydrocarbons and oxidation products are smaller in this case compared to Case A under the same temperature profile.

As shown in Table 5.26, butadiene and methane have the most significant average reductions in composition during cooling by 99.4 % and 99.2 %, whereas the composition for butane did not decrease significantly. Compositions for carbon monoxide decreased by an average significant amount of 85.1 % as the temperature decreased toward the top of the stack. Note that there is no significant change for water and carbon dioxide during cooling.

Table 5.26. Kinetically predicted reductions (%) in compositions for lower weight hydrocarbons and oxidation products in the stack during cooling under the conditions of 17:1 air to fuel ratio, 1000 K temperature profile, and varying flow rates of (a). $3.28 \times 10^5 \text{ cm}^3/\text{s}$, (b). $9.83 \times 10^5 \text{ cm}^3/\text{s}$, and (c). $1.64 \times 10^6 \text{ cm}^3/\text{s}$.

Species	Flow Rate (a)	Flow Rate (b)	Flow Rate (c)
Methane	99.5	98.4	99.7
Ethane	95.6	88.7	85.5
Ethene	98.5	93.0	99.2
Ethyne	92.7	40.2	98.5
Propane	97.8	92.5	98.3
Propene	99.5	80.6	98.3
Propyne	99.5	79.1	97.8
Butane	-	-	-
Butene	99.2	67.9	82.7
Butyne	68.9	93.5	85.5
Butadiene	99.1	99.6	99.4
Butadiyne	99.8	99.4	89.4
Water	-	-	-
Carbon Monoxide	99.9	68.1	87.2
Carbon Dioxide	-	-	-

Compositions for lighter weight hydrocarbons and oxidation products are predicted to have the same flow rate trends as in the 1000 K temperature of Case A results. The percent changes in compositions in this case are shown in Table 5.27. Most of these changes are much larger than those obtained in Case A for the same temperature profile. Ethane, propane, propyne, butyne, and butadiyne have the most significant reductions by 99.9 %. As well, butane, water and carbon dioxide do not change significantly.

Table 5.27. Kinetically predicted changes in composition (%) for lower weight hydrocarbons and oxidation products within the stack under the 1000 K temperature profile, 17:1 air to fuel ratio with increasing flow rate from $3.28 \times 10^5 \text{ cm}^3/\text{s}$ to $1.64 \times 10^6 \text{ cm}^3/\text{s}$.

Species	% Increase	% Decrease
Methane	-	99.5
Ethane	-	99.9
Ethene	-	79.3
Ethyne	-	99.4
Propane	-	99.9
Propene	-	92.8
Propyne	-	99.9
Butane	-	-
Butene	-	99.8
Butyne	-	99.9
Butadiene	-	62.2
Butadiyne	-	99.9
Water	-	-
Carbon Monoxide	99.4	-
Carbon Dioxide	-	-

5.2.2.2.2. Kinetic Results for 1400 K Temperature Profile

Kinetic results from the temperature profile with an initial internal combustion chamber temperature of 1400 K and a 17:1 air to fuel ratio yield trends that are similar to the temperature profile of 1400 K and a 14 air to 1 fuel ratio. Compositions for oxidation products and light hydrocarbon species within the stack have similar trends for product compositions for varying flow rates, but are smaller in magnitude in this case compared to Case A under the same temperature profile.

The cooling of gases results in a composition for lighter weight hydrocarbons and oxidation products. Reductions for this case are shown in Table 5.28 for the three flow rates tested. Note that once again butadiene and butadiyne have the most significant

average decreases in composition by 99.8 %, whereas compositions for butane, water, and carbon dioxide did not change.

Table 5.28. Kinetically predicted reductions (%) in compositions from inlet lower weight hydrocarbons and oxidation products in the stack during cooling under the conditions of 17:1 air to fuel ratio, 1400 K temperature profile, and varying flow rates of (a). 3.28×10^5 cm³/s, (b). 9.83×10^5 cm³/s, and (c). 1.64×10^6 cm³/s.

Species	Flow Rate (a)	Flow Rate (b)	Flow Rate (c)
Methane	99.6	99.7	93.4
Ethane	99.1	99.9	50.2
Ethene	97.1	96.5	96.3
Ethyne	87.3	79.6	75.4
Propane	99.9	97.0	62.4
Propene	99.9	97.2	98.0
Propyne	97.0	99.9	95.8
Butane	-	-	-
Butene	98.7	79.7	32.1
Butyne	80.0	99.9	95.0
Butadiene	99.6	99.9	99.9
Butadiyne	99.6	99.9	99.9
Water	-	-	-
Carbon Monoxide	98.3	98.3	98.3
Carbon Dioxide	-	-	-

As previously mentioned, composition trends over increasing flow rates are the same as Case A 1400 K temperature profile results. With the exception of ethane and butane, all lower weight hydrocarbons are reduced when flow rates are increased. However, oxidation products in this case do not change significantly. Table 5.29 indicates that propyne has the most significant reduction by 99.9 % as flow rates are increased.

Table 5.29. Kinetically predicted changes in composition (%) for lower weight hydrocarbons and oxidation products within the stack under the 1400 K temperature profile, 17:1 air to fuel ratio with increasing flow rate from $3.28 \times 10^5 \text{ cm}^3/\text{s}$ to $1.64 \times 10^6 \text{ cm}^3/\text{s}$.

Species	% Increase	% Decrease
Methane	-	91.3
Ethane	-	97.4
Ethene	-	-
Ethyne	-	2.90
Propane	-	99.7
Propene	-	93.8
Propyne	-	99.9
Butane	-	-
Butene	-	94.7
Butyne	-	97.9
Butadiene	-	17.6
Butadiyne	-	98.4
Water	-	-
Carbon Monoxide	-	-
Carbon Dioxide	-	-

5.2.2.2.3. Kinetic Results for 1623 K Temperature Profile

The kinetic results for the 1623 K temperature profile yield similar results as the temperature profile of 1623 K in Case A, but this case has smaller compositions for light hydrocarbons and oxidation products when compared to Case A. Compositions for oxidation products and light hydrocarbon species within the stack have similar trends for varying flow rates.

The majority of species show a reduction as the temperature gets lower in the stack. Reductions for compositions are shown in Table 5.30. Once again, butadiyne has the most average significant decrease in composition by 99.7 %, whereas the composition for butane, water, and carbon dioxide does not decrease significantly.

Table 5.30. Kinetically predicted reductions (%) in compositions from inlet lower weight hydrocarbons and oxidation products in the stack during cooling under the conditions of 17:1 air to fuel ratio, 1623 K temperature profile, and varying flow rates of (a). $3.28 \times 10^5 \text{ cm}^3/\text{s}$, (b). $9.83 \times 10^5 \text{ cm}^3/\text{s}$, and (c). $1.64 \times 10^6 \text{ cm}^3/\text{s}$.

Species	Flow Rate (a)	Flow Rate (b)	Flow Rate (c)
Methane	91.3	89.5	88.2
Ethane	87.3	85.4	83.9
Ethene	92.1	90.7	90.0
Ethyne	74.6	73.1	71.7
Propane	95.9	93.7	92.7
Propene	94.6	93.4	92.6
Propyne	96.9	96.5	96.1
Butane	-	-	-
Butene	82.3	80.1	78.3
Butyne	98.5	98.3	98.3
Butadiene	98.0	97.8	97.9
Butadiyne	99.7	99.7	99.7
Water	-	-	-
Carbon Monoxide	92.8	92.5	92.3
Carbon Dioxide	-	-	-

Inlet flow rate trends for product compositions are similar to those previously mentioned, including those of the temperature profile of 1623 K in Case A, but different from the 1000 K and 1400 K temperature profiles. In this case, all hydrocarbons are reduced, as well as carbon monoxide. Refer to Table 5.31 for percent changes in these species. As in Case A, propane has the most significant reduction by 73.7 %. There is no change predicted to occur for butane, water, and carbon dioxide as the flow rates are increased.

Table 5.31. Kinetically predicted changes in composition (%) for lower weight hydrocarbons and oxidation products within the stack under the 1623 K temperature profile, 17:1 air to fuel ratio with increasing flow rate from $3.28 \times 10^5 \text{ cm}^3/\text{s}$ to $1.64 \times 10^6 \text{ cm}^3/\text{s}$.

Species	% Increase	% Decrease
Methane	-	60.7
Ethane	-	49.9
Ethene	-	27.8
Ethyne	-	37.5
Propane	-	73.7
Propene	-	59.1
Propyne	-	64.3
Butane	-	-
Butene	-	48.5
Butyne	-	32.7
Butadiene	-	9.80
Butadiyne	-	20.2
Water	-	-
Carbon Monoxide	-	25.0
Carbon Dioxide	-	-

5.2.2.3. Sulphur-Containing Species Results

5.2.2.3.1. Kinetic Results for 1000 K Temperature Profile

As with the predictions for the 1000 K temperature profile and 14:1 air to fuel, predictions for sulphur-containing species show a decreasing trend during the cooling process, and an increasing trend as the flow rates are increased. There is an overall increase in compositions for hydrogen sulphide, carbon sulphide, and carbonyl sulphide when ranging the air to fuel ratio from 14:1 to 17:1, but a decrease for sulphur dioxide. The most abundant species is sulphur dioxide and least abundant species is carbon sulphide.

During the cooling process, carbonyl sulphide compositions decrease by an average significant amount of 99.6 %, hydrogen sulphide by 98.9 %, carbon sulphide by

98.8 %, and sulphur dioxide by only 2.13 %. Increasing flow rates result in an increase of 75.8 % for hydrogen sulphide, 67.1 % for carbonyl sulphide, 47.7 % for carbon sulphide, and insignificantly for sulphur dioxide.

5.2.2.3.2. Kinetic Results for 1400 K Temperature Profile

Compositions of sulphur-containing species within the stack under the 1400 K temperature profile show similar results to Case A under the same temperature profile. As well, an overall general decrease in sulphur species compositions occurs as air to fuel ratios are changed from 14:1 to 17:1.

Sulphur species are found to decrease during the cooling process and increase with increasing inlet flow rate. Compositions for hydrogen sulphide, carbon sulphide, and carbonyl sulphide are reduced by 99.9 %, while sulphur dioxide is reduced by 2.09 % during cooling. Increasing flow rates results in increases of 45.3 % for hydrogen sulphide, 1.48 % for carbon sulphide, and insignificant amounts for carbonyl sulphide and sulphur dioxide. These reductions are much less than those found for the 1000 K temperature profile.

5.2.2.3.3. Kinetic Results for 1623 K Temperature Profile

Kinetic predictions in this case are in agreement with the previous results of temperature profile of 1623 K in Case A, except that sulphur species compositions are smaller than those of Case A. Kinetic predictions conclude that sulphur-containing species compositions have the same trends for varying flow rates and over the temperature range.

Composition reductions during cooling are similar to previous results. They are 99.5 % for hydrogen sulphide, 99.9 % for carbon sulphide, 99.7 % for carbonyl sulphide, and no change for sulphur dioxide. However, in contrast to the temperature profiles of 1000 K and 1400 K, some sulphur-containing species compositions are predicted to decrease with increasing inlet flow rate. Hydrogen sulphide has the most significant reduction by 22.2 %, followed by 21.6 % for carbonyl sulphide, 12.6 % for carbon sulphide, and no change for sulphur dioxide.

5.2.2.4. Aromatic and Poly-Aromatic Hydrocarbon Results

5.2.2.4.1. Kinetic Results for 1000 K Temperature Profile

Aromatic and poly-aromatic hydrocarbons composition results in Case B are in agreement with results from Case A under the same temperature profile. It should also be noted that with the exception of ethyl methyl benzene, product compositions decreased when the air to fuel ratio is changed from 14:1 to 17:1.

Results for both single ring and poly-aromatic species show the same product composition trends over the temperature as Case A results. However, percent composition reductions and increases during cooling are somewhat different. This difference is due to larger oxygen content in the inlet composition. Table 5.32 shows that the most significant reduction during cooling is methyl benzene by 95.1% and no significant reduction for phenol. Table 5.33 shows that during cooling, benzo(a)phenanthrene and methyl phenanthrene compositions are predicted to have the most significant increases by 91.0 % and 92.9 % respectively. It should be noted that

acenaphthalene, fluoranthene, ethynyl naphthalene, and pyrene are not significantly changed.

Table 5.32. Kinetically predicted reductions (%) in compositions for single ring aromatic species in the stack under the conditions of 17:1 air to fuel ratio, 1000 K temperature profile, and varying flow rates of (a). $3.28 \times 10^5 \text{ cm}^3/\text{s}$, (b). $9.83 \times 10^5 \text{ cm}^3/\text{s}$, and (c). $1.64 \times 10^6 \text{ cm}^3/\text{s}$.

Aromatic Species	Flow Rate (a)	Flow Rate (b)	Flow Rate (c)
Benzene	96.9	99.0	88.9
Phenol	-	-	-
Methyl Benzene	99.9	99.9	85.5
Benzaldehyde	99.4	98.9	75.6
Hydroxyl Methyl Benzene	97.9	82.7	97.0
Ethyl Benzene	89.4	89.6	82.5
Ethenyl Benzene	92.7	97.4	93.2
Ethynyl Benzene	2.69	-	-
Dimethyl Benzene	65.3	63.2	61.0
Ethyl Methyl Benzene	88.7	98.1	95.6
Ethenyl Methyl Benzene	98.1	89.2	87.9

Percent changes in composition that occur when increasing flow rate are slightly different from those obtained in Case A. In this case, ethenyl methyl benzene is decreasing with increasing flow rate. The most significant increase is ethenyl benzene by 99.9 % and the most significant decrease is ethyl methyl benzene by 100 %. As well, in this case indene compositions are increasing with increasing flow rate in this case. The most significant increases are naphthalene, methyl naphthalene, ethenyl naphthalene, and cyclopenta(cd)pyrene by 99.9 % and the most significant decrease is biphenyl and biphenylene by 99.9 %. These percent changes can be found in Tables 5.34 and 5.35.

Table 5.33. Kinetically predicted increases (%) in compositions for poly-aromatic species in the stack under the conditions of 17:1 air to fuel ratio, 1000 K temperature profile, and varying flow rates of (a). $3.28 \times 10^5 \text{ cm}^3/\text{s}$, (b). $9.83 \times 10^5 \text{ cm}^3/\text{s}$, and (c). $1.64 \times 10^6 \text{ cm}^3/\text{s}$.

Poly-Aromatic Species	Flow Rate (a)	Flow Rate (b)	Flow Rate (c)
Naphthalene	80.4	79.4	82.3
Hydroxyl Naphthalene	89.8	71.1	90.6
Acenaphthalene	-	-	-
Fluorene	80.1	95.0	88.5
Fluoranthene	-	-	-
Indene	54.8	62.4	75.0
Methyl Indene	87.8	81.2	66.1
Methyl Naphthalene	90.9	72.4	69.0
Benzo(a)indene	87.7	79.4	48.1
Ethyl Naphthalene	90.9	79.1	92.3
Ethenyl Naphthalene	88.9	86.5	84.9
Ethynyl Naphthalene	-	-	-
Benzo(a)phenanthrene	95.6	92.9	84.6
Phenanthrene	91.1	89.4	83.9
Anthracene	92.0	89.0	84.5
Pyrene	-	-	-
4H-cylopenta(def)phenanthrene	96.3	87.9	86.3
Methyl Phenanthrene	96.8	82.6	89.4
Benzo(ghi)fluorene	86.6	90.7	87.2
Biphenyl	84.4	85.1	89.4
Biphenylene	3.65	4.76	12.29
Cyclopenta(cd)pyrene	79.2	95.9	89.8

Table 5.34. Kinetically predicted changes (%) in compositions for single ring aromatic species in the stack as inlet flow rates are increased from $3.28 \times 10^5 \text{ cm}^3/\text{s}$ to $1.64 \times 10^6 \text{ cm}^3/\text{s}$ under the 17:1 air to fuel ratio and 1000 K temperature profile.

Aromatic Species	Increase (%)	Decrease (%)
Benzene	-	82.6
Phenol	34.2	-
Methyl Benzene	-	98.0
Benzaldehyde	-	97.3
Hydroxyl Methyl Benzene	98.1	-
Ethyl Benzene	92.5	-
Ethenyl Benzene	99.9	-
Ethynyl Benzene	-	98.4
Dimethyl Benzene	-	90.1
Ethyl Methyl Benzene	-	100.
Ethenyl Methyl Benzene	-	99.9

Table 5.35. Kinetically predicted changes (%) in compositions for poly-aromatic species in the stack as inlet flow rates are increased from $3.28 \times 10^5 \text{ cm}^3/\text{s}$ to $1.64 \times 10^6 \text{ cm}^3/\text{s}$ under the 17:1 air to fuel ratio and 1000 K temperature profile.

Aromatic Species	Increase (%)	Decrease (%)
Naphthalene	99.9	-
Hydroxyl Naphthalene	-	95.3
Acenaphthalene	78.0	-
Fluorene	97.1	-
Fluoranthene	-	35.8
Indene	99.8	-
Methyl Indene	98.6	-
Methyl Naphthalene	99.9	-
Benzo(a)indene	96.5	-
Ethyl Naphthalene	-	98.8
Ethenyl Naphthalene	99.9	-
Ethynyl Naphthalene	52.9	-
Benzo(a)phenanthrene	-	80.0
Phenanthrene	-	59.2
Anthracene	54.6	-
Pyrene	98.5	-
4H-cyclopenta(def)phenanthrene	67.1	-
Methyl Phenanthrene	-	21.7
Benzo(ghi)fluorene	-	98.1
Biphenyl	-	99.9
Biphenylene	-	99.9
Cyclopenta(cd)pyrene	99.9	-

5.2.2.4.2. Kinetic Results for 1400 K Temperature Profile

When compared to Case A, compositions of aromatic and poly-aromatic hydrocarbons within the incinerator stack have similar product composition trends over the temperature range and for varying flow rates. Single ring aromatic species are predicted to decrease during the cooling process and poly-aromatic species are predicted to increase. It should be noted that with the exception of indene and ethenyl methyl benzene, aromatic and poly-aromatic compositions decrease as air to fuel ratio is changed from 14:1 to 17:1.

Table 5.36 show that the most significant reduction in composition is ethenyl benzene by 95.8 %, while no change for phenol. Table 5.37 shows that during cooling, methyl phenanthrene compositions are predicted to have the most significant increase by 97.8 %. Biphenylene is predicted to have no significant change.

Table 5.36. Kinetically predicted reductions (%) in compositions for single ring aromatic species in the stack under the conditions of 17:1 air to fuel ratio, 1400 K temperature profile, and varying flow rates of (a). $3.28 \times 10^5 \text{ cm}^3/\text{s}$, (b). $9.83 \times 10^5 \text{ cm}^3/\text{s}$, and (c). $1.64 \times 10^6 \text{ cm}^3/\text{s}$.

Aromatic Species	Flow Rate (a)	Flow Rate (b)	Flow Rate (c)
Benzene	98.9	88.7	88.7
Phenol	-	-	-
Methyl Benzene	87.0	98.7	99.7
Benzaldehyde	90.4	90.9	90.5
Hydroxyl Methyl Benzene	88.2	90.4	95.7
Ethyl Benzene	77.1	98.4	95.7
Ethenyl Benzene	97.6	91.9	97.9
Ethynyl Benzene	95.6	80.6	94.6
Dimethyl Benzene	77.1	93.2	96.1
Ethyl Methyl Benzene	90.9	91.0	91.7
Ethenyl Methyl Benzene	94.4	89.4	79.0

Table 5.37. Kinetically predicted increases (%) in compositions for poly-aromatic species in the stack under the conditions of 17:1 air to fuel ratio, 1400 K temperature profile, and varying flow rates of (a). $3.28 \times 10^5 \text{ cm}^3/\text{s}$, (b). $9.83 \times 10^5 \text{ cm}^3/\text{s}$, and (c). $1.64 \times 10^6 \text{ cm}^3/\text{s}$.

Poly-Aromatic Species	Flow Rate (a)	Flow Rate (b)	Flow Rate (c)
Naphthalene	76.3	76.0	75.2
Hydroxyl Naphthalene	81.9	89.8	76.3
Acenaphthalene	79.4	75.0	83.7
Fluorene	31.6	86.7	52.4
Fluoranthene	75.8	69.1	98.5
Indene	15.6	25.4	43.0
Methyl Indene	79.0	90.2	83.9
Methyl Naphthalene	20.5	6.51	24.5
Benzo(a)indene	86.9	94.2	82.9
Ethyl Naphthalene	96.4	81.2	76.1
Ethenyl Naphthalene	54.8	76.0	77.1
Ethynyl Naphthalene	71.5	84.8	78.0
Benzo(a)phenanthrene	91.9	77.1	90.1
Phenanthrene	92.1	72.6	77.0
Anthracene	75.8	79.6	78.3
Pyrene	-	-	3.21
4H-cylopenta(def)phenanthrene	75.1	74.6	99.8
Methyl Phenanthrene	98.1	97.6	97.6
Benzo(ghi)fluorene	90.9	95.8	99.9
Biphenyl	60.2	67.4	69.2
Biphenylene	-	-	-
Cyclopenta(cd)pyrene	79.2	95.9	93.5

Changes in composition that occur when increasing flow rate are similar for single ring and poly-aromatic species from those obtained in Case A. The sole difference from the trends in these results is that in this case hydroxyl methyl benzene compositions decreases with increasing flow rate. Methyl benzene increases by the most significant amount of 48.5 % and the most significant decrease is for ethyl methyl benzene by 99.9 %, which are not the same as Case A. Refer to Table 5.38. Note that benzene and phenol does not change significantly as the flow rate is increased.

Table 5.38. Kinetically predicted changes (%) in compositions for single ring aromatic species in the stack as inlet flow rates are increased from $3.28 \times 10^5 \text{ cm}^3/\text{s}$ to $1.64 \times 10^6 \text{ cm}^3/\text{s}$ under the 17:1 air to fuel ratio and 1400 K temperature profile.

Aromatic Species	Increase (%)	Decrease (%)
Benzene	-	-
Phenol	-	-
Methyl Benzene	48.5	-
Benzaldehyde	21.0	-
Hydroxyl Methyl Benzene	-	80.2
Ethyl Benzene	-	98.5
Ethenyl Benzene	-	59.4
Ethynyl Benzene	-	95.5
Dimethyl Benzene	-	88.0
Ethyl Methyl Benzene	-	99.9
Ethenyl Methyl Benzene	-	95.0

Table 5.39 shows results that are extremely similar to those from Case A. The only difference is that in this case benzo(a)phenanthrene and 4H-cyclopenta(def)phenanthrene are increasing with increasing flow rate and anthracene is decreasing with increasing flow rate. The most significant increases are fluoranthene by 98.0 % and ethyl naphthalene by 95.8 %, and the most significant decrease is benzo(ghi)fluorene by 95.8 %. There is no change for acenaphthalene and biphenylene.

Table 5.39. Kinetically predicted changes (%) in compositions for poly-aromatic species in the stack as inlet flow rates are increased from $3.28 \times 10^5 \text{ cm}^3/\text{s}$ to $1.64 \times 10^6 \text{ cm}^3/\text{s}$ under the 17:1 air to fuel ratio and 1400 K temperature profile.

Aromatic Species	Increase (%)	Decrease (%)
Naphthalene	73.3	-
Hydroxyl Naphthalene	-	94.5
Acenaphthalene	-	-
Fluorene	68.2	-
Fluoranthene	98.0	-
Indene	-	49.1
Methyl Indene	41.7	-
Methyl Naphthalene	85.6	-
Benzo(a)indene	83.9	-
Ethyl Naphthalene	95.8	-
Ethenyl Naphthalene	78.7	-
Ethynyl Naphthalene	58.9	-
Benzo(a)phenanthrene	91.0	-
Phenanthrene	-	40.9
Anthracene	-	80.9
Pyrene	88.7	-
4H-cyclopenta(def)phenanthrene	3.84	-
Methyl Phenanthrene	23.6	-
Benzo(ghi)fluorene	-	95.8
Biphenyl	3.32	-
Biphenylene	-	-
Cyclopenta(cd)pyrene	40.3	-

5.2.2.4.3. Kinetic Results for 1623 K Temperature Profile

Under the conditions of 17:1 air to fuel ratio and the temperature profile with an initial internal combustion temperature of 1623 K, the compositions of aromatic and poly-aromatic hydrocarbons within the incinerator stack have the same results as those found in Case A under the same temperature profile. They have the same product composition trends as a function of temperature and of inlet flow rate, but smaller compositions in terms of magnitude.

Single ring aromatic species are kinetically predicted to decrease and poly-aromatic species are predicted to increase during the cooling process. Most species compositions change significantly. Table 5.40 indicates that the most significant reduction in composition during cooling is for ethynyl benzene by 99.0 % and ethyl benzene by 98.9 %. In addition, the kinetic compositions for phenol do not change significantly. Table 5.41 shows that the most significantly increased poly-aromatic species is indene by 95.3 % and the most insignificant change is for pyrene.

Table 5.40. Kinetically predicted reductions (%) in compositions for single ring aromatic species in the stack under the conditions of 17:1 air to fuel ratio, 1623 K temperature profile, and varying flow rates of (a). $3.28 \times 10^5 \text{ cm}^3/\text{s}$, (b). $9.83 \times 10^5 \text{ cm}^3/\text{s}$, and (c). $1.64 \times 10^6 \text{ cm}^3/\text{s}$.

Aromatic Species	Flow Rate (a)	Flow Rate (b)	Flow Rate (c)
Benzene	77.2	75.6	75.1
Phenol	-	-	-
Methyl Benzene	98.4	97.7	97.3
Benzaldehyde	98.7	98.2	97.8
Hydroxyl Methyl Benzene	96.5	95.5	94.8
Ethyl Benzene	99.3	98.8	98.5
Ethenyl Benzene	98.8	99.9	95.7
Ethynyl Benzene	98.4	99.2	99.4
Dimethyl Benzene	57.1	57.6	63.1
Ethyl Methyl Benzene	33.3	33.1	32.6
Ethenyl Methyl Benzene	82.5	78.2	63.9

Increasing the flow rate has the same trends as those obtained in Case A, however the magnitude of changes is slightly different. In terms of trends, the sole difference for single ring aromatics in this case is that ethyl methyl benzene and ethenyl methyl benzene are increasing with increasing inlet flow rate. The only difference for poly-aromatic species is that phenanthrene and anthracene compositions are increasing with increasing

Table 5.41. Kinetically predicted increases (%) in compositions for poly-aromatic species in the stack under the conditions of 17:1 air to fuel ratio, 1623 K temperature profile, and varying flow rates of (a). $3.28 \times 10^5 \text{ cm}^3/\text{s}$, (b). $9.83 \times 10^5 \text{ cm}^3/\text{s}$, and (c). $1.64 \times 10^6 \text{ cm}^3/\text{s}$.

Poly-Aromatic Species	Flow Rate (a)	Flow Rate (b)	Flow Rate (c)
Naphthalene	79.4	85.8	89.0
Hydroxyl Naphthalene	86.8	77.4	75.7
Acenaphthalene	5.57	9.10	6.67
Fluorene	14.2	22.4	24.6
Fluoranthene	8.86	10.7	5.26
Indene	96.2	99.5	90.1
Methyl Indene	10.3	16.8	19.4
Methyl Naphthalene	85.8	79.4	21.0
Benzo(a)indene	14.5	17.7	20.5
Ethyl Naphthalene	79.4	90.2	81.2
Ethenyl Naphthalene	76.0	76.1	86.1
Ethynyl Naphthalene	17.8	22.2	45.6
Benzo(a)phenanthrene	78.8	76.9	83.0
Phenanthrene	13.1	9.95	8.25
Anthracene	48.4	33.1	14.6
Pyrene	-	-	-
4H-cylopenta(def)phenanthrene	82.4	84.6	85.6
Methyl Phenanthrene	75.8	73.5	72.5
Benzo(ghi)fluorene	79.4	79.4	96.5
Biphenyl	44.7	51.9	54.2
Biphenylene	9.89	2.70	1.56
Cyclopenta(cd)pyrene	52.7	36.7	24.0

flow rate. Table 5.42 indicates that the most significantly increased single ring aromatics are ethyl methyl benzene, ethenyl methyl benzene, and ethynyl benzene by 99.9 % and the most significant reduction is ethyl benzene by 84.7 %.

Table 5.42. Kinetically predicted changes (%) in compositions for single ring aromatic species in the stack as inlet flow rates are increased from $3.28 \times 10^5 \text{ cm}^3/\text{s}$ to $1.64 \times 10^6 \text{ cm}^3/\text{s}$ under the 17:1 air to fuel ratio and 1623 K temperature profile.

Aromatic Species	Increase (%)	Decrease (%)
Benzene	-	8.16
Phenol	12.8	-
Methyl Benzene	-	64.1
Benzaldehyde	-	61.7
Hydroxyl Methyl Benzene	-	61.7
Ethyl Benzene	-	84.7
Ethenyl Benzene	99.0	-
Ethynyl Benzene	99.9	-
Dimethyl Benzene	21.6	-
Ethyl Methyl Benzene	99.9	-
Ethenyl Methyl Benzene	99.9	-

Table 5.43 also indicates that the most significantly increased poly-aromatic is ethynyl naphthalene by 99.7 % and the most significant reduction is indene by 93.9 %. As well, there are no significant changes for fluoranthene and pyrene.

Table 5.43. Kinetically predicted changes (%) in compositions for poly-aromatic species in the stack as inlet flow rates are increased from $3.28 \times 10^5 \text{ cm}^3/\text{s}$ to $1.64 \times 10^6 \text{ cm}^3/\text{s}$ under the 17:1 air to fuel ratio and 1623 K temperature profile.

Aromatic Species	Increase (%)	Decrease (%)
Naphthalene	-	74.6
Hydroxyl Naphthalene	-	73.5
Acenaphthalene	-	13.0
Fluorene	-	21.8
Fluoranthene	-	-
Indene	-	93.9
Methyl Indene	-	28.2
Methyl Naphthalene	-	72.5
Benzo(a)indene	-	28.3
Ethyl Naphthalene	-	92.7
Ethenyl Naphthalene	-	73.0
Ethynyl Naphthalene	99.7	-
Benzo(a)phenanthrene	5.15	-
Phenanthrene	94.1	-
Anthracene	99.2	-
Pyrene	-	-
4H-cylopenta(def)phenanthrene	-	83.7
Methyl Phenanthrene	5.57	-
Benzo(ghi)fluorene	-	80.0
Biphenyl	-	20.9
Biphenylene	5.21	-
Cyclopenta(cd)pyrene	-	43.7

5.2.3. Case C: 21:1 Air to Fuel Ratio Results

5.2.3.1. Introduction

Output mole fraction compositions of combustion chamber calculations are used as input mole fraction compositions in these simulations. Flow rate ranges are the same as for Case A and B. As in Case A and B, the three linear temperature profiles shown in Figure 5.8 with initial input temperatures of 1623 K, 1400 K, and 1000 K are used to calculate mole fraction compositions of species at varying locations within the stack.

5.2.3.2. Oxidation Products and Light Hydrocarbon Species Results

5.2.3.2.1. Kinetic Results for 1000 K Temperature Profile

The compositions for oxidation products and light hydrocarbon species within the stack have similar trends compared to Case A and Case B results. These results have the same product composition trends as a function of inlet flow rate. In addition to this, predictions indicate that a decrease in composition magnitude for light hydrocarbons and oxidation products has occurred when changed the air to fuel ratio is increased from 14:1 to 21:1.

Table 5.44 indicates that butadiene and methane have the most significant decrease in composition during cooling by over 99 %, whereas the composition for carbon monoxide has decreased by an average significant amount of 99.5 %. As in Case A and B, butane, water, and carbon dioxide do not change significantly.

Table 5.44. Kinetically predicted reductions (%) in compositions from inlet lower weight hydrocarbons and oxidation products in the stack during cooling under the conditions of 21:1 air to fuel ratio, 1000 K temperature profile, and varying flow rates of (a). 3.28×10^5 cm³/s, (b). 9.83×10^5 cm³/s, and (c). 1.64×10^6 cm³/s.

Species	Flow Rate (a)	Flow Rate (b)	Flow Rate (c)
Methane	99.6	97.9	98.6
Ethane	83.3	99.2	83.4
Ethene	98.1	96.5	96.7
Ethyne	97.6	90.6	88.4
Propane	95.7	82.7	99.9
Propene	98.4	97.5	99.9
Propyne	99.7	92.8	98.8
Butane	-	-	-
Butene	99.9	89.6	92.7
Butyne	97.3	99.5	92.2
Butadiene	99.9	98.5	99.1
Butadiyne	99.4	98.4	95.2
Water	-	-	-
Carbon Monoxide	99.7	98.8	99.9
Carbon Dioxide	-	-	-

Trends for varying flow rates are much the same as those found in Case A and Case B. Table 5.45 gives the percent changes for these species due to increasing flow rate. These values are similar to those in Case B, but are slightly larger than those found in Case A. Note that the most significant reductions are methane by 99.6 %, ethane by 97.2 %, and propyne by 97.6 %. There are no significant changes for butane, water, and carbon dioxide again.

Table 5.45. Kinetically predicted changes in composition (%) for lower weight hydrocarbons and oxidation products within the stack under the 1000 K temperature profile, 21:1 air to fuel ratio with increasing flow rate from $3.28 \times 10^5 \text{ cm}^3/\text{s}$ to $1.64 \times 10^6 \text{ cm}^3/\text{s}$.

Species	% Increase	% Decrease
Methane	-	99.6
Ethane	-	97.2
Ethene	-	12.7
Ethyne	-	16.3
Propane	-	58.8
Propene	-	81.9
Propyne	-	97.6
Butane	-	-
Butene	-	90.6
Butyne	-	95.3
Butadiene	-	66.7
Butadiyne	-	65.3
Water	-	-
Carbon Monoxide	90.8	-
Carbon Dioxide	-	-

5.2.3.2.2. Kinetic Results for 1400 K Temperature Profile

Kinetic results are similar to results found in Case A and Case B. Compositions for oxidation products and light hydrocarbon species within the stack have the same

product compositions as a function of temperature, inlet flow rate, and air to fuel ratio as Case B.

Lower weight hydrocarbon species are predicted to decrease during the cooling process. Table 5.46 gives the percent reductions for these species under given conditions. It indicates that butadiene and butadiyne have the most significant decreases in composition by 99.8 % and 99.9 %. As well, insignificant changes in composition exist for the same species (i.e. butane, water, and carbon dioxide) as in Case A and B.

Table 5.46. Kinetically predicted reductions (%) in compositions from inlet lower weight hydrocarbons and oxidation products in the stack during cooling under the conditions of 21:1 air to fuel ratio, 1400 K temperature profile, and varying flow rates of (a). $3.28 \times 10^5 \text{ cm}^3/\text{s}$, (b). $9.83 \times 10^5 \text{ cm}^3/\text{s}$, and (c). $1.64 \times 10^6 \text{ cm}^3/\text{s}$.

Species	Flow Rate (a)	Flow Rate (b)	Flow Rate (c)
Methane	99.6	99.2	94.8
Ethane	92.5	99.7	99.5
Ethene	97.1	96.5	96.4
Ethyne	87.6	80.7	77.0
Propane	99.3	97.7	98.1
Propene	91.9	93.2	98.3
Propyne	98.5	98.5	91.0
Butane	-	-	-
Butene	82.7	98.1	93.5
Butyne	92.5	92.8	89.6
Butadiene	99.9	99.7	99.9
Butadiyne	99.9	99.9	99.8
Water	-	-	-
Carbon Monoxide	98.3	98.3	98.3
Carbon Dioxide	-	-	-

As previously mentioned, composition trends over increasing flow rates are the same as Case A and Case B 1400 K temperature profile results, but have slightly different percent changes. Most lower weight hydrocarbons are reduced and when increasing inlet flow rates. Table 5.47 indicates that butene has the most significant reduction by 93.8 %

as flow rates are increased. Note that there are no significant reductions for butane, water, carbon monoxide, and carbon dioxide.

Table 5.47. Kinetically predicted changes in composition (%) for lower weight hydrocarbons and oxidation products within the stack under the 1400 K temperature profile, 21:1 air to fuel ratio with increasing flow rate from $3.28 \times 10^5 \text{ cm}^3/\text{s}$ to $1.64 \times 10^6 \text{ cm}^3/\text{s}$.

Species	% Increase	% Decrease
Methane	-	86.6
Ethane	-	49.6
Ethene	-	6.84
Ethyne	-	9.62
Propane	-	90.2
Propene	-	88.4
Propyne	-	45.7
Butane	-	-
Butene	-	93.8
Butyne	-	87.7
Butadiene	-	4.85
Butadiyne	-	3.24
Water	-	-
Carbon Monoxide	-	-
Carbon Dioxide	-	-

5.2.3.2.3. Kinetic Results for 1623 K Temperature Profile

Predictions for this case show trends for product composition as a function of temperature, flow rate, and air to fuel ratio similar to Case A and Case B.

Light hydrocarbons and oxidations are predicted to decrease during cooling of gases. Table 5.48 indicates that butadiyne has the most significant decrease in composition by 99.7 %, whereas the compositions for butane, water and carbon dioxide did not change at all.

Table 5.48 Kinetically predicted reductions (%) in compositions from inlet lower weight hydrocarbons and oxidation products in the stack during cooling under the conditions of 21:1 air to fuel ratio, 1623 K temperature profile, and varying flow rates of (a). $3.28 \times 10^5 \text{ cm}^3/\text{s}$, (b). $9.83 \times 10^5 \text{ cm}^3/\text{s}$, and (c). $1.64 \times 10^6 \text{ cm}^3/\text{s}$.

Species	Flow Rate (a)	Flow Rate (b)	Flow Rate (c)
Methane	91.6	89.3	87.4
Ethane	91.2	88.5	86.9
Ethene	91.8	90.0	88.9
Ethyne	82.0	82.3	78.9
Propane	96.6	94.7	94.1
Propene	94.8	92.8	92.7
Propyne	96.9	96.0	95.3
Butane	-	-	-
Butene	87.6	84.6	82.4
Butyne	98.5	98.2	98.1
Butadiene	98.0	97.8	97.7
Butadiyne	99.8	99.7	99.7
Water	-	-	-
Carbon Monoxide	92.7	92.1	91.8
Carbon Dioxide	-	-	-

Inlet flow rate trends for product compositions are similar to Case A and Case B results, but different from the 1000 K and 1400 K temperature profiles. Results indicate that all hydrocarbons and carbon monoxide are reduced as the flow rates are increased. Percent changes as a function of flow rate are shown in Table 5.49. As in Case A and Case B, propane has the most significant reduction by 68.2 % and butane, water, and carbon dioxide have no significant change.

Table 5.49. Kinetically predicted changes in composition (%) for lower weight hydrocarbons and oxidation products within the stack under the 1623 K temperature profile, 21:1 air to fuel ratio with increasing flow rate from $3.28 \times 10^5 \text{ cm}^3/\text{s}$ to $1.64 \times 10^6 \text{ cm}^3/\text{s}$.

Species	% Increase	% Decrease
Methane	-	62.2
Ethane	-	51.9
Ethene	-	31.5
Ethyne	-	49.1
Propane	-	68.2
Propene	-	57.5
Propyne	-	67.6
Butane	-	-
Butene	-	49.9
Butyne	-	36.7
Butadiene	-	13.4
Butadiyne	-	20.1
Water	-	-
Carbon Monoxide	-	26.0
Carbon Dioxide	-	-

5.2.3.3. Sulphur-Containing Species Results

5.2.3.3.1. Kinetic Results for 1000 K Temperature Profile

Sulphur-containing species have similar results as the previous two air to fuel ratios tested. Predictions show the same product compositions trends with respect to temperature, inlet flow rate, and air to fuel ratio.

The cooling of gases in the stack causes carbonyl sulphide, hydrogen sulphide, and carbon sulphide to decrease by over 99 % and sulphur dioxide to decrease by only 1.67 %. Increasing flow rates cause hydrogen sulphide and carbon sulphide to increase by over 99 % of their original compositions, 93.5 % for carbonyl sulphide, and insignificantly for sulphur dioxide.

5.2.3.3.2. Kinetic Results for 1400 K Temperature Profile

In this case, results indicate much the same patterns as found in Case A and Case B results. Predictions show significant composition reductions during cooling and increases in composition when increasing flow rates. As well, compositions for sulphur-containing species are reduced when the air to fuel ratio is increased from 14:1 to 21:1.

Compositions for hydrogen sulphide, carbon sulphide, and carbonyl sulphide have significant average reductions of 99.9 %, and only 2.14 % reduction for sulphur dioxide during cooling. Increasing the flow rate results in an increase of 50.0 % for hydrogen sulphide, 2.35 % for carbon sulphide, and insignificant amounts for carbonyl sulphide and sulphur dioxide. These values are much the same as in 14:1 and 17:1 results.

5.2.3.3.3. Kinetic Results for 1623 K Temperature Profile

Predictions show the same patterns and trends for compositions as a function of temperature, inlet flow rate, and air to fuel ratio as the previous results.

Average reductions during cooling are 99.5% for hydrogen sulphide, 99.9 % for carbon sulphide, 99.7 % for carbonyl sulphide, and no change for sulphur dioxide. Increasing flow rate results in a reduction of 17.0 % for hydrogen sulphide, 16.4 % for carbonyl sulphide, and no significant change for carbon sulphide and sulphur dioxide. These values are much the same as in previous results with the exception that carbon sulphide is reduced much less in this case.

5.2.3.4. Aromatic and Poly-Aromatic Hydrocarbon Results

5.2.3.4.1. Kinetic Results for 1000 K Temperature Profile

Kinetic results for aromatic and poly-aromatic hydrocarbons within the incinerator stack in this case show similar trends as previous cases. It should also be noted that with the exception of ethyl methyl benzene, product compositions have decreased since the air to fuel ratio as increased from 14:1 to 21:1. Most importantly, single ring aromatics decrease and poly-aromatic species increase during cooling. Table 5.50 shows that the most significant reduction for single ring aromatics is methyl benzene by 99.8 %. As in Case A and B, phenol is not significantly reduced.

Table 5.50. Kinetically predicted reductions (%) in compositions for single ring aromatic species in the stack under the conditions of 21:1 air to fuel ratio, 1000 K temperature profile, and varying flow rates of (a). $3.28 \times 10^5 \text{ cm}^3/\text{s}$, (b). $9.83 \times 10^5 \text{ cm}^3/\text{s}$, and (c). $1.64 \times 10^6 \text{ cm}^3/\text{s}$.

Aromatic Species	Flow Rate (a)	Flow Rate (b)	Flow Rate (c)
Benzene	98.8	96.9	97.4
Phenol	-	-	-
Methyl Benzene	99.9	99.8	99.7
Benzaldehyde	99.7	98.5	99.7
Hydroxyl Methyl Benzene	98.9	91.9	90.8
Ethyl Benzene	94.1	98.7	95.1
Ethenyl Benzene	90.6	94.9	95.8
Ethynyl Benzene	33.1	36.9	46.5
Dimethyl Benzene	42.5	74.0	52.9
Ethyl Methyl Benzene	93.9	99.2	92.1
Ethenyl Methyl Benzene	95.0	98.2	90.9

In addition, Table 5.51 indicates that the most significant increase amongst poly-aromatic species during cooling is 4H-cyclopenta(def)phenanthrene and methyl phenanthrene by 97.1 % and 95.6 % respectively. However, note that acenaphthalene, fluoranthene, ethynyl naphthalene, and pyrene are not significantly changed.

Table 5.51. Kinetically predicted increases (%) in compositions for poly-aromatic species in the stack under the conditions of 21:1 air to fuel ratio, 1000 K temperature profile, and varying flow rates of (a). $3.28 \times 10^5 \text{ cm}^3/\text{s}$, (b). $9.83 \times 10^5 \text{ cm}^3/\text{s}$, and (c). $1.64 \times 10^6 \text{ cm}^3/\text{s}$.

Poly-Aromatic Species	Flow Rate (a)	Flow Rate (b)	Flow Rate (c)
Naphthalene	66.1	77.4	78.1
Hydroxyl Naphthalene	90.0	95.0	96.1
Acenaphthalene	-	-	-
Fluorene	41.9	42.1	65.4
Fluoranthene	-	-	-
Indene	70.7	85.7	92.3
Methyl Indene	93.8	92.7	90.2
Methyl Naphthalene	79.4	79.6	93.6
Benzo(a)indene	92.6	92.9	96.2
Ethyl Naphthalene	88.3	90.6	91.4
Ethenyl Naphthalene	90.1	92.9	96.2
Ethynyl Naphthalene	-	-	-
Benzo(a)phenanthrene	91.5	93.7	93.8
Phenanthrene	91.4	90.1	89.9
Anthracene	90.4	92.7	98.0
Pyrene	-	-	-
4H-cyclopenta(def)phenanthrene	95.2	96.0	99.9
Methyl Phenanthrene	95.3	95.5	96.1
Benzo(ghi)fluorene	92.1	93.0	93.4
Biphenyl	88.4	89.0	93.3
Biphenylene	2.26	2.52	7.39
Cyclopenta(cd)pyrene	95.5	93.3	93.0

For single ring aromatic and poly-aromatic species, changing the flow rate results in trends in composition similar to previous results. The difference from Case A is that methyl benzene compositions increase with increasing flow rate and from Case B in that methyl benzene and ethenyl methyl benzene compositions increase with increasing flow rate. Compared to Case A, indene compositions increase with increasing flow rate and anthracene decreases with increasing flow rate. When compared to Case B, anthracene decreases (rather than increases) with increasing inlet flow rates. Percent changes for these species are shown in Tables 5.52 and 5.53.

Table 5.52. Kinetically predicted changes (%) in compositions for single ring aromatic species in the stack as inlet flow rates are increased from $3.28 \times 10^5 \text{ cm}^3/\text{s}$ to $1.64 \times 10^6 \text{ cm}^3/\text{s}$ under the 21:1 air to fuel ratio and 1000 K temperature profile.

Aromatic Species	Increase (%)	Decrease (%)
Benzene	-	88.6
Phenol	13.4	-
Methyl Benzene	56.2	-
Benzaldehyde	-	98.6
Hydroxyl Methyl Benzene	96.0	-
Ethyl Benzene	99.9	-
Ethenyl Benzene	98.1	-
Ethynyl Benzene	-	5.89
Dimethyl Benzene	-	89.7
Ethyl Methyl Benzene	-	23.0
Ethenyl Methyl Benzene	85.6	-

Unlike Case A and Case B, benzaldehyde has the most significant reduction by 98.6 % when increasing flow rates. The most significant increase is for ethyl benzene by 99.9 %.

Table 5.53. Kinetically predicted changes (%) in compositions for poly-aromatic species in the stack as inlet flow rates are increased from $3.28 \times 10^5 \text{ cm}^3/\text{s}$ to $1.64 \times 10^6 \text{ cm}^3/\text{s}$ under the 21:1 air to fuel ratio and 1000 K temperature profile.

Aromatic Species	Increase (%)	Decrease (%)
Naphthalene	82.6	-
Hydroxyl Naphthalene	-	49.8
Acenaphthalene	84.3	-
Fluorene	11.9	-
Fluoranthene	12.6	-
Indene	99.9	-
Methyl Indene	86.8	-
Methyl Naphthalene	86.9	-
Benzo(a)indene	78.5	-
Ethyl Naphthalene	-	99.9
Ethenyl Naphthalene	99.9	-
Ethynyl Naphthalene	11.2	-
Benzo(a)phenanthrene	-	75.9
Phenanthrene	-	14.7
Anthracene	-	79.3
Pyrene	10.4	-
4H-cyclopenta(def)phenanthrene	65.5	-
Methyl Phenanthrene	-	69.9
Benzo(ghi)fluorene	-	78.0
Biphenyl	-	61.6
Biphenylene	-	62.3
Cyclopenta(cd)pyrene	35.4	-

The most significant increases in composition while increasing flow rates for poly-aromatic species are indene and ethenyl naphthalene by 99.9 %. As well, the most significant reduction is for ethyl naphthalene, which is not in agreement with previous cases.

5.2.3.4.2. Kinetic Results for 1400 K Temperature Profile

Predictions for aromatic and poly-aromatic hydrocarbons within the incinerator stack are in general agreement with results obtained from Case A and Case B. With the exception of indene and ethenyl methyl benzene, aromatic and poly-aromatic compositions decrease as air to fuel ratio is changed from 14:1 to 21:1. Single ring

aromatic species are predicted to decrease and poly-aromatic species are predicted to increase during the cooling process. As well, species' compositions change when flow rates are increased.

Table 5.54 indicates that the most significant reduction during cooling is ethenyl benzene by 98.4 % and ethyl methyl benzene by 99.2 %. Phenol is insignificantly reduced.

Table 5.54. Kinetically predicted reductions (%) in compositions for single ring aromatic species in the stack under the conditions of 21:1 air to fuel ratio, 1400 K temperature profile, and varying flow rates of (a). $3.28 \times 10^5 \text{ cm}^3/\text{s}$, (b). $9.83 \times 10^5 \text{ cm}^3/\text{s}$, and (c). $1.64 \times 10^6 \text{ cm}^3/\text{s}$.

Aromatic Species	Flow Rate (a)	Flow Rate (b)	Flow Rate (c)
Benzene	85.6	87.2	88.8
Phenol	-	-	-
Methyl Benzene	85.8	98.1	99.9
Benzaldehyde	98.4	91.1	99.9
Hydroxyl Methyl Benzene	99.2	91.2	89.0
Ethyl Benzene	85.3	91.7	93.7
Ethenyl Benzene	99.6	99.5	96.2
Ethynyl Benzene	99.0	99.1	91.9
Dimethyl Benzene	98.1	96.1	95.0
Ethyl Methyl Benzene	99.9	98.9	98.7
Ethenyl Methyl Benzene	86.5	87.8	90.9

Table 5.55 indicates that 4H-cyclopenta(def)phenanthrene and methyl phenanthrene are predicted to have the most significant increase by 97.5 % and 96.2 %.

As in Case A and B, biphenylene has no significant change.

Table 5.55. Kinetically predicted increases (%) in compositions for poly-aromatic species in the stack under the conditions of 21:1 air to fuel ratio, 1400 K temperature profile, and varying flow rates of (a). $3.28 \times 10^5 \text{ cm}^3/\text{s}$, (b). $9.83 \times 10^5 \text{ cm}^3/\text{s}$, and (c). $1.64 \times 10^6 \text{ cm}^3/\text{s}$.

Poly-Aromatic Species	Flow Rate (a)	Flow Rate (b)	Flow Rate (c)
Naphthalene	75.9	79.5	87.1
Hydroxyl Naphthalene	83.4	89.2	96.1
Acenaphthalene	89.2	90.3	97.1
Fluorene	98.1	88.8	79.4
Fluoranthene	95.9	89.6	97.1
Indene	28.7	21.0	15.4
Methyl Indene	83.1	84.6	85.4
Methyl Naphthalene	11.9	20.0	12.8
Benzo(a)indene	96.6	96.4	90.2
Ethyl Naphthalene	89.3	96.0	96.1
Ethenyl Naphthalene	96.2	89.4	93.2
Ethynyl Naphthalene	97.9	97.7	89.7
Benzo(a)phenanthrene	97.2	94.8	90.2
Phenanthrene	90.4	97.8	91.7
Anthracene	83.5	95.6	93.1
Pyrene	26.0	16.2	14.2
4H-cylopenta(def)phenanthrene	97.6	99.7	95.2
Methyl Phenanthrene	98.5	97.4	92.6
Benzo(ghi)fluorene	98.0	94.5	88.7
Biphenyl	60.6	67.0	68.3
Biphenylene	-	-	-
Cyclopenta(cd)pyrene	90.1	91.6	88.4

Trends in product compositions as a result of increasing flow rate are similar for from those in Case A and Case B. However, benzaldehyde and hydroxyl methyl benzene decrease with increasing inlet flow rate in contrast to Case A where these species increased. In Case B, benzaldehyde also increased with increasing flow rate. Table 5.56 indicates that the most significant increase is methyl benzene by 99.0 % and the most significant decrease is dimethyl benzene by 98.8 %. As in both Case A and B, phenol and benzene have only changed by an insignificant amount.

Table 5.56. Kinetically predicted changes (%) in compositions for single ring aromatic species in the stack as inlet flow rates are increased from $3.28 \times 10^5 \text{ cm}^3/\text{s}$ to $1.64 \times 10^6 \text{ cm}^3/\text{s}$ under the 21:1 air to fuel ratio and 1400 K temperature profile.

Aromatic Species	Increase (%)	Decrease (%)
Benzene	-	-
Phenol	-	-
Methyl Benzene	99.0	-
Benzaldehyde	-	60.3
Hydroxyl Methyl Benzene	-	91.7
Ethyl Benzene	-	97.8
Ethenyl Benzene	-	37.3
Ethynyl Benzene	-	50.7
Dimethyl Benzene	-	98.8
Ethyl Methyl Benzene	-	95.3
Ethenyl Methyl Benzene	-	83.9

Poly-aromatic species show similar results when compared to Case A and Case B. The difference from Case A is that in this case benzo(a)phenanthrene and 4H-cyclopenta(def)phenanthrene increase and anthracene and methyl phenanthrene decrease with increasing flow rate. The only difference from Case B is that methyl phenanthrene decreases with increasing flow rate in for case. Table 5.57 indicates that the most significant increases are pyrene and cyclopenta(cd)pyrene by 99.9 % and the most

significant reduction is anthracene by 99.9 % and benzo(ghi)fluorene by 93.6 %. Note that biphenylene has no significant change, like Case A and B.

Table 5.57. Kinetically predicted changes (%) in compositions for poly-aromatic species in the stack as inlet flow rates are increased from $3.28 \times 10^5 \text{ cm}^3/\text{s}$ to $1.64 \times 10^6 \text{ cm}^3/\text{s}$ under the 21:1 air to fuel ratio and 1400 K temperature profile.

Aromatic Species	Increase (%)	Decrease (%)
Naphthalene	43.5	-
Hydroxyl Naphthalene	-	65.8
Acenaphthalene	-	25.6
Fluorene	64.5	-
Fluoranthene	81.6	-
Indene	-	20.3
Methyl Indene	52.2	-
Methyl Naphthalene	96.6	-
Benzo(a)indene	66.2	-
Ethyl Naphthalene	25.5	-
Ethenyl Naphthalene	93.8	-
Ethynyl Naphthalene	31.5	-
Benzo(a)phenanthrene	84.7	-
Phenanthrene	-	84.7
Anthracene	-	99.9
Pyrene	99.9	-
4H-cyclopenta(def)phenanthrene	75.6	-
Methyl Phenanthrene	-	72.5
Benzo(ghi)fluorene	-	93.6
Biphenyl	5.40	-
Biphenylene	-	-
Cyclopenta(cd)pyrene	99.9	-

5.2.3.4.3. Kinetic Results for 1623 K Temperature Profile

Kinetic results for aromatic and poly-aromatic species under the temperature profile of 1623 K and 21:1 air to fuel ratio are in agreement with trends from Case A and Case B.

Lighter weight aromatic species are predicted to decrease and poly-aromatic species are predicted to increase during the cooling process. Table 5.58 indicates that the most significant reduction for lighter aromatics during cooling is ethyl benzene and ethenyl benzene by 98.5 % and 98.1 %. Phenol is not significantly reduced.

Table 5.58. Kinetically predicted reductions (%) in compositions for single ring aromatic species in the stack under the conditions of 21:1 air to fuel ratio, 1623 K temperature profile, and varying flow rates of (a). $3.28 \times 10^5 \text{ cm}^3/\text{s}$, (b). $9.83 \times 10^5 \text{ cm}^3/\text{s}$, and (c). $1.64 \times 10^6 \text{ cm}^3/\text{s}$.

Aromatic Species	Flow Rate (a)	Flow Rate (b)	Flow Rate (c)
Benzene	76.6	75.0	74.5
Phenol	-	-	-
Methyl Benzene	98.4	97.4	96.7
Benzaldehyde	98.6	97.9	97.5
Hydroxyl Methyl Benzene	97.0	95.6	94.6
Ethyl Benzene	99.3	98.4	97.7
Ethenyl Benzene	94.9	99.3	99.9
Ethynyl Benzene	94.3	99.0	99.9
Dimethyl Benzene	64.4	68.9	77.1
Ethyl Methyl Benzene	97.3	92.5	91.7
Ethenyl Methyl Benzene	94.4	91.8	89.9

Table 5.59 indicates that the most abundant increase in poly-aromatic species during cooling is indene by 95.0 %. However, pyrene is not predicted to change significantly.

Table 5.59. Kinetically predicted increases (%) in compositions for poly-aromatic species in the stack under the conditions of 21:1 air to fuel ratio, 1623 K temperature profile, and varying flow rates of (a). $3.28 \times 10^5 \text{ cm}^3/\text{s}$, (b). $9.83 \times 10^5 \text{ cm}^3/\text{s}$, and (c). $1.64 \times 10^6 \text{ cm}^3/\text{s}$.

Poly-Aromatic Species	Flow Rate (a)	Flow Rate (b)	Flow Rate (c)
Naphthalene	94.4	91.0	90.6
Hydroxyl Naphthalene	91.4	94.1	95.0
Acenaphthalene	12.5	8.77	6.25
Fluorene	12.3	27.3	31.6
Fluoranthene	42.1	6.25	2.56
Indene	89.0	97.3	98.6
Methyl Indene	16.3	21.4	25.5
Methyl Naphthalene	68.5	91.0	78.6
Benzo(a)indene	15.0	19.3	22.9
Ethyl Naphthalene	88.9	90.2	92.2
Ethenyl Naphthalene	87.2	88.9	89.9
Ethynyl Naphthalene	17.8	21.0	28.1
Benzo(a)phenanthrene	77.1	76.0	75.1
Phenanthrene	13.5	25.2	25.2
Anthracene	28.9	53.2	82.5
Pyrene	-	-	-
4H-cyclopenta(def)phenanthrene	82.9	85.7	86.9
Methyl Phenanthrene	75.0	72.6	71.5
Benzo(ghi)fluorene	79.3	79.4	79.4
Biphenyl	47.6	54.8	57.1
Biphenylene	5.71	1.40	-
Cyclopenta(cd)pyrene	41.8	37.3	35.8

As previously mentioned, overall aromatic and poly-aromatic composition trends for increasing flow rate are similar to those found in Case A and Case B. However, there are a few slight differences between the cases. When compared with Case A, ethyl methyl benzene and ethenyl methyl benzene compositions increase with increasing flow rate in this case. In addition, the results in this case are identical to the results from Case B. Table 5.60 indicates that the greatest reduction for single ring aromatics is ethyl benzene by 88.0 % and the greatest increase is ethenyl methyl benzene by 99.8 %. In addition, phenol is the only single-ring aromatic species that does not change significantly when increasing the flow rate.

Table 5.60. Kinetically predicted changes (%) in compositions for single ring aromatic species in the stack as inlet flow rates are increased from $3.28 \times 10^5 \text{ cm}^3/\text{s}$ to $1.64 \times 10^6 \text{ cm}^3/\text{s}$ under the 21:1 air to fuel ratio and 1623 K temperature profile.

Aromatic Species	Increase (%)	Decrease (%)
Benzene	-	10.7
Phenol	-	-
Methyl Benzene	-	69.7
Benzaldehyde	-	65.4
Hydroxyl Methyl Benzene	-	67.0
Ethyl Benzene	-	88.0
Ethenyl Benzene	54.1	-
Ethynyl Benzene	70.4	-
Dimethyl Benzene	87.6	-
Ethyl Methyl Benzene	98.5	-
Ethenyl Methyl Benzene	99.8	-

Table 5.61 indicates the percent changes amongst aromatic species. The changes in aromatics are similar to those obtained in Case A, but are slightly different compared to those in Case B. In this case, phenanthrene and anthracene decrease with increasing flow rate, while for Case B they both increase. The most significant reduction in poly-aromatic

species is ethenyl naphthalene by 90.9 % and the most significant increase is ethynyl naphthalene by 21.1 %. As well, there are no significant changes for fluoranthene and pyrene.

Table 5.61. Kinetically predicted changes (%) in compositions for poly-aromatic species in the stack as inlet flow rates are increased from $3.28 \times 10^5 \text{ cm}^3/\text{s}$ to $1.64 \times 10^6 \text{ cm}^3/\text{s}$ under the 21:1 air to fuel ratio and 1623 K temperature profile.

Aromatic Species	Increase (%)	Decrease (%)
Naphthalene	-	34.9
Hydroxyl Naphthalene	-	35.1
Acenaphthalene	-	12.5
Fluorene	-	24.2
Fluoranthene	-	-
Indene	-	89.8
Methyl Indene	-	32.0
Methyl Naphthalene	-	52.4
Benzo(a)indene	-	31.8
Ethyl Naphthalene	-	75.7
Ethenyl Naphthalene	-	90.9
Ethynyl Naphthalene	21.1	-
Benzo(a)phenanthrene	8.73	-
Phenanthrene	-	10.6
Anthracene	-	83.3
Pyrene	-	-
4H-cylopenta(def)phenanthrene	-	83.9
Methyl Phenanthrene	8.52	-
Benzo(ghi)fluorene	-	80.1
Biphenyl	-	23.9
Biphenylene	2.78	-
Cyclopenta(cd)pyrene	-	40.6

Aromatic species compositions are predicted to change as the air to fuel ratio is increased from 14:1 to 21:1. Table 5.62 shows the percent changes in composition for all species discussed including lower weight hydrocarbons, oxidation species, sulphur-containing species, and aromatic species as air to fuel ratio is increased.

Table 5.62. Kinetically predicted changes (ie: ↑ for increase and ↓ for decrease) in composition (%) for species at entry of the incinerator stack, when ranging air to fuel ratio from 14:1 to 21:1 and three temperature profiles with initial internal combustion temperatures of 1000 K, 1400 K, and 1623 K.

Species	T _{initial} = 1000 K	T _{initial} = 1400 K	T _{initial} = 1623 K
Methane	86.9 ↓	88.3 ↓	94.3 ↓
Ethane	96.1 ↓	93.1 ↓	81.2 ↓
Ethene	52.6 ↓	34.7 ↓	42.4 ↓
Ethyne	49.7 ↓	70.8 ↓	74.2 ↓
Propane	89.6 ↓	64.0 ↓	97.3 ↓
Propene	73.6 ↓	98.3 ↓	93.8 ↓
Propyne	77.1 ↓	98.8 ↓	94.5 ↓
Butane	31.4 ↓	31.5 ↓	31.5 ↓
Butene	86.2 ↓	80.3 ↓	79.7 ↓
Butyne	91.4 ↓	76.3 ↓	86.8 ↓
Butadiene	85.0 ↓	65.7 ↓	72.0 ↓
Butadiyne	50.2 ↓	78.8 ↓	81.9 ↓
Water	31.6 ↓	31.8 ↓	31.8 ↓
Carbon Monoxide	58.9 ↓	48.9 ↓	54.6 ↓
Carbon Dioxide	31.1 ↓	31.6 ↓	31.6 ↓
Hydrogen Sulphide	99.1 ↑	75.5 ↓	82.3 ↓
Sulphur Dioxide	32.2 ↓	32.1 ↓	31.9 ↓
Carbon Sulphide	93.4 ↑	83.2 ↓	85.6 ↓
Carbonyl Sulphide	94.5 ↑	78.9 ↓	82.5 ↓
Benzene	52.7 ↓	68.6 ↓	71.8 ↓
Phenol	67.7 ↓	74.5 ↓	78.3 ↓
Methyl Benzene	68.3 ↓	84.7 ↓	96.7 ↓
Benzaldehyde	93.2 ↓	92.8 ↓	96.2 ↓
Hydroxyl Methyl Benzene	99.7 ↓	78.6 ↓	97.4 ↓
Ethyl Benzene	99.9 ↓	99.9 ↓	99.7 ↓
Ethenyl Benzene	99.9 ↓	99.9 ↓	99.9 ↓

Table 5.62 (Continued)

Species	T _{initial} = 1000 K	T _{initial} = 1400 K	T _{initial} = 1623 K
Ethynyl Benzene	69.1 ↓	99.7 ↓	85.8 ↓
Dimethyl Benzene	97.3 ↓	99.9 ↓	98.8 ↓
Ethyl Methyl Benzene	96.7 ↑	96.7 ↓	99.3 ↓
Ethenyl Methyl Benzene	99.5 ↓	99.9 ↑	97.4 ↓
Naphthalene	98.6 ↓	99.1 ↓	99.3 ↓
Hydroxyl Naphthalene	98.5 ↓	99.4 ↓	99.4 ↓
Acenaphthalene	97.8 ↓	99.2 ↓	98.1 ↓
Fluorene	94.2 ↓	93.2 ↓	98.7 ↓
Fluoranthene	97.6 ↓	99.1 ↓	98.1 ↓
Indene	83.9 ↓	95.8 ↑	97.2 ↓
Methyl Indene	77.5 ↓	98.4 ↓	96.6 ↓
Methyl Naphthalene	90.7 ↓	99.0 ↓	97.9 ↓
Benzo(a)indene	84.0 ↓	92.9 ↓	98.1 ↓
Ethyl Naphthalene	87.1 ↓	98.2 ↓	99.9 ↓
Ethenyl Naphthalene	99.2 ↓	97.5 ↓	99.5 ↓
Ethynyl Naphthalene	97.1 ↓	96.7 ↓	97.1 ↓
Benzo(a)phenanthrene	95.7 ↓	93.3 ↓	99.5 ↓
Phenanthrene	56.0 ↓	62.8 ↓	97.8 ↓
Anthracene	86.7 ↓	94.9 ↓	99.5 ↓
Pyrene	96.6 ↓	89.7 ↓	99.5 ↓
4H-cylopenta(def)phenanthrene	97.4 ↓	94.7 ↓	99.6 ↓
Methyl Phenanthrene	96.5 ↓	89.0 ↓	99.1 ↓
Benzo(ghi)fluorene	97.4 ↓	99.3 ↓	99.7 ↓
Biphenyl	75.1 ↓	76.6 ↓	82.0 ↓
Biphenylene	82.7 ↓	54.6 ↓	60.7 ↓
Cyclopenta(cd)pyrene	99.2 ↓	97.3 ↓	99.9 ↓

5.3. Summary

According to previous studies, there are three distinct temperature regions in the combustion chamber; reaction zone (1600 K to 1800 K); a post combustion zone (1200 K to 1600 K); and a quenching zone (800 K to 1200 K). The reaction zone is a temperature range at which many species are combusted, and some major oxidation products are produced. The post combustion zone is where many aromatic and poly-aromatic species are formed. According to this study in the post combustion zone temperature range, the most significant products are benzene, phenol, naphthalene, biphenyl, and biphenylene. In the quenching zone, the major species methane, ethyne, and benzene, along with other species that are kinetically predicted to have values close to equilibrium values. The significant species at this stage are ethyne, methane, carbon monoxide, sulphur dioxide, carbon sulphide, and carbonyl sulphide. Compositions for ethane, propane, oxygen, and hydrogen sulphide increase with increasing flow rates for all three air to fuel ratios. However, methane and butane do not change significantly. All remaining species decrease with increasing flow rate.

Simulations of the incinerator stack predict the formation of many poly-aromatic species during the cooling process. All conditions tested including three air to fuel ratios, three flow rates, and three temperature profiles yielded similar results. Under the 1000 K temperature profile, hydrogen sulphide, carbon sulphide, carbonyl sulphide, and ethyl methyl benzene all increase in magnitude, whereas only ethenyl methyl benzene and indene increase under the 1400 K temperature profile as the air to fuel ratio is varied from 14:1 to 21:1. The remaining species studied under the 1000 K and 1400 K temperature profiles and all species under the 1623 K temperature profile are predicted to decrease as

air to fuel ratio is varied from 14:1 to 21:1, but show a general decrease in composition when ranging the air to fuel ratio from 14 to 1, 17 to 1, and 21 to 1.

At initial entry of the stack where the temperature is at maximum, many smaller volatile species including lower weight hydrocarbons, oxidation products, and lower weight aromatic species are predicted to be at maximum concentration. As these species move toward the top of the stack where the temperature is reduced, their concentrations are significantly reduced by up to 99 % because they are being consumed by reactions that are producing large quantities of poly-aromatic species. Thus, poly-aromatic concentrations are most significant at the top of the stack. The most abundant poly-aromatic species present are biphenylene and biphenyl, and the least abundant species is cyclopenta(cd)pyrene.

These results give similar quantitative trends compared to those of a sour gas flare emission study. The next chapter makes comparison to sour gas flares as well as previous studies done on incineration.

Chapter 6. Discussion

6.1. Introduction

In this chapter, a detailed discussion of the results of the equilibrium and kinetic simulations is given. As well, a comparison to previous studies on incineration modeling and gas flare emissions is made.

6.2. Equilibrium Model

6.2.1. Excess Oxygen Combustion Results

Equilibrium results from the excess oxygen simulations indicate large amounts of oxidation products where there exists a dramatic decrease at 1500 K. This dramatic decrease at 1500 K appears to be a result of aromatic formation of 2-methyl naphthalene. 2-methyl naphthalene is predicted to form at 1500 K by a dramatic amount. However, no light hydrocarbon species are predicted to form. This may be due to high levels of oxygen reacting to fully oxidize these species into oxidative products such as carbon dioxide, carbon monoxide, and water. Several sulphur-containing species are predicted under equilibrium, including hydrogen sulphide, sulphur dioxide, and carbonyl sulphide. Hydrogen sulphide is increasing from 900 K to 2000 K, sulphur dioxide is increasing to 1300 K and stays constant at the higher temperatures, and carbonyl sulphide increases from 800 K to 1500 K and goes to zero above 1500 K. Again, this may be a result of aromatic formation at this temperature. Results from this study for sulphur-containing species are in agreement with theory due to the fact that increasing amounts of sulphur dioxide are predicted with increasing temperature, and amounts of hydrogen sulphide and

carbonyl sulphide, an oxidation product of sour gas combustion, increase with increasing temperature.

6.2.2. Decreasing Oxygen Combustion Results

The trends obtained when decreasing the oxygen content are quite similar to those of excess oxygen combustion, since oxygen levels are still in excess compared to those of stoichiometric amounts. There are no light hydrocarbon species predicted, the only aromatic species predicted is 2-methyl naphthalene, and sulphur-containing species formed include sulphur dioxide, hydrogen sulphide, and carbonyl sulphide. Once again, water, carbon monoxide, carbon dioxide, and carbonyl sulphide all decrease at 1500 K and 2-methyl naphthalene increases at 1500 K.

Larger concentrations for many species, including carbon monoxide, carbon dioxide, water, sulphur dioxide, hydrogen sulphide, carbonyl sulphide, and 2-methyl naphthalene are predicted as oxygen content decreases. This is due to the fact that relative concentrations of hydrocarbons and hydrogen sulphide in the input were increased to compensate for the decrease in O₂ content. Thus, larger compositions are produced as a result of more hydrocarbons and hydrogen sulphide in the feed. The most abundant increase are in carbon monoxide by 62.6 %, hydrogen sulphide by 96.3 %, and carbonyl sulphide by 96.3 % as oxygen content is decreased by 80 %.

6.2.3. Pyrolysis Results

Lack of oxygen plays a large role in the formation of many complex chemical species, including poly-aromatic hydrocarbons, which are soot precursors. Unlike the results for excess oxygen and decreasing oxygen, pyrolysis results indicate the presence of many species, including light hydrocarbon species, oxidation products, sulphur-containing products, and many aromatic species. The oxygen-contained species are likely formed as a result of reactions involving input carbon dioxide.

Light hydrocarbons have an overall decreasing composition trend until 1500 K where compositions go to zero. As well, equilibrium pyrolysis predictions indicate larger concentrations for smaller hydrocarbons (*i.e.* methane has a larger concentration compared to ethane).

Trends are in agreement with previous equilibrium studies completed by Chagger *et al* (1997). Chagger *et al* (1997) studied the nature of hydrocarbon emissions from a propane-rich flame in an incinerator (see section 2.2 for simulation conditions). Concentrations for light hydrocarbons decrease as the temperature is increased. The most abundant light hydrocarbon species are methane and ethyne, as in this case. According to Marinov *et al* (1996), these lighter hydrocarbons play an important role in the formation of aromatic species, where they undergo fast initiation reactions to produce radicals which later recombine and react to form benzene (Marinov *et al* 1996).

Oxidation products, including carbon dioxide, carbon monoxide, and water are predicted at relatively lower concentrations compared to the corresponding results of excess oxygen and decreasing oxygen, but give the same overall trends. This is a result of

lower oxygen levels under pyrolysis conditions compared to those of excess oxygen and decreasing oxygen conditions.

Unlike excess oxygen and decreasing oxygen results, several aromatic and poly-aromatic species are predicted. The majority of aromatic species are at their peak concentrations at approximately 1000 K and decrease toward the higher temperatures. The most abundant species are benzene and naphthalene. In addition, chrysene concentrations are predicted under equilibrium conditions, although it is not predicted under kinetic conditions. Chrysene increases up to 1300 K and then dramatically decreases up to 1500 K.

The results obtained for light hydrocarbons and aromatic species are in agreement with a study completed by Gueret *et al* (1997). Gueret *et al* (1997) studied the thermodynamics of natural gas pyrolysis under the temperatures of 773 K to 2573 K and a pressure of 1 atm. It indicates that light hydrocarbons and aromatic species decrease toward the higher temperatures and that smaller hydrocarbons (i.e. methane) have higher compositions than larger hydrocarbons (i.e. ethane) (Gueret *et al*, 1997).

Many sulphur-containing species are predicted under pyrolysis conditions that are not predicted under excess oxygen and decreasing oxygen content. Aside from hydrogen sulphide, the most abundant species present are 3-methyl thiophene and carbon disulphide. These sulphur compounds are produced from the complex reactions involving carbon-contained radicals and hydrogen sulphide. There are no published kinetic or equilibrium studies on the thermal distraction of sulphur-containing waste gas. Thus, many of these complex sulphur species can only be predicted under equilibrium

conditions. These species include carbon disulphide, thiophene, 3-methyl thiophene, and benzo(b)thiophene.

6.2.4. Stoichiometric Air Combustion Results

As expected, combustion products under stoichiometric conditions yield similar results to the simulations under variable oxygen content. Compositions for carbon dioxide, carbon monoxide, and water are similar to those of excess oxygen and decreasing oxygen conditions. Their compositions decrease at 1500 K. The decrease in composition for oxidation species at 1500 K appears to be a result of the formation of carbon disulphide and aromatic formation. Stoichiometric results yield methane as the only light hydrocarbon with an increasing trend between 1300 K to 1500 K and goes to zero above this temperature, since it is expected for most of the initial hydrocarbon concentrations to be used up in such a stoichiometric reaction. This result is not the same as under excess oxygen, decreasing oxygen, and pyrolysis conditions. However, it can be noted that lack of oxygen content results in an increase in light hydrocarbon species since excess oxygen and decreasing oxygen results yield no light hydrocarbons, stoichiometric conditions yield only methane, and pyrolysis yields several light hydrocarbons.

The results for the sulphur-containing species under stoichiometric combustion yield similar trends for sulphur dioxide, hydrogen sulphide, and carbonyl sulphide compared to those of excess oxygen and decreasing oxygen. Carbon sulphide and carbon disulphide are formed at higher temperatures, but their trends are different than pyrolysis results. Under stoichiometric conditions, compositions for carbon sulphide and carbon disulphide form between temperatures of approximately 1300 K to 1500 K and 1500 K to

2000 K, whereas pyrolysis results indicate that these species exist over the entire temperature range. Thus, it can be concluded that as the amount of oxygen present is reduced, more complex sulphur containing species are formed under equilibrium conditions, again not an unexpected result. In addition, it should be noted that the decrease in composition for carbon sulphide and carbonyl sulphide above 1500 K may be a result of the formation of carbon disulphide.

Predictions for aromatic and poly-aromatic species yield results similar to those of excess oxygen and decreasing oxygen conditions. The only aromatic species predicted at equilibrium is 2-methyl naphthalene at temperatures above 1500 K, where its composition follows the exact same trend as excess oxygen and decreasing oxygen results.

6.3. Kinetic Model

The equilibrium simulations give an indication of product trends and predictions of species, particularly those with no published kinetic rates. However, incinerators do not operate under equilibrium conditions, therefore, kinetic simulations are necessary to get an accurate picture of product trends.

6.3.1. Combustion Chamber Model

Kinetic predictions for combustion chamber compositions for the three flow rates yield similar trends over the temperature range. In all three cases, three distinct temperature regions of the reactor model were simulated and showed significant changes in composition. These regions include approximately between 1600 K and 1800 K

(reaction zone), 1200 K to 1600 K (post combustion zone), and up to 1200 K (quenching zone). The most abundant species for three cases over the temperature range are methane, ethyne, carbon dioxide, sulphur dioxide, phenol, benzene, naphthalene, methyl indene, biphenyl, and biphenylene. Increasing the inlet flow rates (effectively decreasing the residence time) results in ethane, propane, oxygen, and hydrogen sulphide increasing in composition; the remaining species compositions decreasing in composition; and methane and butane remaining unchanged.

Previous studies have indicated that high concentrations of lighter weight hydrocarbons enhance the formation of aromatic and poly-aromatic hydrocarbons (Marinov *et al*, 1996; Frenklach and Wang, 1997). In this case, lower weight hydrocarbon species are at their peak concentrations at the lower temperatures of 800 K to 1000 K and gradually decrease with increasing temperature up to 1800 K. Several aromatic and poly-aromatic species form at the lower temperatures of the post combustion zone (*i.e.* 1200 K). The most abundant aromatic species formed are phenol, benzene, biphenyl, biphenylene, naphthalene, and methyl indene. Many more aromatics and poly-aromatic hydrocarbons are formed at lower concentration levels. Other aromatic species include methyl benzene, benzaldehyde, hydroxyl methyl benzene, ethyl benzene, ethenyl benzene, ethynyl benzene, dimethyl benzene, ethyl methyl benzene, and ethenyl methyl benzene. As well, other poly-aromatic species include hydroxyl naphthalene, acenaphthalene, fluorene, fluoranthene, indene, methyl naphthalene, benzo(a)indene, ethyl naphthalene, ethenyl naphthalene, ethynyl naphthalene, benzo(a)phenanthrene, phenanthrene, anthracene, pyrene, 4H-cyclopenta(def)phenanthrene, methyl phenanthrene, benzo(ghi)fluorene, and cyclopenta(cd)pyrene.

6.3.2. Incineration Stack Model

Kinetic calculations for the incineration stack in all three cases yield trends that are similar for the three temperature profiles. Under all conditions tested, concentrations for light hydrocarbons, oxidation products, and light aromatic species are at a maximum at the initial entry of the stack where the temperature is at its peak. These concentrations decrease significantly as these species move toward the top of the stack where the temperature is at its minimum. Some of the species are reduced by 99% of the original value. Thus, compositions for poly-aromatic species increase with decreasing temperature. The most abundant poly-aromatic species present are biphenyl and biphenylene, and the least abundant species present is cyclopenta(cd)pyrene.

Changes in magnitude occur when the air to fuel ratio is varied from 14:1 to 21:1. The 1000 K temperature profile gives results that indicate that hydrogen sulphide, carbon sulphide, carbonyl sulphide, and ethyl methyl benzene all increase in magnitude as the air to fuel ratio is varied from 14:1 to 21:1. The 1400 K temperature profile gives results that ethenyl methyl benzene and indene increase as air to fuel ratio is varied. The results for the remaining species in the 1000 K and 1400 K temperature profiles and all species from the 1623 K temperature profile indicate a decrease as the air to fuel ratio is varied from 14:1 to 21:1. These changes in magnitude may be a result of inlet feed into the combustion chamber.

These trends are somewhat comparable to previous studies by Marinov *et al* (1996) and Frenklach and Wang (1997). These studies involve detailed investigations of aromatic formation in premixed light hydrocarbon flames. These studies indicate that kinetic compositions are dependent on temperature and the presence of oxygen. As well,

these studies suggest that the majority of lower weight hydrocarbons, including methane, ethyne, and propane, and oxidation products including carbon dioxide and carbon monoxide decrease as temperature decreases. It also indicates that lower weight aromatic species compositions decrease and poly-aromatic species increase at lower temperatures (i.e. as cooling occurs in this case) (Marinov *et al*, 1996). In this study, species such as benzene, methyl benzene, ethyl benzene, ethenyl benzene, and ethynyl benzene show a decrease in composition as temperature is reduced. Poly-aromatic species including naphthalene, biphenyl, ethynyl naphthalene, phenanthrene, and pyrene all increase in composition as the temperature is decreased (Frenklach and Wang, 1997).

6.4. Comparison Between Equilibrium Model and Kinetic Model Results

A comparison of equilibrium and kinetic simulations is useful in that it gives an indication of species concentrations that are limited by kinetics. Trends for the kinetic results in the combustion chamber and the incinerator stack are comparable to equilibrium results, especially at the higher temperatures.

6.4.1. Combustion Chamber Comparison

Kinetic combustion chamber results are predicted to have similar trends under all conditions, thus a general comparison is made to excess oxygen equilibrium results. Note that all kinetic air to fuel ratio results contain excess oxygen levels.

Kinetic trends of oxidation products, including water and carbon dioxide, agree with equilibrium predictions under the excess oxygen conditions above 1000 K. The exception is that carbon dioxide concentrations dramatically decrease at 1500 K in

equilibrium simulations, whereas kinetic compositions remain large and constant above 1500 K. Direct comparison between kinetics and equilibrium indicate that thermodynamic predictions overestimate the concentrations of these species below temperatures of 1000 K. As well, carbon monoxide concentrations under equilibrium conditions agree with kinetic trends only between 1200 K and 1500 K. Equilibrium predictions underestimate the concentrations below 1200 K and above 1500 K. Figure 6.1 gives the comparison for oxidation product trends of excess oxygen equilibrium conditions and combustion chamber kinetic conditions of 14:1 air to fuel ratio and a flow rate of $3.28 \times 10^5 \text{ cm}^3/\text{s}$.

Equilibrium concentration trends, under excess oxygen conditions, for lighter weight hydrocarbons do not agree with kinetics since no light hydrocarbon species are predicted to form under excess oxygen equilibrium.

Equilibrium trends for sulphur-containing species agree with kinetics at slightly different temperatures, depending on the species. Under excess oxygen equilibrium conditions, sulphur dioxide concentrations agree with kinetics over the entire temperature of 800 K to 1800 K, carbonyl sulphide concentrations agree with kinetics between 1200 K and 1500 K, hydrogen sulphide concentrations agree at temperatures above 1400 K, and carbon sulphide concentrations do not agree with kinetics because it is at zero under excess oxygen equilibrium conditions. Thermodynamic predictions underestimate these species concentrations below the given temperatures. Figure 6.2 shows a comparison for sulphur-containing species trends under excess oxygen equilibrium and combustion chamber kinetic conditions of 14:1 air to fuel ratio and flow rate of $3.28 \times 10^5 \text{ cm}^3/\text{s}$.

Figure 6.1. Comparison for oxidation product trends of excess oxygen equilibrium conditions and combustion chamber kinetic conditions of 14:1 air to fuel ratio and a flow rate of $3.28 \times 10^5 \text{ cm}^3/\text{s}$.

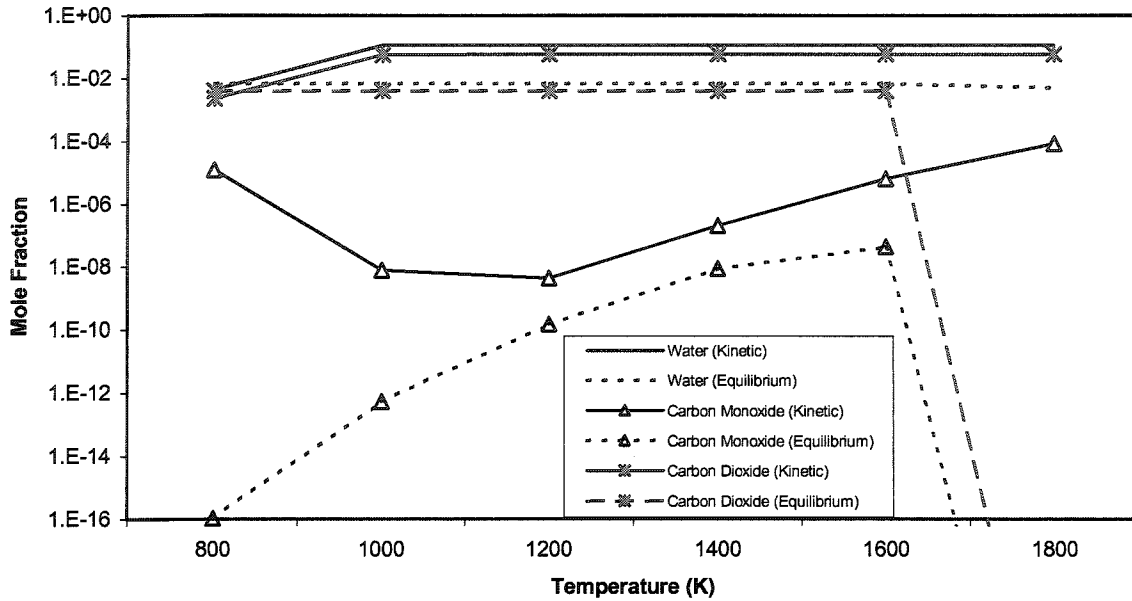
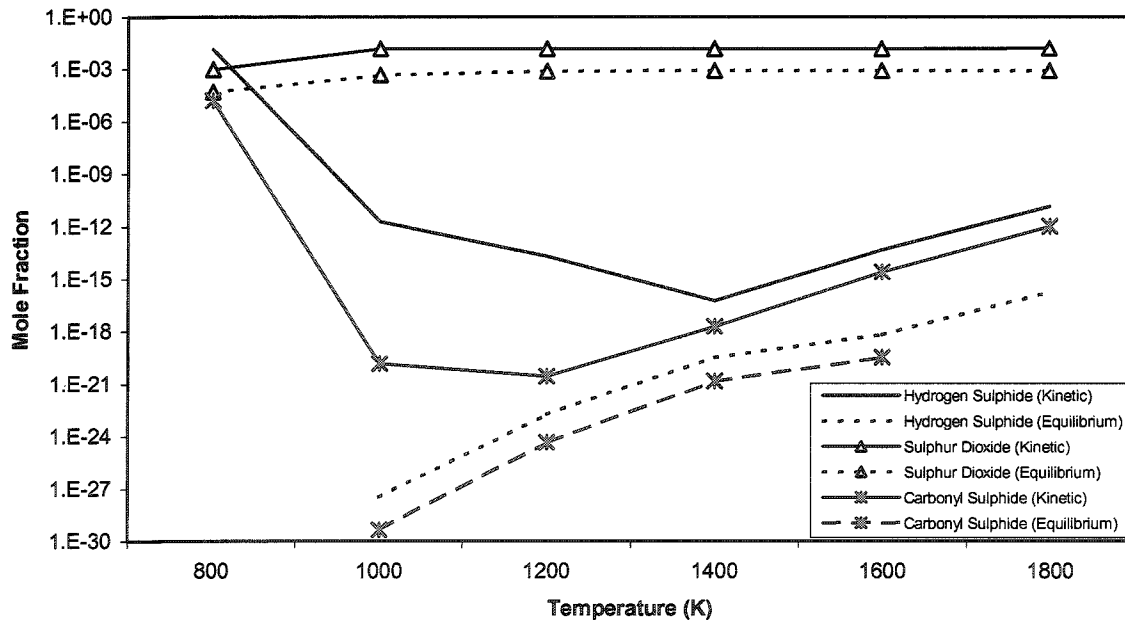


Figure 6.2. Comparison for sulphur-containing species product trends of excess oxygen equilibrium conditions and combustion chamber kinetic conditions of 14:1 air to fuel ratio and a flow rate of $3.28 \times 10^5 \text{ cm}^3/\text{s}$.



As mentioned in section 6.1, several complex sulphur species, including carbon disulphide, thiophene, 3-methyl thiophene, and benzo(b)thiophene, can only be predicted under equilibrium conditions because there is no published kinetic data.

Equilibrium trends, under excess oxygen conditions, for all single-ring aromatic species are not in agreement with kinetics, since no single-ring aromatic species formed under excess oxygen equilibrium. These species include benzene, phenol, methyl benzene, benzaldehyde, hydroxyl methyl benzene, ethyl benzene, ethenyl benzene, ethynyl benzene, dimethyl benzene, ethyl methyl benzene, and ethenyl methyl benzene.

The equilibrium trends, under excess oxygen conditions, for most poly-aromatic species do not agree with kinetics, since the only poly-aromatic species formed under equilibrium is 2-methyl naphthalene. These poly-aromatic species formed using kinetics include naphthalene, hydroxyl naphthalene, acenaphthalene, fluorene, fluoranthene, indene, methyl indene, benzo(a)indene, ethyl naphthalene, ethenyl naphthalene, ethynyl naphthalene, benzo(a)phenanthrene, phenanthrene, anthracene, pyrene, 4H-cyclopenta(def)phenanthrene, methyl phenanthrene, benzo(ghi)fluorene, biphenyl, biphenylene, and cyclopenta(cd)pyrene. Equilibrium trends for 2-methyl naphthalene are in agreement with kinetics above 1750 K. Thermodynamic predictions underestimate kinetic values below this temperature.

The majority of the species that are predicted under equilibrium conditions are in agreement with kinetic calculations above certain temperatures within the combustion chamber. Equilibrium trends below these temperatures disagree with kinetics indicating that the reactions are kinetically controlled.

6.4.2. Incineration Stack Comparison

Excess oxygen equilibrium trends for oxidation products, including carbon monoxide, carbon dioxide, and water agree with kinetic results obtained from temperature profiles of 1000 K, 1400 K, and 1623 K. Both sets of results yield a slight decreasing trend with decreasing temperature. The exception is that carbon monoxide and carbon dioxide equilibrium trends agree with kinetics for temperature profiles of 1000 K and 1400 K, but do not agree with results from the 1623 K temperature profile. The equilibrium concentrations give a dramatic increase at 1500 K as temperature is decreasing, whereas the kinetic results under the 1623 K temperature profile shows a general decrease in composition with decreasing temperature. Thermodynamic predictions are underestimating carbon monoxide and carbon dioxide above 1500 K.

Trends for light hydrocarbons under excess oxygen equilibrium conditions do not agree with kinetic results from the stack. No light hydrocarbon species are predicted to form under excess oxygen equilibrium, whereas kinetics show large amounts of these species. A general decrease in composition for all light hydrocarbons is predicted under the 1000 K, 1400 K, and 1623 K temperature profiles. From these results, it can be concluded that the reactions involving light hydrocarbons are kinetically controlled.

Excess oxygen equilibrium trends for sulphur-containing species agree with kinetics in stack predictions. Sulphur dioxide trends under equilibrium agree with all three temperature profiles that are used in the kinetic stack calculations. Hydrogen sulphide trends under equilibrium agree with kinetic trends from the 1623 K and 1400 K temperature profiles, but not the 1000 K temperature profile. Under equilibrium, hydrogen sulphide goes to zero below 900 K, whereas kinetics show a general decreasing

composition trend with decreasing temperature toward 800 K. Carbonyl sulphide equilibrium concentrations are in agreement with kinetic results from the 1400 K temperature profile, but do not agree with the 1000 K and 1623 K temperature profiles. Under excess oxygen equilibrium conditions, carbonyl sulphide goes to zero at temperatures below 900 K and above 1500 K, whereas kinetics indicate a decreasing composition trend with decreasing temperature at temperatures below 900 K and above 1500 K.

Aromatic species equilibrium trends do not agree with any kinetic results for the incinerator stack. Under excess oxygen equilibrium, the only aromatic species formed is 2-methyl naphthalene at 1500 K to 1750 K. Kinetic trends indicate the formation of several aromatic and poly-aromatic species during cooling for all three temperature profiles. Single-ring aromatic species show an overall decreasing trend and poly-aromatic species show an overall increasing trend with decreasing temperature. Since these results are not in agreement, it can be concluded that the formation of aromatic and poly-aromatic species is controlled by kinetics.

Several species that are predicted under equilibrium conditions agree with kinetic results under certain temperature profiles in the incinerator stack. Equilibrium predictions beyond these temperatures are thought to be invalid compared to stack calculations. In these cases, the kinetic calculations are used to predict the behaviour of the species concentrations inside the stack during the cooling process.

6.5. Comparison to Gas Flaring

As previously discussed, waste gas incineration is used in the oil and gas industry as an alternative to flaring. It is thought that incineration is a better choice for disposing of any waste gas, but there have been no studies in this area. In this study, a qualitative comparison is made between sour gas incineration and sour gas flaring.

Kinetic results obtained from combustion chamber calculations are in agreement with studies completed on sour gas flares. A study completed by the Alberta Research Council (Stroscher, 1996) identified many of the same compounds exiting a sour gas flare during combustion as were identified in significant amounts in this study. Stroscher (1996) indicates large amounts of methane, ethyne, and carbon dioxide, as well as smaller amounts of ethane, carbon-3 hydrocarbons, carbon-4 hydrocarbons, and carbon monoxide. Stroscher (1996) also identified sulphur dioxide, hydrogen sulphide, and carbonyl sulphide, where sulphur dioxide amounts were the most significant. As well, phenol and benzene were produced in relatively large amounts. In addition, other species including methyl benzene, dimethyl benzene, ethyl benzene, ethynyl benzene, ethenyl benzene, and benzaldehyde were all produced in significant amounts. Many poly-aromatic species identified in Stroscher (1996) were also identified including naphthalene, biphenyl, and biphenylene in relatively large amounts, among other species including methyl naphthalene, dimethyl naphthalene, ethyl naphthalene, fluorene, phenanthrene, fluoranthene, pyrene, 4Hcyclopenta(def)phenanthrene, and cyclopenta(cd)pyrene (Stroscher, 1996).

Many of the same species identified exiting the flare are present in this study as exiting from the incinerator stack. These species generally are produced in larger

amounts from the flare compared to that of the simulated stack. This includes oxidation products such as carbon dioxide and carbon monoxide; light hydrocarbons such as methane, ethane, ethene, ethyne, propane, propene, propyne, butane, butene, butyne, butadiene, and butadiyne; and sulphur-containing species such as hydrogen sulphide, sulphur dioxide, carbonyl sulphide. In addition, these species include aromatics such as phenol, benzene, methyl benzene, dimethyl benzene, ethyl benzene, ethynyl benzene, ethenyl benzene, benzaldehyde, naphthalene, biphenyl, biphenylene, methyl naphthalene, dimethyl naphthalene, ethyl naphthalene, fluorene, phenanthrene, fluoranthene, pyrene, 4Hcyclopenta(def)phenanthrene, and cyclopenta(cd)pyrene (Stroscher, 1996). A list of these species is given in Table 6.1.

Equilibrium simulations predict species (where there is not kinetic data available) that are not present in the simulated stack, but are present in the results from Stroscher (1996). They include carbon disulphide, thiophene, 3-methyl thiophene, benzo(b)thiophene, and chrysene. These species are present in larger amounts from a sour gas flare compared to that of the simulations and they follow all of the same trends.

There are compounds found in the emissions from sour gas flaring that are not found exiting the incinerator. These species include 2-methyl-2-propanoic acid, methoxy benzene, 2-thiazolamine, benzofuran, butyl benzene, azulene, benzo(c)cinnoline, dibenzothiophene, and benzo(a)pyrene. This is a result of less efficient combustion in the gas flare. Gas flaring has less efficient combustion than the simulated stack because simulations in this study assume ideal plug flow for the incinerator, which means greater temperature control, oxygen control, and mixing in the enclosed combustion chamber,

Table 6.1. Hydrocarbons and sulphur compounds identified in emissions from a sour oilfield battery flare (25% hydrogen sulphide) in Alberta and a direct comparison to this study (Stroscher, 1996).

Compound	Amount identified (mg/m ³)	Identified in this study– Y (Yes), N (No)
Carbon Monoxide	8.0	Y
Carbon Dioxide	6870.0	Y
Methane	83.1	Y
Ethane	4.9	Y
Ethene	6.0	Y
Ethyne	36.4	Y
Carbon-3 hydrocarbons	5.7	Y
Carbon-4 hydrocarbons	2.9	Y
Sulphur Dioxide	6910	Y
Hydrogen Sulphide	126	Y
Carbonyl Sulphide	64	Y
Carbon Disulphide	482	Y
Thiophene	179.2	Y
3-Methyl Thiophene	2.7	Y
Benzo(b)thiophene	156.6	Y
Benzene	64.3	Y
Methyl Benzene	20.5	Y
Ethyl Benzene	7.1	Y
Dimethyl Benzene	6.5	Y
Ethenyl Benzene	34.4	Y
Ethynyl Benzene	41.9	Y
2-Methyl-2-Propenoic Acid	2.2	N
Methoxy Benzene	1.4	N
2-Thiazolamine	0.9	N
Benzaldehyde	12.6	Y
Benzofuran	3.6	N
Phenol	12.2	Y
Ethenyl Methyl Benzene	1.7	Y
Ethynyl Methyl Benzene	13.8	Y
Butyl Benzene	0.9	N
Naphthalene	61.5	Y
Azulene	34.4	N
Methyl Naphthalene	1.5	Y
Biphenyl	8.0	Y
Ethyl Naphthalene	6.7	Y
Dimethyl Naphthalene	12.0	Y
Biphenylene	13.2	Y
Fluorene	54.21	Y
Benzo(c)cinnoline	3.81	N
Dibenzothiophene	82.2	N
Phenanthrene	34.1	Y
4H-Cyclopenta(def)phenanthrene	3.21	Y
Fluoranthene	14.1	Y
Pyrene	83.3	Y
Cyclopenta(cd)pyrene	9.7	Y
Chrysene	2.4	Y
Benzo(a)pyrene	0.46	N

which leads to better combustion. These parameters under gas flare conditions are extremely difficult to control.

Stroscher (1996) identifies many of the same trends found in emissions exiting the stack. Compositions for sulphur dioxide and phenol are identified in large amounts, and ethenyl methyl benzene are found in much smaller amounts compared to the remaining composition (Stroscher, 1996). Flare emissions are largely affected by oxygen content and flow rate. Stroscher (1996) identifies that increasing wind speed and stack flow rate causes a decrease in a flare's combustion efficiency, thus changing concentrations of species being emitted.

6.6. Summary

The majority of the results obtained from both equilibrium and kinetic models are in agreement with previous studies completed by Marinov *et al* (1996), Frenklach and Wang (1997), and Chagger *et al* (1997). Results indicate that equilibrium compositions are temperature dependent and oxygen content dependent; and that kinetic compositions are temperature dependent, inlet flow rate dependent, and oxygen content dependent. Kinetic concentrations for several species are directly compared to equilibrium trends and values. Equilibrium concentrations closely resemble kinetic concentrations at high temperatures where reactions are fast. At the lower temperatures, equilibrium predictions actually underestimate or overestimate concentrations for a number of species, indicating that at these temperatures reactions are slow and equilibrium is not reached. In addition, many of the kinetic predictions for the stack and equilibrium predictions are comparable to studies on emissions of sour gas flares (Stroscher, 1996).

In summary, it should be noted that the results shown in this study are representative of a real system, since the parameters used for modeling are taken from Questor Incineration Technologies. The assumptions used for the reactor are ideal for this study, but are not sufficient in the case of a real incinerator. The next chapter draws the major conclusions together and makes some new recommendations for future research.

Chapter 7. Conclusions and Recommendations

In this study, thermodynamic and kinetic simulations of sour gas incineration have been performed. Key reactions and key factors that affect the formation of volatile organic compounds and aromatic species under incineration conditions have been identified. In addition, a comparison between sour waste gas incineration and sour gas flaring emissions is made. The key results are summarized in this chapter as well as conclusions and recommendations for future research.

7.1. Reactor Model Verification

In Chapter 3, the reactor model assumptions and requirements are discussed. It is assumed that the reactor model is under steady state conditions. As well, the gas is assumed to be ideal as it is at high temperature and atmospheric pressure. The incinerator flow is assumed to be plug flow. Two of three criteria outlined by Cutler *et al* (1988) demonstrates that the reactor in this case is approximated by plug flow. There is little published data available on the characteristic mixing times and temperature profiles within the combustion chamber and the incineration stack. The calculations of these times are outside the scope of this study, but will be part of future studies.

7.2. Equilibrium Model

Equilibrium calculations were performed under varying oxygen levels. Excess oxygen combustion, as well as decreasing oxygen combustion yields similar trends for all species studied. As expected, the most abundant species formed are carbon monoxide,

carbon dioxide, and water. No lighter weight hydrocarbon species are predicted to form under excess oxygen and decreasing oxygen conditions. Sulphur-containing compounds, including sulphur dioxide, hydrogen sulphide, and carbonyl sulphide, are predicted under equilibrium where sulphur dioxide is the most abundant species over the entire temperature range. The only aromatic species formed is 2-methyl naphthalene. It should be noted that as the oxygen content is decreased, larger compositions for water, carbon monoxide, carbon dioxide, sulphur dioxide, hydrogen sulphide, carbonyl sulphide, and 2-methyl naphthalene are formed. In addition, stoichiometric equilibrium combustion results are similar to the previous results.

Pyrolysis equilibrium results show different behaviour for most species. A number of light hydrocarbon species are predicted to form and the concentrations decrease with increasing temperature. Oxidation products, including carbon dioxide, carbon monoxide, and water, are predicted to form, but at lower concentrations compared to excess oxygen results. As well, carbon monoxide is the most abundant among these species over the temperature range. Several sulphur-containing species are predicted to form under equilibrium conditions, these species include hydrogen sulphide, sulphur dioxide, carbonyl sulphide, carbon sulphide, carbon disulphide, thiophene, 3-methyl thiophene, and benzo(b)thiophene. Sulphur dioxide and carbonyl sulphide are formed as a result of the presence of carbon dioxide in the initial input composition. 3-methyl thiophene is the most abundant at the lower temperatures and sulphur dioxide at the higher temperatures. It appears as though benzene is formed as a result of the carbon-3 radical recombination reactions. Many aromatic species are predicted to form under equilibrium conditions at decreasing concentrations with increasing temperatures.

Benzene and methyl benzene are amongst the most abundant aromatics. In addition, poly-aromatic species including naphthalene and ethyl naphthalene are the most abundant at the lower temperatures, and methyl naphthalene at the higher temperatures.

Under pyrolysis conditions, lack of oxygen causes more complex species to form under equilibrium conditions. There is no kinetic data for carbon disulphide, thiophene, 3-methyl thiophene, benzo(b)thiophene, and chrysene, but these species are found in products of sour gas combustion in the field. As such, it may be possible to use the equilibrium results for these species in subsequent modelling of sour gas combustion.

7.3. Kinetic Model

7.3.1. Combustion Chamber Calculations

Three distinct temperature regions occur in combustion chambers. These include a reaction zone (approximately above 1600 K), a post combustion zone (approximately 1200 K – 1600 K), and a quenching zone (approximately up to 1200 K). In this study, these three zones were simulated to determine the major products formed. In the reaction zone temperature, the major oxidation products are produced. In this study, the significant species produced at this stage are ethyne, methane, carbon monoxide, sulphur dioxide, carbon sulphide, and carbonyl sulphide. The post combustion zone is in the temperature range where many aromatic and poly-aromatic species are formed. According to this study, the most significant are benzene, phenol, naphthalene, biphenyl, and biphenylene. In the quenching zone, the major species are methane, ethyne, and benzene, along with other species that reach values close to equilibrium values.

It should be noted that increasing the air content (ie: oxygen content) in the air to fuel ratio from 14 to 21 has shown the same general decreasing trend over the temperature range. As well, increasing the inlet flow rate results in increasing compositions for ethane, propane, oxygen, and hydrogen sulphide, no change for methane and butane, and decreasing compositions for the remaining species studied.

These results are in agreement with previous studies, including those on sour gas flaring. Lower weight hydrocarbon species are precursors to the formation of aromatic species and poly-aromatic species. The results of this study indicate the formation of benzene occurs after the formation of the first phenyl radical, which enhances the later formation of poly-aromatic hydrocarbons.

Lastly, some species compositions may be predicted by equilibrium calculations, especially at the higher temperatures where reactions are fast. Equilibrium predictions are valid at these temperatures, but tend to fail at the lower temperatures. This is a result of the fact that lower temperature reactions are kinetically limited and do not reach equilibrium.

7.3.2. Incineration Stack Calculations

The temperature profiles with initial combustion temperature of 1000 K, 1400 K, and 1623 K all show similar trends, but yield different compositions for species. At entry of the stack, lower weight hydrocarbons, oxidation products, and smaller aromatic species are predicted to be at their peak concentration. At this point, the most abundant species present for the three temperature profiles are methane, butane, ethyne, water, sulphur dioxide, phenol, biphenyl, and biphenylene. As the temperature decreases in the

stack toward the top, their concentrations drastically decrease, and large concentrations of poly-aromatic species are produced as a result. This is to be expected because smaller volatile organic species are reacting to produce large quantities of poly-aromatic hydrocarbons. It should be noted that each individual temperature profile yielded similar trends under all air to fuel ratios and flow rates, but differs in magnitude of species' compositions.

Stack compositions are also dependent on inlet flow rate and on oxygen content. Changes in magnitude for all species are predicted when increasing the oxygen content condition in the combustion chamber inlet flow. Under the 1000 K temperature profile, hydrogen sulphide, carbon sulphide, carbonyl sulphide, and ethyl methyl benzene all increase in magnitude, whereas only ethenyl methyl benzene and indene increase under the 1400 K temperature profile as the air to fuel ratio is varied from 14:1 to 21:1. The remaining species studied under the 1000 K and 1400 K temperature profiles and all species under the 1623 K temperature profile are predicted to decrease as air to fuel ratio is varied from 14:1 to 21:1. As well, changes in composition magnitude are predicted for all species when inlet flow rate is increased. Depending on the species, compositions decrease and increase as the inlet flow rate is increased. However, these trends are consistent for each individual temperature profile under varying conditions.

Stack results show that lower weight hydrocarbon species and smaller aromatic compounds aid in the formation of poly-aromatic species inside the incinerator stack, since the existing presence of benzene and its derivatives are the precursors of poly-aromatic formation.

Some species compositions that are predicted kinetically agree with equilibrium predictions. It appears that these compositions are especially predictable under the 1000 K temperature profile. The higher temperature profiles yield different trends than those found at the specified temperatures under equilibrium conditions. The equilibrium predictions resemble the combustion chamber compositions more closely than the stack compositions. This is a result of the higher temperatures in the combustion chamber where kinetics are fast and therefore approach equilibrium.

Stack calculations are in agreement with results from previous results on the cooling of flue gases in incineration. They are also similar to many of the same qualitative trends as sour gas flaring in terms of emissions. However, the compounds released from sour gas flares are in larger amounts than they are found in the simulated stack. These species are listed in Table 6.1. In addition, equilibrium calculations predict some species that are identified in sour gas flare emissions, but not under kinetic calculations. These species are again identified in larger amounts in sour gas flares. They include carbon disulphide, thiophene, 3-methyl thiophene, benzo(a)thiophene, and chrysene. In contrast, sour gas emissions identify a number of species that are not identified in the simulated stack. They include 2-methy-propanoic acid, methoxy benzene, 2-thiazolamine, benzofuran, butyl benzene, azulene, benzo(c)cinnoline, dibenzothiophene, and benzo(a)pyrene (Stroscher, 1996). These differences are likely due to the fact that the simulated stack was based on conditions of an idealized plug flow reactor with better oxygen control, temperature control, and better mixing. The gas flare do not have the necessary control over these parameters, therefore resulting in less efficient combustion.

7.4. General Recommendations

As previously mentioned, this study is a basis for further research within the field of waste gas destruction. Although this study has given some definitive results, much more research is needed in order to identify major relationships that are important in reducing or even eliminating toxic emissions released from the combustion of sour gas. A number of general recommendations are discussed below.

Although the constant temperature requirement for a plug flow reactor did not agree with the criteria given by Cutler *et al* (1988), the plug flow reactor model is still used. However, characteristic mixing times and temperature profiles within the combustion chamber and incinerator stack are required to further this work, since this study only provides a basis for these calculations.

Previous studies completed on the combustion of waste gas during incineration are limited. The mechanism used in this study was compiled from a number of mechanisms on hydrocarbon fuel combustion and sulphur-contained fuel combustion. Nonetheless, experimental determination of chemical reactions taking place inside the combustion chamber and the incinerator stack are necessary.

In qualitatively comparing these emission compositions to gas flaring studies, more experimental studies are necessary on the characterization of emissions from waste gas incinerators. A complete experimental identification of compounds from incineration emissions would be a more comparable tool to emission characterization of gas flares.

Since these simulations are performed under high air: fuel ratio, the formation and emission of nitrogen oxide compounds occurred, especially at the higher temperatures.

Nitrogen reacts with oxygen at these temperatures. Further research is needed to determine likely routes of formation and emission of these compounds.

Further research is also needed to determine the most appropriate reactor model to simulate a flare, as the plug flow reactor is not because there is never perfect mixing or sufficient residence time in an incinerator.

7.5. *Summary*

Waste gas incineration is becoming more widely used within the oil and gas industry and there are limited resources available on its emissions. This study provides some definitive results of the emissions released. Equilibrium calculations indicate that species compositions are temperature dependent, and oxygen content dependent. Kinetic calculations indicate that species compositions are temperature dependent, inlet flow rate dependent, and oxygen content dependent. In addition, this study provides the basic trends for species compositions both in the combustion chamber and the incinerator stack. It is found that majority of poly-aromatic species are formed within the stack during the cooling of gases. It is concluded to be a result of reactions taking place between smaller volatile organic compounds produced in the combustion chamber, including lower weight hydrocarbons, complex sulphur species, oxidation products, and lower weight aromatic species.

The results from this study are in agreement with previous studies completed by Marinov *et al* (1996), Frenklach and Wang (1997), and Chagger *et al* (1997). As well, composition trends found in this study are qualitatively comparable studies on sour gas flares (Stroscher, 1996).

Since this study only provides a basis on an ideal incinerator, further research on waste gas incineration is necessary. Although it has given some definitive results, much more research is needed in order to identify major relationships and trends that are important in reducing or even eliminating toxic emissions released from the combustion of waste gas in the oil and gas industry.

References

- Anders, L.C., Yngve, U.Z., and Conny, E.O. (1986). Polynuclear Aromatic Compounds in Flue Gases and Ambient Air in the Vicinity of a Municipal Incineration Plant. *Atmospheric Environment*, **20**: 2279-2282.
- Atkins, P. (2001). *Physical Chemistry, 6th Edition*. (W.H. Freeman and Company: New York, 1999).
- Burcat, A.(2001). Retrieved October 1, 2002, from <http://garfield.chem.elte.hu/Burcat/burcat.html>
- Chagger, H.K., Jones, J.M., Pourkashanian, M., Williams, A. (1997). The nature of hydrocarbon emissions formed during the cooling of combustion products. *Fuel*, **76**: 861-864.
- Chemkin 3.7. Collection Software User Manuel, Revision B. **January 2003**.
- Cutler, A.H. Antal, M.J., Jones, M. (1988). A Critical Evaluation of the Plug-Flow Idealization of Tubular-Flow Reactor Data. *Ind. Eng. Chem. Res*, **27**: 691-697.
- Delta Combustion Solutions (2003). Retrieved on January 20, 2003 from <http://www.deltacombustion.com/web>.
- Flare Efficiency Study*, EPA-600/2-83-052, U.S. Environmental Protection Agency, Cincinnati, OH, July, 1983.
- Frenklach, M., Clary, D.W., Gardiner, W.C., Stein, S.E. (1985). Detailed Kinetic Modeling of Soot Formation in Shock-Tube Pyrolysis of Acetylene, *Twentieth Symposium (International) on Combustion*, The Combustion Institute, p. 887.
- Frenklach, M., and Warnatz, J. (1987). *Combustion Science and Technology*, **51**: 265.
- Frenklach, M. and Wang, H. (1997). A Detailed Kinetic Modeling Study of Aromatics Formation in Laminar Premixed Acetylene and Ethylene Flames. *Combustion and Flame*, **110**: 173-221.
- Gueret, C., Daroux, M., Billaud, F. (1997). Methane Pyrolysis: Thermodynamics. *Chemical Engineering Science*, **52**: 815-827.
- Howard, B. (2001). Retrieved October 1, 2002 from Massachusetts Institute of Technology Combustion Research Group <http://web.mit.edu/anish/www/MITcomb.html>

- Canada's Clean Combustion Network (2003). Retrieved on March 5, 2003 from <http://combustion-net.com>.
- International Energy Annual* 1998; DOE/EIA-0219(98); Energy Information Administration, Office of Energy Markets and End Use, U.S. Department of Energy; Washington, D.C., 2000.
- Johnson, M.R.; Kostiuk, L.W.; Spangelo, J.L. (2001). A Characterization of Solution Gas Flaring in Alberta. *Air & Waste Management Association*, **51**: 1167-1177.
- Konnov, A.A. (1997). Retrieved on October 5, 2002 from <http://homepages.vub.ac.bc/~akonnov>
- Leahey, D.M., Preston, K., Strosher, M. (2001). Theoretical and Observational Assessments of Flare Efficiencies. *Air & Waste Management Association*, **51**: 1610-1616.
- Management of Routine Solution Gas Flaring in Alberta: Report and Recommendations of The Flaring Project Team*. Clean Air Strategic Team, June 1998.
- Marinov, N.M., Pitz, W.J., Westbrook, C.K., Castaldi, M.J., and Senkan, S.M. (1996). Modeling of Aromatic and Polycyclic Aromatic Hydrocarbon Formation in Premixed Methane and Ethane Flames. *Combustion Science and Technology*, **116-117**: 211-287.
- McCrillis, R.C. *Flares as a means of destroying volatile organic and toxic compounds*. EPA/600/D-88/106, US Environmental Protection Agency, Research Triangle, NC. 1988.
- Meridian Engineering and Technology (1997). Retrieved on March 5, 2003 from <http://www.meridianeng.com/airpollld.html>,
- Motyka, D.; Mascarenhas, A. (2002). Incineration Innovation. *Hydrocarbon Engineering*, p. 75.
- NIST Database (2003). Retrieved on March 5, 2003 from <http://webbook.nist.gov/chemistry>
- Olsen, D.B., Gardiner, W.C. Jr. (1977). An Evaluation of Methane Combustion Mechanisms. *Journal of Physical Chemistry*, **81**: 2514.
- Pohl, J.H. and Soelberg, N.R. *Evaluation of the efficiency of industrial flares: Flare head design and gas composition*. PB-86-100559/XAB. Energy and Environmental Research Corporation, Irvine, CA. 1985.

- Pohl, J.H. and Soelberg, N.R. *Evaluation of the efficiency of industrial flares : H₂S gas mixtures and pilot-assisted flares*. PB-87-102372/XAB. Energy and Environmental Research Corporation. Irvine, CA. **1986a**.
- Pohl, J.H. and Soelberg, N.R. *The combustion and destruction of sour gas mixtures in flare flames*. Combustion Institute, Pittsburg, PA. 21st International Symposium on Combustion, Munich, Federal Republic of Germany, August 3, **1986**.
- Questor Incineration Technologies (2003). Retrieved on April 20, 2003 from <http://www.questortech.com/>.
- Stroscher, M.T. (2000). Characterization of Emissions from Diffusion Flare Systems. *Air & Waste Management Association*, **50**: 1723-1733.
- Stroscher, M. *Investigations of Flare Gas Emissions in Alberta*. Environmental Technologies, Alberta Research Council (1996).
- Stone, D.K.; Lynch, S.K.; Pandullo, R.F.; Evans, L.B. *Flares*. United States Environmental Protection Agency, December 1995.
- Stull, D.R.; Westrum, E.F.; Sinke, G.C. *The Chemical Thermodynamics of Organic Compounds* (John Wiley & Sons Inc., New York: 1969).
- TRC Thermodynamic Tables: Hydrocarbons*. (1982). Thermodynamics Research Center, The Texas A&M University System. College Station, Texas.
- TRC Thermodynamic Tables: Non-Hydrocarbons*. (1982). Thermodynamics Research Center, The Texas A&M University System. College Station, Texas.
- Tsuchiya, K., Kenshu, K., Hiroyuki, M. (1996). Studies on the Oxidation Mechanism of H₂S Based on Direct Examination of Key Reactions. *International Journal of Chemical Kinetics*, **29**: 57-66.
- University of Leeds, 1998, <http://www.chem.leeds.ac.uk/Combustion/Combustion.html>
- Warnatz, J. *Eighteenth Symposium (International) on Combustion*, p.136. The Combustion Institute, Pittsburg, PA. **1981**.
- Westbrook, C.K., Creighton, J., Lund, C. and Dryer, F.L. (1977). A Numerical Model of Chemical Kinetics of Combustion in a Turbulent Flow Reactor. *Journal of Physical Chemistry*, **81**: 2542-2554.
- Westbrook, C.K., Dryer, F.L. (1984). Chemical Kinetic Modeling of Hydrocarbon Combustion. *Prog. Energy Combustion Science*, **10**: 1-57.

Woiki, D., Roth, P. (1994). Kinetics of the High Temperature H₂S Decomposition. *Journal of Physical Chemistry*, **98**: 12958-12963.

Yasuda, K. and Takahashi, M. (1998). *Journal of Air and Waste Management Association*, **48**: 441.

Zhang, X.J. **1998**. *J. Environ. Sci. Health*, A33(2): 279.

Appendix 1. Chemkin Input File

ELEMENTS

C H O A R N S

END

SPECIES

H2 CH4 C2H2 C2H4 C2H6 C3H4 C3H6 C4H2 O2 H2O H2O2 CO CO2 CH2O CH2CO
 C H CH CH2 SCH2 CH3 C2H C2H3 C2H5 C3H2 H2CCCH H2CCCCH O OH HO2
 HCO CH3O CH3OH CH3CO CH2OH HCCO CH2HCO C2H3O CH3HCO C3H3
 CH2CHCCH N2 AR CN HCN N NH NO HNO NH2 H2NO NCO N2O NO2 N2H2
 HOCN H2CN NNH NH3 N2H3 C2N2 HNCO S SH H2S SO SO2 SO3 HSO2 HOSO
 HOSO2 SN S2 CS COS HSNO HSO HOS HSOH H2SO HOSHO HS2 H2S2 H2SO4
 HOSOH C4H10 C3H6OH O2C3H6OH C3H5O2 C3H5O2H C3H5O NC3H7O2
 NC3H7O2H IC3H7O2 IC3H7O2H IC3H7O NC3H7O C3H8 IC3H7 NC3H7 PC3H4
 SC3H5 TC3H5 C3H6O C2H5CHO C2H5CO C3H5 IC4H7 C4H C4H5 C4H6 H2C4O
 C4H4 IC4H5 NC4H5 C4H8 T2C4H8 C2C4H8 IC4H3 NC4H3 C6H6 C6H5O C6H5
 C6H5CH3 C6H5CH2 C6H5CHO C6H5CO C6H5CCH2 C6H5CCO HOC6H4CH3
 C6H5CH2OH C6H4O2 OC6H4CH3 C6H5C2H5 C6H4C2H3 C6H4C2H C6H5C2H3
 C6H5C2H C6H5CHCH CH3C6H4CH3 CH3C6H4CH2 CH3C6H4C2H5
 CH3C6H4C2H3 C10H8 C10H9 C10H10 C10H7 C10H7O C10H7OH ACENPHTHLN
 FLUORENE FLRNTHN INDENYL INDENE CH3INDENE CH3INDENYL
 C10H7CH3 C10H7CH2 BZ(A)NDENE C10H7C2H5 C10H7C2H3 C10H7CCH2
 C10H7CCH C10H6CCH PHNTHRYL-1 PHNTHRYL-9 BZ(A)NDNYL C-C5H5
 C-C5H6 BZ(A)PHNTHRN PHNTHRN PHNTHROL-1 PHNTHROL-9 ANTHRACN
 PHNTHROXY-1 PHNTHROXY-9 FLUORYL PYRENE HC4-P(DEF)PTHN
 CH3PHNTHRN HC4-P(DEF)PTHYL BZ(GHI)FLN CH3CY24PD CH3CY24PD1
 CYC6H7 CH3DCY24PD FULVENE FULVENYL C-C5H4O CS2 C4H4S C7H5N
 C8H6O N-C10H22 C6H5OH N-UNDECANE AZULENE C8H6S C12H8O
 A3-M-THIOP BUTYL-BZ ME1-NAP ME2-NAP A1-E-NAP A2,3-DIMNAP
 A4CYP(DEF)PHTRN CY(CD)PYRENE BZ(A)PYR CHRYSENE C8H8O C7H6O2
 C4H8O3 C14H8O2 A1,3-DIMBZ BIPHNYLN ACENHTHN BIPHENYL BZ(A)PYR*S
 A2C6H5-2 CHRYSEN*4 PYC2H-2 C8H6 HA2R5 ACENHTHN A2R5H2 C12H9
 C6H5C3H2 PYRENE*2

END

Appendix 2.1.

Equilibrium input composition file for excess oxygen combustion at constant temperature of 800 K and constant pressure of 1 atm.

```
REAC H2 7.4729 x 10-6
REAC CH4 1.6964 x 10-3
REAC C2H6 3.9980 x 10-4
REAC O2 2.0874 x 10-1
REAC CO2 4.0354 x 10-4
REAC N2 7.7829 x 10-1
REAC AR 9.3063 x 10-3
REAC H2S 8.5191 x 10-4
REAC C3H8 2.1298 x 10-4
REAC C4H10 8.9675 x 10-5
TEMP 800
PRES 1
TP
END
```

Appendix 2.2.

Equilibrium input composition file for decreasing oxygen combustion by 20 % at constant temperature of 800 K and constant pressure of 1 atm.

```
REAC H2 7.7985 x 10-6
REAC CH4 1.7703 x 10-3
REAC C2H6 4.1722 x 10-4
REAC O2 1.7427 x 10-1
REAC CO2 4.2112 x 10-4
REAC N2 8.1220 x 10-1
REAC AR 9.7117 x 10-3
REAC H2S 8.8903 x 10-4
REAC C3H8 2.2226 x 10-4
REAC C4H10 9.3582 x 10-5
TEMP 800
PRES 1
TP
END
```

Appendix 2.3.

Equilibrium input composition file for pyrolysis combustion at constant temperature of 800 K and constant pressure of 1 atm.

```
REAC H2 9.4444 x 10-6
REAC CH4 2.1439 x 10-3
REAC C2H6 5.0527 x 10-4
REAC O2 0.0000 x 100
REAC CO2 5.1000 x 10-4
REAC N2 9.8361 x 10-1
REAC AR 1.1761 x 10-2
REAC H2S 1.0767 x 10-3
REAC C3H8 2.6917 x 10-4
REAC C4H10 1.1333 x 10-4
TEMP 800
PRES 1
TP
END
```

Appendix 2.4.

Equilibrium input composition file for stoichiometric combustion at constant temperature of 800 K and constant pressure of 1 atm.

```
REAC H2 1.6246 x 10-4
REAC CH4 3.6879 x 10-2
REAC C2H6 8.6918 x 10-3
REAC O2 1.9292 x 10-1
REAC CO2 1.9577 x 10-3
REAC N2 7.2572 x 10-1
REAC AR 8.5618 x 10-3
REAC H2S 1.8521 x 10-2
REAC C3H8 4.6302 x 10-3
REAC C4H10 1.9496 x 10-3
TEMP 800
PRES 1
TP
END
```

Appendix 3.1.

Plug input file used for modeling the combustion chamber under isothermal conditions at a temperature of 1800 K, pressure of 1 atm, fuel flow rate of $3.28 \times 10^5 \text{ cm}^3/\text{s}$, and 14:1 air to fuel ratio.

```
XEND 244.  
DIAM 337.82  
ISO  
TEMP 1800.  
PRES 1.0  
VDOT 30725745.  
REAC H2S 0.01538  
REAC H2 0.00031  
REAC O2 0.19570  
REAC N2 0.73437  
REAC CO2 0.00185  
REAC CH4 0.03046  
REAC C2H6 0.00731  
REAC C3H8 0.00398  
REAC C4H10 0.00178  
REAC AR 0.00886  
DX 244.  
END
```

Appendix 3.2.

Plug input file used for modeling the incinerator stack under the conditions of a linear temperature profile with an initial temperature of 1623 K at entry of the stack, pressure of 1 atm, fuel flow rate of $1.64 \times 10^6 \text{ cm}^3/\text{s}$, and a 14:1 air to fuel ratio.

```
XEND 975.  
DIAM 337.82  
TFIX  
TPRO 0      1623.  
TPRO 15     1619.92305  
TPRO 25     1617.87175  
TPRO 35     1615.82045  
TPRO 45     1613.76915  
TPRO 55     1611.71785  
TPRO 65     1609.66655  
TPRO 75     1607.61525  
TPRO 85     1605.56395  
TPRO 95     1603.51265  
TPRO 105    1601.46135  
TPRO 115    1599.41005  
TPRO 125    1597.35875  
TPRO 135    1595.30745  
TPRO 145    1593.25615  
TPRO 155    1591.20485  
TPRO 165    1589.15355  
TPRO 175    1587.10225  
TPRO 185    1585.05095  
TPRO 195    1582.99965  
TPRO 205    1580.94835  
TPRO 215    1578.89705  
TPRO 225    1576.84575  
TPRO 235    1574.79445  
TPRO 245    1572.74315  
TPRO 255    1570.69185  
TPRO 265    1568.64055  
TPRO 275    1566.58925  
TPRO 285    1564.53795  
TPRO 295    1562.48665  
TPRO 305    1560.43535  
TPRO 315    1558.38405  
TPRO 325    1556.33275  
TPRO 335    1554.28145  
TPRO 345    1552.23015  
TPRO 355    1550.17885  
TPRO 365    1548.12755  
TPRO 375    1546.07625  
TPRO 385    1544.02495  
TPRO 395    1541.97365  
TPRO 405    1539.92235  
TPRO 415    1537.87105  
TPRO 425    1535.81975
```

Appendix 3.2 (continued)

TPRO	435	1533.76845
TPRO	445	1531.71715
TPRO	455	1529.66585
TPRO	465	1527.61455
TPRO	475	1525.56325
TPRO	485	1523.51195
TPRO	495	1521.46065
TPRO	505	1519.40935
TPRO	515	1517.35805
TPRO	525	1515.30675
TPRO	535	1513.25545
TPRO	545	1511.20415
TPRO	555	1509.15285
TPRO	565	1507.10155
TPRO	575	1505.05025
TPRO	585	1502.99895
TPRO	595	1500.94765
TPRO	605	1498.89635
TPRO	615	1496.84505
TPRO	625	1494.79375
TPRO	635	1492.74245
TPRO	645	1490.69115
TPRO	655	1488.63985
TPRO	665	1486.58855
TPRO	675	1484.53725
TPRO	685	1482.48595
TPRO	695	1480.43465
TPRO	705	1478.38335
TPRO	715	1476.33205
TPRO	725	1474.28075
TPRO	735	1472.22945
TPRO	745	1470.17815
TPRO	755	1468.12685
TPRO	765	1466.07555
TPRO	775	1464.02425
TPRO	785	1461.97295
TPRO	795	1459.92165
TPRO	805	1457.87035
TPRO	815	1455.81905
TPRO	825	1453.76775
TPRO	835	1451.71645
TPRO	845	1449.66515
TPRO	855	1447.61385
TPRO	865	1445.56255
TPRO	875	1443.51125
TPRO	885	1441.45995
TPRO	895	1439.40865
TPRO	905	1437.35735
TPRO	915	1435.30605
TPRO	925	1433.25475
TPRO	935	1431.20345
TPRO	945	1429.15215
TPRO	955	1427.10085
TPRO	965	1425.04955

Appendix 3.2 (continued)

TPRO 975 1422.99825
PRES 1.0
VEL 1545.
REAC H2 2.898E-06
REAC CH4 1.188E-13
REAC C2H2 5.593E-10
REAC C2H4 5.288E-14
REAC C2H6 4.698E-22
REAC C3H4 2.103E-21
REAC C3H6 4.092E-22
REAC C4H2 5.071E-16
REAC O2 6.182E-02
REAC H2O 1.138E-01
REAC H2O2 8.061E-09
REAC CO 4.545E-06
REAC CO2 5.820E-02
REAC CH2O 3.487E-15
REAC CH2CO 3.759E-16
REAC C 8.938E-22
REAC H 8.523E-08
REAC CH 4.817E-15
REAC CH2 1.207E-14
REAC SCH2 2.186E-16
REAC CH3 9.406E-14
REAC C2H 3.643E-14
REAC C2H3 3.022E-15
REAC C2H5 6.689E-21
REAC C3H2 6.834E-19
REAC H2CCCH 5.455E-16
REAC H2CCCCH 1.736E-19
REAC O 3.356E-06
REAC OH 1.435E-04
REAC HO2 1.591E-07
REAC HCO 4.706E-16
REAC CH3O 8.591E-17
REAC CH3OH 7.892E-08
REAC CH3CO 7.144E-05
REAC CH2OH 7.820E-20
REAC HCCO 2.095E-13
REAC CH2HCO 5.011E-05
REAC C2H3O 2.486E-11
REAC CH3HCO 2.236E-04
REAC C3H3 1.036E-19
REAC CH2CHCCH 2.172E-08
REAC N2 7.296E-01
REAC AR 8.863E-03
REAC CN 6.492E-14
REAC C2N2 4.647E-17
REAC HCN 3.386E-10
REAC N 2.022E-11
REAC NH 1.840E-13
REAC NO 1.001E-02
REAC HNO 4.621E-09
REAC NH2 4.511E-14

Appendix 3.2 (continued)

REAC H2NO 5.097E-14
REAC NCO 1.124E-14
REAC N2O 4.368E-08
REAC NO2 1.403E-05
REAC N2H2 1.943E-19
REAC HOCN 1.030E-08
REAC H2CN 2.520E-18
REAC NNH 1.536E-13
REAC NH3 3.496E-13
REAC N2H3 4.144E-22
REAC HNCO 3.757E-13
REAC S 8.394E-13
REAC SH 1.594E-13
REAC H2S 3.399E-14
REAC SO 1.475E-07
REAC SO2 1.529E-02
REAC SO3 9.833E-05
REAC HSO2 5.957E-13
REAC HOSO 1.026E-08
REAC HOSO2 1.645E-09
REAC SN 7.003E-14
REAC S2 3.053E-17
REAC CS 5.327E-24
REAC COS 1.818E-15
REAC HSNO 0.000E+00
REAC HSO 6.426E-12
REAC HOS 9.957E-13
REAC HSOH 1.275E-14
REAC H2SO 9.508E-18
REAC HOSHO 1.635E-14
REAC HS2 1.770E-21
REAC H2S2 7.532E-25
REAC H2SO4 8.467E-10
REAC HOSOH 0.000E+00
REAC C4H10 1.781E-03
REAC C3H6OH 0.000E+00
REAC O2C3H6OH 0.000E+00
REAC C3H5O2 0.000E+00
REAC C3H5O2H 0.000E+00
REAC C3H5O 0.000E+00
REAC NC3H7O2 0.000E+00
REAC NC3H7O2H 0.000E+00
REAC IC3H7O2 0.000E+00
REAC IC3H7O2H 0.000E+00
REAC IC3H7O 0.000E+00
REAC NC3H7O 0.000E+00
REAC C3H8 7.424E-31
REAC IC3H7 1.457E-30
REAC NC3H7 1.522E-30
REAC PC3H4 3.834E-21
REAC SC3H5 5.253E-25
REAC TC3H5 1.232E-26
REAC C2H5CHO 2.271E-20
REAC C3H6O 3.423E-20

Appendix 3.2 (continued)

REAC C2H5CO 4.398E-27
REAC C3H5 8.718E-23
REAC IC4H7 6.580E-28
REAC C4H 4.582E-25
REAC C4H5 0.000E+00
REAC C4H6 1.486E-23
REAC H2C4O 2.726E-16
REAC C4H4 2.660E-15
REAC IC4H5 1.205E-20
REAC NC4H5 1.401E-22
REAC C4H8 3.602E-27
REAC T2C4H8 4.615E-25
REAC C2C4H8 2.232E-25
REAC IC4H3 7.398E-17
REAC NC4H3 9.348E-16
REAC C6H6 1.387E-13
REAC C6H5O 3.857E-09
REAC C6H5 6.451E-14
REAC C6H5OH 4.920E-12
REAC C6H5CH3 3.236E-23
REAC C6H5CH2 2.952E-23
REAC C6H5CHO 1.893E-23
REAC C6H5CO 8.356E-23
REAC C6H5CCH2 2.194E-26
REAC C6H5CCO 2.388E-25
REAC HOC6H4CH3 5.454E-25
REAC C6H5CH2OH 1.011E-23
REAC C6H4O2 0.000E+00
REAC OC6H4CH3 2.712E-26
REAC C6H5C2H5 3.330E-34
REAC C6H4C2H3 3.261E-30
REAC C6H4C2H 4.776E-24
REAC C6H5C2H3 3.805E-28
REAC C6H5C2H 4.178E-23
REAC C6H5CHCH 5.320E-29
REAC CH3C6H4CH3 3.039E-32
REAC CH3C6H4CH2 5.253E-31
REAC CH3C6H4C2H5 3.939E-31
REAC CH3C6H4C2H3 2.373E-61
REAC C10H8 1.229E-38
REAC C10H9 3.928E-45
REAC C10H10 3.015E-39
REAC C10H7 1.567E-41
REAC C10H7O 8.735E-41
REAC C10H7OH 4.379E-40
REAC ACENPHTHLN 2.130E-38
REAC FLUORENE 8.986E-41
REAC FLRNTHN 1.632E-44
REAC INDENYL 7.639E-38
REAC INDENE 1.880E-40
REAC CH3INDENE 7.852E-35
REAC CH3INDENYL 1.370E-30
REAC C10H7CH3 3.696E-45
REAC C10H7CH2 6.626E-44

Appendix 3.2 (continued)

REAC BZ(A)NDENE 1.284E-41
REAC C10H7C2H5 1.434E-54
REAC C10H7C2H3 3.016E-47
REAC C10H7CCH2 1.991E-45
REAC C10H7CCH 7.259E-39
REAC C10H6CCH 1.150E-40
REAC PHNTHRYL-1 9.966E-47
REAC PHNTHRYL-9 2.656E-47
REAC BZ(A)NDNYL 1.643E-37
REAC C-C5H5 3.099E-13
REAC C-C5H6 2.347E-15
REAC BZ(A)PHNTHRN 7.905E-47
REAC PHNTHRN 9.126E-44
REAC PHNTHROL-1 4.043E-46
REAC PHNTHROL-9 4.039E-46
REAC ANTHRACN 8.017E-45
REAC PHNTHROXY-1 5.387E-46
REAC PHNTHROXY-9 1.698E-46
REAC FLUORYL 8.408E-38
REAC PYRENE 9.663E-42
REAC HC4-P(DEF)PTHN 4.478E-40
REAC CH3PHNTHRN 4.337E-40
REAC HC4-P(DEF)PTHYL 4.208E-37
REAC BZ(GHI)FLN 5.046E-44
REAC CH3CY24PD 1.719E-25
REAC CH3CY24PD1 9.998E-22
REAC CYC6H7 1.669E-22
REAC CH3DCY24PD 3.003E-25
REAC FULVENE 3.264E-17
REAC FULVENYL 2.343E-19
REAC C-C5H4O 1.352E-13
REAC BIPHENYL 4.147E-20
REAC C12H9 4.593E-21
REAC C6H5C3H2 3.788E-22
REAC BIPHNYLN 5.643E-17
REAC C8H6 0.000E+00
REAC CHRYSENE 0.000E+00
REAC CHRYSEN*4 0.000E+00
REAC BZ(A)PYR 0.000E+00
REAC CY(CD)PYRENE 1.556E-59
REAC PYC2H-2 0.000E+00
REAC BZ(A)PYR*S 0.000E+00
REAC PYRENE*2 0.000E+00
REAC ACENHHTN 0.000E+00
REAC HA2R5 7.541E-45
REAC A2R5H2 2.205E-47
REAC A2C6H5-2 1.096E-76
DX 15.
END



